SEPARATION OF HEAVY METALS FROM WATER USING FIBROIN AS ADSORBENT

by

Muhammad Usman Farooq

A thesis
presented to the University of Waterloo
in fulfillment of the
thesis requirement for the degree of
Doctor of Philosophy
in
Chemical Engineering

Waterloo, Ontario, Canada, 2013

AUTHOR'S DECLARATION

I hereby declare that I am the sole author of this thesis. This is a true copy of the thesis, including any required final revisions, as accepted by my examiners.

I understand that my thesis may be made electronically available to the public.

ABSTRACT

Discharge of untreated industrial effluents containing heavy metals is hazardous to the environment as they are highly toxic, accumulates in the food chain and persistent in nature. Because of these adverse effects, their removal from wastewater is a substantial step in the protection of the environment and human health. Biosorption is found to be an eco-friendly, economical and lucrative separation technique in the removal of metal ions from effluent. This study explores the seperation potential of a new sorbent, fibroin (constituent of natural silk spun by *Bombyx mori)* for the removal of lead, chromium, copper and cobalt ions from effluent water.

The biosorbent was prepared by the separation of cocoon into its constituents, fibroin and sericin. The removal of sericin from fibroin, called silk degumming, was carried out by water extraction method. Effect of temperature (55-95^{o}C) on the kinetics and quantity of sericin removed was studied. The separation kinetics was approximated by the intraparticle diffusion model and the pseudo-second-order equation.

Biosorption characteristics of fibroin for the removal of lead, chromium, copper, and cobalt ions from aqueous solution were investigated through a batch study. The effect of initial solution concentration, contact time and temperature on the sorption process was investigated. The adsorption equilibrium was described by the Langmuir isotherm. The thermodynamic parameters, the change in enthalpy (ΔH) and change in entropy (ΔS), were calculated by using Van't Hoff plot. An accurate mathematical expression was used to calculate Gibbs free energy (ΔG), for the adsorption of all metals on fibroin.

For the kinetic data analysis, pseudo-second-order equation was modified based on the fact that the term q_e in the kinetic equation should be the equilibrium uptake corresponding to the instantaneous metal concentration in the solution. In order to evaluate the rate constant k_2, sorption kinetic data was fitted to the modified pseudo-second-order equation. The calculated values of rate constant k_2, for the adsorption of all metals on fibroin, were used to the modified pseudo-second-order model to predict the kinetic data. A good comparison was observed between the experimental data and model calculations. The kinetic data was also fitted to the intraparticle diffusion model which showed a multi linear trend.

The metal ions were desorbed from fibroin up to ten cycles of adsorption and desorption by using 0.05M ethylenediaminetetraacetic acid (EDTA). The removal of metal ions from fibroin was found to be rapid since complete desorption occurred within 15min. The uptake capacity of fibroin and adsorption/desorption kinetics remained almost the same even after ten cycles. The rate constants for both adsorption and desorption were also calculated by fitting the kinetic data to the modified pseudo-second-order model.

The dynamic adsorption was studied in a flow-through column packed with fibroin for the removal of all metals. Experiments were performed in order to study the effect of influent concentration (12-75ppm), influent flow rate (0.15-0.24ml/min) and regeneration of fibroin bed (upto 4 cycles). Whereas the bed height, column diameter and amount of adsorbent packed were kept constant during this study. Fibroin bed saturated with metal ions was regenerated effectively by using 0.5M EDTA solution. After four consecutive cycles of adsorption and desorption, no change in the uptake capacity was observed. The bed depth service time model, the Thomas model and the Yoon-Nelson model were used to analyze the breakthrough data. The calculated values of Yoon-Nelson constants were used to predict the breakthrough curves. A good comparison was observed between experimental data and the Yoon-Nelson model calculations.

An investigation was conducted to check if the adsorption of metal ions was carried out either by the surface of the fibroin or they were adsorbed deep inside its polymer network, and bulk was used. For this study, silk fibroin was transformed into thin films of three different thicknesses having same surface area. Batch experiments were conducted to study the thickness effect of fibroin films for the adsorption of metal ions. A constant amount of metal uptake for all three fibroin films showed that the adsorption was not a surface phenomenon, but the bulk body of the fibroin was used for this separation. Kinetic data was fitted to the modified pseudo-second-order model. The kinetic rate constant k_2 was not significantly affected by the film thickness which abrogated the possibility of simple diffusion mechanism for metal sorption into fibroin. Fibroin films loaded with metal ions were desorbed once dipped in deionized water. The desorption kinetics was again described by the modified pseudo-kinetic-model. The calculated values of desorption rate constant k_d were used to predict the kinetics of film

desorption. A good comparison was observed between the modified pseudo-second-order model calculations and experimental desorption data of fibroin films.

DEDICATION

I am dedicating my whole PhD work to all the innocent victims of suicide attacks who lost their lives during war against terrorism in Pakistan. Dedicating to the families who lost their love ones without knowing why and who killed them! I am also dedicating my work to all police and army officials who shed their blood to safeguard those innocent lives.

ACKNOWLEDGEMENTS

First and foremost, I thank Allah (swt) for endowing me with health, strength, patience and knowledge to complete my studies from the beginning till today.

I am heartily thankful to my supervisor Prof. Dr. Xianshe Feng. I acknowledge all his encouragement, valuable time and guidance given to me with deep gratitude and appreciation. It was never possible to accomplish this thesis without his continuous support, attention in detail and personal involvement in all the phases of this research which enables me to develop an understanding of the subject. I am indebted to him more than he knows.

My heartiest thanks is to my dear friend Prodip Kundu for his affection, support, keen interest and encouragement during the whole tenure of my research. He always gave me the encouragement whenever I got disappointed and helped me every time I got stuck during small tasks.

I also want to thank Higher Education Commission of Pakistan for providing me the funding for this project. I especially extend my gratitude to Mrs. Saima Naurin and Miss Madiha Aslam, for their support, great help and efforts they made to make this dream come true.

I have no words to thank my dad Dr. Altaf-ur-Rehman Barque and my mom Mrs. Salma Naheed, for their support and prayers for me. I was not able to complete my studies without their encouragement. Here, I also want to thank my wife Dr. Asma Rafique. Her understanding and great help made me able to achieve my target.

I would like to express my appreciation to my senior lab fellows Dr. G. Francisco and Dr. Jennifer who were always helpful to me by the day I have joined the lab.

I am always thankful for all the care, love and support given to me by all my colleagues and friends, Yiji Hu, Ying, YiYi, Dihuwa, JingJing Sun, Shahaab, and Charlie. They all made this five year time really memorable. I have best wishes for them for their bright future.

Finally, I want to thank my friends Abdual Whaab Tareen, Muhammad ShahJahan, Usman Awaisi, Ahmad Aslam, Ferwa Syed and Sunaina Somrro. The only

thing I have for them is my love. I wish, in their life, they not only achieve everything they have aspiration for, but something beyond it.

Table of Contents

List of Tables

List of Figures

NOMENCLATURE

A	Absorbance
a_e	Activity of adsorbate in solution at equilibrium, (mol/L)
b	Langmuir adsorption constant, (L/mol)
C	Final concentration of adsorbate in solution, (mol/L)
C_o	Initial concentration of adsorbate in solution, (mol/L) or (mg/g)
C_e	Equilibrium concentration of adsorbate in solution, (mol/L) or (mg/g)
C_b	Effluent concentration at breakthrough, (mol/L)
C_s	Concentration of standard reference solution, (mol/L)
C_m	Maximum equilibrium capacity in bed, (mol)
c	Boundary layer effect, (mol/g)
F	Effluent flow rate, (L/min)
ΔG	Gibbs free energy, (kJ/mol)
ΔH	Enthalpy change of adsorption, (kJ/mol)
I	Intensity of sample beam, (W/m^2)
I_o	Intensity of reference beam, (W/m^2)
I_e	Ionic strength of solute at adsorption equilibrium, (mol/L)
k_d	Kinetic rate constant for desorption, (g/mol.min)
K_f	Freundlich adsorption constant, ($L/mol^{1-\frac{1}{n}}.g$)
k_1	Pseudo-first-order rate constant, (min^{-1})
k_2	Pseudo-second-order rate constant, (g/mol.min)
k_i	Intraparticle diffusion rate constant, ($mol/g.min^{1/2}$) or ($mg/g.min^{1/2}$)
k_y	Adsorption rate constant for Yoon-Nelson model, (min^{-1})
k_a	Adsorption rate constant for Adams-Bohart model, (L/mol.min)
k_b	Adsorption rate constant for BDST model, (L/mol.min)
k_t	Adsorption rate constant for Thomas model, (L/mol.min)
k_f	Equilibrium adsorption constant, (L/mol)
m	Mass of adsorbent, (g)
N_o	Saturation concentration of effluent, (mol/L)
1/n	Heterogeneity factor

P	Debye-Huckel limiting law constant
θ_e	Fraction of surface of adsorbent covered at equilibrium
q_e	Metal uptake at adsorption equilibrium, (mol/g) or (mg/g)
q_m	Metal uptake at adsorption saturation, (mol/g)
q_t	Metal uptake at time t, (mol/g) or (mg/g)
q_o	Maximum solid phase concentration for Thomas model, (mol/g)
R	Universal gas constant, (J/mol.K)
S_c	Cross sectional area of adsorption column, (cm^2)
ΔS	Entropy change of adsorption, (kJ/mol.K)
T	Temperature, (K) or (^oC)
t	Time, (min)
t_b	Service time at breakthrough, (min)
u	Linear flow rate of effluent, (cm/min)
V	Volume of effluent solution in adsorption experiment, (L) or (ml)
Z	Bed height in adsorption column, (cm)
z	Charge (Number $\mid z_+z_-\mid$) carried by solute at adsorption equilibrium

GREEK SYMBOLS

β	Kinetic coefficient of external mass transfer, (L/min)
Υ_e	Activity coefficient at adsorption equilibrium
τ	Time to achieve 50% breakthrough in Yoon-Nelson model, (min)

ABBREVATIONS

BDST, Bed depth service time model

EDTA, Ethylenediaminetetraacetic acid

YN, Yoon-Nelson Model

CHAPTER 1

INTRODUCTION

The infrastructure of our civilization has been based on the predominant use of metals, and most of them are unstable in a habitable environment. As a result of corrosion, they are getting dispersed in our surroundings as a mobile product hazardous to life. We are penetrating a lot of hazardous metals by our technological processes in order to make our life more comfortable. The life cycle of metals begins in mining industries and ends with waste disposal in the earth crust [1].

Elements are pure chemical substances, if they are triggering some environmental pollution, it is a great challenge to destroy or annihilate them. Their quantity in our nearest surroundings, i.e., within the planet of the earth is constant. Geological, biological and social processes may change only their displacement, mobility and chemical activity of elements. These elements include metals. The concentration of heavy metals in the environment must be within certain limits, favorable for homeostatic of our organisms which are a part of our environment. The optimal concentration for each metal species is different for different biological species [2,3].

1.1 MOTIVATION AND OBJECTIVES

Protection of ground-water and marine water is a complex issue and a vital public concern. Once contaminated, it can be technically difficult and enormously expensive to clean up. One way to protect these waters from contamination is through the control of industrial discharges. Often though, control processes are not adequate in treating high flow rates or those with relatively low contaminant concentrations [4]. This proposal involves an adsorption process for removing heavy metals from industrial wastewater streams. The specific contaminating heavy metals addressed in this work are *lead*,

chromium, *copper* and *cobalt* removal, which have become a serious concern because of their toxicity to aquatic life. The proposed adsorption process has several advantages: naturally occurring biopolymer fibroin was used as an adsorbent, continuous adsorption-desorption cycles, and a high efficiency for the metal removal from effluent water stream [5].

Fibroin is a constituent of natural silk, spun by a silk worm *Bombyx Mori*. The silk consists of two major constituent fibroin and sericin. These two constituents are proteins that contain functional groups of amino acids, and they are widely used in different industries including cosmetic, pharmaceutical, textile and food. In the present study, the research focus is on fibroin one of the two constituents, though both proteins have similar characteristics in certain aspects. The basic difference in these two natural compounds is their hydrophobic and hydrophilic properties. Fibroin is less hydrophilic than sericin. The hydrophobic property and the presence of amino acids as functional groups make it a suitable material for the removal of heavy metals from effluent stream of water. Fibroin will be shown to be effective for the removal of heavy metals. This work also represents a new contribution to the environmental sciences and technology because to our knowledge, fibroin has not been used for such applications [6,7].

In present research, four representative heavy metals, Lead, Chromium, Copper and Cobalt, have been used for separation from effluent water stream. These metals are major pollutants to the ground water. The kinetics and equilibrium study of metals adsorption on fibroin was carried out, and the information generated would prove fibroin as a potential adsorbent for practical applications. Fibroin was shown to be a biosorbent, which could be regenerated by ethylenediaminetetraacetic acid (EDTA). As a biopolymer, fibroin does not involve any significant manufacturing cost or by-products harmful to the environment. It's a common trend that if we synthesize a polymer or sorbent for water cleaning purposes, there will be a lot of byproducts exerting indirect hazardous impacts on the environment. The execution, development and implementation (at later stages) of this naturally occurring biopolymer will be a green technology friendly to the environment. The major objectives of this research were:

- To investigate the degumming of silkworm cocoon to separate sericin from fibroin.

- To identify the mechanism involved in the removal of metal ions (i.e., lead, chromium, copper and cobalt) by fibroin, and also examine the adsorption kinetics and equilibrium models for these systems.
- To find out the feasibility of using fibroin for adsorption of the metal ions by taking thermodynamics and reusability of the adsorbent into account.
- In order to scale up the adsorption process, column study was conducted to determine the dynamic parameters related to breakthrough.
- To find out whether adsorption of metal ions on fibroin is a surface phenomenon or is characterized by the whole material as bulk.

1.2 THESIS OUTLINE

The first chapter was an introduction and background of heavy metals as pollutants and their impacts on the environment. The adsorbent to be used for the separation of these metal ions from waste water was also discussed.

The literature relevant to this research was reviewed in the second chapter. It involved a critical review of most biosorbents used for metal removal, adsorption models, experimental procedures and analytical techniques adopted by different researchers.

Instead of buying pure fibroin, silk worm *Bombyx Mori* cocoons were processed to remove sericin in order to get fibroin. The removal of sericin from cocoon was conducted, and the sericin removal kinetics was studied. This topic was addressed in chapter 3. The information collected will be useful for designing cocoon degumming processes.

Fibroin was tested for the adsorption of metals, and the equilibrium and kinetics of the adsorption was investigated. Regeneration of fibrin was also carried out by using ethylenediaminetetraacetic acid, and the kinetic data of the metal desorption from fibroin was modeled. This part of the thesis work was presented in chapter 4.

Once it was found that fibroin worked well for the adsorption of metal ions and could also be regenerated for another cycle of adsorption, the work continued with dynamic column adsorption. Breakthrough curves were determined experimentally and the breakthrough data were fitted to empirical models. A cyclic process consisting of

adsorption, regeneration (desorption) was carried out continuously, and this was presented in chapter 5.

Fibroin is a fibrous material, having a large surface area but difficult to determine. Fibroin films were developed after tremendous effort, and fibroin films of different thicknesses were used to investigate whether the sorption of metal ions occurred on surface or in bulk. The equilibrium and kinetic data were compared to those obtained with fibroin fibers. These were presented in chapter 6.

The conclusions drawn from this study and the prospects of using fibroin for metal removal from water were discussed in chapter 7.

CHAPTER 2

BIOSORPTION OF HEAVY METALS: A LITERATURE REVIEW

2.1 HEAVY METALS AND THEIR IMPACT AS POLLUTANT

The term "heavy metal" denotes any metallic element that has a relatively high density and is toxic or poisonous even at low concentrations [8]. "Heavy metal" is a general collective term, which generally applies to a group of metals and metalloids with an atomic density greater than 4g/cm^3 [9]. However, chemical properties of heavy metal are more important than its density. Examples of heavy metals are lead (Pb), cadmium (Cd), zinc (Zn), mercury (Hg), arsenic (As), silver (Ag), chromium (Cr), copper (Cu), iron (Fe), and the platinum group elements. Any substance in the environment, which causes intolerable effects, impairing the welfare of the environment, reducing the quality of life and may eventually cause death, is a pollutant. Hence, environmental pollution is the presence of a pollutant in the environment (e.g., air, water and soil) which may be poisonous or toxic and will be harmful to living things in the environment.

2.1.1 OCCURRENCE AND RECOVERY OF HEAVY METALS

Heavy metals occur as natural constituents of the earth crust, and are persistent environmental contaminants since they cannot be degraded or destroyed. In a very small amount, they enter the body system through food, air, and water and accumulate in the body over a period of time [4,10]. They exist in their ores in the rocks in different chemical forms, from which they are recovered as minerals. Heavy metal ores include sulphides (such as iron, arsenic, lead, lead-zinc, cobalt, gold, silver and nickel) and oxides (such as aluminium, manganese, gold, selenium and antimony). Some heavy metals have both

sulphide and oxide ores such as iron, copper and cobalt. Therefore, we will see sulphides of lead, cadmium, arsenic and mercury would be found naturally together with sulphides of iron (pyrite, FeS_2) and copper (chalcopyrite, $CuFeS_2$) as minors, which are the by-products of various hydrometallurgical processes or as part of exhaust fumes in pyrometallurgical and other downstream processes after mining. Some metals are left behind as stakeouts scattered in open and partially covered pits, during mining processes; some are transported through wind and flood, causing various hazards to the environment [11]. Heavy metals are basically extracted from their ores by mineral processing operations.

2.1.2 BIO-IMPORTANCE OF HEAVY METALS

Some heavy metals (like Fe, Zn, Ca and Mg) are of bio-importance to human being, and their daily medicinal and dietary allowances have been recommended. However, some others (like As, Cd, Pb, and methylated forms of Hg) have been found to have no known bio-importance in human biochemistry and physiology, and consumption even at very low concentrations can be toxic [5]. Even for the essential heavy metals for human body, intakes in diet have to be maintained at certain limits, as excess intake will result in poisoning or toxicity, which is evident by certain known medical symptoms that can be diagnosed clinically. Zinc is a ‘masculine’ element that balances copper in the male body, and is essential for the reproductive system. It is an important co-factor for dehydrogenating enzymes and in carbonic anhydrase. Zinc deficiency may lead to anaemia and retardation of growth and development [12]. Calcium is a very essential element in human metabolism for the production of strong bones and teeth. Its tolerance limit is relatively high as compared to other bio useful metals, that is, at 50mg/l of drinking water. The daily dietary requirement of calcium rises at the highest across both sexes and all ages of humans, and high doses of calcium can be well-tolerated in the body because of the regulating hormones that are thyrocalcitonin and parathormone. Magnesium is an important electrolytic constituent of the blood. It is present in the blood plasma and body fluids, interstitial and cell fluids. Its daily dietary requirement varies and increases from infants to adults and from males to females. The highest daily requirement of magnesium is for pregnant and lactating women [9,13]. Arsenic has been reported to be

an essential nutritional trace element but its function in the human biological system is still unclear. Silver is a trace element which is toxic even in very low concentration in drinking water and any level of concentration of silver in drinking water has been banned, both by the World Health Organization (WHO) and National Agency for Food and Drugs Administration and Control (NAFDAC). Lead, cadmium and mercury have been reported not to have any known function in human biochemistry or physiology, and are not found naturally in living organisms [8,14]. Therefore, intake of even very low concentrations of these metals in diet is very harmful for them.

2.1.3 TOXICITY OF HEAVY METALS

The biotoxic effects of heavy metals refer to the harmful effects of heavy metals to the body when they are consumed above the bio-recommended limits. All heavy metals have specific toxicity signs, but some signs common to cadmium, lead, arsenic, mercury, zinc, copper and aluminium poisoning include gastrointestinal disorders, stomatitis, tremor, hemoglobinuria, ataxia, paralysis, vomiting and convulsion, depression, and pneumonia when volatile vapours and fumes are inhaled [11]. The nature of effects could be acute, chronic or sub-chronic, depending upon the period of exposure and concentration. The elements can be neurotoxic, carcinogenic, mutagenic or teratogenic. Cadmium is toxic at even very low concentrations. In humans, exposure for long time results in renal dysfunction, characterized by tubular proteinuria. High exposure can lead to obstructive lung disease, cadmium pneumonitis, caused by inhalation of dusts and fumes. The features of the poisoning are chest pain, cough with foamy and bloody sputum, and death of the lining of the lung tissues because of excessive accumulation of watery fluids. Cadmium can also lead to bone defects, viz; osteomalacia, osteoporosis and spontaneous fractures, increased blood pressure and myocardic dysfunctions. The symptoms include nausea, vomiting, abdominal cramps, dyspnea and muscular weakness and these symptoms depend upon severity of exposure. Severe exposure may lead to pulmonary odema and death. Pulmonary effects (emphysema, bronchiolitis and alveolitis) and renal effects may be due to subchronic inhalational exposure to cadmium and its compounds [15]. Lead is the most significant toxic heavy metal, and the inorganic forms are absorbed through ingestion from food and

water, and inhalation from air polluted with lead compounds. Lead has teratogenic effect which is very serious. Lead poisoning also causes inhibition of the production of hemoglobin, abnormalities in kidney functions, damages joints and causes dysfunction in reproductive and cardiovascular system and lead to acute and chronic damage to the central and peripheral nervous system. It also has a severe effect on gastrointestinal tract and damages urinary tract resulting in hematuria (bloody urine). Regarding nervous system, it can cause severe and permanent brain damage.

Organic form of lead predominantly affects central nervous system as compared to inorganic form that affects gastrointestinal system and other biological systems. Lead can cause poor development of grey matter of brain in children thus resulting in poor intelligent quotient. Ca and Zn deficiencies increase its absorption in body. Acute and chronic toxic effects of lead lead to psychosis. The effect of zinc poisoning is the same as that of lead and so Zn poisoning can be diagnosed wrongly as lead poisoning [16]. Zinc, when taken orally, is considered to be relatively non toxic. However, when taken in excess amount, it can cause systemic dysfunctions that result in impairment of growth and reproduction. The clinical signs of zinc toxicosis are vomiting, diarrhea, hematuria (bloody urine), icterus (yellow mucus membrane), liver failure, kidney failure and anemia. Mercury is a toxic metal and has no known function in human biochemistry and physiology. Spontaneous abortion, congenital malformation and gastrointestinal disorders (like corrosive esophagitis and hematochezia) are the toxic effects of inorganic forms of mercury. Organic forms of mercury, which include monomethyl and dimenthylmecury presents clinically with erethism (an abnormal irritation or sensitivity of an organ or body part to stimulation), acrodynia (Pink disease, which is characterized by rash and desquamation of the hands and feet), gingivitis, stomatitis, neurological disorders, total damage to the brain and centeral nervous system and are also associated with congenital malformation [17]. Arsenic toxcicity symptoms also depend upon its chemical form. Arsenic causes protein coagulation, makes complexes with coenzymes and prevents the production of adenosine triphosphate during respiration (INECAR, 2000). It is possibly carcinogenic in compounds of all its oxidation states and high-level exposure can result in diseases causing death. Arsenic toxicity also presents as a disorder, which is clinically similar to, and often confused with Guillain-Barre syndrome, an anti-immune disorder

which occurs when the body's immune system is impaired and it attacks part of the peripheral nervous system, resulting in nerve inflammation leading to muscle weakness [4,18].

2.2 SOURCES OF HEAVY METAL CONTAMINATION

Heavy metal contamination exists in waste streams of many industries, for example metal plating facilities, mining operations, and tanneries. The soil surrounding many military bases is also contaminated and poses a risk of metal contamination groundwater and surface water. The metals that are released from these activities include cadmium, chromium, lead, and mercury. Heavy metals are not biodegradable and excreted from the body and accumulate in living organisms, causing various diseases and disorders. Processes for treatment of metal contaminated waste streams include chemical precipitation, membrane filtration, ion exchange, carbon adsorption, and co-precipitation/adsorption [19,20].

2.2.1 REMOVEL OF HEAVY METALS FROM WATER

Purification of metal contaminated waste streams needs cost effective treatment. Natural materials that are available in large quantities, or certain waste products from industrial or agricultural operations, can be used for the removal of heavy metals as inexpensive sorbents [21]. After these materials have been expended, they can be disposed of without expensive regeneration because of their low cost. Cost is an important parameter for selecting sorbent materials. However, cost information is seldom reported, and the expense of individual sorbent varies depending on the degree of processing required and local availability [22]. In general, a sorbent can be assumed as ``low cost" if it has any of these characteristics; that it requires little processing, is abundant in nature, or is a by-product or waste material from another industry. Of course, improved sorption capacity may compensate the cost for additional processing [23]. A number of scattered researches have already been conducted on a wide variety of sorbents. Some of the reported low-cost sorbents are bark/tannin-rich materials, lignin, chitin/chitosan, dead biomass, seaweed/algae/alginate, xanthate, zeolite clay, fly ash, peat, bone gelatin beads,

leaf mould, moss, iron-oxide-coated sand, modified wool, modified cotton [24,25]. In the above adsorbents, some are natural and rest made from different chemical processes. Each of the adsorbent has its own advantages, chemical binding properties related to efficiency in the capture of heavy metals [26].

2.2.2 ADSORPTION A TECHNIQUE FOR SEPARATION OF HEAVY METALS

Adsorption can be defined as selective collection and concentration onto solid surfaces of particular types of molecules contained in a liquid or a gas [27]. This unit operation helps to selectively capture and remove gases or liquids of mixed systems, even at small concentrations, from gaseous or liquid streams using a wide variety of specific materials known as *adsorbents. Adsorbate* is the material which is adsorbed onto the adsorbent. Two mechanisms are normally involved in adsorbtion, chemical adsorption and physical adsorption. When gaseous or liquid molecules reach the surface of an adsorbent and remain there without any chemical reaction, it is ***physical*** *adsorption* or *physisorption.* The mechanism of physisorption may be due to intermolecular, electrostatic or van der Waals forces, or may depend on the physical configuration of the adsorbent, for example, the pore structure of the adsorbent. Physical adsorbents typically have large surface areas [28]. The quality of adsorbent is determined by the properties of the material being adsorbed (molecular size, boiling point, molecular weight, and polarity) and the properties of the surface of the adsorbent (polarity, pore size, and spacing) [29]. In order to improve physical adsorption, the following parameters can be considered; increase the adsorbate concentration, increase the adsorbate area, select the best absorbent for the specific system, remove some contaminants before adsorption, reduce the adsorption temperature, increase the adsorption contact time, frequently replace or regenerate the adsorbent [30]. When molecules of a gas or liquid adhere to the surface of the adsorbent by means of a chemical reaction and the formation of chemical bonds, it is called ***chemical*** *adsorption* or *chemisorption*. With chemisorption, regeneration is often difficult or impossible. Chemisorption usually requires high temperature which provides the activation energy to break chemical bonds [31].

2.3 THE EQUILIBRIUM AND KINETIC MODELS

Adsorption equilibrium studies are important to determine the efficacy of adsorption. In addition to this, it is also necessary to identify the adsorption mechanism. Kinetic models can be exploited to investigate the mechanism of biosorption and its potential rate-controlling steps that may include mass transport and chemical reaction processes. In addition, to select the optimum condition for full-scale removal processes, information on the kinetics of metal uptake is required. Adsorption kinetics is expressed as the solute removal rate. In practice, kinetic studies were carried out in batch systems by using various initial sorbate concentrations, sorbent doses, particle sizes, agitation speeds, pH values and temperatures along with different sorbent and sorbate types. Then data regression was used to determine the best-fitting kinetic rate equation. The linear least-square method can also be applied to the linearly transformed kinetic rate equations for fitting the experimental data to determine the rate constant [32]. To understand the adsorption kinetics and rate-limiting step, several kinetic models have been proposed in the literature. Examples include pseudo-first and pseudo-second order rate models, Weber and Morris sorption kinetic model, Adam–Bohart–Thomas relation, first-order reversible reaction model, external mass transfer model, first-order equation of Bhattacharya and Venkobachar Elovich's model and Ritchie's equation [33]. The pseudo-first and second-order kinetic models are the most appreciated models to study the biosorption kinetics of heavy metals and quantify the extent of uptake in biosorption kinetics [34].

2.3.1 MODELS FOR KINETIC STUDY OF ADSORPTION

Sorption is not a single step process. It involves the transport of the sorbate particles from aqueous phase to the surface of the solid adsorbent, followed by the diffusion of these solute particles into the interior of the adsorbent. The overall adsorption process may be controlled by one or more steps, such as film or external diffusion, pore diffusion, surface diffusion and adsorption on the pore surface, or the combination of more than one steps [35]. To understand the significance of diffusion mechanism, accurate estimates of the diffusivities of the sorbent particles must be determined using diffusion

controlled kinetic models based on the experimental data. Due to porosity of the certain adsorbent, the intraparticle diffusion is expected in the kinetics of adsorption process [36]. In order to reveal the mechanisms and the rate controlling steps, the kinetic data can be fitted to intraparticle diffusion model proposed by Weber and Morris in 1962 [37,38]. The intraparticle diffusion model is commonly expressed by the following equation:

$$q_t = k_i\sqrt{t} + c \qquad (2.1)$$

where c (mol/g) is a constant that gives information about the boundary layer effect and k_i (mol/g.min$^{1/2}$) is the intraparticle diffusion rate constant. If the intraparticle diffusion is involved in the adsorption process, then a plot of the uptake q_t versus square root of time will result in a straight line with an intercept c which reflects the boundary layer effect on adsorption. The larger the intercept, the greater would be the contribution of the surface sorption in the rate-controlling step. If the line passes through the origin then the intraparticle diffusion would be the only rate controlling step. The intraparticle rate constant k_i can be evaluated from the slope of the linear plot of q_t versus √t. If the kinetic data fitting to the intraparticle diffusion model exhibits multi-linear plots which do not pass through the origin, it is indicative of some degree of boundary layer control and this further shows that the intraparticle diffusion is not the only rate-controlling step, and other processes may also affect the rate of sorption significantly [39].

In previous studies, the intraparticle diffusion model has been applied in three different forms:

(1) q_t (the amount of adsorption at any time) is plotted against √t (the square root of time) to get a straight line that is forced to pass through the origin [40-42];

(2) Multi-linearity in q_t versus √t plot is considered (that is, two or three steps are involved to follow the whole adsorption process). In this form, the external surface adsorption or instantaneous adsorption occurs in the first step; the second step is the gradual adsorption step, where intraparticle diffusion is controlled; and the third step is the final equilibrium step, where the solute moves slowly from larger pores to micro pores causing a slow adsorption rate. The time required for the second step usually depends on the variations of the system (including solute concentration, temperature, and adsorbent particle size), which is difficult to be predicted or controlled [43-47];

(3) q_t is plotted against √t to obtain a straight line but does not necessarily pass through the origin; that is, there is a non-zero intercept. Almost all the intercepts reported in the literature are positive, indicating that rapid adsorption occurs within a short period of time. To our knowledge, this type of initial adsorption behavior has not been reported [48-53].

The kinetics experimental data can also be analyzed by using different kinetic models. The most commonly used ones are pseudo-first order equation and pseudo-second order equation, in order to determine whether adsorption is limited by chemical complexation or not. The original form of ***pseudo-first order*** reaction is [32,54,55]:

$$\frac{dq_t}{dt} = k_1 (q_e - q_t) \qquad (2.2)$$

and that of the ***pseudo-second order*** reaction is [56-58]:

$$\frac{dq_t}{dt} = k_2 (q_e - q_t)^2 \qquad (2.3)$$

where t is the time (min), q_t and q_e are the quantities of the metal on adsorbent at time t and at equilibrium, respectively ($mol.g^{-1}$), k_1 (min^{-1}) and k_2 ($g.mol^{-1}.min^{-1}$) the rate constants of the pseudo-first order and pseudo-second order adsorption respectively. To evaluate k_1, equation 2.2 can be rearranged as follows:

$$\ln(q_e - q_t) = \ln q_e - k_1 t \qquad (2.4)$$

Thus a plot of $\ln(q_e - q_t)$ vs t will be a straight line with a slope equal to $-k_1$ and an intercept gives the $\ln q_e$. However, if the intercept does not equal to the equilibrium uptake of metal ions, the adsorption is not likely to be first-order even if this plot has high correlation coefficient with the experimental data. For the pseudo-second order equation, equation 2.3 can be written as:

$$\frac{t}{q_t} = \frac{1}{k_2 q_e^2} + \frac{1}{q_e} t \qquad (2.5)$$

A plot of $\frac{t}{q_t}$ vs t will be a straight line with a slope $\frac{1}{q_e}$ and an intercept $\frac{1}{k_2 q_e^2}$. Hence we can obtain k_2 from the intercept and slope of the plot [59].

2.3.2 EQUILIBRIUM STUDIES OF ADSORPTION

Biosorption of heavy metal is defined as a passive non-metabolically mediated process of metal binding by biosorbent [60]. Agricultural waste and industrial by-products, bacteria, yeasts, fungi, and algae can function as biosorbents of heavy metals. Biosorption is considered to be a fast physical or chemical process, and its rate is governed by the type of the process. In other words, it can be defined as a general term for a number of passive accumulation processes which in any particular case may include ion exchange, coordination, complexation, chelation, adsorption and micro-precipitation [61]. Proper analysis and design of adsorption/biosorption separation processes require relevant adsorption/biosorption equilibria as one piece of the vital information. In equilibrium, there is a certain relationship between solute concentration in solution and adsorbed state (i.e., the amount of solute adsorbed per unit mass of adsorbent). Their sorption equilibrium is a function of temperature. Therefore, the adsorption equilibrium relationship at a given temperature is referred as adsorption isotherm. Several adsorption isotherms originally used for gas adsorption are available and are readily adopted to correlate the adsorption equilibria in heavy metals biosorption. Some important examples are Freundlich, Langmuir, Redlich–Paterson and Sips equation. The most commonly used among them are Freundlich and Langmuir equations. The application of these isotherms on biosorbent-assisted heavy metals removal from water and wastewater will be discussed later [31].

2.3.2.1 FREUNDLICH ISOTHERM

Freundlich isotherm[32,62] is an empirical equation. This equation is one of the most commonly used isotherms for the description of adsorption equilibrium. Freundlich isotherm is able to describe the adsorption of organic and inorganic compounds on a large variety of adsorbents. This equation is in the form of:

$$q_e = K_f C_e^{1/n} \qquad (2.6)$$

which can also be expressed in the linearized form:

$$\log q_e = \log K_f + \frac{1}{n}\log c_e \qquad (2.7)$$

The plot of $\log q_e$ versus $\log C_e$ has a slope equal to 1/n and an intercept of $\log K_f$. $\log K_f$ is equivalent to $\log q_e$ when C_e equals to unity [32]. When n ≠1, the K_f value depends on the units of q_e and C_e used. On average, a favorable adsorption tends to have Freundlich constant *n* between 1 and 10. A larger value of n (smaller value of 1/n) indicates stronger interaction between biosorbent and heavy metal while 1/n equal to 1 indicates linear adsorption leading to identical adsorption energies for all sites. Freundlich isotherm has the ability to fit many experimental adsorption–desorption data, and is especially excellent to fit in the data from highly heterogeneous sorbent systems. This isotherm can thus be used to represent the biosorption isotherm. However, in some cases the Freundlich isotherm is not suitable for biosorption.

2.3.2.2 LANGMUIR ISOTHERM

Another commonly used model for describing heavy metals sorption to biosorbent is the Langmuir model [63]. Langmuir equation describes the relationship of the coverage of molecules on a solid surface and concentration of a medium at a fixed temperature. This isotherm is based on three assumptions: (1) adsorption is limited to monolayer coverage, (2) all surface sites are alike and each site can only accommodate one adsorbed molecule, and (3) the ability of a molecule to be adsorbed on a given site is independent of its neighboring sites occupancy [34]. At adsorption equilibrium, the rates of adsorption and desorption from the surface are equal. The Langmuir equation can be written as:

$$q_e = q_m \frac{bc_e}{1+bc_e} \qquad (2.8)$$

which can also be written in different linear forms:

$$\frac{c_e}{q_e} = \frac{1}{q_m} c_e + \frac{1}{b q_m} \quad (2.9)$$

$$q_e = q_m - \left(\frac{1}{b}\right) \frac{q_e}{c_e} \quad (2.10)$$

$$\frac{q_e}{c_e} = b q_m - b q_e \quad (2.11)$$

In biosorption, the saturation limit of various biomass is affected by several factors such as the number of sites in the biosorbent material, the accessibility of the sites, the chemical state of the sites (i.e., availability) and the affinity between the site and the metal (i.e., binding strength). In covalent metal binding case, supposing that an occupied site is theoretically available, the extent to which the site is to be dwelled upon by a given metal depends further on the binding strength and concentration of that metal in opposition to the metals already occupying that site.

A decrease in b value with temperature signifies exothermicity of the adsorption process (physical adsorption), while the opposite trend indicates that the process needs thermal energy (endothermic), which is often relevant to chemisorption. In physical adsorption, the bonding between heavy metals and active sites of the biosorbent gets weaker at higher temperatures in contrast with chemisorption bonding which becomes stronger. The exothermicity or endothermicity of the biosorption is determined by heat of adsorption. This thermodynamic property is commonly obtained using Van't Hoff equation, which relates the equilibrium adsorption constant to the temperature [51,64,65].

2.4 BIOMATERIALS AS NATURAL ADSORBENT

Many microorganisms have been shown to be capable of concentrating heavy metals from their aqueous environment, and the term biosorption is used to describe for such passive, non-metabolically mediated process of metal binding by living or dead biomass [65]. At present, different biomaterials are being used as adsorbents for heavy metals. Distinctive adsorption equilibria and kinetic models are extensively used in explaining the biosorption of heavy metals. In general, up till now, most studies on the biosorption of heavy metal ions by different biosorbent types have been directed toward the uptake of single metal in preference to multicomponent systems. In particular, the

Langmuir and Freundlich models are the most common isotherms for correlating biosorption experimental data, though other isotherms, which were initially established for gas phase applications, can also be extended onto biosorption systems. Abundant of research has been done for the separation of heavy metals, and the topics addressing specifically this separation by using a natural adsorbent are being cited and discussed here.

Ucun et al.[66] investigated the biosorption properties of copper(II) and zinc(II) on a cone biomass of *Pinus sylvestris* by using batch techniques. They carried out this biosorption studies with single metal solutions. The removal of copper(II) and zinc(II) from aqueous solutions increases with pH and sharply decreases when pH of the solution was decreased. The biosorption capacity is greatly affected by pH. It was concluded that the adsorption is favored by an increase in pH. The maximum biosorption capacity of *P. sylvestris* for Cu(II) was 26mg/g and for Zn(II) it was 16mg/g at C_o=10mg/L. The biomass exhibited a high biosorption capacity in 1h at C_o=60mg/L and m=0.5g/L. The adsorption isotherms were used for a mathematical description of biosorption of metal ions onto cone biomass. It was found that the adsorption equilibrium data fitted well to the adsorption models. In their research, the Freundlich and Langmuir model could describe the adsorption equilibrium of these metals on cone biomass. The biosorption constants were found from the Freundlich and Langmuir isotherms at 25°C. It is found that the biosorption data of metals on cone biomass fitted in both the Freundlich and Langmuir adsorption models. The results of their study indicate the possibilities of cleaning the environment with the use of natural resources.

Sarı and Tuzen[67] focused on the biosorption of As(III) and As(V) ions onto *Inonotus hispidus* biomass from aqueous solutions. They found the biosorption capacity of *I. hispidus* biomass 51.9mg/g and 59.6mg/g for As(III) and As(V), respectively at optimum conditions of pH6 for As(III) and pH2 for As(V). The metal ions were desorbed from *I. Hispidus* using 1M HCl and 1M HNO_3. The high stability of *I. hispidus* permitted 10 times of adsorption–elution process along the studies with a decrease of about 11–28% in recovery of As(III) and 10–25% for As(V). The kinetic data signified that the biosorption of As(III) and As(V) ions onto *I. hispidus* followed the pseudo-second-order kinetic model well. The thermodynamic calculations showed the feasibility, exothermic

and spontaneous nature of the biosorption of As(III) and As(V) ion onto *I. hispidus* biomass. It was concluded that *I. hispidus* is a good adsorbent for As(III) and As(V) removal from aqueous solution. Furthermore, it can be considered to be a promising biosorbent for the treatment of wastewater containing As(III) and As(V) ions, because *I. hispidus* is a low-cost biomass with a considerably high biosorption capacity.

Batch experiments were conducted by Li et al.[68] to study the copper(II) removal by formaldehyde inactivated *Cladosporium cladosporioides*, *Gliomastix murorum* and *Bjerkandera* sp., at conditions of agitated speed of 150rpm, temperature of 25^{o}C, biosorbent dose of 2g.L^{-1} and contact time of 12h. For each biomass, they found that the optimum pH was 6.0 and the equilibrium contact time was about 2h. Without acid or alkali treatment for improving adsorption properties, the experimental maximum copper(II) biosorptions were relatively high: 7.74mg.g^{-1} for *C. cladosporioides*, 9.01mg.g^{-1} for *G. murorum*, and 12.08mg.g^{-1} for *Bjerkandera* sp.. The biosorption data of all the dead fungal biomasses were quite fitted to Langmuir isotherm model and pseudo second-order kinetic model; first-order Lagergren kinetic model gave good adjustment to the data of *Bjerkandera* sp. but did not fit into the data of *C. cladosporioides* and *G. murorum* very well. In their work, they derived the pH, contact time and initial copper(II) concentration influencing the copper(II) biosorption process of dead *Bjerkandera* sp., *G. murorum* and *C. cladosporioides* biomasses. These fungal biomasses have relatively high capacity for the removal of copper(II) from aqueous solutions.

Zhu et al.[69] used Peanut hull, which is an agricultural by-product that is abundantly available, as adsorbent for the removal of Cu(II) from aqueous solutions. The extent of adsorption was investigated as a function of pH, contact time, adsorbate concentration and temperature. They found out that the Cu(II) removal is pH-dependent, reaching to a maximum at pH5.5. The biosorption process followed pseudo-second-order kinetics, and equilibrium was attained in 2h. The rate constant increased with an increase in the temperature, an indication of endothermic biosorption. The activation energy of Cu(II) biosorption was determined to be 17.02kJ/mol based on the Arrhenius equation, which shows that biosorption may be an activated chemical biosorption. They analyzed the equilibrium data using the Langmuir, Freundlich, and Dubinin-Radushkevich (D-R)

isotherm models. The equilibrium biosorption capacity of Cu(II) determined from the Langmuir equation was 21.25mg.g^{-1} at 30°C. The mean free energy *E* (kJ/mol) from the D-R isotherm also indicated a chemical ion-exchange mechanism. The thermodynamic parameters such as changes in Gibbs free energy (ΔG^o), enthalpy (ΔH^o) and entropy (ΔS^o) were used to predict the nature of the biosorption process. The negative ΔG^o values at various temperatures confirmed that the biosorption processes are spontaneous.

The work of Zhu et al.[69] indicates that peanut hull can be used as an effective adsorbent for the treatment of Cu-bearing aqueous waste stream. Adsorption data indicates the applicability of pseudo-second-order kinetics. The activation energy and mean free energy calculated from the Arrhenius equation and D-R isotherm respectively; confirm the chemical biosorption mechanism. Compared to various other sorbents reported in the literature, the peanut hull in this study showed a good promise for practical applicability due to easy availability of the material and easy recovery of metal entrapped by combustion method.

Table 2.1 summarizes some of literature work on the adsorption equilibrium data for numerous biosorbents that followed the Langmuir model.

Table 2.1 Analytical results of equilibrium data reported in literature.

Adsorbate	**Concentration (mg.L^{-1})**	**Adsorbent**	**Fitted Model**	**Reference**
Cd(II)	100 – 1250	*Dates' Pedicels*	Langmuir Model	Yazid et al. 2011 [65]
As(III) & As(V)	10-500	Macrofungus (*Inonotus hispidus*)	Langmuir Model	Sarı and Tuzen 2009 [67]
Cu(II)	5-300	*Cladosporium cladosporioides*	Langmuir Model	Li et al. 2009 [68]
Cu(II)	30	*Peanut hull*	Langmuir Model	Zhu et al. 2009 [69]
Pb(II)	10-1000	*Ficus Religiosa leaves*	Langmuir Model	Qaiser at al. 2009 [70]
Pb(II) & Cd(II)	10-400	*Macrofungus (Amanita Rubescens)*	Langmuir Model	Sarı and Tuzen 2009 [71]

Qaiser et al.[70] investigated the biosorption of lead by *Ficus religiosa* leaves in powder and immobilized form. They conducted batch experiments to determine the biosorption capacity, equilibrium time, effect of pH and temperature. They found that the maximum biosorption capacity of lead was 37.45mg.g^{-1} at pH4.0. The temperature change in the range of 20–40°C affected the biosorption capacity, and the maximum removal was observed at 25°C. In their research, the thermodynamic parameters were determined from the experimental data. They also used the Langmuir and Freundlich models to describe the equilibrium data. The Langmuir model fitted the data better with a correlation coefficient of 0.97. The kinetics of biosorption followed pseudo-second order model. For continuous biosorption experiments, the FRLs biomass was immobilized in a polysulfone matrix. Breakthrough curves were analyzed at different flow rates, pH and bed depth. Bed depth service time (BDST) and the Thomas models were used to explain the experimental data. A solution of 0.05M HNO_3 did well to elute lead from biomass. The release of Ca, Mg and Na ions during lead biosorption revealed that ion exchange was the major removal mechanism.

Sarı and Tuzen[71] also studied the biosorption characteristics of Pb(II) and Cd(II) ions from aqueous solutions using macrofungus (*Amanita rubescens*) biomass as a function of pH, biomass dosage, contact time, and temperature. They applied Langmuir, Freundlich and Dubinin–Radushkevich models to explain the biosorption isotherm of the metal ions. The Langmuir model fitted in the equilibrium data better than the Freundlich isotherm. The maximum biosorption capacity of *A. rubescens* for Pb(II) and Cd(II) was determined to be 38.4 and 27.3mg.g^{-1}, respectively, at pH5.0, contact time of 30min, biomass dosage of 4g.L^{-1}, and temperature of 20°C. The metal ions were desorbed from *A. Rubescens* using 1M HCl and 1M HNO_3. The recovery for both metal ions was found to be higher than 90%. The high stability of *A. rubescens* permitted ten times of adsorption–elution process along the studies with a decrease of about 10% in recovery of both metal ions. They calculated the mean free energy values evaluated from the D–R model, indicating that the biosorption of Pb(II) and Cd(II) onto *A. rubescens* biomass took place by chemical ion-exchange. The calculated thermodynamic parameters (ΔG°, ΔH° and ΔS°) showed that the biosorption of Pb(II) and Cd(II) ions onto *A. rubescens* biomass was feasible, spontaneous and exothermic under examined conditions. Their

experimental data was also tested in terms of biosorption kinetics using pseudo-first-order and pseudo-second-order kinetic models. The results showed that the biosorption of both Pb(II) and Cd(II) followed the pseudo-second-order kinetics. Since *A. rubescens* is a low-cost biomass with a considerably high biosorption capacity, it is a potential biosorbent for the treatment of wastewater containing Pb(II) and Cd(II) ions.

Blazquez et al.[72] used pine cone shell (PCS) as biosorbent for the removal of Cu(II) from aqueous solutions. The biosorbent was characterized by potentiometric titrations, pore size distribution, surface area, and elemental analysis and FTIR analyses. Batch adsorption experiments were performed as a function of biosorbent dosage, particle size, solution pH, contact time, and initial metal ion concentration. Experimental data was fitted to equilibrium and kinetic models to evaluate models constants. Equilibrium data fitted well with Langmuir isotherm model. The maximum biosorption capacity of PCS for Cu(II) at pH5.0 and temperature 25^{o}C was determined to be 6.81mg.g^{-1}. Pseudo-second-order model fitted well to the kinetic data with a correlation coefficient greater than 0.99. In the same study, dynamic biosorption was also accomplished by using a packed-bed column and the key column parameters were determined. Pine cone shell was shown to be a potential biosorbent for Cu(II) removal from aqueous solutions.

Nauclea diderrichii seed biomass was investigated for the adsorption of Cd(II) and Hg(II) at National Center for Nano Science and Technology Beijing, China by Omorogie et al.[73]. The gathered experimental data were fitted into kinetic and thermodynamic models. For the kinetics of adsorption, the data were fitted best into pseudo-second order kinetic model among others. Their results showed that the uptake of Cd(II) onto Nauclea diderrichii seed biosorbent surface was faster than Hg(II) but the reason was not justified in discussion. Moreover, the experimental results revealed that the biosorption of Cd(II) and Hg(II) was endothermic. The highest temperature applied to the adsorption in the study was 333K at which the maximum metal uptake q_e for Cd(II) and Hg(II) was 6.30 and 6.15mg.g^{-1}, respectively. The highest initial biosorption rates for Cd(II) and Hg(II) were 56.19 and 4.39mg.g^{-1}.min^{-1}, respectively. For the calculation of thermodynamic parameters, Erying equation was applied to the equilibrium data.

Singha and Das[74] carried out a biosorption research involving six different biosorbents, namely rice straw, rice bran, rice husk, coconut shell, neem leaves, and

hyacinth roots for the removal of Pb(II) from aqueous solutions. Experiments were carried out as a batch process and different kinetic models were applied to the adsorption data to investigate the nature of adsorption for Pb(II) on each biosorbent. The adsorption kinetic data was best represented by pseudo-second order adsorption model for all the adsorbents except for rice husk which was described by intraparticle diffusion model. The adsorption of Pb(II) onto rice bran, hyacinth roots, and rice straw were governed predominately by film diffusion, but the adsorption on rice husk was controlled by intraparticle diffusion. The adsorption onto coconut shell and neem leaves was governed by film diffusion and intraparticle diffusion equally. The numerical values of mass transfer coefficients indicated that the adsorption rate from liquid to solid phase was fairly fast for each biosorbent. The thermodynamic study showed that the adsorption was endothermic in nature for all the adsorbents. Dubinin-Radushkevich isotherm fitted well to the equilibrium data and was evident of chemical adsorption for all biosorbents studied in this work.

2.5 FIBROIN AS AN ADSORBENT

Silk is increasingly being exploited for biomedical purposes. In recent years, it has been studied for applications in the emerging field of tissue engineering, particularly in the areas of oxygen and water vapour permeation, biocompatibility and biodegradability. Silk thread from *Bombyx mori* has a fibrous core of fibroin, the structural protein responsible for biocompatibility and bioactivity, surrounded by a family of ‘‘gummy’’ proteins, called sericin, which can be removed during the degumming process [75,76].

Sericin is a more hydrophilic protein, whose primary structure is rich in polar residues, but some of its fractions are not completely water soluble due to β-sheet portions [77]. Sericin can be classified into three fractions, depending on their solubility in water as sericin A, sericin B and sericin C. Sericin A is the outermost layer and it contains about 17.2% of nitrogen and amino acids like sericin, threonine, glycine, and aspartic acid. Sericin B is the middle layer containing 16.8% of nitrogen. Sericin C is the innermost layer, which is adjacent to fibroin filament, and it contains sulphur and 16.6% of nitrogen [78].

Silk fibroin is a kind of polypeptide with functional amino acids in its structure. The electric charges in its molecular chains originating from the dissociation of acidic groups provide vast potentials for the retention of specific metal species [79]. Fibroin is a glycoprotein composed of two equimolar protein subunits of 25 and 370 kDa covalently linked by disulphide bonds. Fibroin filament has a crystalline and an amorphous domain. The amorphous domain is characterized by the presence of amino acids with bulkier side chains, whereas the crystalline domain is characterized by high percentage of alanine, glycine, and serine (12, 30, 44% respectively) [80-83], which contain short side chains to permit close packing densities for overlaying sheets. The β-sheet form and crystalline form have been reported for silk fibroin, having a molecular mass of 350-415K, whereas anti-parallel β-sheet structure, forming microfibrils, is responsible for the crystalline nature of the silk fiber. The microfibrils are organized into fibril bundles, with several bundles leading finally to a single silk thread. Based on the literature information about the presence of amino group in fibroin structure, it can be a good adsorbent for heavy metals [84,85].

Chen et al.[86] carried out a study for the adsorption of Cu^{2+} using fibroin as an adsorbent. They investigated the selective retention of Cu^{2+} with silk fibroin at pH6.0, and a novel on-line procedure for separation/ pre-concentration of Cu^{2+} from complex sample matrices was developed. An on-line solid-phase extraction procedure for pre-concentration of Cu^{2+} by exploiting silk fibroin as the sorbent was developed. The silk fibroin provides abundant functional groups for retaining metal species of interest and the retained metal ions could readily be desorbed by employing a suitable stripping reagent. In addition to this, the silk fibroin entails a distinct advantage over the conventional adsorbents because it is an environmental-friendly material which can be easily obtained and recycled after use, facilitating rapid biodegradation. This material, thus, shows vast potentials as a bio-compatible material for sample pretreatment.

2.6 FIBROIN FILMS

The separation studies involve adsorption of different heavy metals on fibroin, but due to its fibrous nature, it is unclear whether metal sorption occurs on surface or in the bulk. To clarify this, fibroin could be converted into solid films and then the metal

adsorption behavior can be observed to determine whether it is a bulk property or surface phenomenon.

Fibroin can be converted into films, and the procedure may involve several steps (i) conversion of fibroin threads into solution form by adding certain salts to break hydrogen bonding, (ii) removal of salts from the solution using dialysis, (iii) casting fibroin films from the fibroin solution [87-89].

Sah and Pramanilk[90] carried out a study aiming at the preparation of silk fibroin solution for possible applications in tissue engineering. They used *Bombyx mori* silkworm cocoon to extract fibroin protein by degumming in aqueous Na_2CO_3 solution. Then they dissolved the fibroin into LiBr aqueous solutions. The fibroin protein solution was purified and studied for the protein content. In this study, the degumming of cocoon and its solubility were significantly dependent on the salt concentration, treatment temperature, and time. A concentration of 0.02M Na_2CO_3, temperature of 80°C and time more than 40min were found to be favorable degumming conditions. The proper conditions for the dissolution of fibroin into aqueous solutions were found to be 9.3M LiBr, 70°C temperature, and 6h dissolving time. It was shown that there was no glue like sericin over the fibroin surface at the above degumming conditions. The fibroin protein content of the solution was measured by Bradford protein assay. The regenerated silk fibroin can be used for fabrication of porous fibroin scaffolds for various tissue engineering applications.

2.7 COLUMN STUDY

Biosorption process can be performed under a batch or continuous mode, and a continuous adsorption process is often preferred for the separation of heavy metals in practical applications. The same adsorption column can be utilized for adsorption and desorption cycle studies.

Mukhopadhyay et al.[91] used Aspergillus niger biomass for the dynamic adsorption of copper, and the continuous adsorption column data were fitted to fixed bed model and reduced lumped diffusion model successfully. By varying the bed heights and flow rates of effluent, the experimental adsorption rate and the breakthrough curves were fitted to the models. In the initial adsorption period the solute removal was fast, but with

the passage of time the bed got saturated and the removal rate gradually decreased. This was due to the decrease in driving force of adsorption. The breakthrough data was evaluated using fixed bed model and reduced lumped diffusion model, which had a good agreement with the experimental data. It was observed that both models could predict column dynamics accurately at high flow rates.

Chitosan and its derivatives have been employed as a sorbent by many researchers for the removal of heavy metals. Most of the work has been carried out in batch mode in order to investigate kinetics, equilibrium and thermodynamics of the adsorption process [92].

Kavianinia et al.[93] synthesized a chitosan-based bioadsorbent. They improved the thermal stability of chitosan matrix by the use of pyromellitic dianhydride (PMDA) for hydrogel crosslinking, and employed it for the removal of Cu(II) from aqueous solutions in a fixed bed column. The effects of bed height, influent Cu(II) concentration, and flow rate on the dynamic adsorption were studied. It was shown that the lower a flow rate, a lower effluent concentration and a higher bed height led to an extended breakthrough and exhaustion time. The dynamic adsorption data were analyzed using Adams–Bohart, the Thomas, and the Yoon–Nelson models. Regeneration of the chitosan–PMDA was also conducted using 0.1mol.L^{-1} HCl. The uptake was reduced to 93.5% in the second cycle and the time to achieve breakthrough was reduced from 400 to 250min.

Vilar et al.[94] investigated marine algae gelidium and algal composite material for continuous removal of Cu(II) from aqueous solutions in a packed bed column. The effects of solution pH, influent concentration, and temperature were investigated. The metal uptake capacity was slightly affected by the temperature. At a given influent flow rate, the breakthrough time was decreased as the inlet copper concentration increased. An increase in ionic strength of influent solution caused a reduction in the sorption capacity of the biosorbents, which was responsible for the decrease in breakthrough time. The biosorption behavior was studied during one sorption–desorption cycle of Cu(II) in the column fed with 50 and 25mg.L^{-1} of Cu(II) in aqueous solutions, at pH5.3, leading to a maximum uptake capacity of 13 and 3mg.g^{-1}, respectively, for algae gelidium and composite material. A 100% desorption was obtained by using 0.1M HNO_3 solution as a

desorbent, and no change was observed on the uptake capacity of the composite material after two consecutive sorption–desorption cycles. For the simulation of copper adsorption in packed bed column, the mass transfer model was derived by considering film and intraparticle resistances and the equilibrium based on the Langmuir equation (adsorption) or by the mass action law (desorption) [95].

Rao et al.[96] used *Syzygium cumini* leaf powder as a biosorbent in a fixed bed mini column. They reported the effects of flow rate, initial Cd(II) concentration and bed height as experimental parameters to obtain breakthrough curves. The maximum uptake of Cd(II) in the adsorption column was 29.08mg.g^{-1} at pH5.5, initial Cd(II) concentration 100mg.L^{-1}, bed height 5cm and flow rate 40ml.min^{-1}. Bohart–Adams, BDST, Thomas and Yoon–Nelson models were applied to the data for predicting breakthrough curves and to determine the characteristic parameters. The characteristic parameters of the respective models such as service time (Hutchins BDST model), adsorption capacity (Thomas model) and time required for 50% breakthrough (Yoon–Nelson model) were determined. The utilization of the column adsorption data for design of a commercial column were discussed in their study. HCl was used as a desorbent. A desorption of 98% of Cd(II) using 0.05N HCl solution was made obtained.

Zhang et al.[97] used carboxymethyl straw to eliminate methylene blue (MB) in a fixed-bed column. The straw based adsorbent showed a high MB uptake in the column. Various models such as Thomas, Clark, Adams–Bohart, Yoon–Nelson, Wolborska, and BDST models were employed to fit the experimental data. Among these, Thomas model was found to be the most suitable to describe the adsorption behavior, according to the monolayer chemical adsorption mechanism. The effects of initial solution pH, bed height, temperature, initial MB concentration and flow rate on the column adsorption were studied in details based on the Thomas model. It was found that these operating conditions can greatly affect the breakthrough curves, while temperature has little influence on the MB adsorption of the modified straw.

2.7.1 MODELING OF ADSORPTION COLUMN DATA

For a continuous process, a fixed-bed adsorber is usually used. The effectiveness of a biomass can be evaluated from the breakthrough curve of the effluent concentration

(or the concentration–time profile). A typical S-shaped breakthrough curve is usually observed [98]. In order to predict the breakthrough curve of an adsorption process in a fixed bed, the Bohart–Adams, Thomas and Yoon-Nelson models have been often used. Moreover, the required bed height is an important parameter in designing an adsorption column. This can be determined from the breakthrough curve and the bed-depth service-time (BDST) model. In the present study, the effectiveness of fibroin as a biosorbent will be evaluated. The adsorption capacity of fibroin in a continuous fixed-bed column will also be determined. For a proper design of an adsorption column, an accurate prediction of the breakthrough curve is needed. Therefore, the experimental results obtained from the continuous system will be fitted to the above mentioned models for adsorption [99].

Most of the earlier investigations on heavy metal biosorption were restricted to batch equilibrium studies. The sorption capacity of biosorbents obtained from batch equilibrium experiments is useful in providing fundamental information about the effectiveness of metal-biosorbents system. However, this data may not be applicable to most of the treatment systems (such as column operations) where contact time is not sufficient for the attainment of equilibrium. Hence, there is a need to perform biosorption studies using adsorbent filled columns. Several investigators have identified packed column as the most effective arrangement for cyclic sorption-desorption[100,101] as it makes the best use of concentration difference known as a driving force for heavy metal sorption. Present laboratory-scale study would aim at investigating the effectiveness of fibroin for removal of toxic metal ions from aqueous environment.

The study will be conducted in a fixed bed column with parameters including influent concentration and flow rate. The breakthrough curves for the adsorption of metal ions will be analyzed by using bed depth service time (BDST) model, Thomas model and Yoon-Nelson model.

Among the available adsorber types for biosorption, packed bed columns offer several advantages, viz., simple to operate, high process yield, and easy scale-up. The use of batch process is economically not feasible for small and medium-flow treatment application due to high costs involved in the process [102,103]. In such cases, fixed bed column could provide additional advantages over freely dipped adsorbent into contaminated water. The advantages include ease of regeneration and reuse of the

biomass, easy solid–liquid separation operation, and minimal clogging in the fixed bed [104]. Although biosorption studies dealing with fixed bed columns involving immobilized biomass is not totally new, they are limited in using either dead, inactivated or resting biomass in miniscule columns [105]. Moreover, immobilized adsorption bed has not been well studied, particularly in packed columns, for heavy-metal removal, which seems to offer dual advantages of high biosorption efficiency and easy regeneration of the column. However, the previous studies involved mainly the sorption of metals in a continuously operated column with no further cycles tested. Therefore, the present work is aimed at investigating and comparing the regeneration and reuse of fibroin in the biosorption of copper, lead, chromium and cobalt in individual packed bed columns operated under continuous mode. To analyze the performance of the column in the removal of the metals, several parameters, as outlined below, will be used.

The loading behavior of the metal ions, to be removed from solution in a packed bed, is usually expressed in terms of the ratio of effluent to initial metal concentrations C/C_o as a function of time (t) or volume (V) of the eluate for a given bed height (z) and is termed the isoplane or breakthrough curve.

The maximum (equilibrium) capacity q_m of a packed bed column is calculated from area under the plot of adsorbed metal concentration versus time. This is more conveniently expressed as:

$$q_m = F \int_0^t C \, \mathrm{dt} \qquad (2.12)$$

where C is the adsorbed metal concentration (mol/L) and F is the flow rate (L/min) at which the metal solution is passed through the column for a time period t until column bed get saturated.

The expression developed by Thomas [106], calculates the maximum solid phase amount of the solute on the adsorbent and the adsorption rate constant for a continuous adsorption process in the column. The linearized form of the model is given as:

$$\ln\left(\frac{C_o}{C} - 1\right) = k_t \frac{mq_o}{F} - k_t \frac{VC_o}{F} \qquad (2.13)$$

where k_t is the Thomas rate constant (L/mol.min), q_o is the maximum solid phase concentration (mol/g) and m is the amount of adsorbent (g) in the column, F is the volumetric flow rate (L/min) and V is the effluent volume (L). To determine the Thomas rate constant (k_t) and maximum solid phase concentration (q_o) the experimental data can be fitted by plotting $\ln(\frac{C_o}{C} - 1)$ versus effluent volume V [107].

On the basis of the Adams–Bohart and the Thomas model, equation 2.14 is the fundamental equation describing the relationship between C/C_o and t in a flowing system.

$$ln\frac{C}{C_o} = k_a C_o t - k_a N_o \frac{z}{u} \qquad (2.14)$$

where z is the bed depth (cm), the linear flow rate (cm/min) u is defined as the ratio of the flow rate F (L/min) to the cross-sectional area S_c (cm^2), k_a is the adsorption rate constant (L/mol.min), and N_o is the saturation concentration (mol/L).

For describing the concentration distribution in the bed for low concentration range (low C/C_o) in the breakthrough curve, the following relationship by Wolborska[108] can be used.

$$ln\frac{C}{C_o} = \frac{\beta C_o}{N_o} t - \frac{\beta z}{u} \qquad (2.15)$$

where β is the kinetic coefficient of external mass transfer (L/min).

The expression of the Wolborska solution is equivalent to the Adams–Bohart relation if the constant k_a is equal to β/N_o. The parameters in these two models can be determined from a plot of $\ln(C/C_o)$ against t for a given bed height and flow rate. Apparently, the terms k_a and N_o seem to be fixed only for particular values of z and F in a column [109,110].

One of the most successful models used in analyzing breakthrough data from column tests has been the bed depth-service time (BDST) model. It was originally proposed by Bohart and Adams[111]. It shares a common basis with the Adams–Bohart model. Later, Hutchins[112] described the liner form of this model by the following equation:

$$t_b = \frac{N_o}{uC_o} z - \frac{1}{k_b C_o} \ln\left(\frac{C_o}{C_b} - 1\right) \qquad (2.16)$$

where t_b is the service time at breakthrough (min), and C_b is the effluent concentration at breakthrough (mol/L). A straight line obtained by plotting t_b versus z yields the values of saturation concentration of bed (N_o) and kinetic constant k_b from its slope and intercept, respectively. The value of N_o can also be calculated in a more convenient way as follows. At 50% breakthrough, C_o/C_b=2 and t_b=$t_{0.5,}$ the final term in the BDST equation becomes zero resulting in the following relationship [105]:

$$t_{0.5} = yz \qquad (2.17)$$

$$y = \frac{N_o}{uC_o} = \text{constant} \qquad (2.18)$$

Thus a plot of time at 50% breakthrough against bed height should be a straight line passing through the origin, allowing N_o to be calculated.

Another simple theoretical model developed by Yoon-Nelson[113] could also be used to investigate the breakthrough behavior of metal adsorption on the column bed. The linearized form of Yoon-Nelson Model for a single component system is described by the following equation:

$$ln\left(\frac{C}{C_o - C}\right) = k_y(t - \tau) \qquad (2.19)$$

where C_o is inlet concentration of effluent (mol/L), C is effluent concentration at any time (mol/L), k_y is Yoon-Nelson rate constant (min^{-1}), t is time (min) and τ (min) is the time when $C/C_o = 0.5$.

$$t = \tau + \frac{1}{k_y} ln\left(\frac{C}{C_o - C}\right) \qquad (2.20)$$

From the linear dependencies of $ln\left(\frac{C}{C_o - C}\right)$ versus time t, model parameter k_y and τ can be calculated for a given flow rate and initial concentration. In order to validate the experimental data, breakthrough curve could be regenerated by using calculated values of

k_y and τ from data fitting to Yoon-Nelson. To regenerate breakthrough curves, YN model equation could be rearranged as follows [114].

$$\frac{C}{C_o} = \frac{C_o.\exp[k_y(t-\tau)]}{1+\exp[k_y(t-\tau)]C_o} \qquad (2.21)$$

2.8 SEPARATION OF SILK FIBROIN AND SERICIN FROM COCOON

Extraction of silk fibroin from cocoon is accomplished by a process called "Degumming process", usually by one of the following methods.

(1) Extraction with water at a high temperature,

(2) Extraction with water at a high temperature and under pressure.

(3) Extraction with a soap solution.

(4) Extraction with a synthetic detergent.

(5) Extraction with an acid.

(6) Removal of sericin by using enzymes[115].

2.8.1 EXTRACTION WITH WATER

This is the easiest extraction method to get sericin solution, and it is also used in this study. The cocoon shells of *Bombyx Mori* were cut into pieces (about $1cm^2$) and thoroughly washed with water. Then the cocoon shells were boiled with water at 95^oC - 100^oC for different time periods. Fibroin was filtered out using non-woven fabrics and glass microfiber filters [116].

2.8.2 EXTRACTION WITH WATER UNDER PRESSURE AT 120°C

Sericin cannot be dissolved in water at room temperature, but it is highly susceptible to dissolve in boiling water. However, long treatment can damage the fibroin. In the silk industry, autoclaves (commonly at 120^oC and 2 atmospheres for 1-2 hr) are normally used to treat the fiber [117]. However, incomplete degumming may occur. Therefore, sometimes soap or synthetic detergent is added to improve the degumming effect. This process is very difficult to control and it is not widely used in the silk industry nowadays.

2.8.3 EXTRACTION WITH SOAP SOLUTION

Marseilles soap is an outstanding soap for sericin extraction. This process can be carried out using 10-20g.L^{-1} soap at 92-98^{o}C for 2-4 hours at pH10.2-10.5. Generally, alkali causes hydrolysis of the polypeptide chains in the fibers. In addition, alkali hydrolysis can attack the end of a peptide chain easily. Due to the sensitive nature of fibroin itself and the chemical similarity of fibroin and sericin, this process tends to attack both the sericin and fibroin at high temperatures. Moreover, the most important requirement for this process is that soft water should be used to avoid the calcium soap formation. Nowadays, soap solutions are replaced by synthetic detergents because they have advantages over soap in reducing the extraction time and damaging the fiber [118].

2.8.4 EXTRACTION WITH SYNTHETIC DETERGENTS

Synthetic detergent can be used to minimize the fiber damage and reduce the time of treatment (e.g., 30-40min at 98^{o}C) compared with soap. In the extraction process of sericin, non-ionic synthetic detergent can reduce the impact on the tensile strength of the fiber. Normally, efficient degumming can be achieved using 2.5g.L^{-1} nonionic synthetic detergent at pH11.5 for 30min. However, a relatively high temperature (e.g., at 98^{o}C) and a high pH (e.g., at pH11.5) pose problem to this process. Therefore, the operating temperature, time of treatment and amount of detergent should be properly controlled to prevent fibroin damage [119].

2.8.5 EXTRACTION WITH ACIDS

Some acids (such as sulphuric, hydrochloric, tartaric and citric acids) can be used as degumming agents as well. Because alkaline solutions are safer to fibroin degradation than acid solutions, this process has not received much attention in the silk industry. Strong acids (e.g., sulphuric and hydrochloric acids) cannot be used to achieve complete degumming without damaging fibroin [119].

2.8.6 REMOVAL WITH ENZYMES

Enzymes are present in living cells, catalyzing a specific chemical reaction acting as biocatalysts. They can be used at atmospheric pressure and in mild conditions of temperature and pH (e.g., at 40^{o}C, pH8.0). Different enzymes help in hydrolysis, reduction, oxidation, coagulation and decomposition reactions. Hydrolytic enzymes are commonly used in the textile industry; e.g., cellulase, trypsin and papain [118,119].

CHAPTER 3

SEPARATION OF SERICIN FROM SILK FIBROIN

3.1 INTRODUCTION

There are various methods for removing sericin and fibroin from silkworm cocoon. Some of them were discussed in the literature review. Here sericin is extracted from the cocoon with hot water, and the effect of temperature on sericin removal is studied.

The sericin present on the silk fiber coats the filaments into three distinct layers [7]. The outer most layer consists of sericin A, intricate by small glands in the silk worm auxiliary to the main silk glands. An interior layer consists of sericin B, produced by the main glands of the silk worm. The pigment present is stratified near the common boundary. The third and inner most layer is sericin C, which is particularly resistant to enzyme action [77]. The removal of sericin from fibroin surface involves the following steps: the sericin are hydrated and charged with hydroxyl ions, the dispersion of the glutinized sericin by the reulsion of similarly charged moieties, the dispersed sericin is further stabilized by hydrolysis [78].

The objective of this work was not to present the conditions of degumming the natural silk coming from *Bombyx mori* but to present an application of silkworm cocoon fibroin for heavy metal removal from water. This chapter focusses on removal of sericin from silkworm cocoon to produce fibroin. The kinetics of sericin removal is studied as well.

3.2 EXPERIMENTAL

The silk worm *Bombyx mori* cocoon from Brazil was used for extraction of sericin to obtain fibroin. Deionized water was provided by the University of Waterloo. A UV-Vis Spectrophotometer (Shimadzu UV mini 1240) was used for the analysis of the sericin solution samples.

The extraction of sericin was carried out by the water extraction method. Cocoon shells were cut into pieces with an average size of 1×1 cm. The pieces of cocoon were washed with deionized water at room temperature to remove any impurities and dust particles. Water was removed from the cocoon pieces by a strainer. Then the cocoon pieces were dried in an oven at 80^{o}C until a constant weight was achieved. A conical flask (100ml) was filled with 50ml deionized water and 1g of the dry cocoon sample. The flask was sealed and immersed in a HAAKE FISONS DC3 water bath to maintain a constant temperature. The solution samples were taken out from the flask for analysis for a period of 0-9 h. Each sample consists of approximately 2ml volume, and it was put back into the flask after absorbance measurement. The above procedure was repeated at different temperatures ranging from 55 to 95^{o}C.

To prepare the calibration curve, the extracted sericin from cocoons was dried, and standard solutions of sericin at known concentrations were prepared. The absorbance of the standard solutions was measured, and the measured absorbance of the protein solution versus the known concentration of the sericin sample was plotted which is presented in Figure A.1. (Appendix A).

3.3 RESULTS AND DISCUSSION

During the experiments, absorbance of sericin samples was analyzed for the quantity of sericin separated from cocoons at five different temperatures (i.e., 55, 65, 75, 85 and 95^{o}C). Figure 3.1 shows the absorbance of sericin samples at a wavelength range of 250–772nm for sericin extracted at different temperature and water extraction durations.

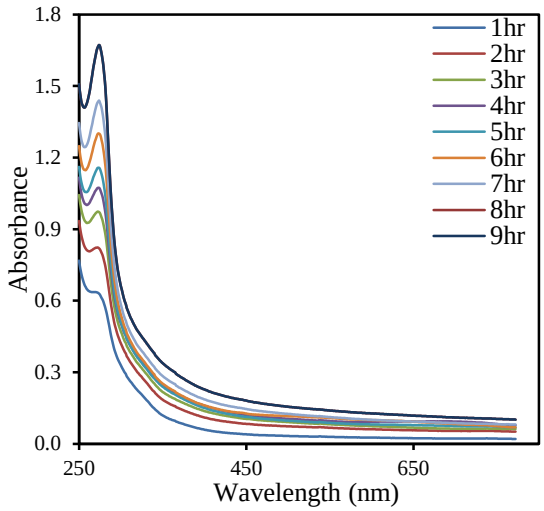

(a) Extraction temperature **95°C**

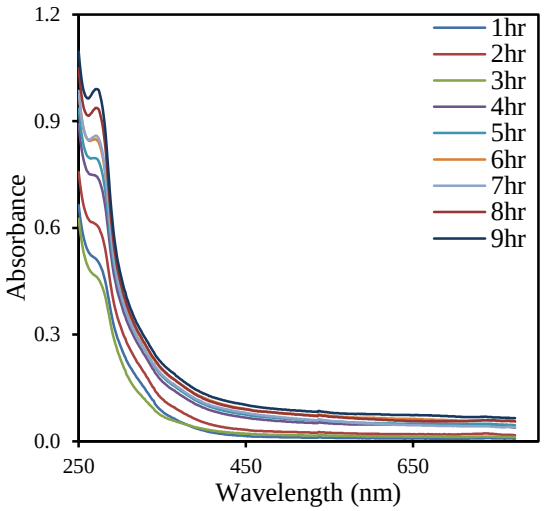

(b) Extraction temperature **85°C**

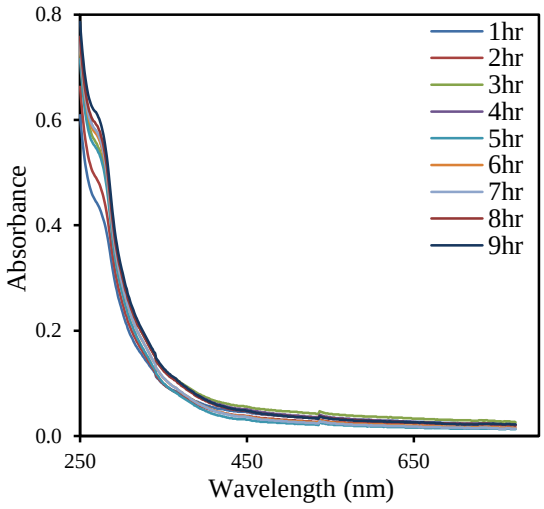

(c) Extraction temperature **75°C**

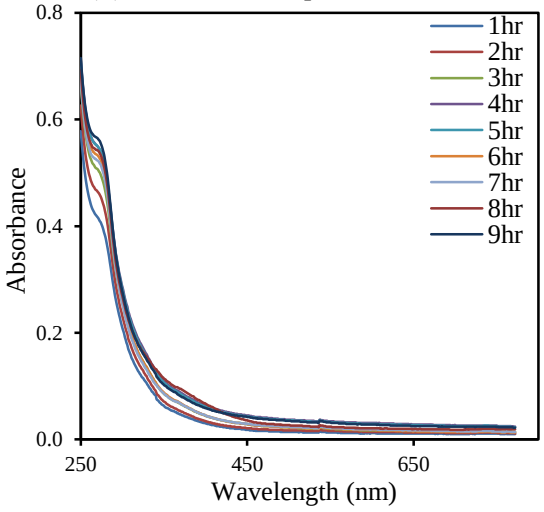

(d) Extraction temperature **65°C**

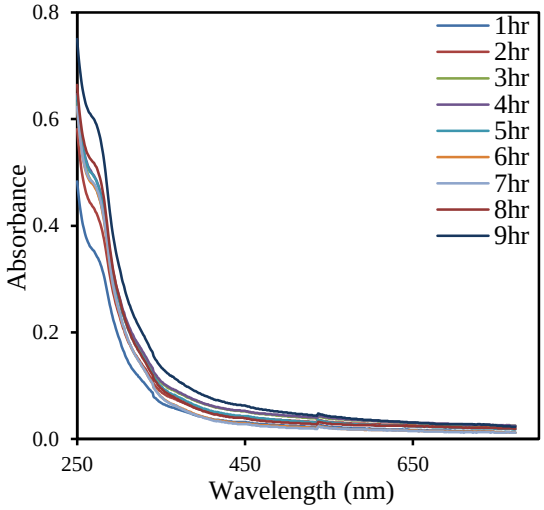

(e) Extraction temperature **55°C**

Figure 3.1 Absorbance spectra of sericin samples extracted from silkworm cocoon at different extraction temperatures and durations.

Proteins in solutions absorb UV light and give an absorbance maxima (peak) at some specific wavelength which is usually around 280nm [78,120]. In this study, the sericin solution shows a peak of the absorbance at a wavelength of 282nm. At lower extraction temperatures (i.e., 55–65^{o}C), the absorbance peak is not so prominent. In contrast, the absorbance peak gets sharper when sericin is extracted at a higher temperature (i.e., 85, 95^{o}C). This may be due to the fact that at lower extraction temperatures, sericin molecules with smaller chain were released from the cocoon, and at higher temperatures, sericin molecules with longer chains would be dissolved in water. The primary reason for the absorbance peak is amino acids with aromatic rings. As sericin with longer chains contains more amino groups, a higher value of absorbance at 282nm was observed. While in case of smaller molecules of sericin with short chains, the result is converse. Thus, it was decided to prepare the calibration curve at a wavelength of 282nm to convert absorbance to sericin concentration.

The effect of extraction time on the separation of sericin from fibroin at a certain temperature can be seen from Figure 3.1. At lower temperatures (i.e., 55, 65 and 75^{o}C) [Figures 3.1 (c),(d),(e)], the magnitude of absorbance peaks at 282nm is very small and almost constant for all the three temperatures. It shows that the separation of sericin from cocoon is less effective at low temperatures. On the other hand, at higher temperatures (i.e., 85 and 95^{o}C) [Figures 3.1 (a),(b)], the magnitude of the absorbance peaks shows a rapid expansion, which indicates an effective removal of sericin from the cocoon. It can also be illustrated that, a larger amount of sericin was removed from cocoon within the same time period (i.e., 9hrs) at 95^{o}C than at other lower temperatures. However, proteins may be damaged at excessively high temperatures, and thus to reduce the possibility of damage in protein structure or destruction in polymer chains, extraction temperatures lower than 95^{o}C were used in this study [79,81].

The absorbance curves of the sericin solutions extracted at temperatures 55-95^{o}C for 9hrs are plotted together in Figure 3.2 for easy comparison. It gives a clearer view of the temperature effect on sericin removal from cocoon. It illustrates that a rise in extraction temperature from 55 to 75^{o}C does not affect the sericin removal very much as the absorbance curves at this temperature range are very close to each other. In contrary, a sharp increase in absorbance peaks can be observed for extraction temperatures 85 and

95°C, because of the high sericin contents in the solution caused by an effective extraction at high temperatures.

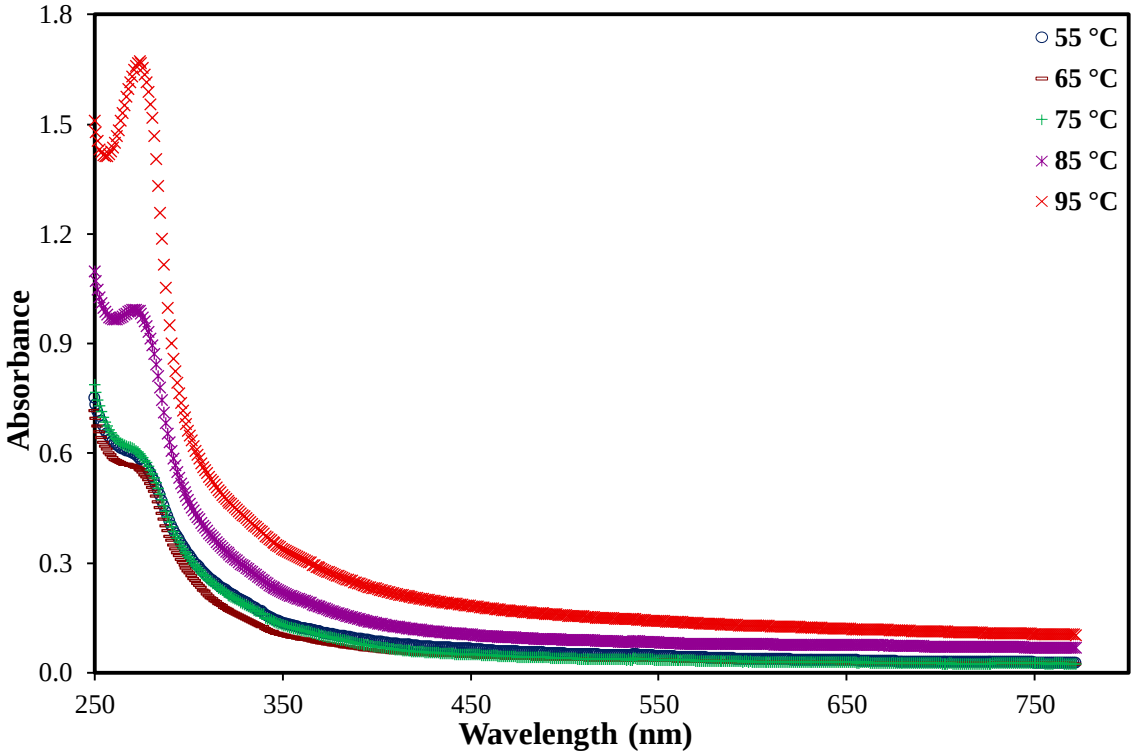

Figure 3.2 Absorbance spectra of sericin samples extracted from silkworm cocoon at 55 – 95°C for 9hr.

The effect of extraction time on the concentration of sericin in the extract at different extraction temperatures is presented in Figure 3.3. The sericin extraction is essentially a result of desorption of sericin from the silkworm cocoon in water. Figure 3.3 represents the accumulative amount of sericin extracted as time proceeds. It is the quantity of sericin separated from 1g of cocoon. Obviously, no additional extraction of sericin took place after 3 hours of immersion of the cocoon in water at temperatures 55 – 85°C and an equilibrium was established between the sericin extracted and the sericin left on the cocoon. At 95°C, however, the extraction of sericin occurred continuously for about 6 hours and then an equilibrium was established. This shows that an increase in temperature favors the extraction of sericin from the cocoon.

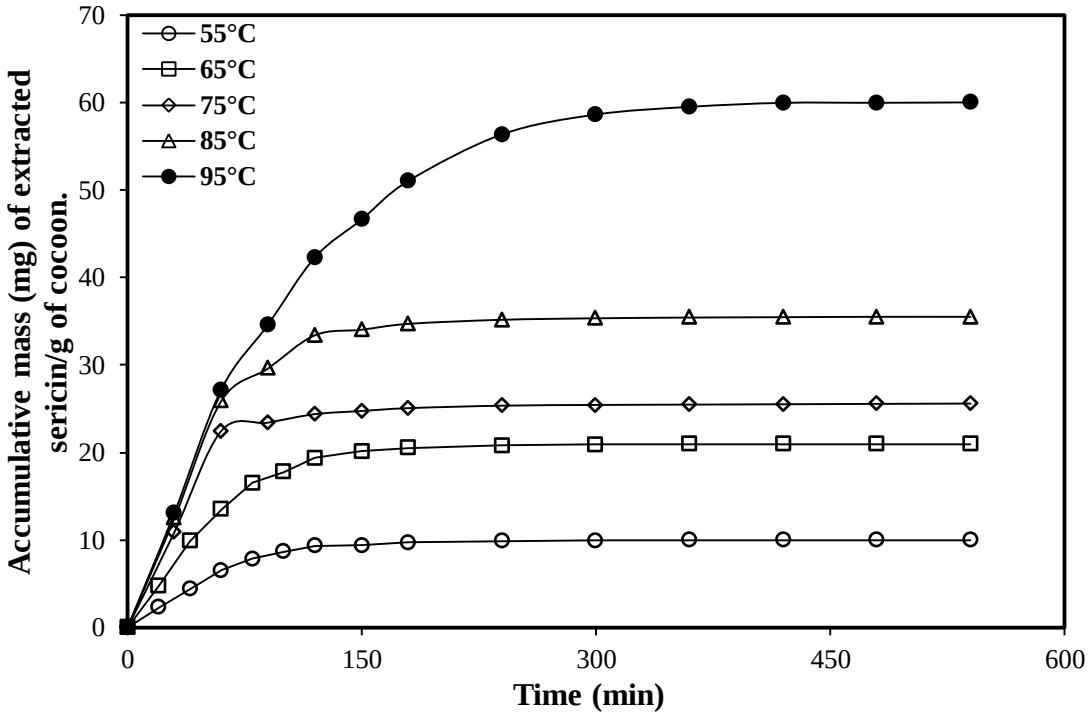

Figure 3.3 Mass of extracted silk sericin vs time at different extraction temperatures.

The objective of the experiment was to remove sericin from cocoon shells in order to get fibroin. At 95^{o}C, once the equilibrium was achieved, the separation of sericin from cocoon stopped. At this temperature, 60.0mg/g of sericin was extracted, whereas the total sercin content present in 1g of cocoon is approximately 250mg. The maximum amount of sericin in cocoon shells is around 25-30% [75,84]. In the sericin extraction experiment, 1g cocoon was immersed in 50ml water. In order to separate more sericin from the cocoon at 95^{o}C, the solid cocoon was placed into a new batch of 50ml deionized water. In this way, the sericin remained on fibroin surface start dissolving in the water again. This sequential water extraction was repeated until the sericin concentration in water reached zero. It took approximately 1L of water to remove all the sericin present in 1g of cocoon.

Figure 3.4 shows the physical appearance of silkworm cocoons and its constituents, fibroin and sericin after separation.

Figure 3.4 Cocoons and its constituents, sericin and fibroin.

COCOONS SPUN BY SILKWORM *BOMBYXMORI*

EXTRACTED SERICIN

SILK FIBROIN

3.3.1 KINETICS OF SERICIN EXTRACTION

The extraction of sericin is the result of desorption of sericin from cocoon shells into the water. In order to investigate the kinetics of the extraction process, pseudo-first-order kinetic model, pseudo-second-order kinetic model and intraparticle diffusion models are used to fit the kinetic data [38,54,56]. Data fitting to pseudo-first-order and pseudo-second-order kinetic models are presented in Figures 3.5 and 3.6, respectively. Table 3.1 shows the model parameters obtained by the data fitting. Although the correlation coefficients are close to unity for both pseudo-first order and pseudo-second order kinetic models, the calculated q_e value is close to the experimental value of q_e for the pseudo-second-order model, which seems adequate to describe the extraction data of sericin from the cocoon shells. In the above discussed models, parameter q_e is the amount of sericin separated at equilibrium (mg/g) and q_t is the amount of sericin separated (mg/g) at time t (min).

For data fitting to the pseudo-first-order kinetic model, once q_t becomes equal to q_e, the term $\ln(q_t-q_e)$ becomes undefined. To avoid this error, only the separation data that satisfies the ratio $\frac{q_t}{q_e} \leq 0.99$ was plotted in Figure 3.5.

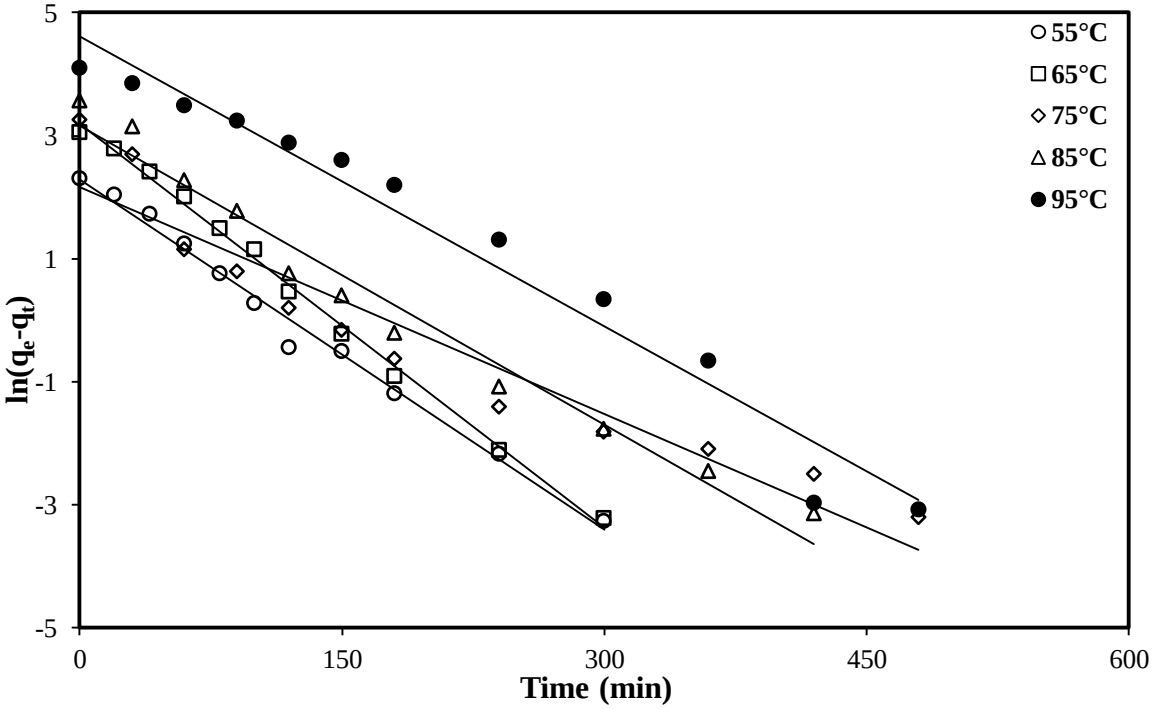

Figure 3.5 Plot of $\ln(q_e-q_t)$ vs time, to test the applicability of the pseudo-first-order model for the extraction of sericin from cocoon. (Extraction temperature 55-95^{o}C)

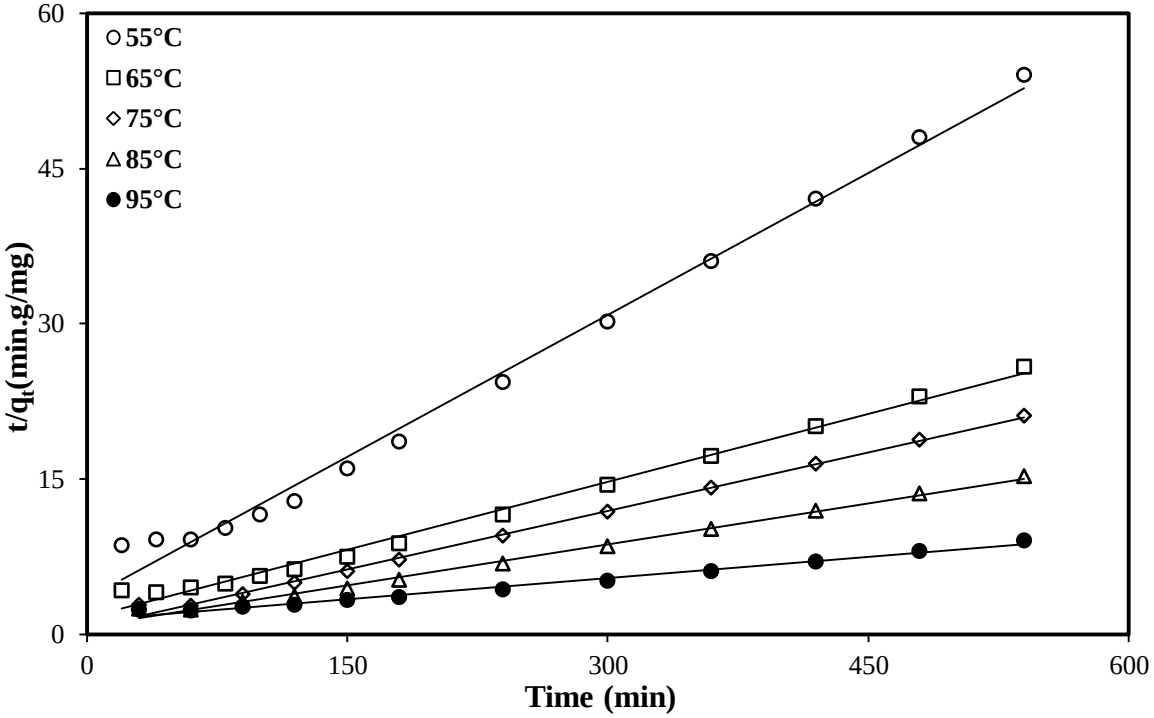

Figure 3.6 Plot of t/q_t vs time, to test the applicability of the pseudo-second-order model for the extraction of sericin from cocoon. (Extraction temperature 55-95^{o}C)

Table 3.1 Data for Pseudo-first-order and Pseudo-second-order kinetics models.

Extraction temperature (^{o}C)	**Pseudo-first-order**			**Pseudo-second-order**			**Experimental q_e (mg/g)**
	R^2	Calculated q_e (mg/g)	Rate Constant k_1(min^{-1})	R^2	Calculated q_e (mg/g)	Rate Constant k_2 (g/mg.min)	
55	0.99	9.89	0.019	0.99	11.0	0.03	10.0
65	0.99	24.2	0.022	0.99	22.9	0.27	20.9
75	0.92	8.75	0.012	0.99	26.7	1.03	25.6
85	0.97	23.5	0.016	0.99	37.9	1.74	35.5
95	0.97	101.4	0.016	0.98	73.5	2.75	60.0

Figure 3.7 illustrates the intraparticle diffusion kinetics of sericin extraction at various temperatures. Kinetic parameters from the linear plots of intraparticle diffusion model are given in Table 3.2. The q_t vs $\sqrt{t}$ plot show multi-linearity, and the first linear portion (Phase I) is represented by a solid trend line and second linear portion (Phase II) is represented by a dotted trend line.

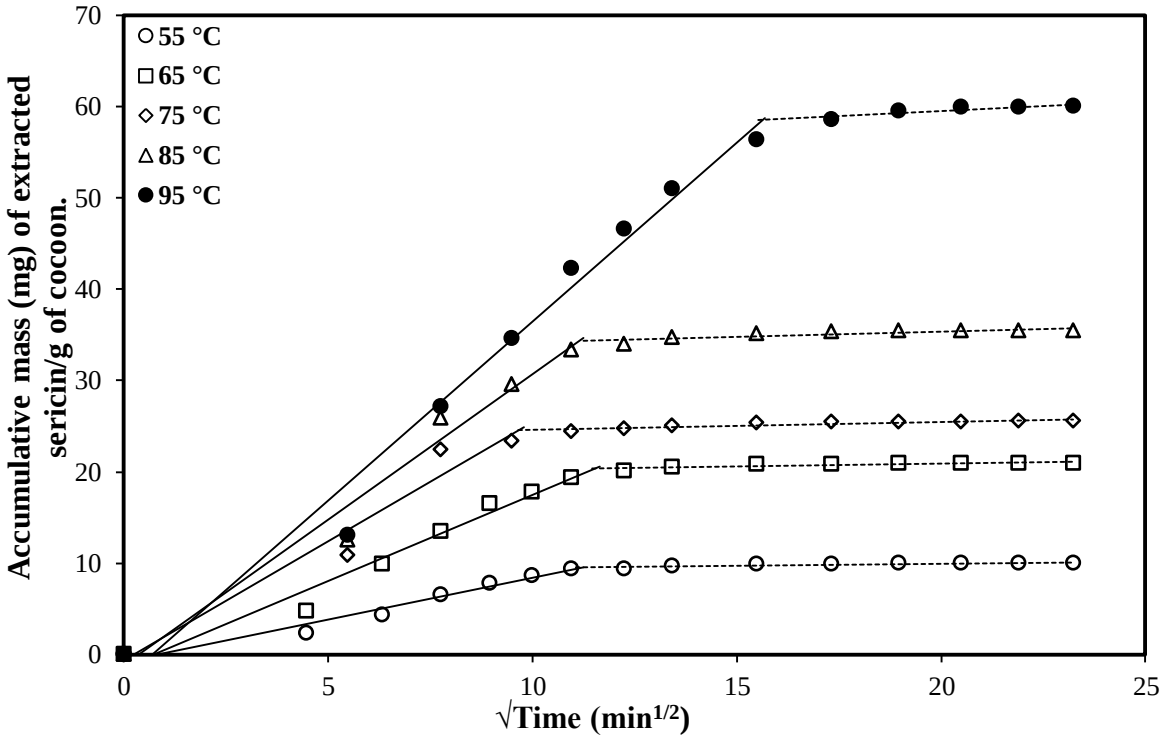

Figure 3.7 Plot of q_t vs √time, to test the applicability of the intraparticle diffusion model for the extraction of sericin from cocoon. (Extraction temperature 55-95^oC)

Phase I: The initial portion of the plot is attributed to the boundary layer diffusion effect or can be considered to be surface dispersion at the beginning of the extraction. This portion of the plot attributes the instantaneous desorption which occurred at the beginning of separation. The values of intraparticle diffusion rate constant k_i, and boundary layer effect c are calculated from the slope and intercept of this portion, respectively. The values of k_i, have been found to increase from 0.91 to 3.92mg/g.min$^{1/2}$ with an increase of desorption temperature from 55 to 95^oC. For the desorption of sericin, the concentration gradient of sericin in the bulk phase (layers of sericin on fibroin) and in water acts as a driving force, which changes with a change in the sericin concentration in solution. Thus, an increase in sericin concentration in water results a decrease in the driving force for sericin extraction, which, causes a decrease in diffusion rate of sericin molecule from the cocoon into water. The values of c have been found negative, no matter what the magnitude is, which neglects the presence of boundary layer effects at the beginning of desorption. Since, at the initial stage of sericin extraction, water was pure and offered no boundary resistance to the desorbing sericin.

Table 3.2 Parameters of intraparticle diffusion model for the extraction of sericin from cocoon at different temperatures.

Extraction temperature (^oC)	Phase I			Phase II		
	k_i (mg/g.min$^{1/2}$)	c (mg/g)	R^2	k_i (mg/g.min$^{1/2}$)	c (mg/g)	R^2
55	0.91	-0.73	0.97	0.05	9.1	0.70
65	1.88	-1.35	0.97	0.06	19.7	0.68
75	2.61	-0.65	0.95	0.09	23.8	0.81
85	3.18	-1.12	0.97	0.11	33.1	0.75
95	3.92	-2.71	0.98	0.23	55.0	0.79

Phase II: The second linear portion of plot is attributed to the intraparticle diffusion at the later extraction stage. The slope of this linear portion characterizes the rate parameter corresponding to the intraparticle diffusion. The intercept of this portion is proportional to the boundary layer thickness [43]. The values of intercept c are in the range of 9.05 to 55.03mg/g for extraction temperatures ranging from 55–95^{o}C. The greater value of c shows a larger effect of boundary layer on desorption of sericin from fibroin surface. The increase in c value could be caused by glutinization of sericin [76]. Where at a high temperature, sericin may get hydrated, and the dispersion of the glutinized particles into water happens fast, causing a significant boundary layer effect.

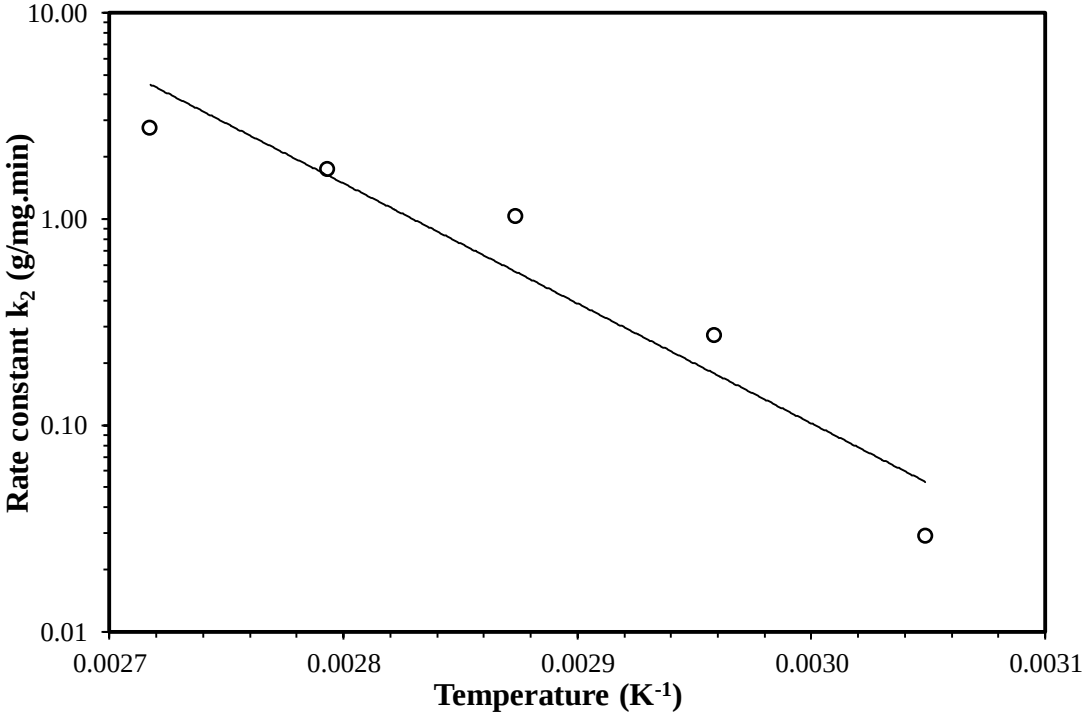

Figure 3.8 Plot of pseudo-second-order rate constant k_2 vs temperature$\frac{1}{T}$.

Figure 3.8 shows the temperature effect and the pseudo-second-order rate constant k_2 for extraction of sericin from cocoon. With a rise in the extraction temperature, there is an increase in the rate constant k_2. It appears to indicate that the chemical "decomplexation" is the rate controlling step for the degumming of sericin from the cocoon.

3.4 CONCLUSIONS

The following conclusions can be drawn for the extraction of sericin from silkworm cocoon to obtain fibroin:

- Sericin can be separated from cocoon with hot water extraction without using any chemicals.
- An increase in temperature increases the rate of sericin extraction.
- The kinetics of sericin extraction is approximated by the intraparticle diffusion model which showed a multi linear trend, it indicates that the intraparticle diffusion in not the only rate controlling step for this separation.
- Pseudo-second-order equation also explained the extraction kinetics; this appears to indicate that the chemical decomplexation could be a contributor of rate controlling for sericin removal from silkworm cocoon by hot water extraction.

CHAPTER 4

HEAVY METAL ADSORPTION ON FIBROIN

4.1 INTRODUCTION

In order to optimize the design of an adsorption system to remove metal ions from solutions, it is important to establish the correlation between equilibrium uptake and solute concentration. An accurate mathematical description of equilibrium adsorption capacity is indispensable for reliable prediction of adsorption parameters and quantitative comparison of adsorption behavior for different adsorbent systems (or for varied experimental conditions within any given system) [121].

Adsorption equilibrium is established when the amount of metal ions adsorbed onto the adsorbent is equal to the amount being desorbed. It is possible to depict the equilibrium adsorption isotherms by plotting the uptake of the metal ion in the solid phase versus that in the liquid phase. The distribution of metal ions between the two phases is a measure of the position of equilibrium in the adsorption process and can generally be expressed by isotherm models. The shape of an isotherm may be considered to predict if a sorption system is ‘‘favorable’’ or ‘‘unfavorable’’. The isotherm shape can also provide qualitative information on the nature of the solute–surface interactions [122].

An analysis of equilibrium data is important not only for developing an equation that can be used to compare different biomaterials under different operational conditions but also to design and optimize the operating conditions [123]. The experimental data for the amount of adsorbate adsorbed on the adsorbent are fitted into an equilibrium isotherm model to determine the model parameters.

A number of adsorption isotherm models are available in literature those are being adopted to correlate adsorption equilibria in heavy metal biosorption. Some known ones

have already been discussed in previous chapter. Adsorption of heavy metal ions by fibroin will be described by Langmuir model.

4.2 THERMODYNAMIC PARAMETERS OF BIOSORPTION

Both energy and entropy factors must be considered in thermodynamics of adsorption, in order to determine whether a process will occur spontaneously or not. The process of lead (Pd), chromium (Cr), copper (Cu) and cobalt (Co) biosorption are assumed to be a reversible process, which represents a heterogeneous equilibrium. For such an equilibrium, the Gibbs free energy (ΔG) can be determined by [124]:

$$\Delta G = -RT\ln k_f \qquad (4.1)$$

where R is the universal gas constant, 8.314 $Jmol^{-1}K^{-1}$, T is the absolute temperature in K, and k_f is the adsorption equilibrium constant derived from equilibrium adsorption model which fits the experimental data (It might have a different notation). In present study, the adsorption equilibrium is defined by Langmuir adsorption model with an adsorption equilibrium constant b having a unit of L/mol. After data fitting to the equilibrium adsorption model, the equilibrium constant b will be determined. Then the value of equilibrium constant b can be used to calculate the thermodynamic parameters from the Van't Hoff equation.

The Gibbs free energy indicates the degree of spontaneity of the adsorption process, where more negative values reflect a more energetically favorable adsorption process. The relationship between the equilibrium constant b and the temperature is given by the Van't Hoff equation. Its linear form is [124]:

$$lnb = \frac{\Delta S}{R} - \frac{\Delta H}{RT} \qquad (4.2)$$

The entropy change of biosorption ΔS and the enthalpy change of biosorption ΔH can be obtained from the slope and intercept of a Van't Hoff plot of lnb vs $\frac{1}{T}$. In the present study, the equilibrium data fits with Langmuir adsorption model, and so thermodynamic parameters are calculated using Langmuir equilibrium constant b.

The Langmuir isotherm is commonly used for description of adsorption data at equilibrium [63,125].

$$q_e = q_m \frac{bC_e}{1+bC_e} \qquad (4.3)$$

where q_e is the adsorption capacity of adsorbent at equilibrium (mmol/g) and q_m (mmol/g) is limiting adsorption capacity when the sorption sites are fully covered with metal ions. It allows for comparison of adsorption performance, particularly in cases where the adsorbent does not reach its full saturation [126]. C_e, is the equilibrium concentration of adsorbate in solution (mmol/L), whereas b is the Langmuir equilibrium constant of adsorption with a unit of L/mol. The Langmuir equilibrium constant has been employed often for calculation of ΔG using equation 4.1 in adsorption studies [127-131]. It should be pointed out that the thermodynamic equilibrium constant in equation 4.1 is unit less, whereas the Langmuir equilibrium constant has a unit of L/mol. Therefore, a simple but hardly asked question in adsorption studies is whether the use of the Langmuir equilibrium constant for calculation of ΔG by equation 4.1 is reasonable. According to Langmuir [132], the adsorption process can be depicted as follows:

$$X + Y \Leftrightarrow XY \qquad (4.4)$$

in which X represents free adsorptive solute molecules, Y is vacant sites on the adsorbent, and XY is the occupied sites. For equation 4.4, the thermodynamic equilibrium constant k_f can be written as follows [133]:

$$k_f = \frac{activity\ of\ occupied\ sites}{(activity\ vaccant\ sites)(activity\ of\ solute\ in\ solution)} \qquad (4.5)$$

It is reasonable to consider that the activity coefficients of the occupied and unoccupied sites are the same [133], and thus equation 4.5 becomes:

$$k_f = \frac{\theta_e}{(1-\theta_e)a_e} \qquad (4.6)$$

in which θ_e is the fraction of the surface covered at equilibrium and a_e is the activity of the adsorbate in solution at equilibrium. The activity of a substance is related to its molar concentration (C_e) by:

$$a_e = \Upsilon_e \frac{C_e}{C_s} \qquad (4.7)$$

where Υ_e is the activity coefficient at the adsorption equilibrium, and C_s is the molar concentration of the standard reference solution which is equal to 1 mol/L [134], and thus:

$$a_e = (\Upsilon_e . C_e).(1L/mol) \qquad (4.8)$$

Substituting equation 4.8 into equation 4.6 will give the following relation:

$$k_f = \frac{\theta_e}{(1-\theta_e)C_e\Upsilon_e} . (1mol.L^{-1}) \qquad (4.9)$$

As θ_e is equal to the ratio of q_e and q_m,

$$\theta_e = \frac{q_e}{q_m} \qquad (4.10)$$

Putting equation 4.10 into equation 4.3 gives:

$$b = \frac{\theta_e}{(1-\theta_e)C_e} \qquad (4.11)$$

Again a comparison of equation 4.9 and 4.11 gives:

$$k_f = \frac{b}{\Upsilon_e} . (1mol.L^{-1}) \qquad (4.12)$$

Replacing k_f in equation 4.1 by equation 4.12 leads to:

$$\Delta G = -RTln\left[\frac{b}{\Upsilon_e} . (1mol.L^{-1})\right] \qquad (4.13)$$

So far, all adsorbates studied in the literature can be roughly divided into two big groups according to their charge characteristics, that is, charged species (e.g., heavy metal ions) and neutral species or species with weak charges (e.g., organic compounds).

According to the Debye-Huckel limiting law, γ_e is a function of the ionic strength (I_e) of the solute at adsorption equilibrium and the charge carried by solute (z):

$$\log \gamma_e = -Pz^2 I_e^{\frac{1}{2}} \qquad (4.14)$$

where P is Debye-Huckel limiting law constant and is unit less. So, according to equation 4.14, for neutral adsorbates or adsorbates with weak charges, equation 4.13 turns to

$$\Delta G = -RT\ln[b\,.\,(1mol.\,L^{-1})] = -RT\ln b \quad (4.15)$$

This implies that for neutral adsorbates or adsorbates with weak charges, the Langmuir equilibrium constant with units of liters per mole can be reasonably used for determination of ΔG. However, for charged adsorbates (e.g., multivalent ions), the Debye-Huckel limiting law, the extended Debye-Huckel law, the Davies equation, and the specific ion interaction model all show that the activity coefficients of charged adsorbates are governed by ionic interactions, and the value of the activity coefficient of a charged adsorbate ranges downward from unity as the concentration of adsorbate is increased [125]. In this case, only for a dilute solution of charged adsorbate, I_e would be negligible, and subsequently, the activity coefficient in equation 4.13 would be close to unity. Therefore, equation 4.13 can be reduced to equation 4.15, indicating that the use of the Langmuir equilibrium constant for determination of ΔG is reasonable only for a dilute solution of a charged adsorbate. In fact, such a constraint has often been ignored in adsorption studies of multivalent cations [125].

Milonjic[135] also questioned the use of the Langmuir equilibrium constant for calculation of ΔG of adsorption and thought that if adsorption took place in dilute solutions, the Langmuir equilibrium constant could be converted to a dimensionless constant by multiplying it by 55.5 mol water per liter (i.e., 1000g divided by the molar mass of water), and ΔG was proposed to be calculated by:

$$\Delta G = -RT\ln(55.5\ b) \qquad (4.16)$$

As discussed above, the activity of a substance is the ratio of the concentration of the substance to a reference concentration (1mol/L), and thus the unit of such a ratio

always cancels. Subsequently, the activity has no unit [134]. Similar value of b should be used in equation 4.2 in order to calculate ΔS and ΔH for the adsorption.

$$\ln[55.5b] = \frac{\Delta S}{R} - \frac{\Delta H}{RT} \qquad (4.17)$$

To calculate thermodynamic parameters is a sensitive issue and most of the work misses interpreting the derived equilibrium constant into thermodynamic equations. As a result, extremely different results may result from the experimental data. Some research work is presented in Table 4.1 in which thermodynamic parameters were incorrectly calculated.

Table 4.1 Articles in which thermodynamic parameters of adsorption are evaluated by the wrong interpretation of equilibrium constant.

Sorption system		**Constant Used**	**Reference**
Solute	Adsorbent		
Cu	Peanut hull	Langmuir Adsorption Constant	Zhu et al.[69]
Cd, Zn, Pb	Penicillium simplicissimum	Langmuir Adsorption Constant	Fan et al.[138]
Cu	Penicillium biomass	Langmuir Adsorption Constant	Zhang et al.[139]
Pb	Natural zeolite	q_m from Langmuir model.	Karatas[95]
Cu, Ni	Activated slag	Langmuir Adsorption Constant	Gupta[140]
Ni	Brown algae	Langmuir Adsorption Constant	Pahlavanzadeh et al.[136]
Ni	Lewatit resin	Langmuir Adsorption Constant	Dizge et al.[137]

Pahlavanzadeh et al.[136] have used brown algae for the removal of Ni(II). Biosorption equilibrium was explained by Langmuir and Freundlich adsorption models and the regression coefficient was higher (>0.99) for Langmuir adsorption model. For the calculation of thermodynamic parameters, they used Langmuir constant with unit L/mol and tabulated the results.

Dizge et al.[137] adopted the same approach to calculate thermodynamic parameters for the adsorption of Ni(II) ions. The equilibrium sorption data were fitted into Langmuir, Freundlich and Tempkin models, and the Langmuir adsorption model was shown to fit the data very well. Dizge used Langmuir adsorption constant for the evaluation of thermodynamic parameters.

4.3 EXPERIMENTAL

4.3.1 MATERIALS

Fibroin is obtained by extracting sericin from the cocoon shells. Lead acetate [$Pb(CH_3COO)_2$], potassium chromate [K_2CrO_4], copper sulfate pentahydrate [$CuSO_4.5H_2O$], cobalt acetate tetrahydrate [$Co(CH_3COO)_2 .4H_2O$] and ethylenediamine tetraacetic acid [$C_{10}H_{16}N_2O_8$] were provided by Sigma Aldrich Canada. Deionized water was provided by chemical engineering department. (***Note:*** In subsequent studies wherever the words lead, chromium, copper and cobalt are discussed, they always mean lead, chromium, copper and cobalt ions, unless otherwise mentioned. Similarly, all concentrations and uptake values are for these metal ions. The term "All Metals" will mean the metal ions of lead, chromium, copper and cobalt.)

4.3.2 BIOSORBENT PREPARATION

In adsorption experiments, fibroin was used as adsorbent, which was obtained by removing sericin from cocoons. The procedure of sericin removal from cocoon to obtain fibroin has been described in Chapter 3 briefly.

10g of washed cocoons were placed in 2L of deionized water, heated at 95^{o}C for up to 9hrs. Then the water was replaced by a fresh batch of 2L deionized water. The amount of sericin that was present in each batch of removed water was measured by using UV-Vis Spectrophotometer (Shimadzu UV mini 1240). The replacement of water was repeated until the amount of sericin present in the water reached to zero. It means there was no more sericin present on the fibroin surface that could dissolve in water. It took about 10L of deionized water in order to make fibroin free of sericin.

Water was removed from the fibroin by using a strainer. The fibroin was air dried in open atmosphere overnight. It was further dried in an oven at 70^{o}C until a constant weight was achieved. Then it was preserved in an airtight glass bottle for further use in the adsorption experiments.

4.3.3 SORPTION EXPERIMENTS

2000ppm stock solution of lead was prepared using lead acetate salt. This stock solution was diluted to get desired lead concentrations. In a 100ml Pyrex beaker, 80ml of lead solution ranging from 50 to 750ppm was taken. Then 1g of fibroin was immersed into the lead solution, and the conductivity of the solution was monitored until the change in the metal concentration completely stopped. In general, the change in the solution concentration took approximately 5 hours to stop. From the changes in lead concentration in the solution, the sorption uptake q_t of lead in fibroin was determined by using the following mass balance equation:

$$q_t = \frac{C_o - C}{m} V \qquad (4.18)$$

where V is the volume of solution (L), m is the weight of adsorbent used (g), C_o is the initial concentration of the solute (mmol/L), and C is the concentration of the solute (mmol/L) at time t.

In order to construct the equilibrium profiles for thermodynamic evaluation of adsorption, experiments were conducted at temperatures 25, 30, 35, 40 and 45^{o}C. However, for temperatures other than room temperature (i.e. 25^{o}C), only the equilibrium data were recorded. For this purpose, the metal solution in a 100ml Pyrex beaker was sealed and placed in a HAAKE FISONS DC3 water bath to maintain a constant temperature during the course of adsorption. At each operating temperature (i.e., 25, 30, 35, 40 and 45^{o}C), the initial metal concentration was in the range of 50 to 750ppm.

Similarly, for chromium, copper and cobalt adsorption, the salts of potassium chromate [K_2CrO_4], copper sulfate pentahydrate [$CuSO_4.5H_2O$], and cobalt acetate tetrahydrate [$Co(CH_3COO)_2 .4H_2O$] were used respectively to make stock solutions of 2000ppm metal concentrations. These solutions were diluted to get different desired concentrations for adsorption experiments.

Batch experiments were also conducted to study the desorption of metal ions from fibroin. 80ml of lead solution was placed in a 100ml Pyrex beaker. Then 1g of fibroin was allowed to contact with this lead solution having an initial concentration of 500ppm. After adsorption equilibrium was achieved, the fibroin sample was taken out of the metal solution, followed by gentle squeezing with a whatman^{Tm} filter paper (grade I pore size 11μm) to remove free metal solution present on its surface. Then the fibroin sample was soaked into 50ml EDTA solution of 0.05M concentration in a 100ml beaker. A small tweezer was used to get fibroin in and out of the solution each time. The solution was agitated with a magnetic stirrer at 30rpm. Samples of the EDTA complex solution were taken out periodically for concentration analysis. Once the metal was completely desorbed from fibroin into the EDTA solution, the fibroin was taken out and rinsed with deionized water repeatedly in order to remove EDTA completely from the fibers and make it prepared for the next adsorption cycle. After this, the fibroin sample was squeezed between filter papers to remove excess moisture, and the same regenerated fibroin sample was used for the subsequent sorption/desorption experiments. This procedure was repeated for up-to ten cycles using the same adsorbent for each metal solution. This will help determine the reusability of the regenerated fibroin.

The same adsorption-desorption cyclic procedure was repeated for other metals. For lead and cobalt, the initial solution concentration for adsorbent loading was kept at 500ppm and for chromium and copper it was 250ppm.

The concentration of metal ions is determined by using a conductivity meter (InoLab Cond Level 2, supplied by WTW Laboratory, Germany). It is an indirect but accurate method to determine the metal concentration in a solution. Using standard solutions of each metal, the conductivity vs concentration graphs were plotted for lead, chromium, copper and cobalt to prepare the calibration curves, which are presented in Appendix A (Figures A.2–A.5).

In the presence of ethylenediamine tetraacetic acid, metal ions can be removed from adsorbent to form a complex with EDTA. Thus, the conductivity meter can no longer be used for measuring the ionic concentration during desorption. As a result, the ionic concentration of metals in EDTA solution was determined by using an inductively coupled plasma mass spectrometry (ICP-MS). It is a mass spectrometry highly sensitive

and capable of determining a range of metals at concentrations below one part in 10^{12} [141]. It is based on inductively coupled plasma as a method of ionization with a mass spectrometer for separating and detecting the ions. Prodigy High Dispersion ICP provided by Teledyne Leeman Laboratories USA was used for the analysis.

4.4 RESULTS AND DISCUSSION

4.4.1 SORPTION EQUILIBRIUM

The effect of temperature on the equilibrium adsorption of metals (i.e., lead, chromium, copper and cobalt) on fibroin was determined in a temperature range of 25℃ – 45℃. Figure 4.1 represents the equilibrium uptake of metals by fibroin in terms of *q* (mmol/g) at different temperatures (i.e., 25℃, 30℃, 35℃, 40℃ and 45℃) versus solution concentration *C* (mmol/L).

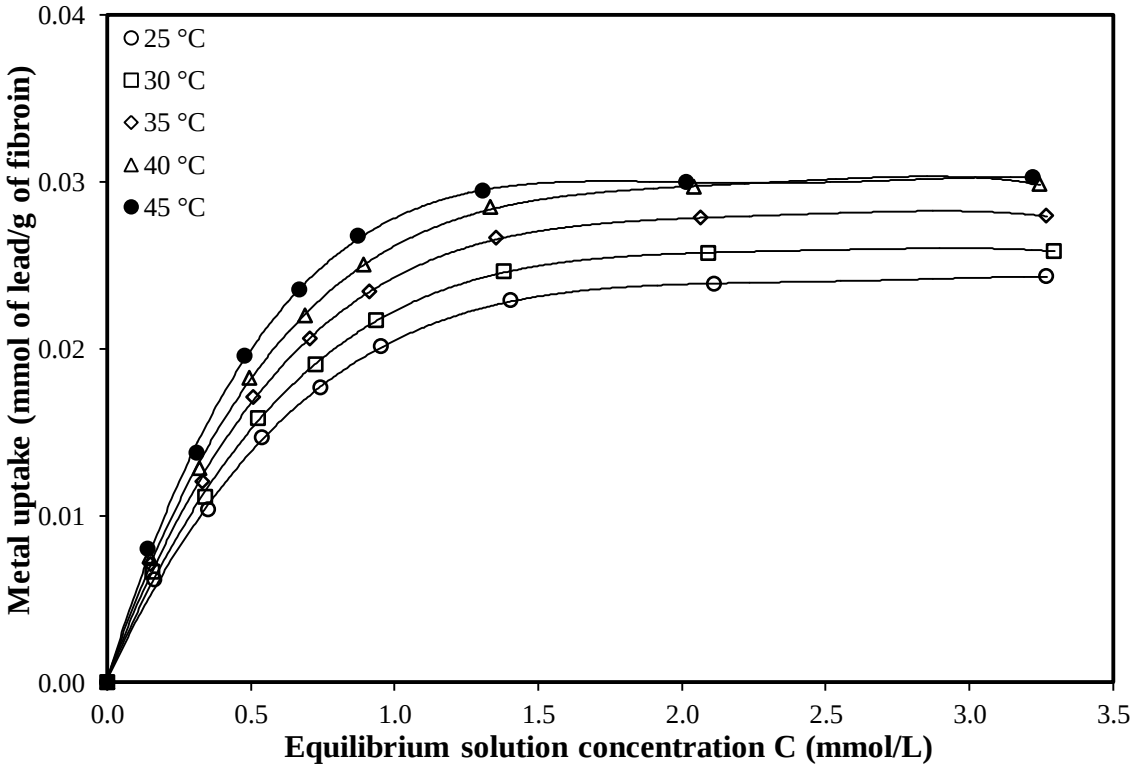

Figure 4.1(a) Equilibrium profiles of ***lead*** adsorption on fibroin at different temperatures.

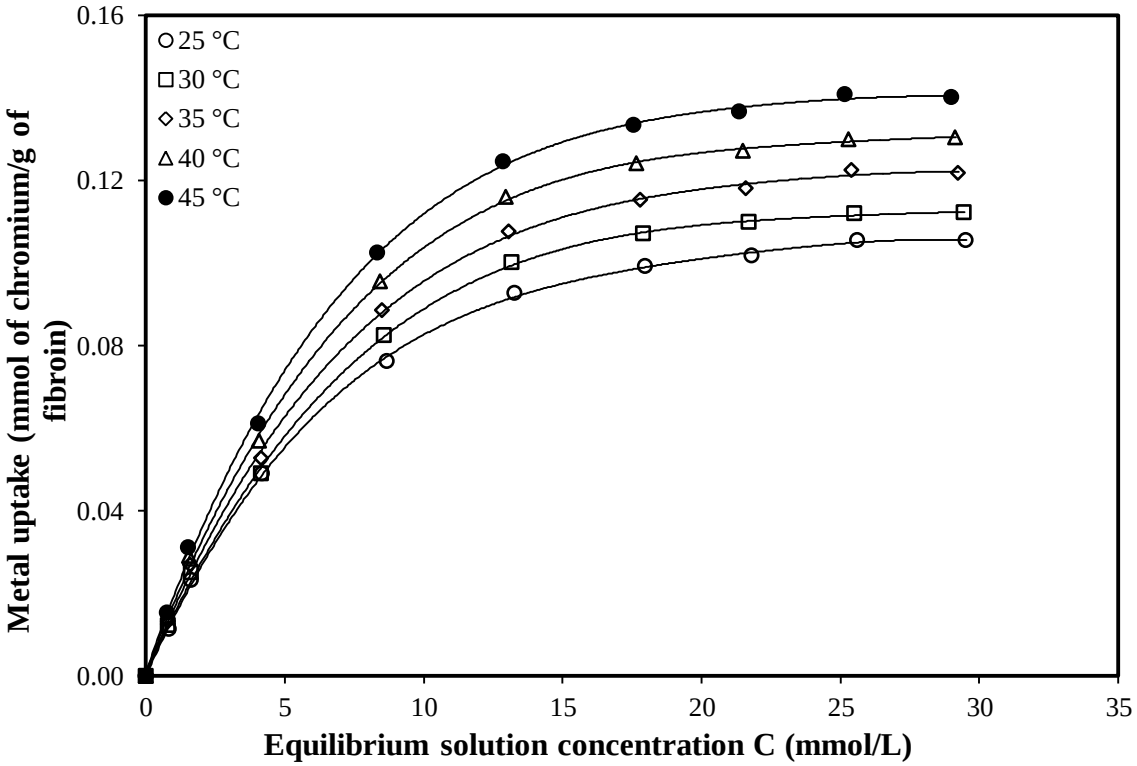

Figure 4.1(b) Equilibrium profiles of ***chromium*** adsorption on fibroin at different temperatures.

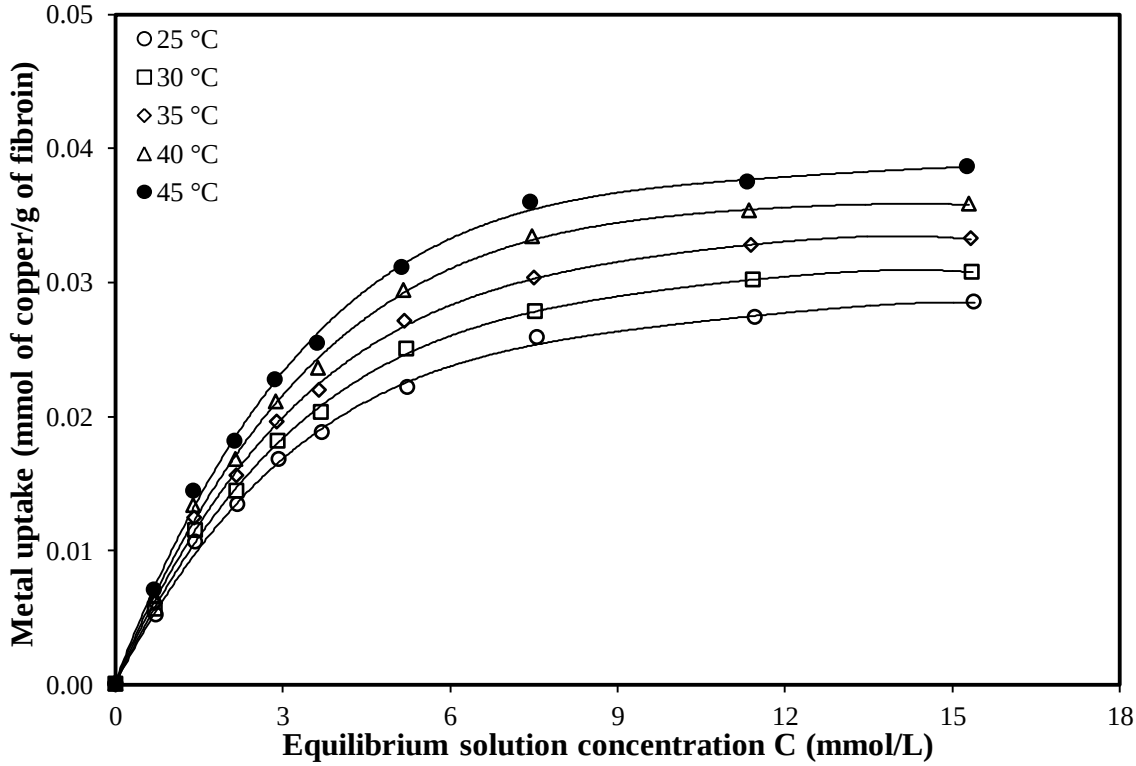

Figure 4.1(c) Equilibrium profiles of ***copper*** adsorption on fibroin at different temperatures.

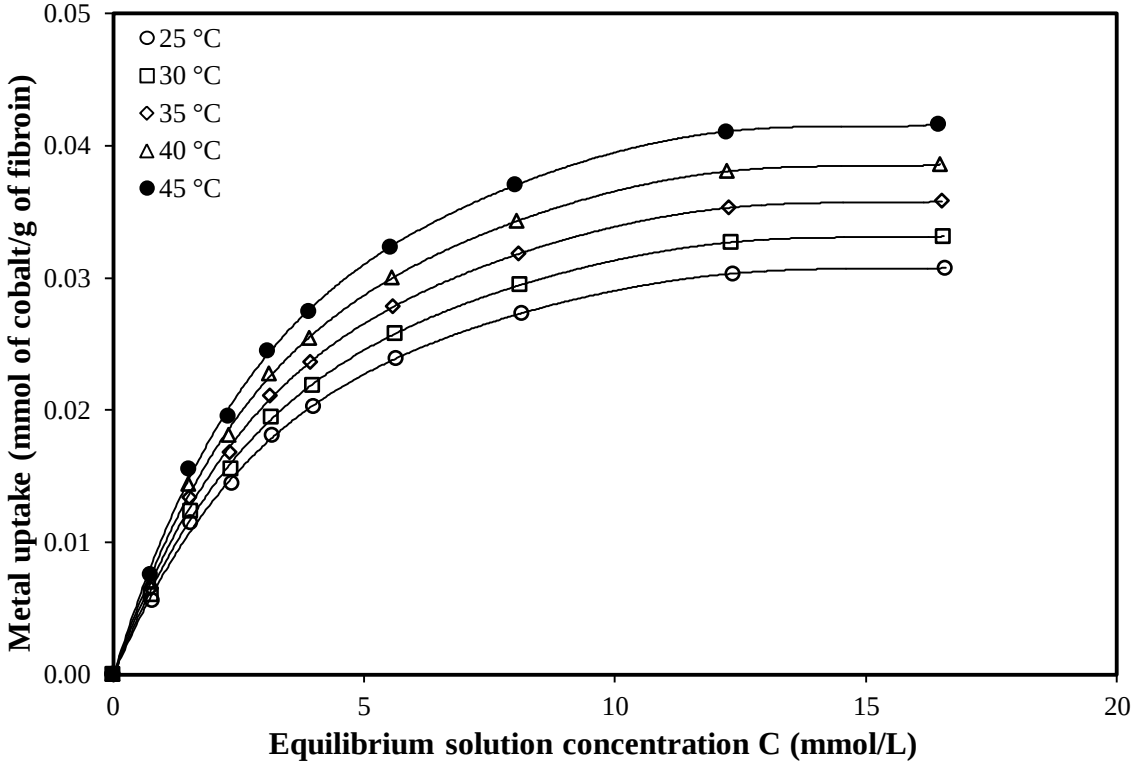

Figure 4.1(d) Equilibrium profiles of ***cobalt*** adsorption on fibroin at different temperatures.

In general, the temperature effects on sorption for different metal–biomaterials systems are incongruent [142]. Figure 4.1 shows that there is an increase in the uptake capacity of fibroin with an increase in the temperature for all the metals studied here. This could be due to the activation of some charged sites on this natural polymer with an increase in temperature which causes more capturing of metal ions.

The equilibrium adsorption data for the sorption of all metals was fitted to Langmuir adsorption model. The linearized form of Langmuir adsorption model is:

$$\frac{c_e}{q_e} = \frac{1}{q_m} c_e + \frac{1}{b q_m} \qquad (4.19)$$

where q_e is equilibrium uptake capacity of adsorbent (mmol/g), C_e is equilibrium solution concentration (mmol/L), q_m is the maximum adsorption capacity of adsorbent (mmol/g) and b is Langmuir adsorption constant (L/mmol). The ratio $\frac{C_e}{q_e}$ is plotted against C_e, as shown in Figure 4.2.

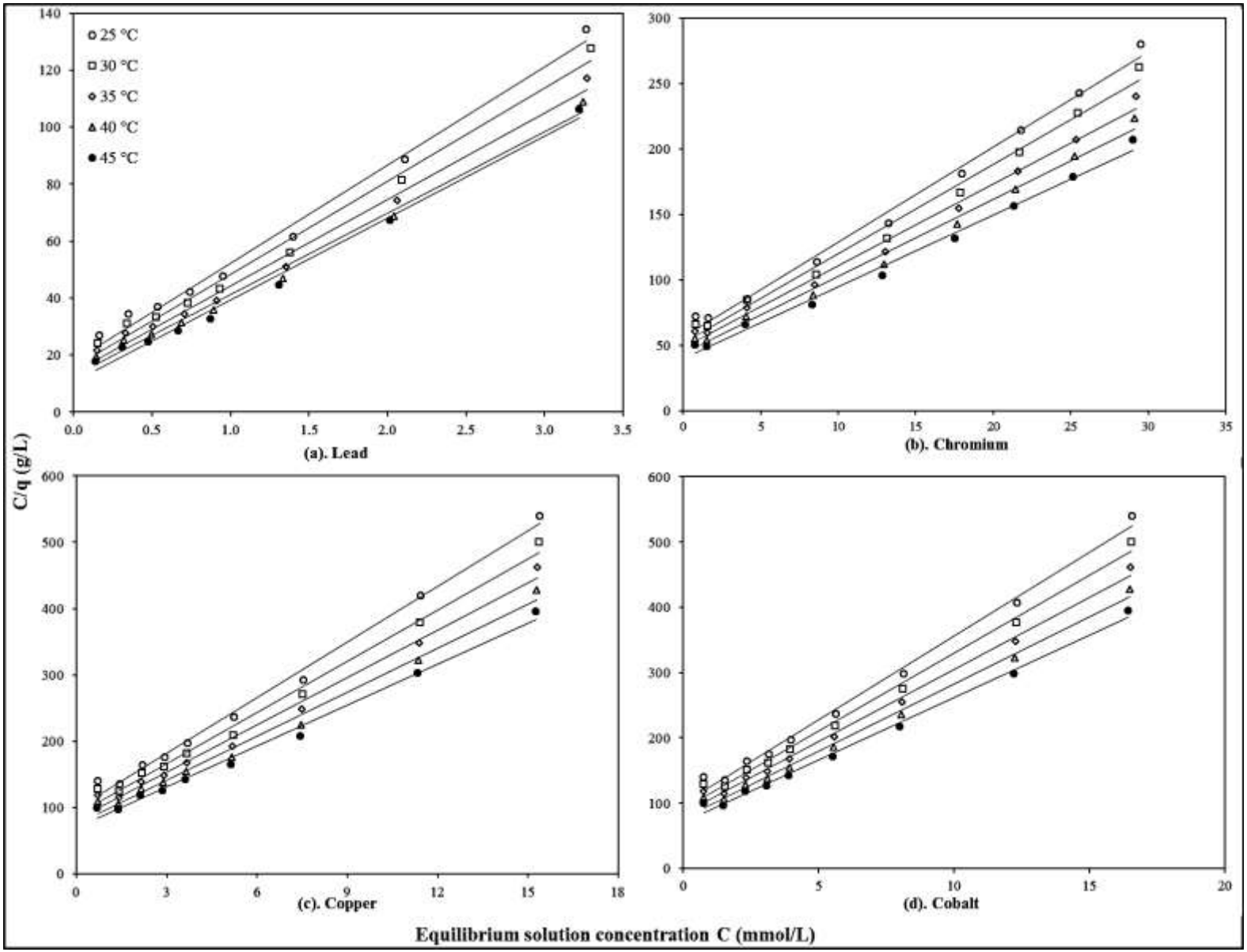

Figure 4.2 Linearized Langmuir isotherms for the adsorption of (a). Lead, (b). Chromium, (c). Copper and (d). Cobalt on fibroin at different temperatures.

where the slope and intercept of the straight line are given by:

$$Slope = \frac{1}{q_m} \quad (4.20)$$

$$Intercept = \frac{1}{bq_m} \quad (4.21)$$

The values of correlation coefficients R^2, Langmuir constants b and q_m for are shown in Table 4.1. Each equilibrium curve, after fitting to the Langmuir model, gives a straight line with a correlation coefficient R^2 close to unity. It shows that the sorption equilibrium data is described well by the Langmuir adsorption model.

Using the adsorption equilibrium parameter b, the Gibb's free energy ΔG can be calculated by using equation 4.16. The constant b used for thermodynamic calculations must have unit L/mol, and the quantity in the bracket in equation (4.16) become dimensionless once multiplied by 55.5mol/L.

Table 4.2 Parameters of the Langmuir adsorption model and Gibb's free energy (ΔG) for the sorption of lead, chromium, copper and cobalt on fibroin at different temperatures.

Metal	Temperature (K)	R^2	b (L/mmol)	q_m (mmol/g)	ΔG (kJ/mol)
Lead	298.15	0.99	1.913	0.029	-28.7
	303.15	0.99	2.089	0.031	-29.4
	308.15	0.99	2.165	0.033	-30.0
	313.15	0.99	2.255	0.035	-30.6
	318.15	0.99	2.748	0.035	-31.6
Chromium	298.15	0.99	0.129	0.138	-22.0
	303.15	0.99	0.130	0.147	-22.4
	308.15	0.99	0.128	0.160	-22.7
	313.15	0.99	0.134	0.169	-23.2
	318.15	0.99	0.136	0.182	-23.6
Copper	298.15	0.99	0.285	0.036	-24.0
	303.15	0.99	0.287	0.039	-24.4
	308.15	0.99	0.289	0.042	-24.8
	313.15	0.99	0.294	0.045	-25.3
	318.15	0.99	0.299	0.048	-25.7
Cobalt	298.15	0.99	0.259	0.039	-23.8
	303.15	0.99	0.262	0.042	-24.2
	308.15	0.99	0.264	0.045	-24.6
	313.15	0.99	0.267	0.049	-25.0
	318.15	0.99	0.270	0.052	-25.4

From Table 4.2, the values of equilibrium adsorption constant ***b*** increase with an increase in adsorption temperature for each metal. Similarly, the maximum uptake capacity of fibroin q_m also tend to increase with an increase in temperature. This may be attributed to the activation of the more sites on the adsorbent surface. The experimental values of maximum uptake capacity of fibroin at 25°C, for all metals, are compared with other sorbents reported in literature. (Appendix B Table B.2).

Negative value of ΔG shows the spontaneity of the adsorption process in regard of energy. With an increase in temperature, the values of ΔG are getting smaller, indicates less energy requirement for adsorption at higher temperature. The decrease in ΔG values with an increase in temperature also indicate that the degree of spontaneity of the reaction increases with the rise in adsorption temperature [143]. The adsorption equilibrium constant *b* is getting larger with an increase in temperature. It also shows that the adsorption process is endothermic.

Similar results were obtained by Fan et al.[138] for the adsorption of cadmium, zinc and lead on Penicillium simplicissimum.

For the calculation of other thermodynamic parameters, the change in enthalpy ΔH and change in entropy ΔS, equation 4.17 is used. By plotting ln(55.5b) vs 1/T gives a straight line with:

$$Slope = -\frac{\Delta H}{R} \qquad (4.22)$$

and

$$Intercept = \frac{\Delta S}{R} \qquad (4.23)$$

The Van't Hoff plots for all metals are presented in Figure 4.3. By using the slope and intercept of Van't Hoff plots, the values of ΔH and ΔS are calculated for all metals and are presented in Table 4.3.

Table 4.3 Thermodynamic parameters, ΔH and ΔS, calculated from the Van't Hoff equation with a temperature range of 25 - 45°C for the adsorption of all metals on fibroin.

Metal	R^2	Enthalpy Change ΔH (kJ/mol)	Entropy Change ΔS (kJ/mol.K)
Lead	0.96	8.30	0.124
Chromium	0.99	2.01	0.081
Copper	0.95	1.73	0.086
Cobalt	0.99	1.54	0.085

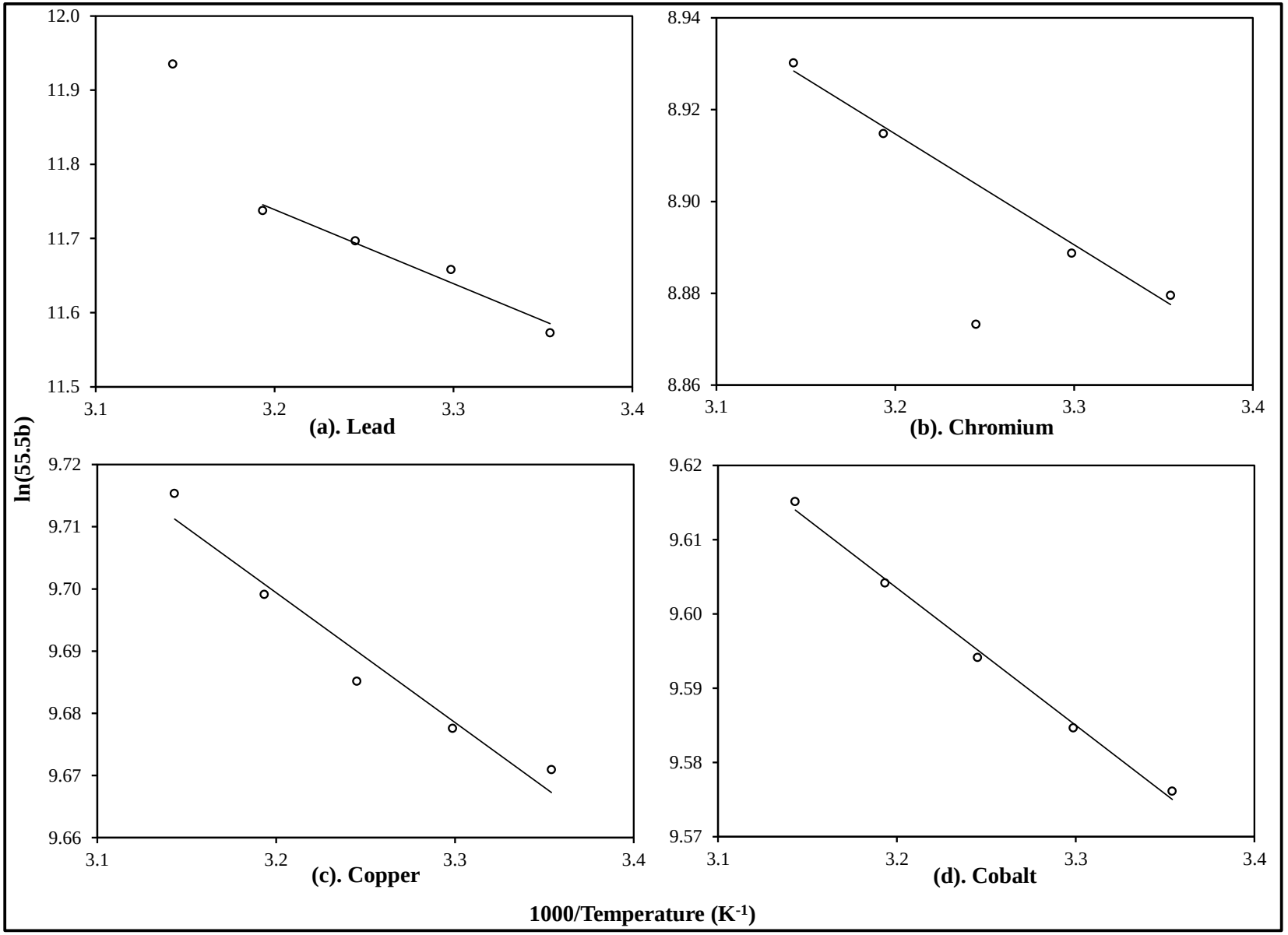

Figure 4.3 Van't Hoff plot of ln(55.5b) vs 1/T for entropy and enthalpy change calculations of (a). Lead, (b). Chromium, (c). Copper and (d). Cobalt adsorption on fibroin.

The values of ΔS, for the adsorption of all the metals are positive but small which indicates little change in the randomness of adsorbate molecules on the solid surface and in the solution. The positive value of ΔH shows that the adsorption of the metals on fibroin surface is endothermic. The heat evolved during physical adsorption generally falls into a range of 0.008-25kJ/mol, while the heat of chemical adsorption generally falls into a range of 80-200kJ/mol [144]. It appears the metal sorption in fibroin is of physical adsorption.

4.4.2 SORPTION KINETICS

In adsorption, the contact time of the adsorbent with the adsorbate is of great importance. The adsorption kinetics of lead, chromium, copper and cobalt on fibroin was determined at different initial metal concentrations. The adsorption temperature for kinetic study was kept constant at 25^{o}C. Figures 4.4(a) – 4.4(d) show the amount of metal adsorbed as a function of time. Generally, the adsorption kinetics can be categorized into two phases, the first phase consists of the initial rapid adsorption of metal ions, followed by the second phase which involves a slow removal of metal ions. In present study, the first phase (time shorter than 50min) was fast and most of the biosorption takes place within this period. At second phase, which is slow enough (time between 50 to 125min), the rate of metal removal slackened and reasonably small amounts of metals were adsorbed on the fibroin. Eventually, an equilibrium was achieved after 125min of the contact time and the metal uptake did not change anymore.

Most researchers relate the initial rapid phase of sorption to the passive physical adsorption or ion exchange at the sorbent surface. However, the slower second phase of adsorption may imply other biosorption mechanisms such as microprecipitation, complexation etc [145].

In order to gain an insight into the mechanism of biosorption such as mass transfer and chemical reaction and to determine the kinetic parameters, the adsorption kinetic data was fitted to the pseudo-first-order, pseudo-second-order and Weber's intraparticle diffusion models. These kinetic and mass transfer models were discussed in Chapter 2 (Literature review) but a little overview is presented here.

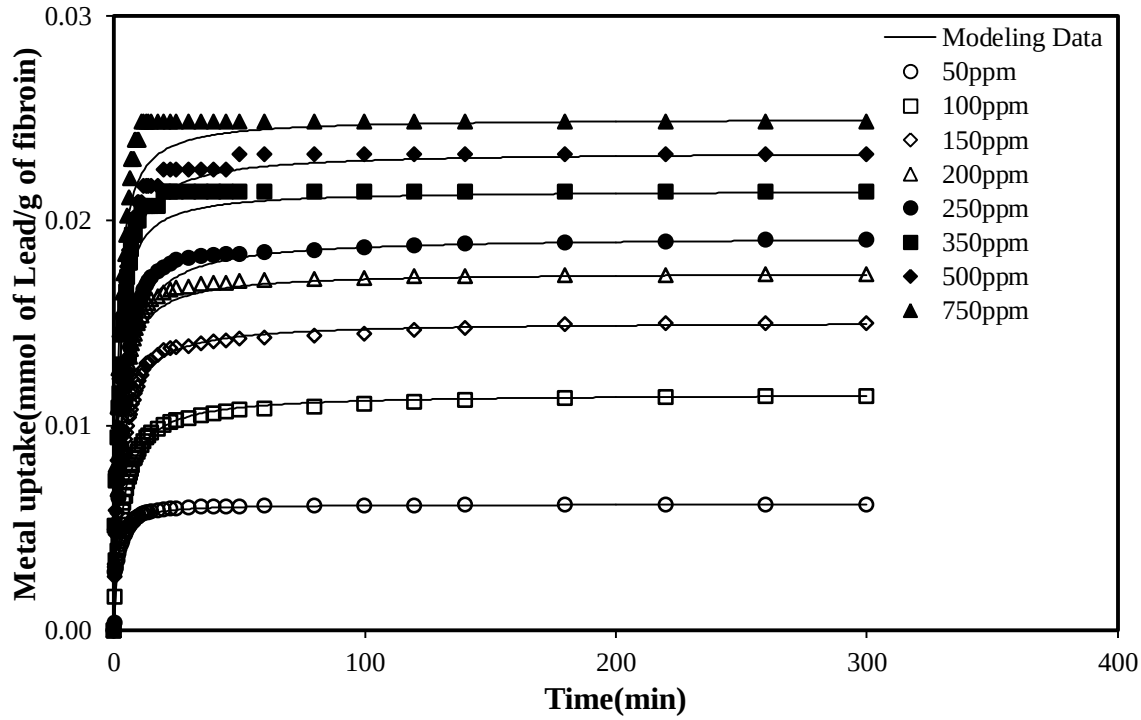

Figure 4.4(a) Comparison of experimental and modeled data for the adsorption of ***lead*** on fibroin. (Adsorption temperature 25^{o}C)

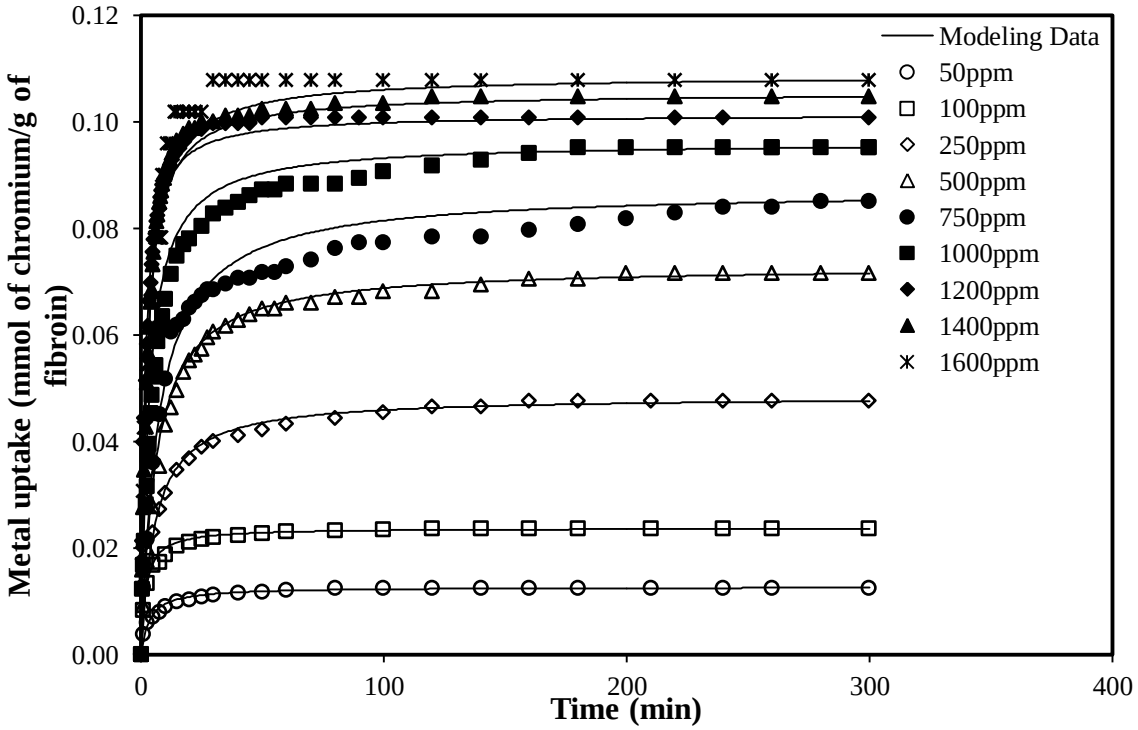

Figure 4.4(b) Comparison of experimental and modeled data for the adsorption of ***chromium*** on fibroin. (Adsorption temperature 25^{o}C)

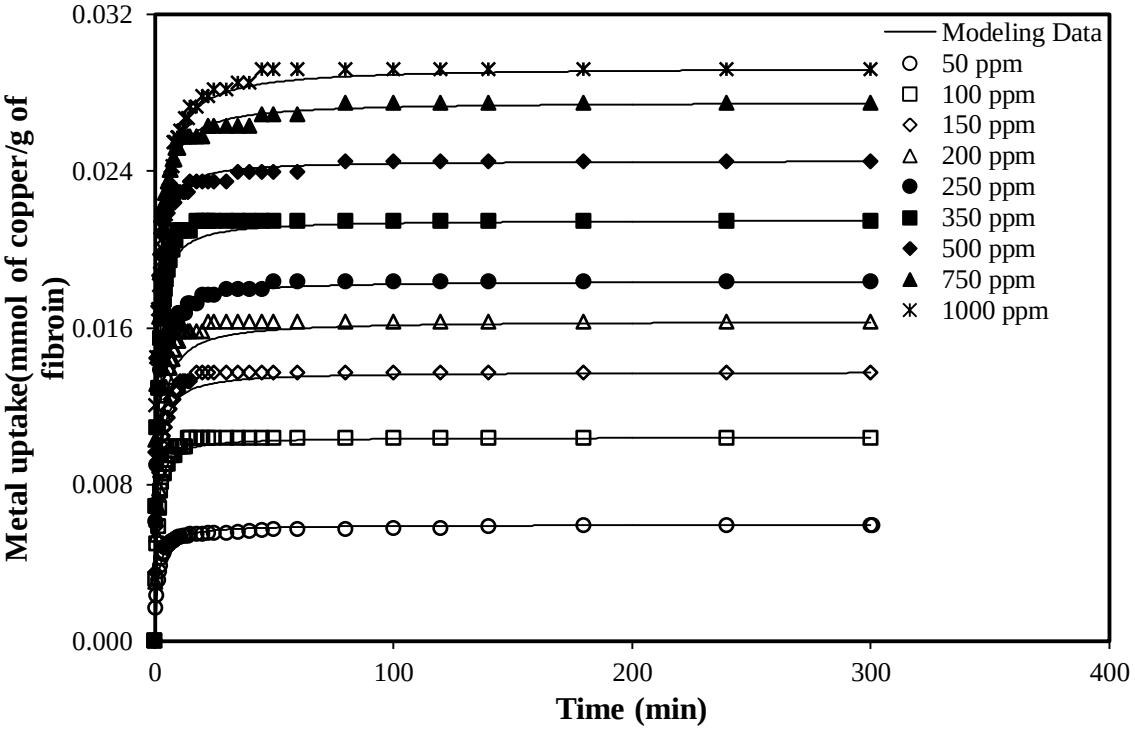

Figure 4.4(c) Comparison of experimental and modeled data for the adsorption of ***copper*** on fibroin. (Adsorption temperature 25^{o}C)

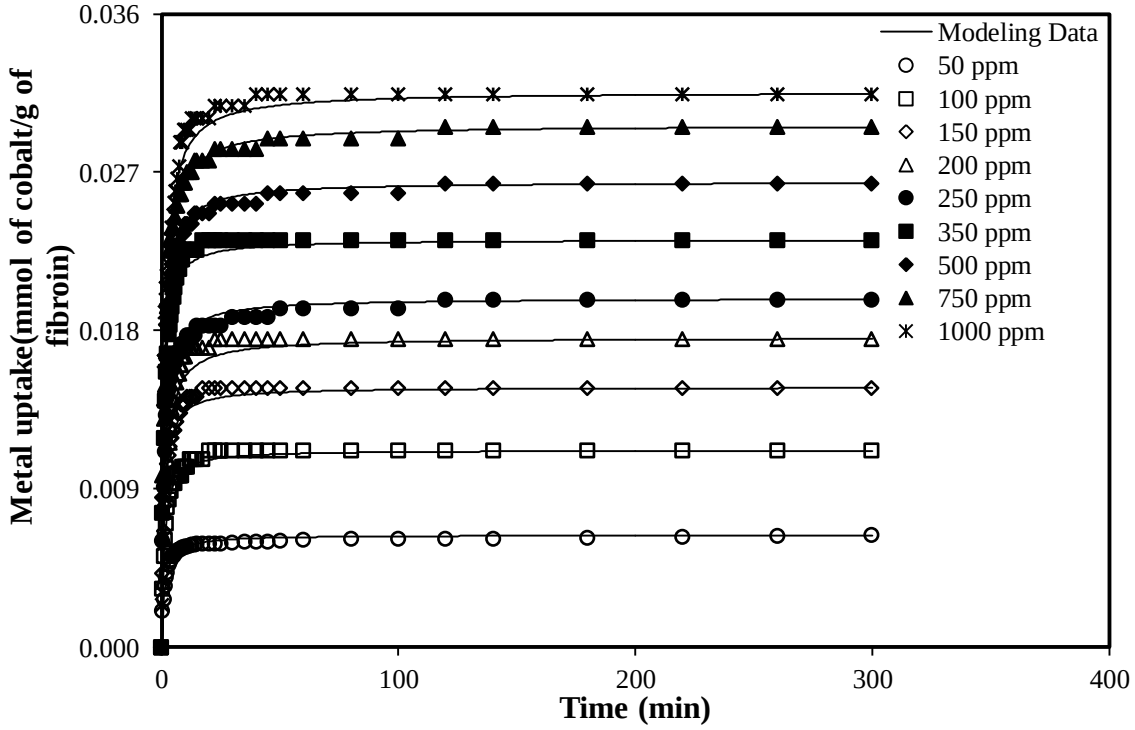

Figure 4.4(d) Comparison of experimental and modeled data for the adsorption of ***cobalt*** on fibroin. (Adsorption temperature 25^{o}C)

The pseudo-first-order kinetic model assumes that the rate of occupation of adsorption sites is proportional to the number of unoccupied sites, whereas the pseudo-second-order model assumes that the sorption capacity is determined by the number of active sites occupied on the biosorbent and that the biosorption may be the rate-limiting step involving valence forces through sharing or exchanging electrons between the biosorbent and the adsorbate [145].

It was found that the experimental data did not fit the pseudo-first-order model, whereas the pseudo-second-order model worked well for the data fitting. The data fitting to the pseudo-second-order kinetic model is presented in Appendix B (Figures B.1 - B.4). The adsorption rate constant k_2 and the equilibrium metal uptake q_e were determined from the data fitting and are presented in Table 4.4. Apparently, the experimental data for all metals seems to fit well to the pseudo-second-order model, with a correlation coefficient R^2 of greater than 0.99. Similarly, the calculated q_e values from the pseudo-second-order model fitting have a very good agreement with the values of experimental q_e over the metal concentration ranges studied here. As shown by data in Table 4.4, the rate constant k_2 did not have a clear correlation with the initial metal concentration of the solution. This shows that the kinetic rate constant k_2 may be not dependent on the initial metal concentration of the solution.

For the adsorption of Cr(VI) on *Salvinia cucullata*, Baral et al.[146] got similar results from the data fitting to the pseudo-second-order kinetic model. They used initial Cr(VI) concentrations ranging from 400 to 700ppm in the adsorption experiments and found that the values the rate constant k_2 evaluated were independent of the initial metal concentration. Ertugay and Bayhan[124] studied the adsorption of Cr(VI) on *Agaricus bisporus* with a concentration range from 50 to 125ppm. The kinetic data fitting to pseudo-second-order model showed that the rate constant k_2 was not dependent on the initial solution concentration. Similar results are reported by some other researchers for adsorption with different initial solution concentrations [59,68,70].

Table 4.4 Experimental data and parameters calculated from pseudo-second-order kinetic model for the adsorption of all metals on fibroin with different initial solution concentration. (Adsorption temperature 25°C)

Metal	Experimental Data					Calculated Data (pseudo-second-order model)		
	Initial Concentration (C_o)		Final Concentration (C_e)		Metal Uptake (q_e)	Metal Uptake (q_e)	Kinetic rate constant (k_2)	R^2
	(ppm)	(mmol/L)	(ppm)	(mmol/L)	(mmol/g)	(mmol/g)	(g/mmol.min)	
Lead	50	0.24	48	0.23	0.006	0.006	144.6	1
	100	0.48	97	0.47	0.011	0.012	26.3	1
	150	0.72	146	0.71	0.015	0.015	24.9	0.99
	200	0.97	196	0.94	0.017	0.018	32.5	1
	250	1.21	245	1.18	0.019	0.019	15.5	0.99
	350	1.69	344	1.66	0.021	0.022	49.2	0.99
	500	2.41	494	2.38	0.023	0.023	26.5	0.99
	750	3.62	744	3.59	0.025	0.025	52.4	0.99
Chromium	50	0.96	49	0.95	0.013	0.013	22.4	0.99
	100	1.92	98	1.89	0.024	0.024	19.1	1
	250	4.81	247	4.75	0.048	0.049	3.4	0.99
	500	9.62	495	9.53	0.072	0.073	1.9	0.99
	750	14.42	744	14.32	0.085	0.086	1.4	0.99
	1000	19.23	994	19.11	0.095	0.097	2.0	0.99
	1200	23.08	1193	22.95	0.101	0.102	7.7	1
	1400	26.92	1393	26.79	0.105	0.106	4.8	1
	1600	30.77	1593	30.63	0.108	0.109	4.7	0.99
Copper	50	0.79	50	0.78	0.006	0.006	105.8	0.99
	100	1.57	99	1.56	0.010	0.010	181.1	1
	150	2.36	149	2.35	0.014	0.014	103.8	1
	200	3.15	199	3.13	0.016	0.016	63.9	0.99
	250	3.94	249	3.91	0.018	0.018	55.6	1
	350	5.51	348	5.48	0.022	0.022	93.7	1
	500	7.87	498	7.84	0.025	0.025	51.5	1
	750	11.81	748	11.78	0.028	0.028	34.4	1
	1000	15.75	998	15.71	0.029	0.029	26.8	1
Cobalt	50	0.85	50	0.84	0.006	0.006	109.1	0.99
	100	1.70	99	1.68	0.011	0.011	116.7	1
	150	2.55	149	2.53	0.015	0.015	102.7	1
	200	3.39	199	3.37	0.018	0.018	63.1	0.99
	250	4.24	249	4.22	0.020	0.020	33.9	0.99
	350	5.94	348	5.91	0.023	0.023	88.5	1
	500	8.48	498	8.45	0.026	0.027	31.9	1
	750	12.73	748	12.69	0.030	0.030	26.2	1
	1000	16.97	998	16.93	0.031	0.032	28.9	0.99

The calculated values of kinetic rate constant k_2 and metal uptake at equilibrium q_e from pseudo-second-order model seems to be good, and most previous work reported in the literature was done in the same manner. However, a closer look at this will reveal some issues. In the pseudo-second-order rate equation, q_e is the equilibrium adsorption uptake and it is the difference between q_e and q at a given time determines the adsorption rate at the moment. However, during the batch adsorption experiments, the metal uptake increases as adsorption proceeds. The q_e in the kinetics equation should be the equilibrium uptake corresponding to the instantaneous metal concentration in the solution. Thus the data fitting equation should be modified.

The pseudo-second-order reaction equation is:

$$\frac{dq_t}{dt} = k_2 (q_e - q_t)^2 \qquad (4.24)$$

The Langmuir adsorption model is described by:

$$q_e = q_m \frac{bC_e}{1+bC_e} \qquad (4.25)$$

For a batch adsorption process, a simple mass balance equation gives:

$$mq = C_o V - C_e V \qquad (4.26)$$

where m is the mass of adsorbent (g), q is uptake of metal ion (mmol/g), C_o and C_e are the initial and final concentration of metal ion in the solution respectively (mmol/L) and V is the volume of solution (L). Rearranging equation 4.26 gives:

$$C_e = C_o - \frac{mq}{V} \qquad (4.27)$$

Substituting equation 4.27 into equation 4.25 gives:

$$q_e = \frac{q_m}{1+\frac{1}{b\,(C_o - \frac{mq}{V})}} \qquad (4.28)$$

Then the pseudo-second-order kinetic equation can be written as:

$$\frac{dq_t}{dt} = k \left[\frac{q_m}{1+\frac{1}{b\,(C_o - \frac{mq}{V})}} - q_t \right]^2 \qquad (4.29)$$

Equation 4.29 is derived to explain the kinetics of an adsorption process in which equilibrium uptake q_e is not constant but is changing as adsorption proceeds with time if the adsorption equilibrium follows the Langmuir model using the parameters determined from the equilibrium sorption studies (i.e., b, q_m).

The kinetic rate constant k_2 (g/mmol.min) can be evaluated by fitting the kinetic data to equation 4.29. A numerical solution program in FORTRAN® (provided in Appendix C) was used in this study.

Kinetic data is fitted to the kinetic model (equation 4.29) to evaluate the rate constant k_2 for the adsorption of all metals. For data fitting, the values of q_m, b, C_o, m and V, which are used in equation 4.29, are presented in Table 4.5. The calculated values of rate constant k_2 for each metal are also presented in Table 4.5. The calculated values of k_2 seem independent of the initial concentration.

To check whether the calculated value of rate constant k_2 is correct, the model calculations based on the k_2 so obtained are also presented in Figures 4.4(a), (b), (c) and (d) for comparison with the experimental data. In these diagrams, the regenerated kinetic curves are shown as "modeling data". It can be observed that the modeling data gives a good agreement with the experimental data. Therefore, it can be said that the modified kinetic model worked well to describe the kinetic data of adsorption.

In Table 4.5, it is observed that the calculated values of rate constant k_2 that corresponds to low initial concentrations (i.e., 50 and 100ppm) deviate from the rest of the values in their relevant group. At metal concentrations higher than 100ppm, the calculated k_2 values do not fluctuate significantly. Thus, we decided to use a single k_2 value for the adsorption of an individual metal. The deviation in the calculated k_2 values at lower initial concentrations might be due to experimental errors. In the adsorption experiments conducted with lower initial solution concentrations, the change in solution concentration (i.e., initial and final solution concentration during adsorption) was very small. The mass ratio of adsorbent to the solution was 1/80. With this ratio, there will be no significant difference between the initial and final concentration. Therefore, the k_2 values corresponding to the low initial metal concentrations and showed $\frac{(C_o - C_e)}{100} \leq 2\%$ (k_2 shown by an " * " sign in Table 4.5, whereas the concentrations C_o & C_e, are presented in Table 4.4) were not taken into account in the arithmetic average of k_2 values. The average k_2 values are also shown in Table 4.5.

Table 4.5 Values of kinetic rate constant k_2 calculated from data fitting to equation 4.29 for the adsorption of all metals on fibroin with different initial solution concentrations. (V=0.08L and m=1g and the values of q_m & b, the Langmuir constants, are those calculated for adsorption equilibrium at 25°C)

Lead				**Chromium**			
Langmuir Constants used	Initial Concentration C_o		Rate Constant k_2	Langmuir Constants used	Initial Concentration C_o		Rate Constant k_2
	(ppm)	(mmol/L)	(g/mmol.min)		(ppm)	(mmol/L)	(g/mmol.min)
b=1.913 (L/mmol)	50	0.24	65.8*	b=0.129 (L/mmol)	50	0.96	16.8*
	100	0.48	17.4		100	1.92	16.8*
	150	0.72	19.6		250	4.81	3.1
	200	0.97	22.9		500	9.62	2.0
q_m=0.029 (mmol/g)	250	1.21	15.8	q_m=0.138 (mmol/g)	750	14.42	1.5
	350	1.69	29.3		1000	19.23	3.1
	500	2.41	21.3		1200	23.08	6.1
	750	3.62	29.3		1400	26.92	4.1
					1600	30.77	3.6
Average k_2			22.2	Average k_2			3.3
Copper				**Cobalt**			
Langmuir Constants used	Initial Concentration C_o		Rate Constant k_2	Langmuir Constants used	Initial Concentration C_o		Rate Constant k_2
	(ppm)	(mmol/L)	(g/mmol.min)		(ppm)	(mmol/L)	(g/mmol.min)
b=0.285 (L/mmol)	50	0.79	109.8*	b=0.259 (L/mmol)	50	0.85	110.5*
	100	1.57	99.9*		100	1.70	75.4*
	150	2.36	61.4		150	2.55	59.9
	200	3.15	38.5		200	3.39	36.9
q_m=0.036 (mmol/g)	250	3.94	49.6	q_m=0.039 (mmol/g)	250	4.24	40.3
	350	5.51	52.1		350	5.94	55.8
	500	7.87	60.2		500	8.48	36.9
	750	11.81	34.7		750	12.73	27.1
	1000	15.75	24.8		1000	16.97	25.3
Average k_2			45.9	Average k_2			40.3

The average values of k_2 for each metal adsorption were also used for the regeneration of kinetic data. A comparison of the model calculations and experimental kinetic data for the adsorption of lead, chromium, copper and cobalt is shown in Figures 4.5(a), (b), (c) and (d), respectively. The model predicted kinetic curves also give a good comparison with the experimental data when an average of k_2 values is used in the kinetic model. This set of data can also be compared to the calculated data using the individual k_2 values presented in Figures 4.4(a), (b), (c), and (d).

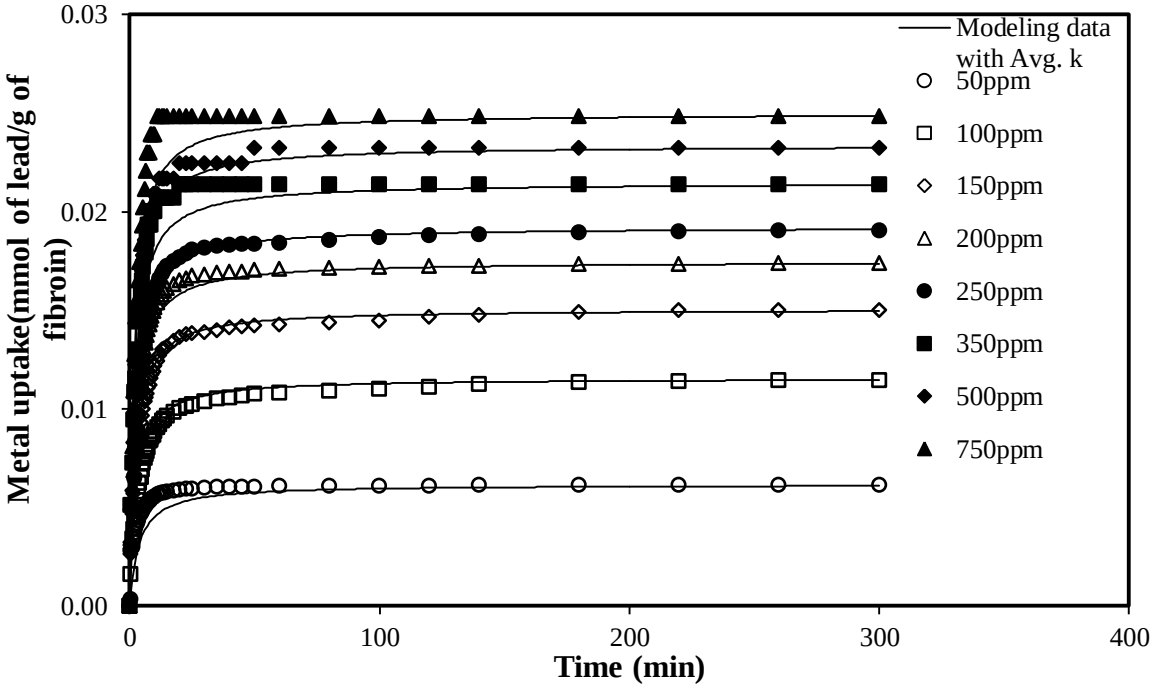

Figure 4.5(a) Comparison of experimental data for the adsorption of ***lead*** on fibroin and regenerated data from kinetic model (equation 4.29) using average value of kinetic rate constant k_2. (Adsorption temperature 25°C)

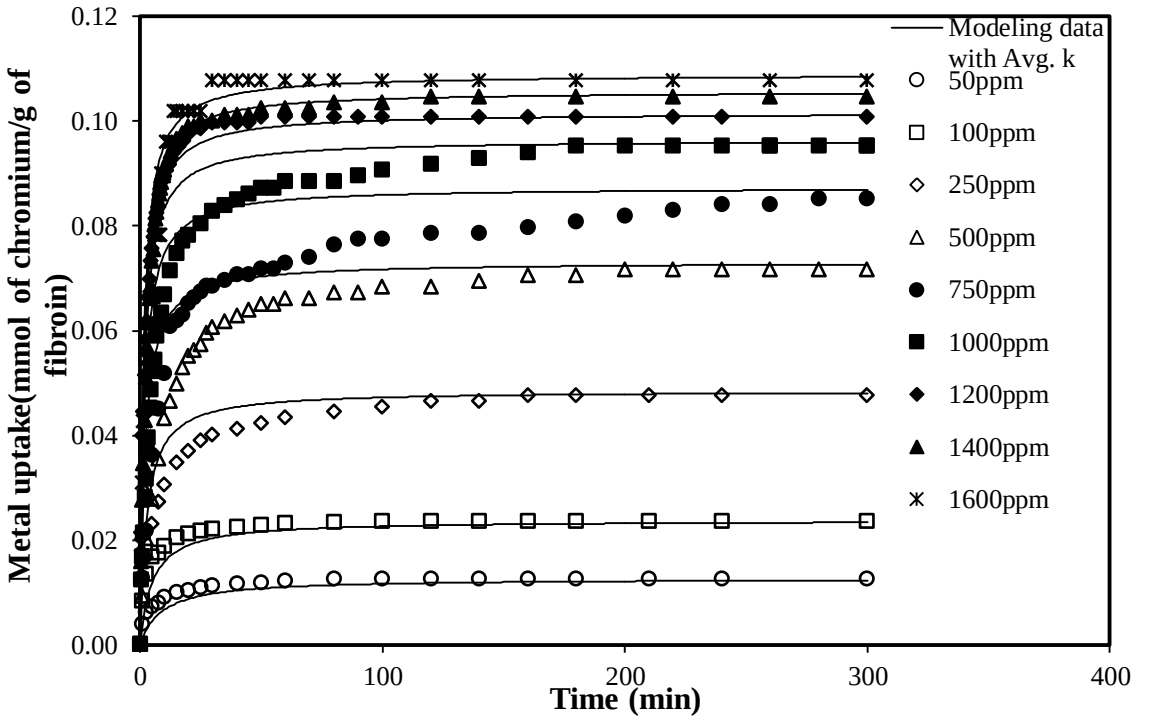

Figure 4.5(b) Comparison of experimental data for the adsorption of ***chromium*** on fibroin and regenerated data from kinetic model (equation 4.29) using average value of kinetic rate constant k_2. (Adsorption temperature 25°C)

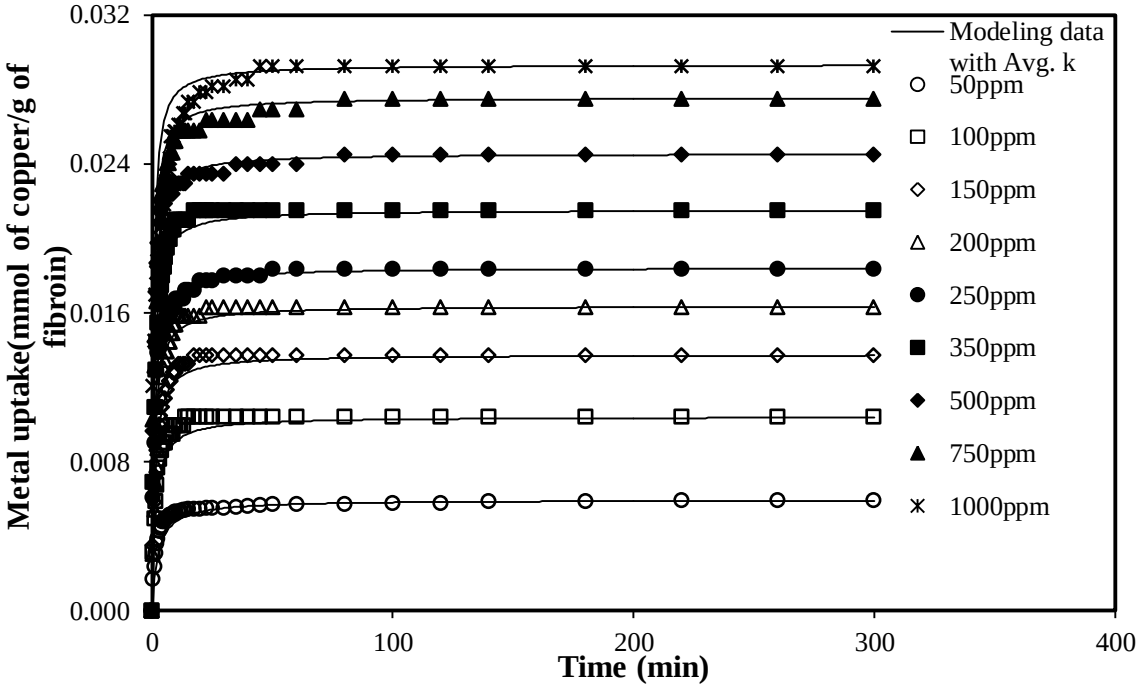

Figure 4.5(c) Comparison of experimental data for the adsorption of ***copper*** on fibroin and regenerated data from kinetic model (equation 4.29) using average value of kinetic rate constant k_2. (Adsorption temperature 25°C)

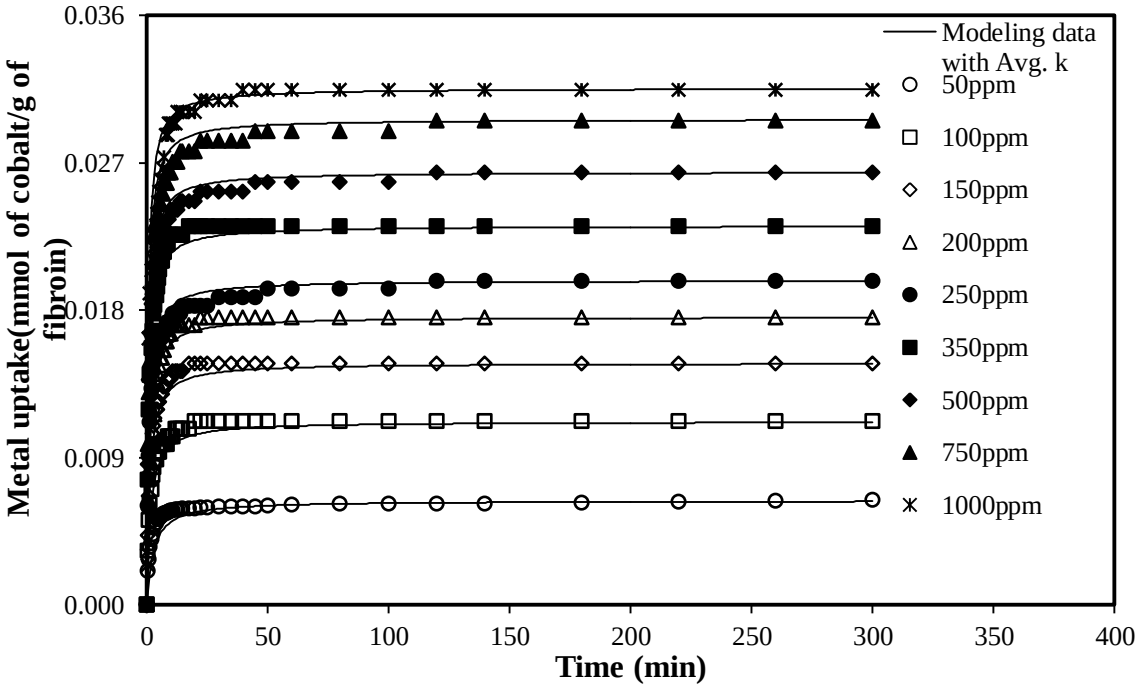

Figure 4.5(d) Comparison of experimental data for the adsorption of ***cobalt*** on fibroin and regenerated data from kinetic model (equation 4.29) using average value of kinetic rate constant k_2. (Adsorption temperature 25°C)

The adsorption kinetic data is also fitted to the intraparticle diffusion model. It showed a multi-linearity trend for lead, chromium, copper and cobalt adsorption. The fitted kinetic data to intra particle diffusion model for lead adsorption is presented in Figure 4.6. The data fitting for other metals (chromium, copper and cobalt) showed the similar trend, and they are presented in Appendix B (Figures B.5- B.7). The data in Figure 4.6 shows two adsorption phases. In the first Phase, the external surface adsorption or instantaneous adsorption occurs. At this stage, the rate of adsorption is pretty fast. In the second phase, gradual adsorption occurs that is controlled by the intra particle diffusion. In this phase the solute moves slowly from the solution into the interior of fibroin. The time required for the second adsorption phase usually depends on the variations of the system (including solute concentration, temperature, and adsorbent particle size), which is difficult to be predicted or controlled [39].

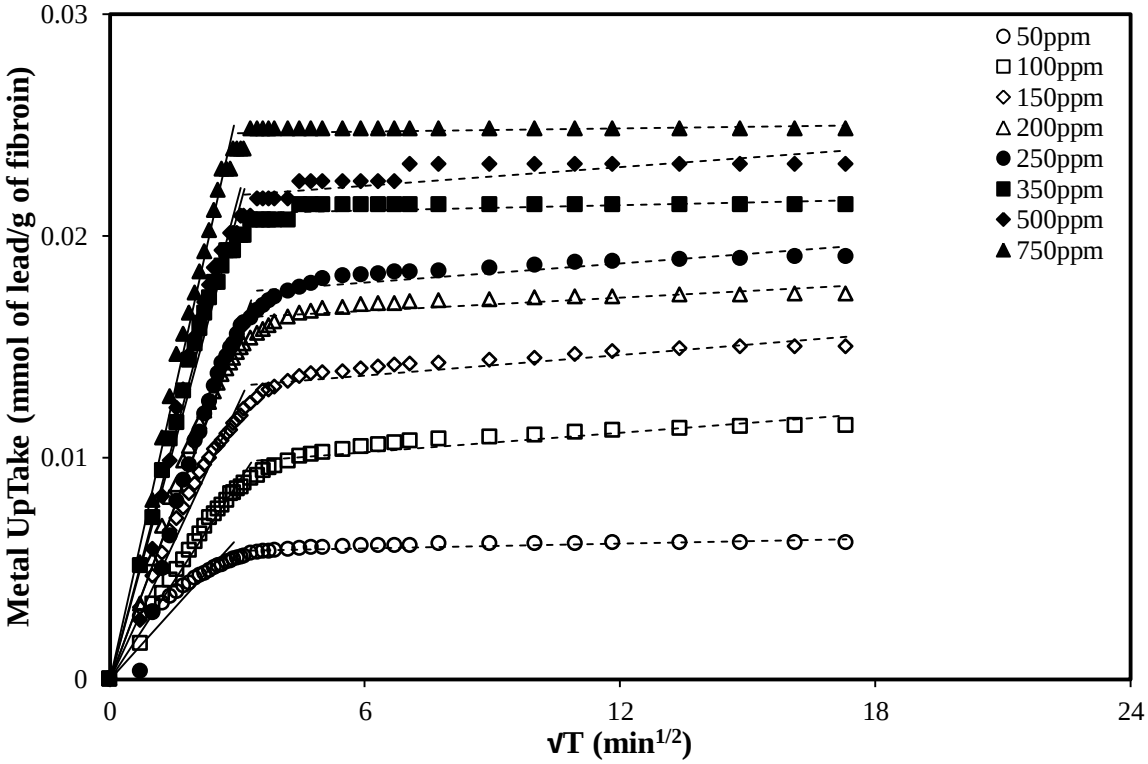

Figure 4.6 Kinetic data fitted to intraparticle diffusion model for the adsorption of ***lead*** with different solution concentrations.

Table 4.6 Parameters of intraparticle diffusion model for the adsorption of all metals on fibroin with different initial solution concentrations.

Metal	Initial Concentration (ppm)	Phase I		Phase II	
		R^2	k_i (mmol/g.min$^{1/2}$)	c (mmol/g)	k_i (mmol/g.min$^{1/2}$)
Lead	50	0.78	0.002	0.006	0.0004
	100	0.98	0.003	0.009	0.0001
	150	0.97	0.004	0.013	0.0002
	200	0.97	0.005	0.016	0.0001
	250	0.96	0.005	0.017	0.0001
	350	0.97	0.007	0.021	0.00004
	500	0.97	0.007	0.021	0.0001
	750	0.99	0.009	0.025	0.00002
Chromium	50	0.88	0.003	0.011	0.0001
	100	0.87	0.006	0.021	0.0002
	250	0.94	0.009	0.038	0.0006
	500	0.98	0.012	0.058	0.0009
	750	0.99	0.016	0.061	0.0015
	1000	0.98	0.021	0.077	0.0012
	1200	0.94	0.032	0.098	0.0002
	1400	0.99	0.031	0.095	0.0007
	1600	0.97	0.029	0.103	0.0004
Copper	50	0.92	0.002	0.005	0.00005
	100	0.89	0.004	0.010	0.00003
	150	0.90	0.005	0.013	0.00004
	200	0.98	0.005	0.016	0.00004
	250	0.75	0.007	0.017	0.00010
	350	0.81	0.008	0.021	0.00002
	500	0.71	0.010	0.023	0.00010
	750	0.88	0.011	0.025	0.00020
	1000	0.77	0.010	0.027	0.00010
Cobalt	50	0.93	0.002	0.006	0.00005
	100	0.80	0.004	0.011	0.00004
	150	0.85	0.005	0.014	0.00003
	200	0.97	0.006	0.017	0.00004
	250	0.86	0.007	0.017	0.00020
	350	0.85	0.009	0.023	0.00004
	500	0.73	0.010	0.024	0.0002
	750	0.85	0.010	0.027	0.0002
	1000	0.84	0.011	0.030	0.0002

The calculated parameters of intra particle diffusion model for the adsorption of lead, chromium, copper and cobalt are presented in Table 4.6. The adsorption rate during phase I is quite fast as compared to phase II. The slope of the second linear portion characterizes the rate parameter corresponding to the intra particle diffusion, whereas the intercept of this portion is proportional to the boundary layer thickness. The values of intraparticle diffusion rate constant, k_i, are found to increase with an increase in the initial metal concentration for all metals. This can be attributed to the driving force of diffusion. The driving force changes with the ionic concentration in the bulk solution. Thus, an increase in the metal concentration results in an increase in the driving force, which will increase the diffusion rate of metal ions into the pores of fibroin.

Due to multi-linearity of kinetic curves, it can be suggested that metal sorption on the fibroin is not only controlled by the intraparticle diffusion and there may be other mechanism involved for this separation. Besides, the plots q_t versus $t^{1/2}$ pass through the origin, it shows that adsorption mechanism is a multi-step process, which can involve adsorption of metal ions on the external surface and then their diffusion into the interior of sorbent (polymer network). In general, the value of intercept c in Phase II gives an idea about the boundary layer effect on sorption. If we look at the calculated values of intercept c for phase II, they seem to be in direct proportion with the initial metal concentration. This increase in c value with an increase in boundary layer also shows a smaller probability of internal mass transfer. Greluk and Hubicki[147] got similar results while performing the sorption of dye on polystyrene anion exchangers.

4.4.3 ADSORPTION-DESORPTION CYCLE STUDY

The adsorption-desorption study was carried out not only to recover the adsorbed metal ions but also to reuse the spent fibroin. This study can also be used to evaluate the feasibility of regenerated adsorbent so that the same adsorbent can be used over and over. Ethylenediaminetetraacetic acid (EDTA) is used as a chelating agent for the desorption of metal ions from fibroin. The presence of nitrogen atoms and short chain carboxylic groups in EDTA helps in the mobility of adsorbed metal ions from adsorbent surface into the solution. Once the metal ions move to the solution, EDTA can bind them strongly due to its charged ionic groups and the metal ions to form a stable complex [148].

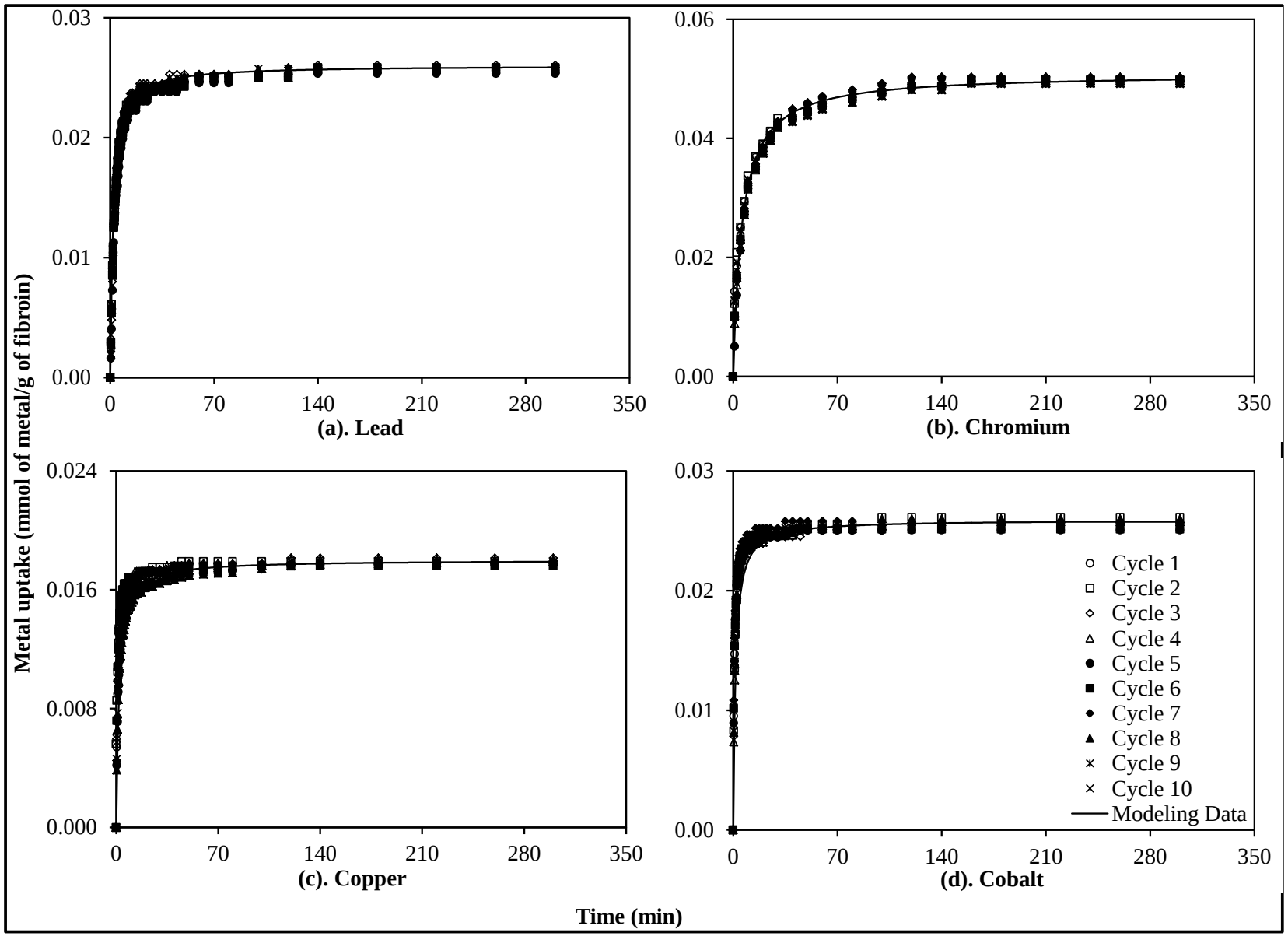

Figure 4.7 Comparison of experimental kinetic data, up to ***ten cycles,*** and modeled data using equation 4.29 for the adsorption of (a). Lead, (b). Chromium, (c). Copper and (d). Cobalt on fibroin. (Initial solution concentration for lead & cobalt was 500ppm, and for chromium & copper it was 250ppm)

In the present study, two major parameters for adsorption-desorption cycles are considered: the kinetics of adsorption for each cycle after regeneration, and the kinetics of desorption for each cycle after each adsorption. Once the kinetic data of adsorption and desorption is observed, the kinetic profiles seem to be very much laying on each other for all cycles. It shows that the uptake capacity of fibroin remains same, and the kinetics of adsorption as well as kinetics of desorption is the same. The kinetic data for ten cycles of adsorption and desorption is taken as a single set for fitting to the model in order to evaluate the rate constant using equation 4.29.

In case of desorption, the initial solution concentration is lower than the final concentration, and the mass balance becomes:

$$mq = C_e V - C_o V \qquad (4.30)$$

By using equation 4.30, the final kinetic equation would be:

$$\frac{dq_t}{dt} = k_d \left[\frac{q_m}{1+\frac{1}{b\,(C_e - \frac{mq}{V})}} - q_t \right]^2 \qquad (4.31)$$

Equation 4.31 describes a batch desorption process in which k_d is rate constant of desorption, and C_e is the final concentration of solution at desorption equilibrium. The other parameters in equation 4.31 are the same as those for adsorption kinetics described earlier. The values of q_m and b, the Langmuir constants, used to solve equation 4.31 are presented in Table 4.7. For data fitting to equation 4.31, a program was developed in FORTRAN® and is presented in Appendix C.

A comparison of the experimental kinetic data (shown by the data points) up to ten cycles for the adsorption of lead, chromium, copper and cobalt, and the modeled data (shown by a solid line) is presented in Figure 4.7. First, the values of rate constant k_2 are evaluated by fitting experimental data to equation 4.29. Then, the evaluated values of k_2 are used to regenerate the data by using equation 4.29 again. Figure 4.7 shows a good agreement between experimental curves and the modeled data for all metals.

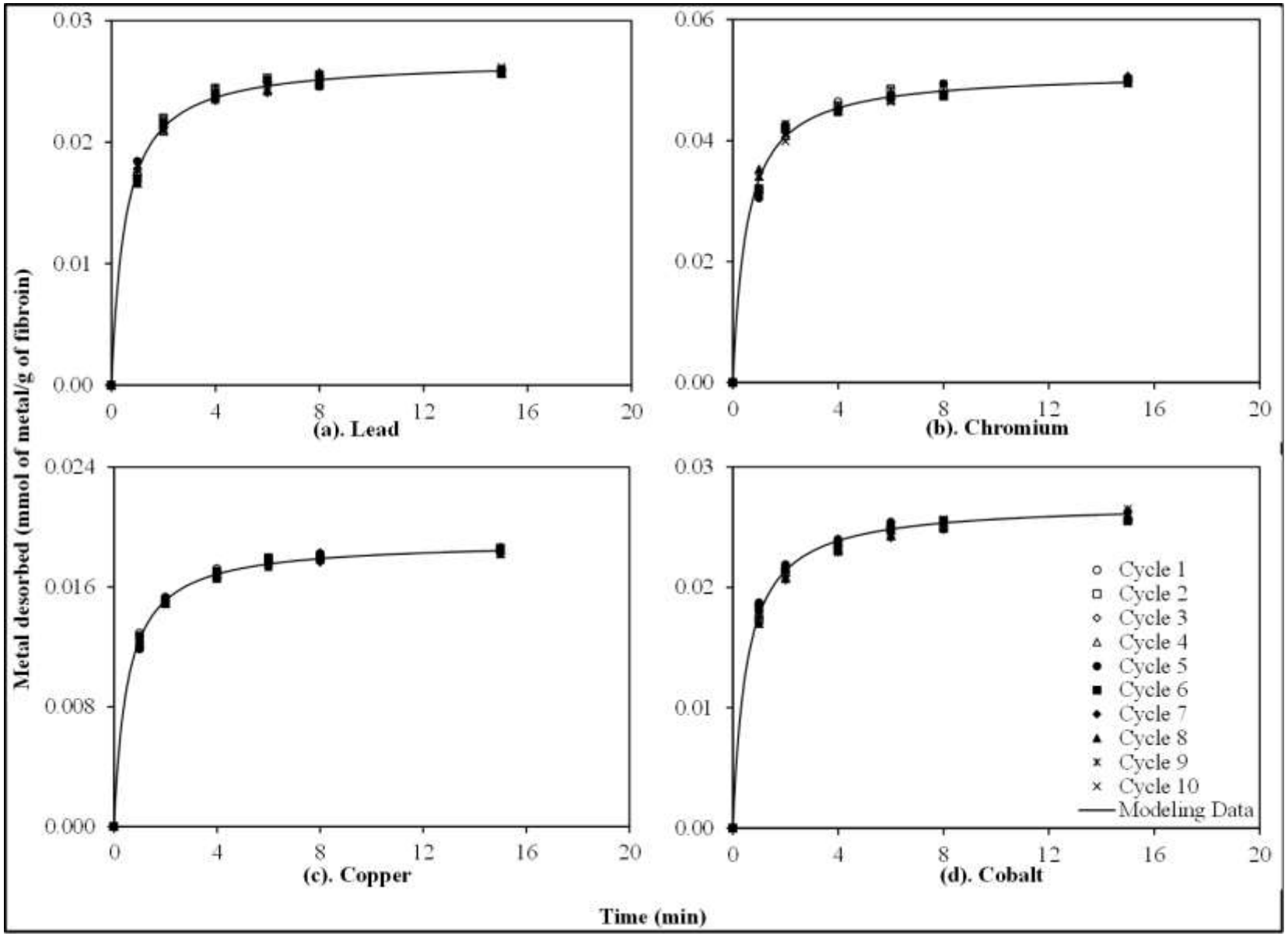

Figure 4.8 Comparison of experimental kinetic data, up to ***ten cycles,*** and modeled data using equation 4.31 for the desorption of (a). Lead, (b). Chromium, (c). Copper and (d). Cobalt from fibroin to EDTA solution.

For the analysis of desorption kinetic data up to ten cycles, similar steps were repeated though equation 4.31 was used. Desorption kinetic data up to ten cycles in comparison with the modeled data is presented in Figure 4.8. It also shows a good agreement between experimental and modeled data. The kinetic data for adsorption and desorption is described quite well by the equations 4.29 and 4.31, respectively.

Table 4.7 Kinetic rate constants of adsorption and desorption, calculated from data fitting to equation 4.29 and 4.31 respectively, for all metals.

Metal	Langmuir constants used for data fitting		Initial concentration used for adsorption		Adsorption rate constant k_2	Desorption rate constant k_d
	b	q_m				
	(L/mmol)	(mmol/g)	(ppm)	(mmol/L)	(g/mmol.min)	(g/mmol.min)
Lead	1.91	0.03	500	2.4	22.5	63.4
Chromium	0.13	0.14	250	4.8	4.3	58.5
Copper	0.29	0.04	250	4.9	48.7	66.5
Cobalt	0.26	0.04	500	8.5	32.6	60.9

The calculated values of adsorption and desorption rate constants are presented in Table 4.7. The values of k_2 reflect an average of ten adsorption cycles. Similarly, the values of k_d, for all metals, also reflect an average of ten desorption cycles. Table 4.7 shows a contrast between the values of rate constant for adsorption and desorption. The values of adsorption rate constants for all metals are lower than the values of desorption rate constants. This could be due to the fact that the metal is desorbed in a very short period of time as compared to the time taken by the adsorption to achieve equilibrium. For the desorption, once the metal ions left the adsorbent surface, they were captured by the EDTA to form a chelate [148,149]. As discussed earlier, the adsorption of metal ions on fibroin surface could be a physical phenomenon, whereas the desorption is driven by the strong charge affinity of free radicals present on EDTA. This could be one of the reasons for the shortened time for desorption and contributed for the higher values of desorption rate constant k_d.

Zhang et al.[139] reported similar results in a study of dynamics of Cu(II) removal by adsorption on a membrane made up of *Penicillium* biomass. This separation was carried out in batch as well as continuous process. They evaluated the sorption performance of *Penicillium* membrane packed bed column in ten adsorption-desorption cycles. For desorption, 0.05M HCl was used as an eluting agent. A comparison of

adsorption and desorption breakthrough curves up to ten cycles was reported. The change in uptake capacity of adsorbent after ten adsorption cycles was almost negligible. The desorption curves obtained for all cycles exhibit a similar trend. The membrane of *Penicillium* biomass was reported as a good adsorbent that can be regenerated and reused for the removal of Cu(II) from aqueous solutions effectively.

Yazid et al.[65] used three different salt solutions as eluting agent while performing the desorption of Cd(II) from *activated dates pedicels.* They used NaCl, KCl and $CaCl_2$ at various concentrations to determine the most efficient agent of desorption. NaCl was found to be the most efficient desorbing agent, and it desorbed around 82% of Cd(II) from biosorbent. The sorption of Cd(II) on *activated dates pedicels* was declared as an ion exchange and Ca^{2+} was more exchangeable for Cd^{2+} than K^+ and Na^+.

4.5 CONCLUSIONS

Batch adsorption experiments for the removal of lead, chromium, copper and cobalt from aqueous solution were carried out where fibroin was used as an adsorbent. The adsorption equilibrium, kinetics and cyclic adsorption-desorption for all metals on fibroin showed the following:

- The adsorption of metal ions from aqueous solution to fibroin followed Langmuir isotherm.
- The calculated adsorption free energy ΔG for metal ions on fibroin suggested that it is a physical adsorption.
- The thermodynamic evaluation of the adsorption indicated that the adsorption is spontaneous and endothermic.
- Kinetic rate constant k_2 is independent of initial adsorbate concentration, but it is different for different metals.
- A multi linear trend of intraparticle diffusion model showed that the adsorption of all metals on fibroin is not only controlled by the intraparticle diffusion and possibly more than one mechanism is involved.
- There is not a considerable change in the uptake capacity and the rate of adsorption even after ten cycles of adsorption and desorption, and thus fibroin can be reused repeatedly as an adsorbent.

CHAPTER 5

PACKED BED ADSORPTION COLUMN

5.1 INTRODUCTION

Columns studies are needed to assess the required contact time, and the results obtained from batch adsorption studies may not be applied directly for field applications for the treatment of wastewater. The characteristics of dynamic adsorption system in contrast with batch adsorption have more emphasis for environmental applications because complete mass transport occurs with the flow of liquid along the length of column. The dynamic behavior of adsorption in column involves saturation along the column in relation to time, adsorbent density and column length simultaneously [93,150]. The efficiency of the adsorption column is generally better than that of the batch adsorption process. In an adsorption column, the adsorbent is packed uniformly; as the liquid flows through the adsorber, the adsorbent will absorb metal ions before approaching its equilibrium [95,151]. In the adsorption column, once the adsorbent gets saturated with the adsorbate, no additional metals ions can be detained and regeneration of the bed is needed. In a batch operation, both the adsorbent and the solution are mixed together. As the adsorbent gradually approaches the adsorption equilibrium, the decrease in metal concentration in the solution slows down. In an adsorption column, the equilibrium established between the adsorbent and solution is dynamic, and there is a concentration front that moves along the column length. There is always a contact with the fresh adsorbent before the column becomes exhausted.

For the removal of metals ions like lead, chromium, copper and cobalt, the kinetics and equilibrium of adsorption have been explored in a batch system. These results are relevant to column studies where fibroin is packed in a column in order to

study its dynamic adsorption behavior. The parameters derived after this study, are useful for adsorber design.

5.2 EXPERIMENTAL

The experimental setup for a continuous adsorption system consists of a 12cm long glass column with a diameter of 0.35cm. 0.8g of fibroin was packed uniformly and firmly into the column with the help of a glass rod. The height of fibroin bed in the column was 10cm. For an even liquid flow across the column's cross-sectional area and to neglect channeling effects, a flow controlling valve was mounted at the exit of the column. The schematic of the column arrangement is shown in Figure 5.1. During the column study, the height of the pack bed (10cm), diameter (0.35cm) and the mass of adsorbent (0.8g) were kept constant. The flow rate was controlled by the valve mounted at the bottom (downstream) of the column. During the operation, the metal concentration in the collected samples of effluent from the downstream of the column was monitored by an InoLab Cond Level 2 conductivity meter. The effect of adsorbate concentration, the effect of effluent flow rate and the reusability of adsorbent for fixed bed column packed with fibroin was studied. (*Note:* Height of column and height of packed bed are two different parameters. In subsequent discussion, height of packed bed i.e., 10cm is used in all calculation.)

To study the effect of initial concentration of adsorbate on the dynamic adsorption, the influent solution of each metal (i.e., Lead, Chromium, Copper and Cobalt) with a concentration of 12, 25, 50 and 75ppm was introduced from a holding flask mounted at the top of the column. The liquid flowed through the column under gravity. During these experiments, the effluent flow rate was kept constant at 0.15ml/min for all influent solutions.

The effect of flow rate on the performance of the adsorption column was studied by varying the flow of effluent (0.15, 0.18, 0.21 and 0.24ml/min) while the inlet concentration of metal ions in the feed solution was kept constant at 12ppm.

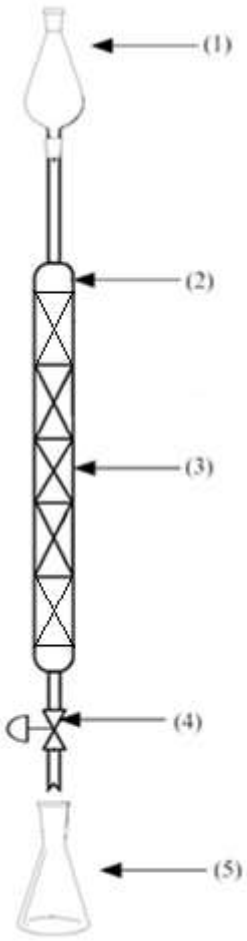

(1). Feed Funnel
(2). Adsorption Column
(3). Fibroin Bed
(4). Flow Control Valve
(5). Sample Collection Flask

Figure 5.1 Schematic diagram of fibroin packed bed column to study dynamic adsorption in laboratory.

The flow of influent through the column was under gravity. In order to setup a constant flow rate through the column, deionized water was introduced into the column and it was measured manually. The opening of the flow control valve was fixed at some specific position and the collected volume in a unit time was recorded. An arithmetic average of ten measurements of flow rate was used. The calculated flow measurements and their average at each flow level are presented in Table B.1 (Appendix B). The influent level into the feed funnel remained almost constant. It offered no change to the influent flow rate flowing through the column.

The reusability of fibroin in the adsorption column was evaluated by using an ethylenediaminetetraacetic acid (EDTA) solution in order to regenerate the bed. The feed solutions of lead, chromium, copper and cobalt to the column were at an inlet concentration of 12ppm and a flow rate 0.15ml/min. The breakthrough data for the adsorption of metals on fibroin bed was recorded. Once the adsorption bed was saturated with metal ions as the outlet concentration from the column became equal to inlet concentration (i.e., $C=C_o$), 0.05M EDTA was introduced into the column at a flow rate of 0.15ml/min for 30min, followed by flowing with deionized water at a flow rate of 0.24ml/min for 10min. This corresponded to 4.5ml of EDTA solution and 2.4ml of deionized water passing through the column. The purpose of EDTA was to desorb the metal ions adsorbed in fibroin bed and then water was flown through the column to rinse it and make it free of EDTA. In order to find whether the bed was regenerated properly with EDTA or not, the water sample collected at the end of water rinse was analyzed for presence of metal ions using conductivity meter. Once it was confirmed that the adsorption bed is free of the metal, the feed metal solution was introduced into the column again with the same flow rate and the inlet concentration, for a second adsorption cycle. The new breakthrough data was recorded until the fibroin bed got saturated with metal ions. The adsorption and desorption steps were repeated for up to four times to test the column performance under cyclic conditions.

5.3 RESULTS AND DISCUSSION

The time for the appearance of breakthrough and the shape of the breakthrough curve are very important characteristics for determining the operation and the dynamic response of adsorption column. In other words, the breakthrough curve gives an insight of performance of a pack bed column. The general position of the breakthrough curve along the time axis depends on the capacity of column with respect to the feed concentration, bed height and the flow rate [152].

Breakthrough curves for metal adsorption are made by plotting the ratio of adsorbate concentration in effluent (C) leaving the column at any time and adsorbate concentration in effluent entering the column (C_o) versus time (t). The ratio (C/C_o) has a magnitude of 0 - 1 while the time range goes until the complete saturation of bed is

achieved and it happens when the metal concentration in inlet and exhaust stream became equal (i.e., $C = C_o$). The amount of metal ions adsorbed in the column can be determined from the area above the breakthrough curve constructed from (C/C_o) vs time.

The method adapted to calculate maximum uptake (equilibrium) capacity q_m of fibroin (mmol/g) packed in adsorption column is calculated by area under the plot of adsorbed metal concentration versus time (i.e., $1\text{-}C/C_o$ vs time). It could be expressed by the mass balance equation:

$$q_m = \frac{C_o.F}{1000\,m}\int_0^t \left(1 - \frac{C}{C_o}\right) \mathrm{dt} \qquad (5.1)$$

where C_o and C are the metal concentration in inlet stream and concentration at any time (ppm or mmol/L), F is the volumetric flow rate at which the effluent solution is passed through the column (L/min) and m is the mass of adsorbent packed into the column (g).

To determine the amount of metal ion adsorbed, the time required to get the bed saturated with metal ions, the height of bed needed to treat unit volume of effluent and the rate of adsorption under flow through column conditions, the breakthrough data were analyzed using a dynamic adsorption model. For breakthrough data analysis, three empirical models, i.e., the Yoon-Nelson model, the bed depth service time model, and the Thomas model, are used to fit the data. These models have been discussed already in Chapter 2 (Literature review). However, a brief discussion about data fitting to these models is presented here. The Yoon-Nelson model is described by the equation:

$$t = \tau + \frac{1}{k_y} ln\left(\frac{C}{C_o - C}\right) \qquad (5.2)$$

For fitting the breakthrough data into the Yoon-Nelson model, time t against $ln\left(\frac{C}{C_o - C}\right)$ is plotted, which gives a straight line. The constants τ and k_y in this model can be calculated from its intercept and slope.

The experimental data is also fitted to the Bed depth service time model, which is described by the following expression:

$$t_b = \frac{N_o}{uC_o} z - \frac{1}{k_b C_o} \ln\left(\frac{C_o}{C} - 1\right) \qquad (5.3)$$

which is similar to the Thomas equation. The vales of k_b and N_o can be calculated from the slope and intercept of t_b vs $ln\left(\frac{C_o}{C} - 1\right)$ plot.

The linearized form of the Thomas model is given as:

$$\ln(\frac{C_o}{C} - 1) = k_t \frac{mq_o}{F} - k_t \frac{VC_o}{F} \qquad (5.4)$$

The Thomas rate constant (k_t) and maximum solid phase concentration (q_o) can be evaluated by plotting $\ln(\frac{C_o}{C} - 1)$ versus effluent volume V, which yields a straight line. The slope of this straight line is used for the calculation of k_t and intercept is used to determine the maximum solid phase concentration q_o.

5.3.1 EFFECTS OF INFLUENT CONCENTRATION

The adsorption performance of fixed bed fibroin column was tested at various inlet metal concentrations ranging from 12 to 75ppm for all metals. The breakthrough curves are in Figures 5.2(a), (b), (c), and (d) for lead, chromium, copper and cobalt, respectively. As expected; at a higher influent concentration, the breakthrough was achieved earlier. At saturation, the amount of metal adsorbed by fibroin bed is calculated using equation 5.1, and the results are shown in Table 5.1.

The change in inlet concentration of influent affects the column performance, and the time to achieve breakthrough decreases with an increase in the inlet concentration of metals in the influent. This is because that at a higher concentration, the binding sites available on fibroin become occupied more quickly with metal ions which caused the adsorbent to exhaust more rapidly. By increasing the influent concentration, the maximum uptake capacity of fibroin q_m also increases. The increase in uptake capacity of fibroin with an increase in metal concentration in the solution has been studied in Chapter 4.

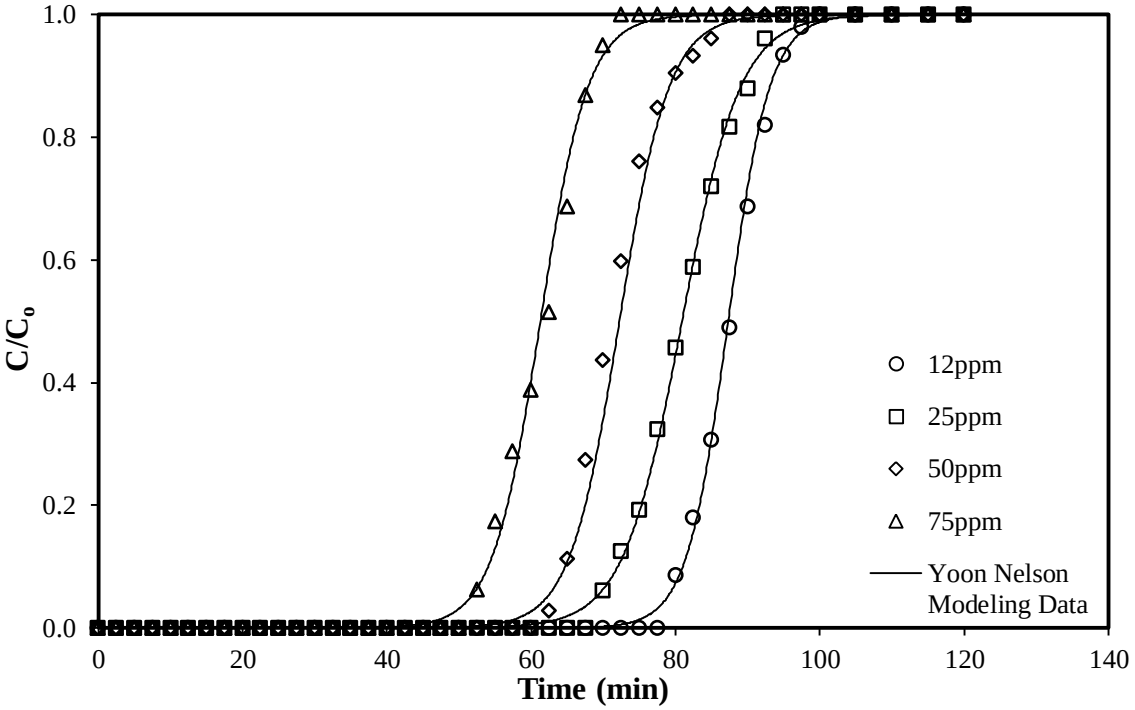

Figure 5.2(a) Comparison of experimental and Yoon-Nelson modeled breakthrough curves for the separation of ***lead*** exiting the fibroin packed bed column at different inlet concentrations.

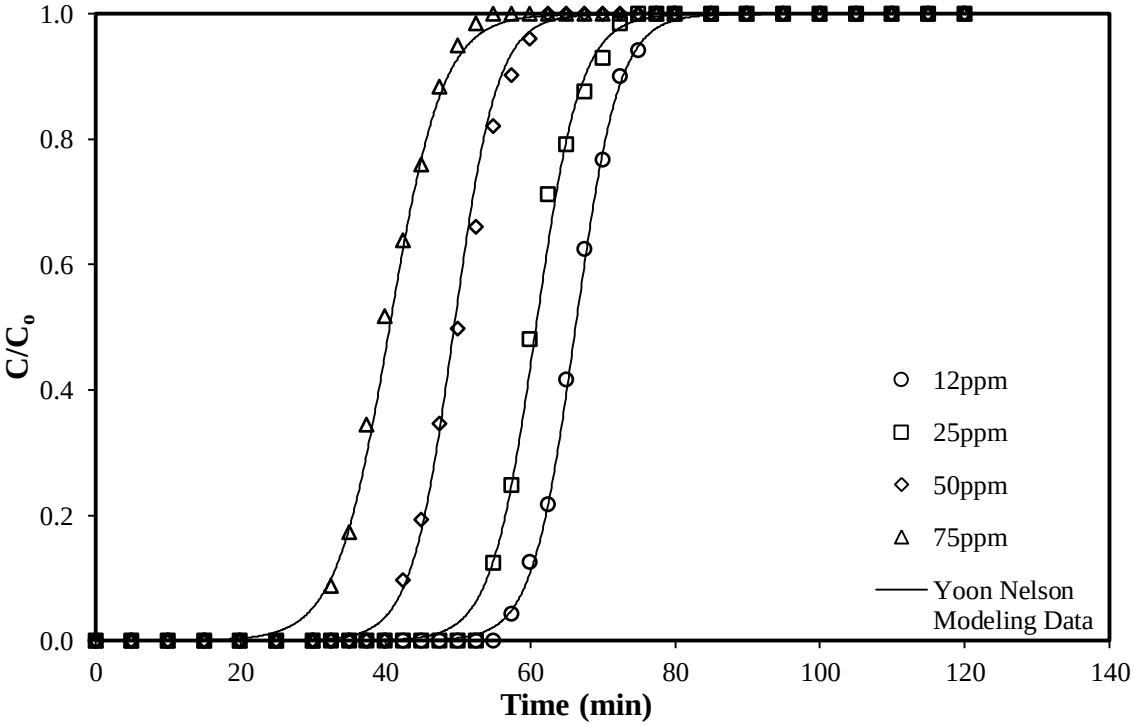

Figure 5.2(b) Comparison of experimental and Yoon-Nelson modeled breakthrough curves for the separation of ***chromium*** exiting the fibroin packed bed column at different inlet concentrations.

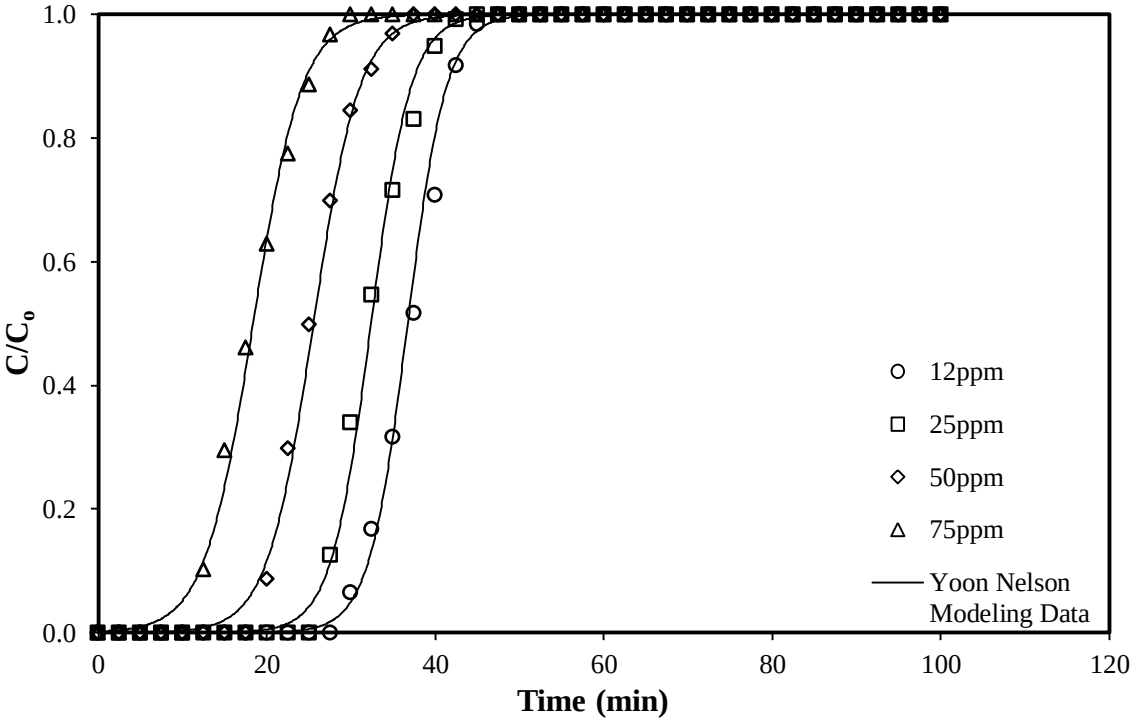

Figure 5.2(c) Comparison of experimental and Yoon-Nelson modeled breakthrough curves for the separation of ***copper*** exiting the fibroin packed bed column at different inlet concentrations.

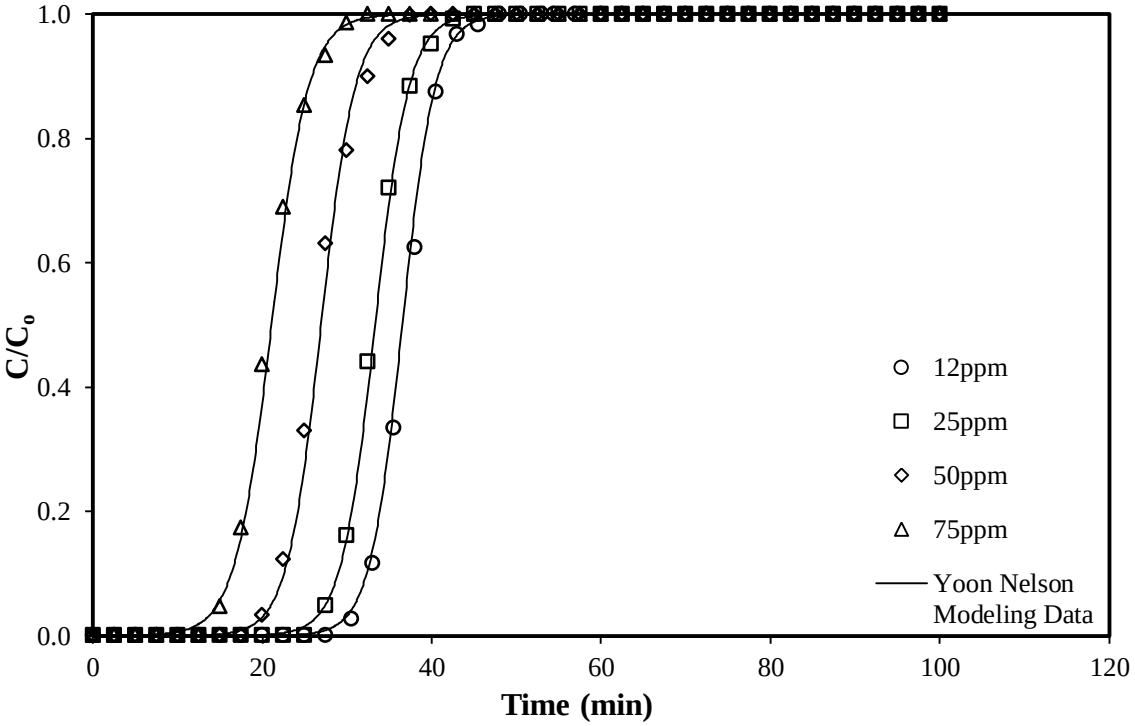

Figure 5.2(d) Comparison of experimental and Yoon-Nelson modeled breakthrough curves for the separation of ***cobalt*** exiting the fibroin packed bed column at different inlet concentrations.

The breakthrough data in Figure 5.2 was fitted to the Yoon-Nelson model, Bed depth service time model and Thomas model. Data fitting to Yoon-Nelson model is presented in Figure 5.3. The calculated parameters of Yoon-Nelson model are presented in Table 5.2. The correlation coefficients R^2 for the data fitting are very close to 1, indicating a good fit of experimental data to the model. The values of τ, time to achieve 50% breakthrough decreases with an increase in the initial influent concentration for all metals studied. The Yoon-Nelson rate constant k_y for the adsorption of copper and cobalt tend to decrease slightly with an increase in the metal ion concentration, whereas no clear trend was observed for lead and chromium.

Table 5.1 Maximum saturation capacity of fibroin packed bed column at different influent concentration with constant flow rate of 0.15ml/min. (Bed height = 10cm, Diameter = 0.35cm, mass of fibroin = 0.8g)

Initial concentration (ppm)	Lead	Chromium	Copper	Cobalt
	Uptake at saturation (10^{-3} mmol/g)			
12	1.11	2.84	1.26	1.41
25	1.87	4.96	2.22	2.40
50	3.39	8.56	4.06	4.38
75	4.24	11.5	5.54	5.37

To validate the model, the calculated values of k_y and τ are used to regenerate the breakthrough curves for all metals. For this purpose, the Yoon-Nelson model equation is rearranged as follows:

$$\frac{C}{C_o} = \frac{C_o.\exp[k_y(t-\tau)]}{1+\exp[k_y(t-\tau)]C_o} \qquad (5.5)$$

The breakthrough curves predicted based on equation 5.5 is also shown in Figures 5.2(a), (b), (c) and (d) (solid lines). There is a good agreement between experimental data and model calculations.

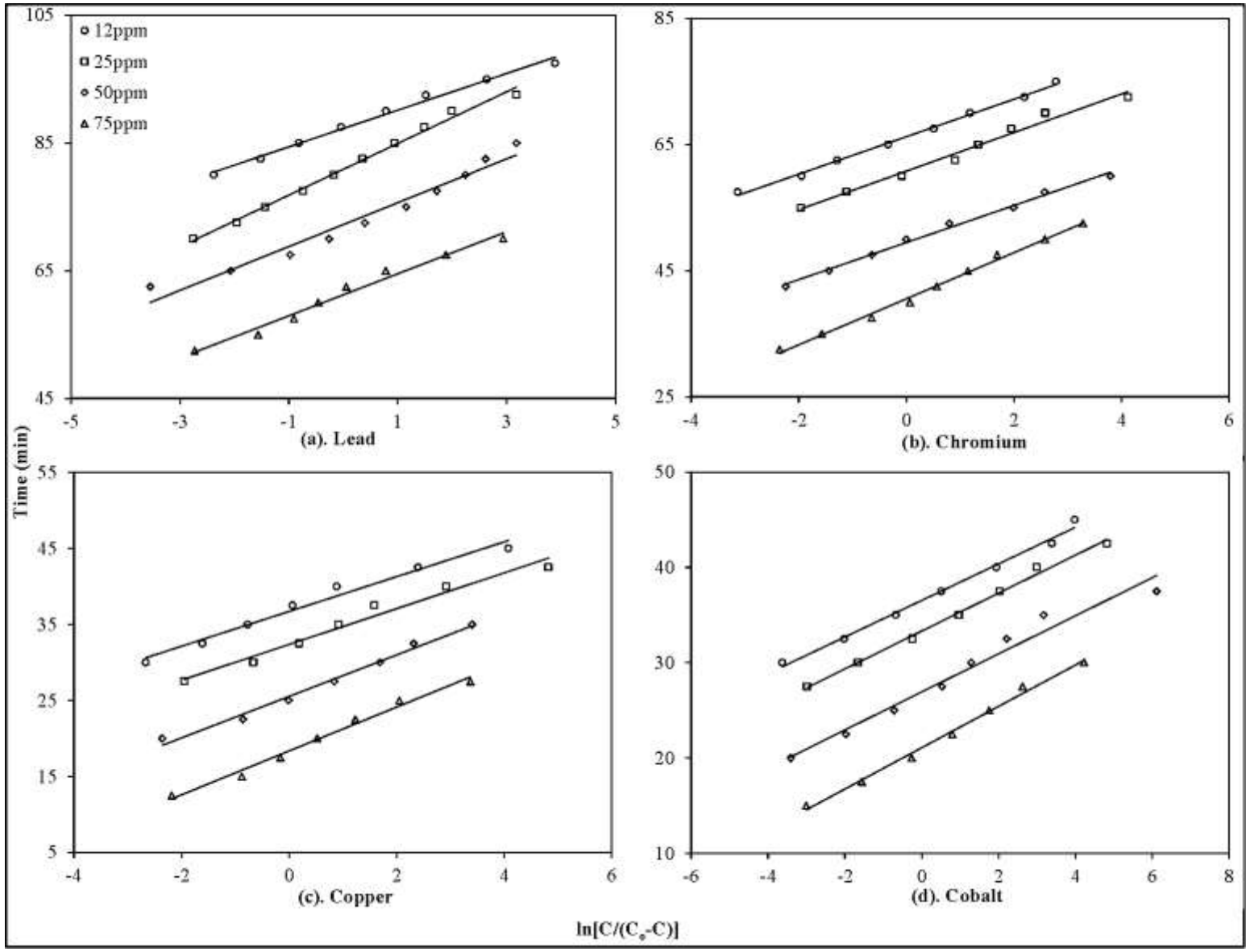

Figure 5.3 Breakthrough data fitting to Yoon-Nelson model for the separation of (a). *Lead* (b). *Chromium* (c). *Copper* and (d). *Cobalt* from effluent exiting the fibroin packed bed column at different inlet concentrations.

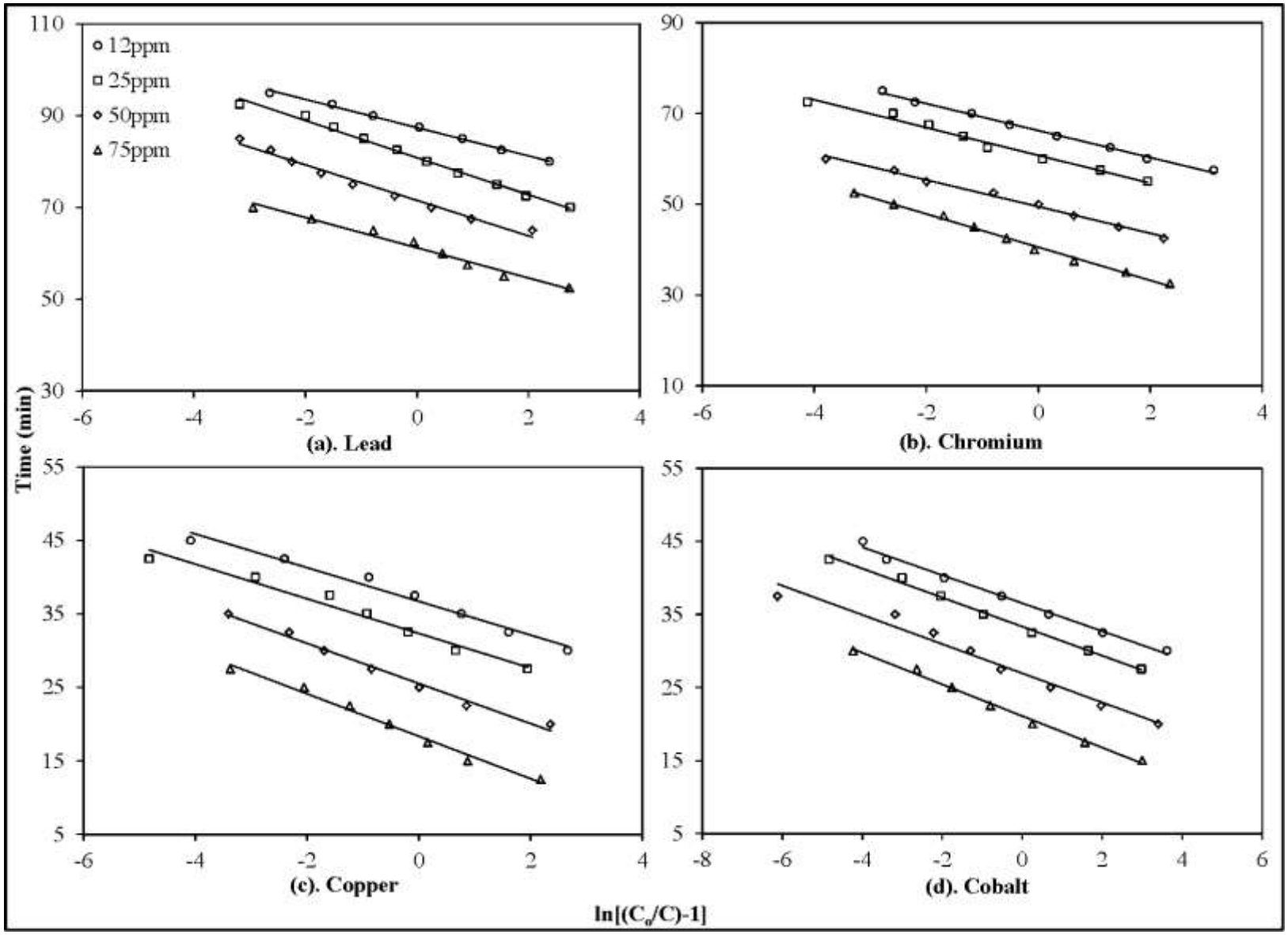

Figure 5.4 Breakthrough data fitting to BDST model for the separation of (a). *Lead* (b). *Chromium* (c). *Copper* and (d). *Cobalt* from effluent exiting the fibroin packed bed column at different inlet concentrations.

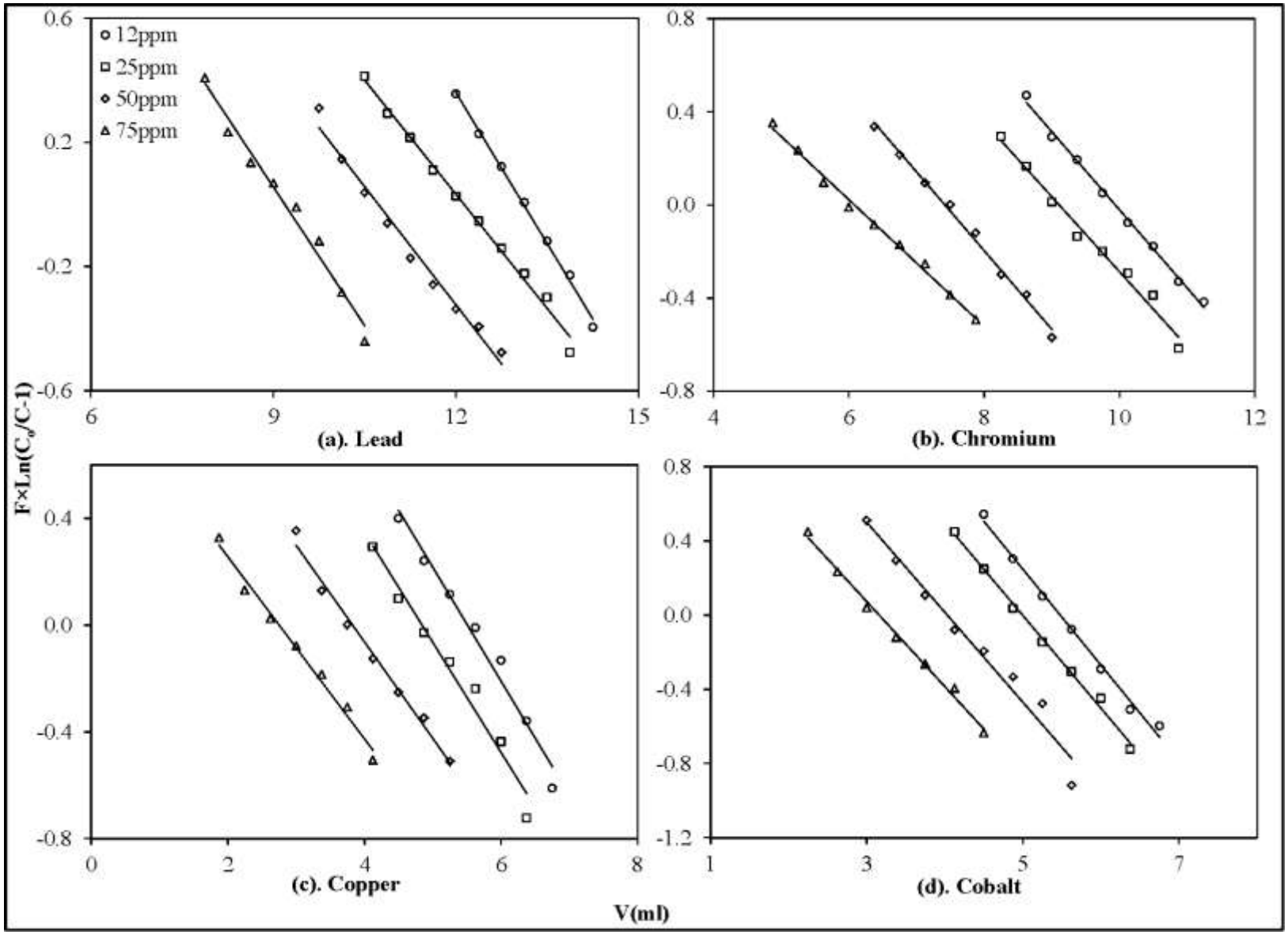

Figure 5.5 Breakthrough data fitting to Thomas model for the separation of (a). *Lead* (b). *Chromium* (c). *Copper* and (d). *Cobalt* from effluent exiting the fibroin packed bed column at different inlet concentrations.

Furthermore, the breakthrough data is fitted to the bed depth service time model, and the data fitting is presented in Figure 5.4. The values of characteristic parameters of the model, i.e., the dynamic sorption capacity of bed (N_o) and dynamic rate constant (k_b), are presented in Table 5.2 as well. A correlation coefficient R^2 close to 1 was obtained for the data fitting. With an increase in initial concentration of influent, the values of N_o also increased, and the rate constant k_b showed an opposite trend. Increasing the initial concentration of influent resulted in a reduction in the dynamic rate constant k_b of the BDST model.

Table 5.2 Parameters of Bed depth service time model, Thomas model and Yoon-Nelson model calculated from breakthrough data fitting of effluents exiting the column with different inlet concentrations.

Metal	Initial Conc. (ppm)	BDST Model			Thomas Model			Yoon-Nelson Model		
		R^2	N_o (mmol/L)	k_b (L/mmol.min)	R^2	q_o (10^{-3} mmol/g)	k_t (L/mmol.min)	R^2	τ (min)	k_y (min^{-1})
Lead	12	0.99	0.80	5.62	0.99	0.95	5.60	0.99	87.3	0.35
	25	0.99	1.52	2.05	0.99	1.83	2.03	0.99	80.9	0.25
	50	0.98	2.69	1.07	0.98	3.24	1.05	0.97	72.2	0.29
	75	0.98	3.48	0.84	0.98	4.16	0.82	0.98	61.3	0.30
Chromium	12	0.99	2.38	1.46	0.99	2.87	1.45	0.99	66.3	0.34
	25	0.98	4.56	0.68	0.98	5.48	0.67	0.98	60.8	0.33
	50	0.99	7.42	0.35	0.99	8.92	0.35	0.99	49.5	0.34
	75	0.99	9.12	0.20	0.99	10.97	0.19	0.99	40.6	0.27
Copper	12	0.98	1.08	2.31	0.98	1.30	2.26	0.98	36.7	0.44
	25	0.97	1.99	1.08	0.97	2.38	1.05	0.97	32.4	0.42
	50	0.99	3.14	0.47	0.99	3.77	0.46	0.99	25.5	0.37
	75	0.99	3.38	0.29	0.99	4.06	0.29	0.99	18.4	0.35
Cobalt	12	0.99	1.16	2.56	0.99	1.40	2.54	0.99	36.5	0.52
	25	0.99	2.20	1.19	0.99	2.65	1.18	0.99	33.3	0.50
	50	0.97	3.56	0.59	0.97	4.28	0.57	0.97	26.9	0.50
	75	0.99	4.18	0.36	0.99	5.03	0.36	0.99	21.1	0.46

Similarly, the Thomas model was also tested to fit the experimental data for the adsorption of metal ions flowing through the fibroin packed bed column at different effluent concentrations. This is shown in Figure 5.5. The model parameters, dynamic rate constant k_t and maximum solid phase concentration $q_{o,}$ are evaluated and are presented in Table 5.2. The Thomas model also gave a good fit to the breakthrough data. The calculated Thomas rate constant k_t decreases with an increase in the influent concentration, while the maximum solid phase concentration q_o increases.

Rao et al.[96] found similar results while performing the dynamic adsorption of Cd(II) flowing through a packed bed column of *Syzygium cumini* leaf powder. With an increase in the initial Cd concentration, an increase in the uptake of adsorption and a decrease in the breakthrough time were reported. The breakthrough data also followed the BDST model, Yoon-Nelson model and the Thomas model; they reported similar effects of influent concentration on the model parameters.

5.3.2 EFFECTS OF INFLUENT FLOW RATE

The adsorption behavior of fibroin bed column was also influenced by the flow rate of influent. Other parameters, initial influent concentration, bed height, column diameter and mass of adsorbent packed into the column, remained constant throughout this study (Table 5.3). The flow rate of influent flowing through the column was changed as 0.15, 0.18, 0.21 and 0.24ml/min. The breakthrough curves for the adsorption of lead, chromium, copper and cobalt are shown in Figures 5.6 (a), (b), (c) and (d), respectively.

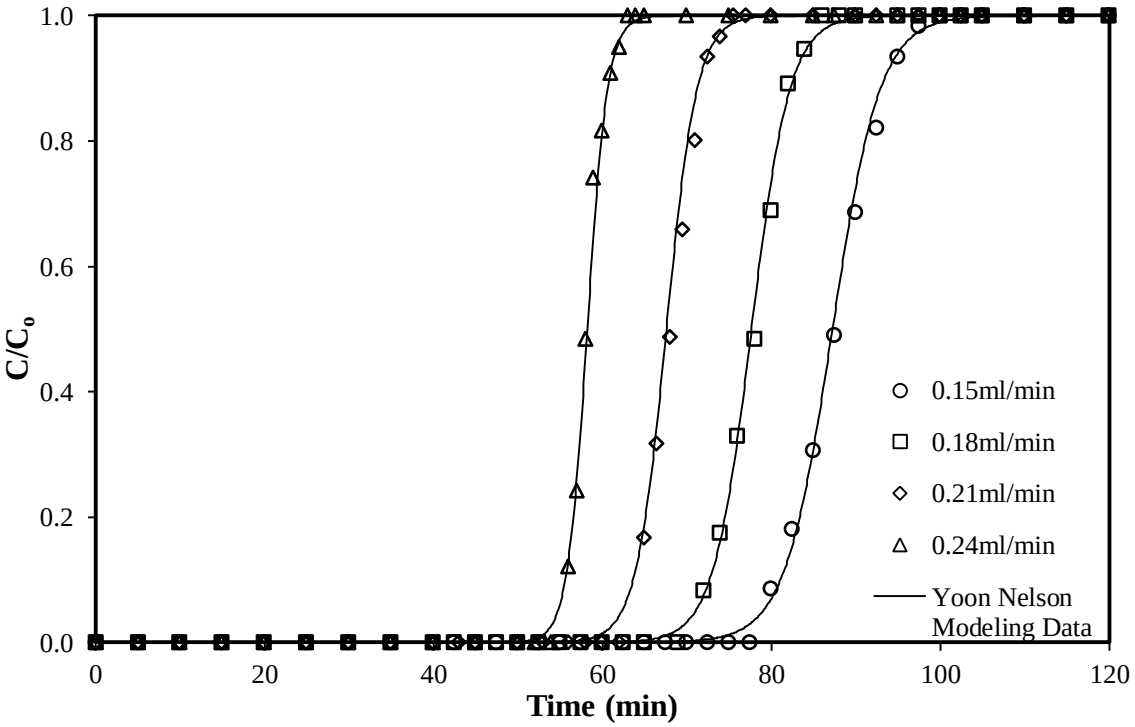

Figure 5.6(a) Comparison of experimental and Yoon-Nelson modeled breakthrough curves for the separation of ***lead*** exiting the fibroin packed bed column at different flow rates.

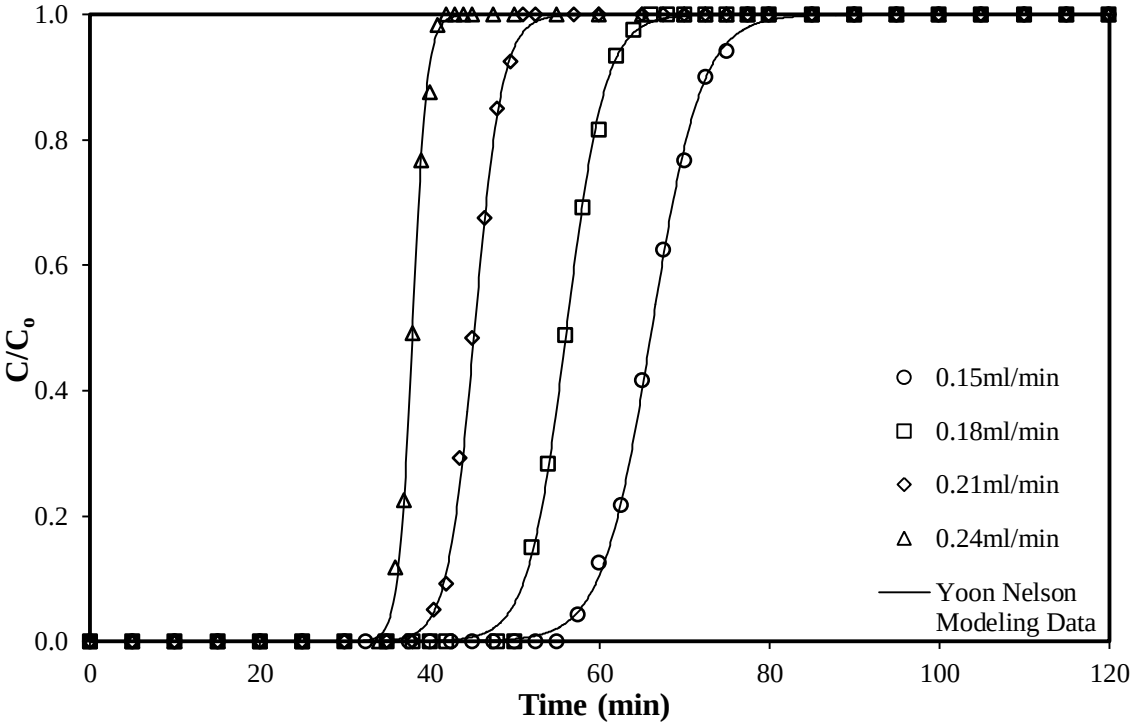

Figure 5.6(b) Comparison of experimental and Yoon-Nelson modeled breakthrough curves for the separation of ***chromium*** exiting the fibroin packed bed column at different flow rates.

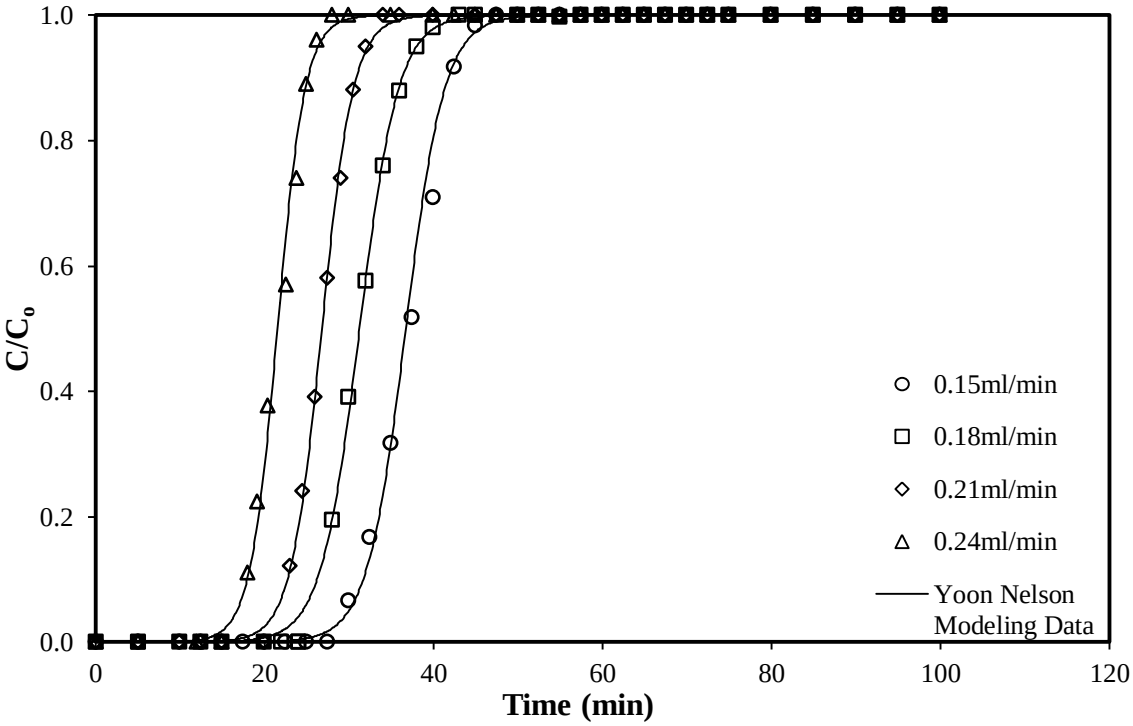

Figure 5.6(c) Comparison of experimental and Yoon-Nelson modeled breakthrough curves for the separation of ***copper*** exiting the fibroin packed bed column at different flow rates.

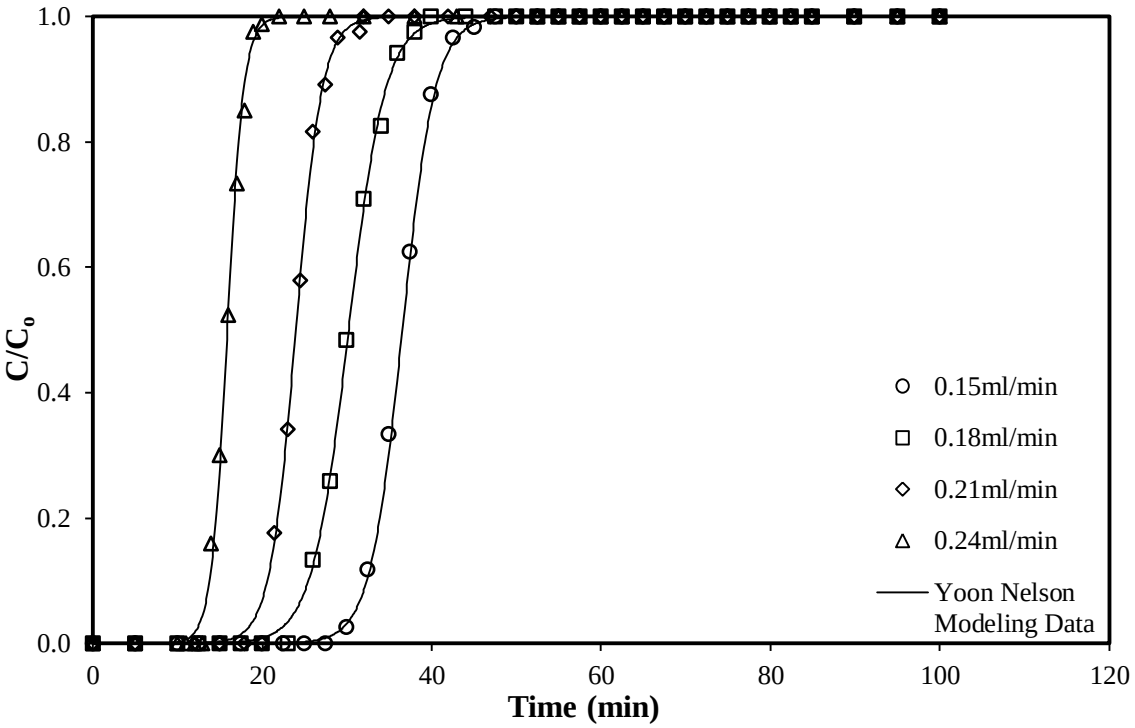

Figure 5.6(d) Comparison of experimental and Yoon-Nelson modeled breakthrough curves for the separation of ***cobalt*** exiting the fibroin packed bed column at different flow rates.

It was observed that with an increase in influent flow rate, the breakthrough was attained in a shorter period of time since the fibroin bed got saturated more quickly. The reason for the reduction in the breakthrough time is that at a higher flow rate, the metal ions were admitted to the adsorption bed faster, which caused the bed to get saturated faster.

Zhang et al.[97] used a fixed bed column packed with straw based adsorbents for the removal of methylene blue from an influent solution. An increase in flow rate of the solution showed the same effect on the uptake capacity of the bed, which was justified by the decrease in contact time between the influent solution and the adsorbent.

The values of maximum uptake capacity of fibroin packed bed column q_m at different flow rates are calculated using equation 5.1, and they are presented in Table 5.3. Apparently, the values of q_m at different influent flow rates are almost constant. This is easy to understand because q_m corresponds to the uptake when fibroin is the adsorption bed was in equilibrium with influent liquid.

Table 5.3 Maximum saturation capacity of fibroin packed bed column at different influent flow rates with constant inlet concentration of 12ppm. (Bed height = 10cm, Diameter = 0.35cm, mass of fibroin = 0.8g)

Inlet Flow Rate (ml/min)	Lead	Chromium	Copper	Cobalt
	Uptake at saturation (10^{-3} mmol/g)			
0.15	1.11	2.84	1.26	1.41
0.18	1.08	2.82	1.24	1.35
0.21	1.07	2.81	1.24	1.34
0.24	1.05	2.81	1.23	1.33

The adsorption breakthrough data were also fitted to the dynamic models, as shown in Figures 5.7 to 5.8. The model parameters so determined are shown in Table 5.4. In general, the data fit the models well. As an illustration, model calculations based on the Yoon-Nelson model are also shown in Figure 5.6, which shows a very good agreement with the experimental data. Note that the Thomas model was not included here simply because it is essentially the same as the BDST model, as shown by equations 5.3 and 5.4.

Table 5.4 Parameters of Bed depth service time model and Yoon-Nelson model calculated from breakthrough data fitting.

Metal	Influent Flow Rate (ml/min)	BDST Model			Yoon-Nelson Model		
		R^2	N_o (mmol/L)	k_b (L/mmol.min)	R^2	τ (min)	k_y (min^{-1})
Lead	0.15	0.99	0.79	5.62	0.99	87.3	0.36
	0.18	0.99	0.84	7.64	0.99	77.7	0.44
	0.21	0.99	0.86	9.60	0.99	67.6	0.56
	0.24	0.99	0.84	14.5	0.99	58.2	0.84
Chromium	0.15	0.99	2.38	1.46	0.99	66.3	0.34
	0.18	0.99	2.42	1.93	0.99	56.1	0.45
	0.21	0.99	2.28	2.70	0.99	45.3	0.62
	0.24	0.98	2.20	5.23	0.98	38.0	1.21
Copper	0.15	0.98	1.08	2.31	0.98	36.7	0.44
	0.18	0.99	1.11	2.31	0.99	31.3	0.44
	0.21	0.99	1.11	2.86	0.99	26.8	0.54
	0.24	0.98	1.02	3.24	0.98	21.5	0.62
Cobalt	0.15	0.99	1.16	2.56	0.99	27.7	0.52
	0.18	0.99	1.15	2.48	0.99	21.0	0.50
	0.21	0.97	1.07	2.83	0.97	16.0	0.58
	0.24	0.98	0.81	2.50	0.98	11.5	1.05

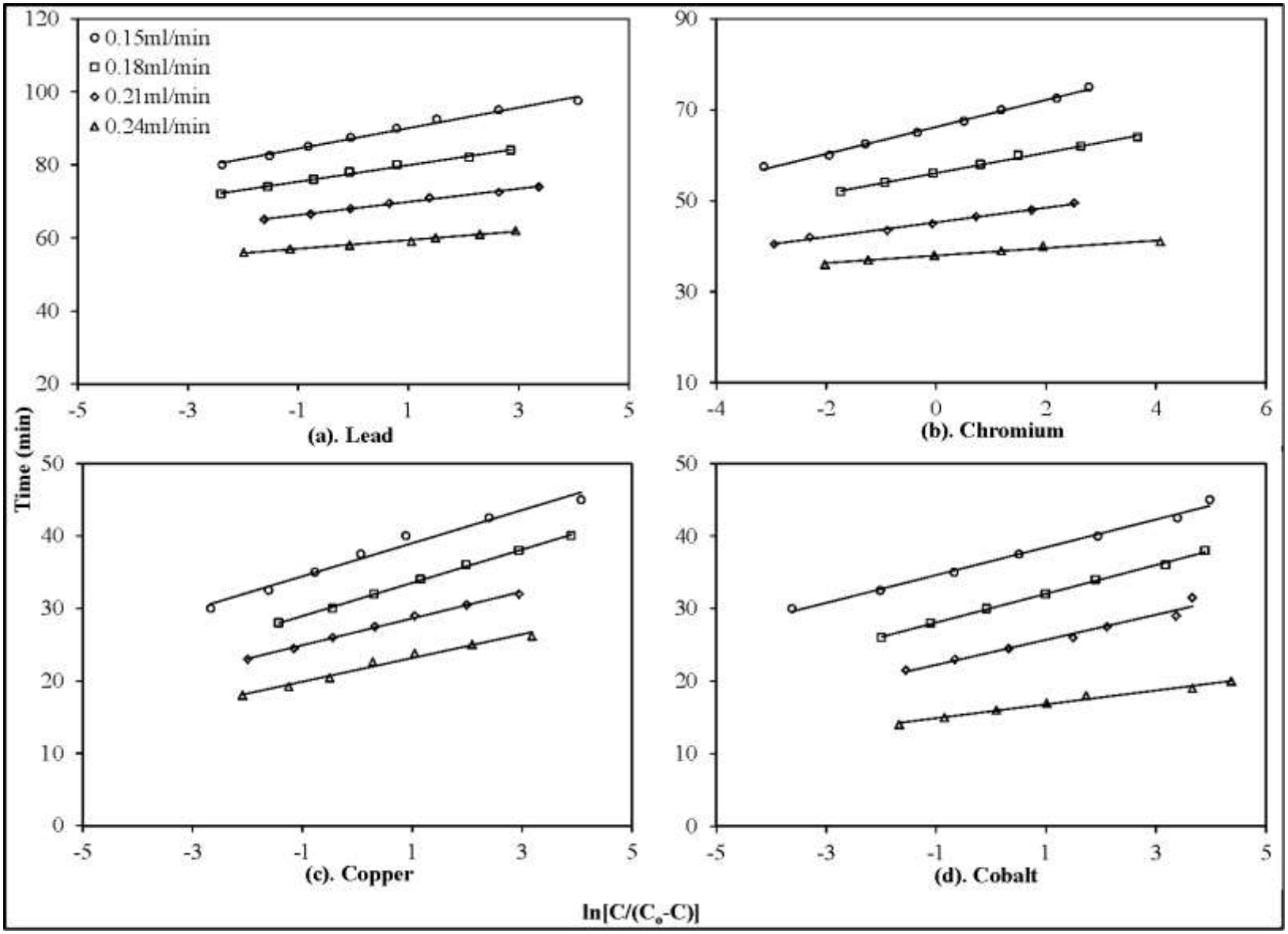

Figure 5.7 Breakthrough data fitting to Yoon-Nelson model for the separation of (a). *Lead* (b). *Chromium* (c). *Copper* and (d). *Cobalt* from effluent exiting the fibroin packed bed column at different flow rates.

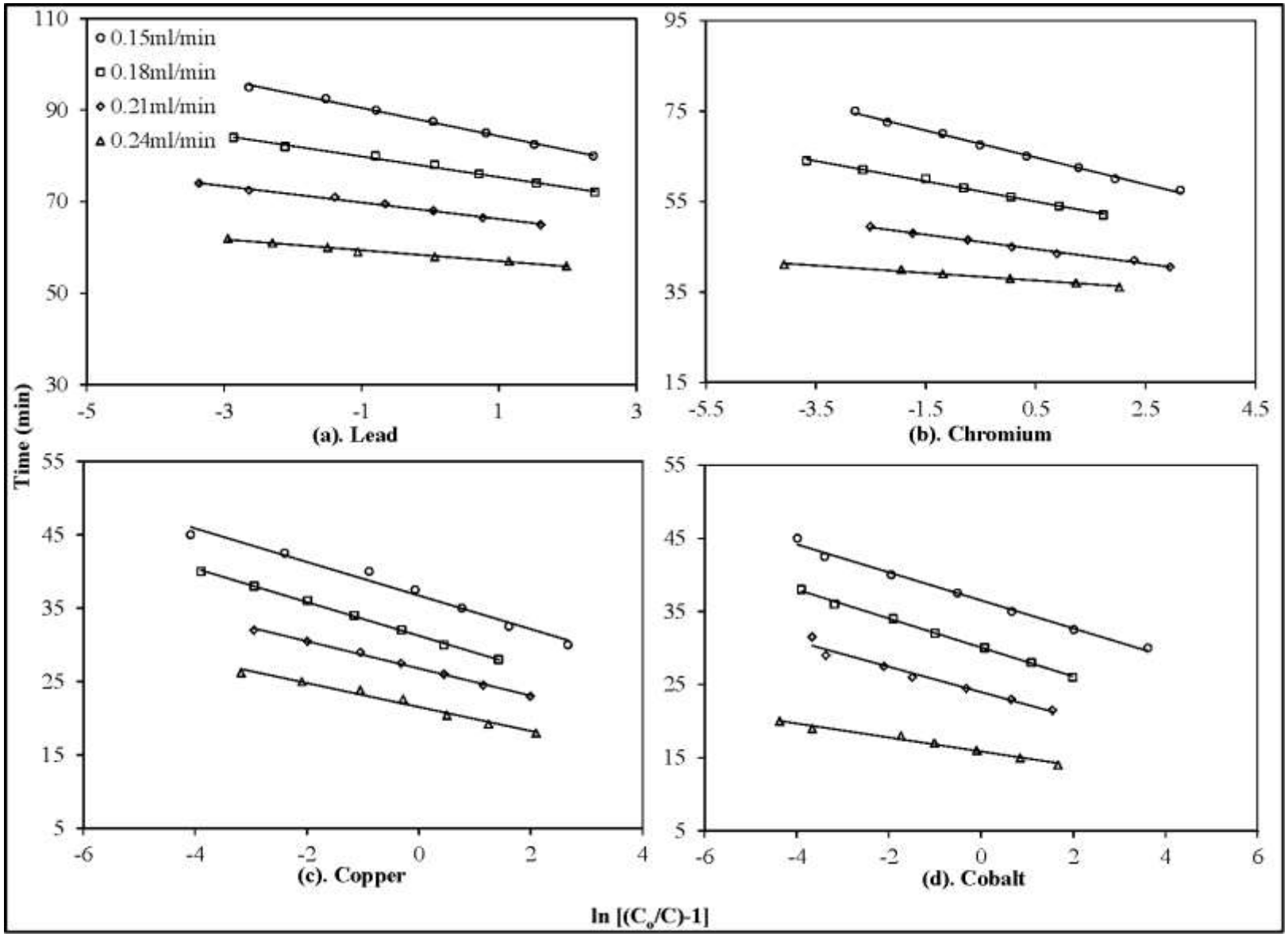

Figure 5.8 Breakthrough data fitting to BDST model for the separation of (a). *Lead* (b). *Chromium* (c). *Copper* and (d). *Cobalt* from effluent exiting the fibroin packed bed column at different flow rates.

The data in Table 5.4 shows that the dynamic rate constant k_b in the BDST model increases with an increase in flow rate for lead, chromium and copper, but no such a clear trend can be observed for cobalt sorption in the column. On the other hand, the adsorption capacity of the bed, N_o, was shown to be not affected by the influent flow rate. For the Yoon-Nelson model, τ was shown to be decreased with the flow rate, while the opposite was true for k_y.

Similar results were claimed by Agrawal et al.[101] while performing a dynamic adsorption studies for chromium adsorption on gelatin nanoparticles.

5.3.3 COLUMN REGENERATION

The regeneration of the adsorbent material is vital to practical uses of adsorption columns. The aim of this study was to remove the adsorbed metal ions from the column bed into a small volume of an eluting solution, which can be subjected to further treatment to recover the metals. To make the adsorbent reusable for cyclic adsorption and desorption, the regeneration should not compromise the capacity of the adsorbent.

After each adsorption cycle, the fibroin bed was regenerated by using 0.05M EDTA solution, and the adsorption breakthrough was evaluated again. This was repeated for at least 4 cycles. In this part of the study, the initial metal concentration, effluent flow rate, column diameter, mass of adsorbent and bed height were kept constant (Table 5.5). The breakthrough curves for the adsorption of lead, chromium, copper and cobalt are presented in Figures 5.9(a), (b), (c) and (d), respectively. It is shown that the uptake capacity of fibroin remains the same after regeneration with EDTA.

The metal uptake capacities are calculated by using equation 5.1 and are presented in Table 5.5. The fibroin bed was shown to be easily regenerated and could be used repeatedly after cyclic regeneration.

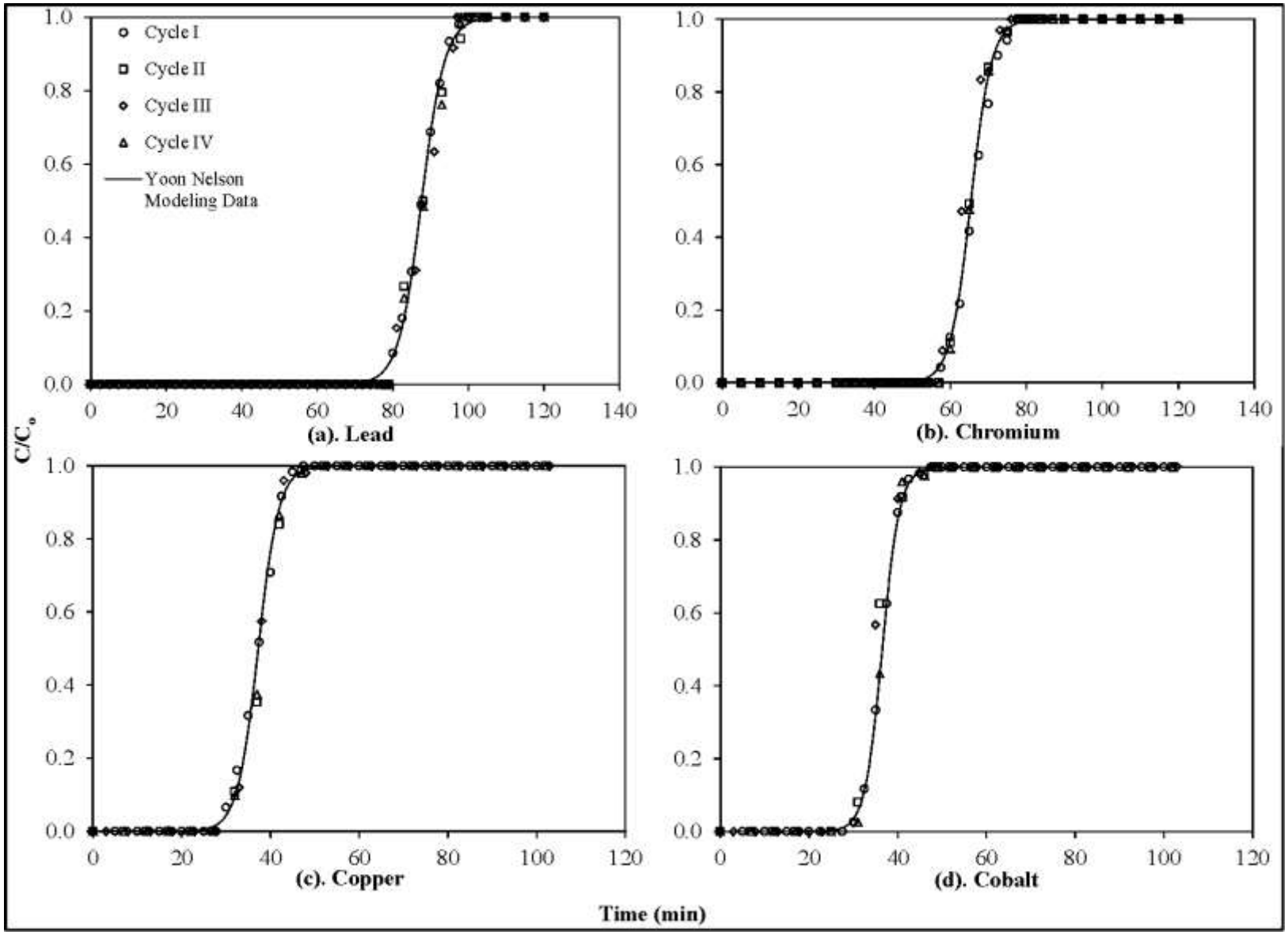

Figure 5.9 Comparison of experimental data and Yoon-Nelson modeled breakthrough curves for the separation of (a). *Lead* (b). *Chromium* (c). *Copper* and (d). *Cobalt*.

Table 5.5 Maximum saturation capacity of fibroin packed bed column for the adsorption of all metals. (Influent concentration = 12ppm, Flow rate = 0.15ml/min, Bed height = 10cm, Diameter = 0.35cm, mass of fibroin = 0.8g)

Adsorption Cycle	Lead	Chromium	Copper	Cobalt
	Uptake at saturation (10^{-3} mmol/g)			
I	1.11	2.86	1.26	1.41
II	1.09	2.87	1.26	1.42
III	1.11	2.86	1.25	1.41
IV	1.11	2.85	1.26	1.41

After regeneration, the adsorber bed showed the same breakthrough behavior, as the metal uptake and the rate of adsorption remained the same. Therefore, the breakthrough data of all four adsorption runs was taken as a single set for fitting to the Yoon-Nelson model, and a good fit to the data is observed (Figure 5.10). The calculated model parameters, time to achieve 50% breakthrough τ and dynamic rate constant k_y are reported in Table 5.6. The values of constants τ and k_y shows a good comparison with the values those were derived while the column was operated under different flow rates and different initial concentrations study (See data in Tables 5.2 and 5.4 for model parameters at 12ppm and 0.15ml/min). The model calculations based on the Yoon-Nelson model using the parameters so obtained are also shown in Figure 5.9 to compare with the experimental data. Again, the fitted Yoon-Nelson model was shown to describe the experimental data well.

Table 5.6 Parameters of Yoon-Nelson model calculated from breakthrough data fitting of multiple adsorption cycles through the column.

Metal	R^2	τ (min)	k_y (min^{-1})
Lead	0.96	87.6	0.33
Chromium	0.97	65.4	0.37
Copper	0.97	37.3	0.43
Cobalt	0.96	36.5	0.51

Clearly, the fibroin packed bed column offered a potential to be used repeatedly for metal biosorption without any loss in its adsorption capacity, and the column regeneration could be done easily with a small amount of EDTA.

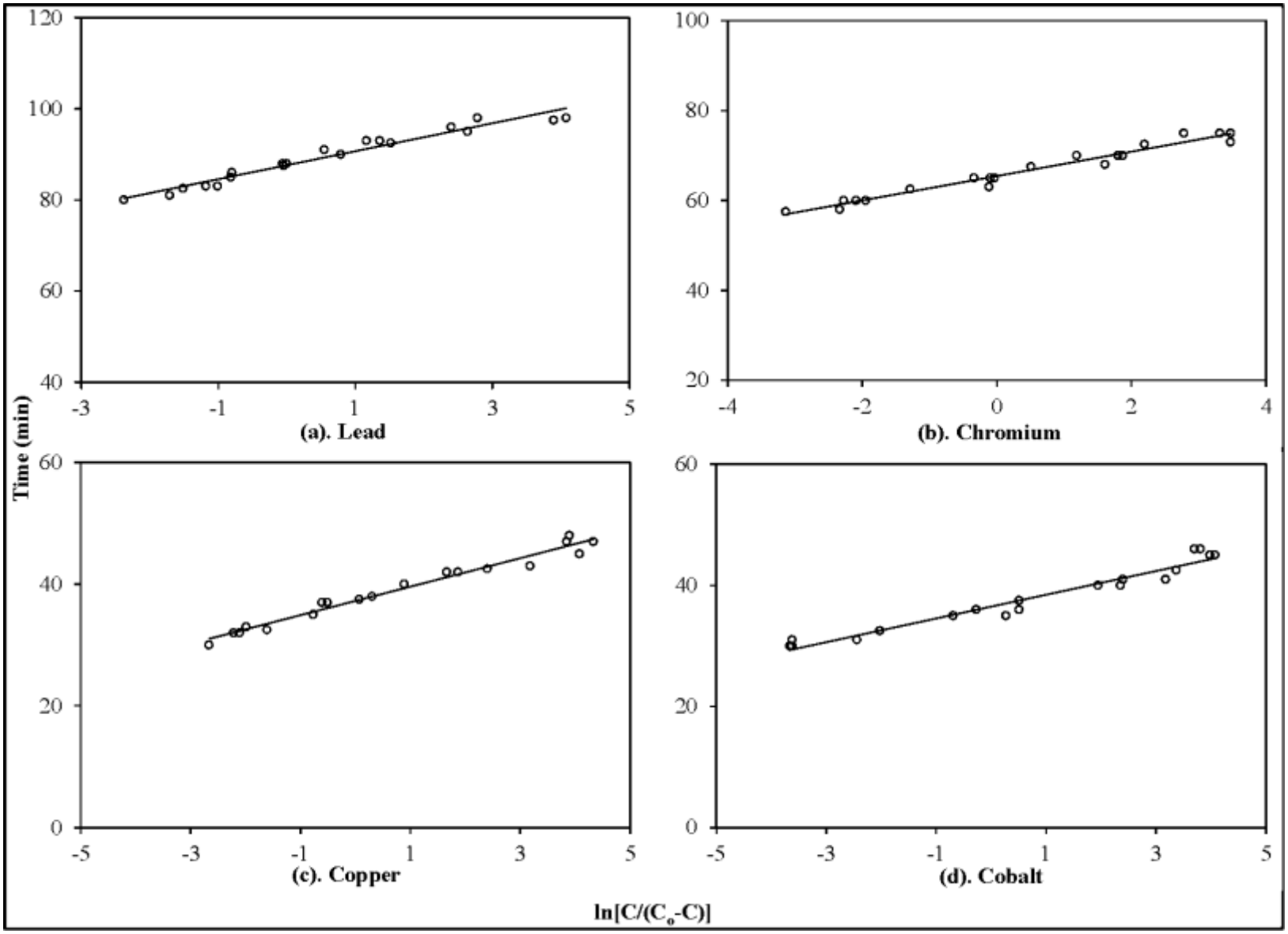

Figure 5.10 Fitting of combined data of four adsorption cycles to Yoon-Nelson model for the separation of (a). *Lead* (b). *Chromium* (c). *Copper* and (d). *Cobalt.*

5.4 CONCLUSIONS

In this chapter, adsorption of lead, chromium, copper and cobalt in a fixed bed column packed with fibroin was studied; the following conclusions can be drawn:

- An increase in saturation capacity of the fibroin bed with an increase in the influent concentration was due to the increase in the equilibrium effluent concentration.
- All the three models (i.e., Yoon-Nelson model, BDST model and Thomas model) fit well with the experimental data; the bed depth service time model and Thomas model, which have essentially a common basis, described the adsorption breakthrough equally well.
- The same adsorbent can be used for multiple adsorption cycles after regeneration with an EDTA solution, and there was no change in its metal uptake capacity after regeneration.

CHAPTER 6

ADSORPTION OF METAL IONS ON FIBROIN FILM

6.1 INTRODUCTION

Fibroin has proved itself a potential adsorbent for lead, chromium, copper and cobalt ions. The adsorption kinetics and equilibrium have been studied. However, an important adsorption aspect still needs to be explained is whether the adsorption of the metal ions is taking place onto the surface of fibroin or the ions adsorb deep inside the polymer network of fibroin. The surface area of adsorbent is one of the commonly measured properties in the evaluation of sorption performance of various adsorbents. Generally, the adsorbents with higher surface area are expected to have greater adsorption capacity than those with less surface area, owing to more exchange sites for the adsorbates [144,145].

Fibroin, in the fiber form, has showed a fast mass transfer due to its large surface area, as shown by the sharp breakthrough curves (Chapter 5). Efforts were made to use homogenous fibroin films, which had well defined areas and weights, for the adsorption study. This will help answer the above question as whether metal sorption occurs on the fibroin surface or in its interior, or both.

6.2 EXPERIMENTAL

6.2.1 PREPARATION OF FIBROIN FILMS

Preparation of fibroin film involves three steps.

- Dissolution of fibroin into a lithium salt solution.
- Separation of the lithium salt from fibroin by precipitation of fibroin in an alcohol.
- Formation of homogenous solution of fibroin in a solvent.
- Casting of fibroin films from the solution.

Lithium bromide forms a strong ionic solution in water and can break the hydrogen bonding between the long chains of fibroin proteins. 100ml of 9.5M lithium bromide solution was taken into a flask of 250ml, was sealed and heated to 85^{o}C. Then, 18g of fibroin was added to the hot lithium bromide solution in order to dissolve the fibroin by breaking the hydrogen bonding in the polymer chain. It took about 7hrs to dissolve fibroin completely at this temperature [153,154].

The fibroin solution was filtered through a stainless steel mesh screen (120 Mesh). The filtered fibroin solution was kept as stock and utilized to get fibroin in a slurry form when needed.

The next step was the separation of LiBr salt from this solution. In the literature, most of the researchers used dialysis for the separation of lithium bromide solution, which is extremely time consuming and uses a large amount of water [155-157]. In the present study, a different technique was developed for the removal of lithium salt from the fibroin. Ethanol was used for liquid-liquid contact [159,160]. About 400ml of ethanol was stirred at 300rpm and 5ml of the fibroin solution was dropped into ethanol drop by drop using a syringe, resulting in a slurry. This solution (lithium salt, ethanol and fibroin) was allowed to settle for about 8hrs, and ethanol and lithium salt was decanted out from the container. The remaining slurry was mixed with 2L of deionized water. After settling, the clear liquid phase (water, residual ethanol and LiBr) was removed, and the fibroin was placed in 2L deionized water. The procedure was repeated multiple times in order to make sure that all the lithium salt was removed from the fibroin. To ensure the complete removal of lithium bromide salt, the conductivity of water was monitored using an InoLab Cond Level 2 conductivity meter. The washing of fibroin slurry with deionized water was done repeatedly till no lithium bromide was detected in the rinsing water.

Then the fibroin slurry was filtered using a Whatman^{Tm} grade I filter paper with a pore size of 11μm to remove the water. This fibroin paste was dissolved in 98% formic acid to form a homogenous solution containing 100ml of formic acid by making a 16% (w/v) solution. This was close to the maximum solubility of fibroin in formic acid. Films having there different thicknesses (named as thickness A, B and C) were cast onto Pyrex® Petri-dishes of 75mm diameter using different weight of the fibroin solution.

After drying of the cast fibroin films for 12hrs, the petri-dishes were dipped into deionized water for about 12 hrs. The resulting fibroin films, swollen in water, were peeled off easily from the glass surface. The fibroin films of three different thicknesses A, B and C with a constant surface area of 72.63cm^2 were used to carry out an adsorption and desorption of the metal ions (i.e., lead, chromium, copper and cobalt). The thickness of each film was measured at ten different spots and an average was taken (Appendix C Table C.2). The specifications of the three films are shown in Table 6.1.

Table 6.1 Specifications of films A, B and C.

Film	Thickness (mm)	Dry Weight (g)
A	0.162	0.493
B	0.069	0.354
C	0.041	0.224

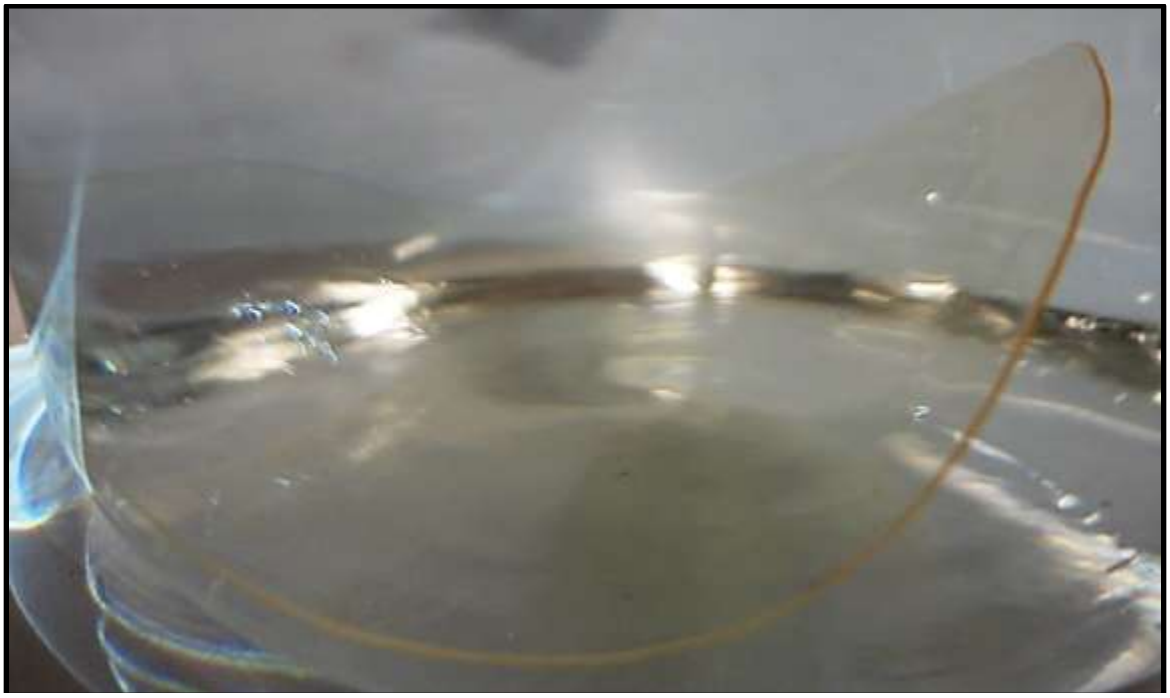

Figure 6.1 Water swollen fibroin film.

6.2.2 ADSORPTION EXPERIMENTS

A stock solution of 2000ppm Pb^{+2} was made by using lead acetate salt [$Pb(CH_3COO)_2$]. This stock solution was diluted to get 25, 100 and 500ppm concentration solutions. For the adsorption experiment, the fibroin film was immersed into a known volume of lead solution. The conductivity of lead solution was monitored

using an InoLab Cond Level 2 conductivity meter. The conductivity is converted to the solution concentration by using the calibration curve of each metal provided in Appendix A (Figures A.2-A.5). The adsorption kinetic data was monitored for 5 hours. From the change in lead concentration in the solution, the equilibrium sorption uptake of lead in fibroin film was calculated by using the following mass balance equation:

$$q_t = \frac{C_o - C_t}{m} V \qquad (6.1)$$

where V is the total volume of solute solution (L), m is the weight of adsorbent used (g), C_o is the initial concentration of the solute (mmol/L), and C_t is the concentration of the solute (mmol/L) in the solution at time t. When the batch sorption eventually reach an equilibrium, the equilibrium uptake was determined using equation 6.1 with C_t=C_e, where C_e is the equilibrium concentration of the metal in the solution.

During adsorption experiments, the ratio of volume of solution to the weight of membrane was kept constant in order to compare the results.

$$\frac{volume\ of\ solution}{weight\ of\ membrane} = constant \qquad (6.2)$$

Adsorption of chromium, copper and cobalt was also performed onto the fibroin films. Potassium chromate [K_2CrO_4], copper sulfate pentahydrate [$CuSO_4.5H_2O$] and cobalt acetate tetrahydrate [$C_o(CH_3COO)_2.4H_2O$] salts were used to make the feed solutions for adsorption experiments of Cr, Cu and C_o adsorption in the fibroin films.

6.2.3 DESORPTION EXPERIMENTS

Desorption study was carried out by using the fibroin films of three thicknesses A, B and C with constant surface area 72.63cm^2. Film A was soaked in lead solution of 80ml with an initial concentration of 500ppm until the equilibrium was achieved. It was done to load fibroin film with lead ions, and the amount of lead ions was calculated by using equation 6.1.

The fibroin film, saturated with known amount of lead ions, was immersed in 100ml of deionized water, and the change in conductivity was measured as metal desorption took place. The change in conductivity of the solution occurred due to migration of lead ions from the polymer network to the water. Eventually an adsorption equilibrium was established between the lead present in fibroin and water. As a result,

there was no more change in the conductivity of water. The conductivity was converted to concentration by using the calibration curve (Appendix A, Figure A.2). Then, the film was taken out of the saturated solution and immersed in 100ml of fresh deionized water for the second series of desorption experiments until a new equilibrium was established between lead in the liquid and the solid medium. Finally, the same fibroin film with a small amount of metal ions was introduced into a third batch of 100ml deionized water to carry out a third series of desorption experiments. Similarly, the fibroin films B and C were soaked into 80ml Pb^{+2} solutions having the initial concentration of 500ppm to load the metal in the films, followed by desorption experiments using the same procedure.

The desorption experiments for chromium, copper and cobalt ions were carried out for the all three films (A, B and C) as well. Potassium chromate [K_2CrO_4], copper sulfate pentahydrate [$CuSO_4.5H_2O$] and cobalt acetate tetrahydrate [$C_o(CH_3COO)_2.4H_2O$] were used to prepare the solutions for chromium, copper and cobalt, respectively. For metal loading in fibroin films, initial solution concentration for chromium and copper was kept 250ppm and for cobalt it was 500ppm.

6.3 RESULTS AND DISCUSSION

Kinetic data for the adsorption of lead, chromium, copper and cobalt on fibroin films (A, B and C) at different metal concentrations (i.e., 25, 100 and 500ppm) is presented in Figure 6.2. The fibroin films had different thicknesses but the same area, and thus the weights of films were also different. Once the metal uptake is normalized by the weight of the film, the kinetic data (i.e., metal uptake vs time) fell on a single line for all three thicknesses. The kinetic curves showed a similar trend once fibroin fibers were used as adsorbent, which is presented in Chapter 4. The uptake capacity of fibroin films, calculated by equation 6.1, is presented in Table 6.2.

To determine the adsorption rate constant k_2, the kinetic data was fitted to the same model used in Chapter 4.

$$\frac{dq_t}{dt} = k_2 \left[\frac{q_m}{1+\frac{1}{b\,(C_o-\frac{mq_t}{V})}} - q_t \right]^2 \qquad (6.3)$$

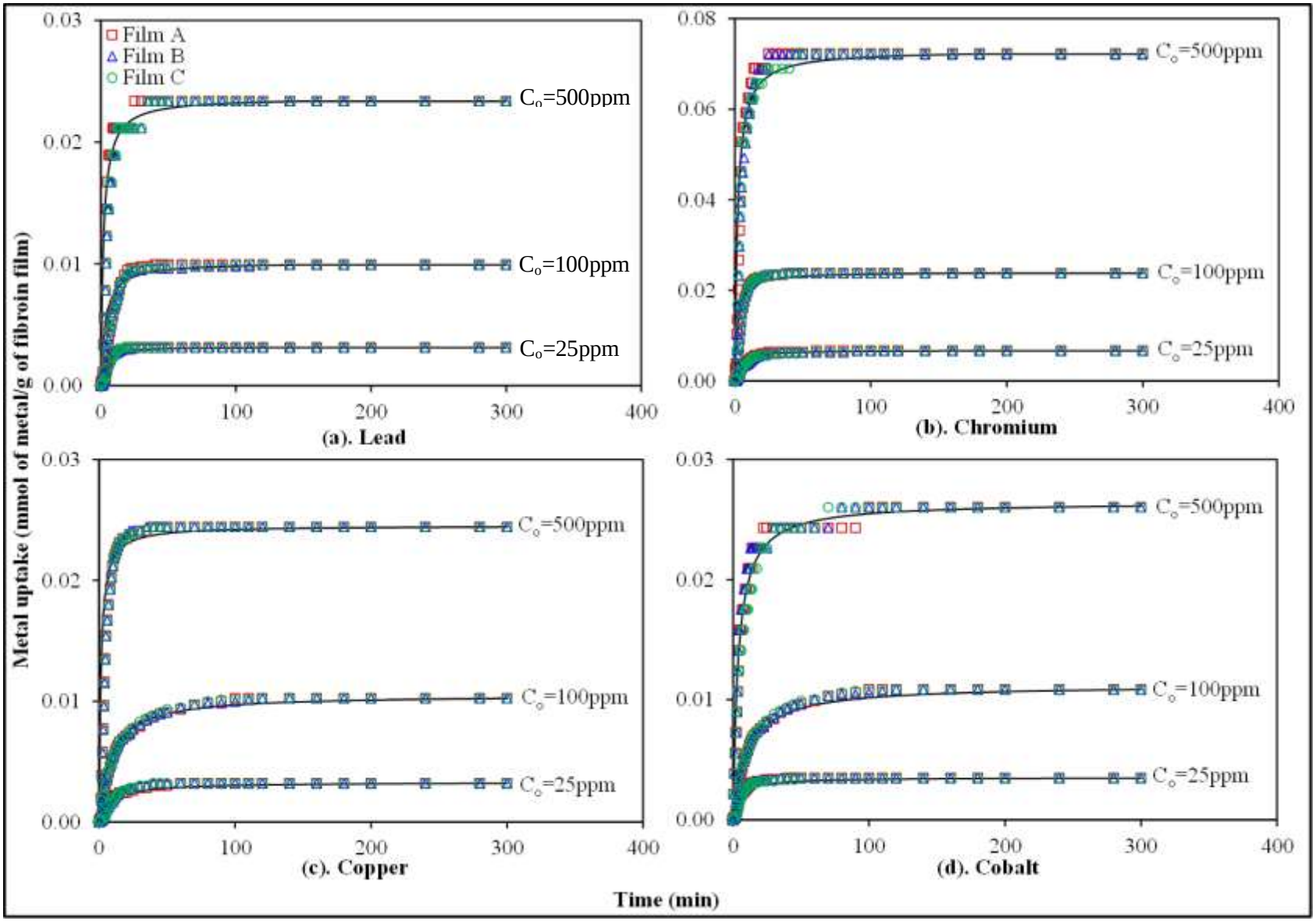

Figure 6.2 Comparison of experimental data and model calculation for the adsorption of (a). *Lead* (b). *Chromium* (c). *Copper* and (d). *Cobalt* on ***fibroin films*** of three thicknesses.

Table 6.2 Metal uptake capacity of ***fibroin films*** of three different thicknesses at initial solution concentration of 25, 100 and 500ppm. (Surface area of ***fibroin films*** 72.63cm^2)

Metal	Initial Solution Concentration		Film	Equilibrium Solution Concentration	Equilibrium Uptake q_e
	(ppm)	(mmol/L)		mmol/L	(10^{-3} mmol/g)
Lead	25	0.12	A	0.11	3.12
			B	0.11	3.13
			C	0.11	3.13
	100	0.48	A	0.44	9.92
			B	0.44	9.92
			C	0.44	9.92
	500	2.41	A	2.31	23.35
			B	2.31	23.35
			C	2.31	23.35
Chromium	25	0.48	A	0.46	6.66
			B	0.46	6.64
			C	0.46	6.67
	100	1.92	A	1.82	23.80
			B	1.82	23.80
			C	1.82	23.79
	500	9.62	A	9.29	72.18
			B	9.29	72.03
			C	9.29	72.27
Copper	25	0.39	A	0.38	3.20
			B	0.38	3.20
			C	0.38	3.20
	100	1.57	A	1.53	10.22
			B	1.53	10.23
			C	1.53	10.23
	500	7.87	A	7.77	24.43
			B	7.77	24.43
			C	7.77	24.42
Cobalt	25	0.42	A	0.41	3.47
			B	0.41	3.47
			C	0.41	3.48
	100	1.70	A	1.65	10.84
			B	1.65	10.84
			C	1.65	10.85
	500	8.48	A	8.37	26.02
			B	8.37	26.01
			C	8.37	26.01

Table 6.3 Values of kinetic rate constant k_2 evaluated from experimental data fitting to equation 6.3 for the adsorption of all metals on *fibroin films* exposed to the solutions having initial concentrations of 25, 100 and 500ppm.

Metal	Initial Solution Concentration (ppm)	Final Solution Concentration (ppm)	Rate Constant k_2 Fibroin Film (g/mmol.min)	Rate constant k_2 Average value (g/mmol.min)
Lead	25	22.0	36.5*	10.2
	100	90.6	10.2	
	500	477.9	10.2	
Chromium	25	23.6	16.8*	6.4
	100	94.8	9.2	
	500	484.3	3.6	
Cobalt	25	24.1	47.2*	8.6
	100	97.3	7.5	
	500	493.5	9.8	
Copper	25	24.0	28.5*	9.9
	100	97.0	8.70	
	500	493.2	11.2	

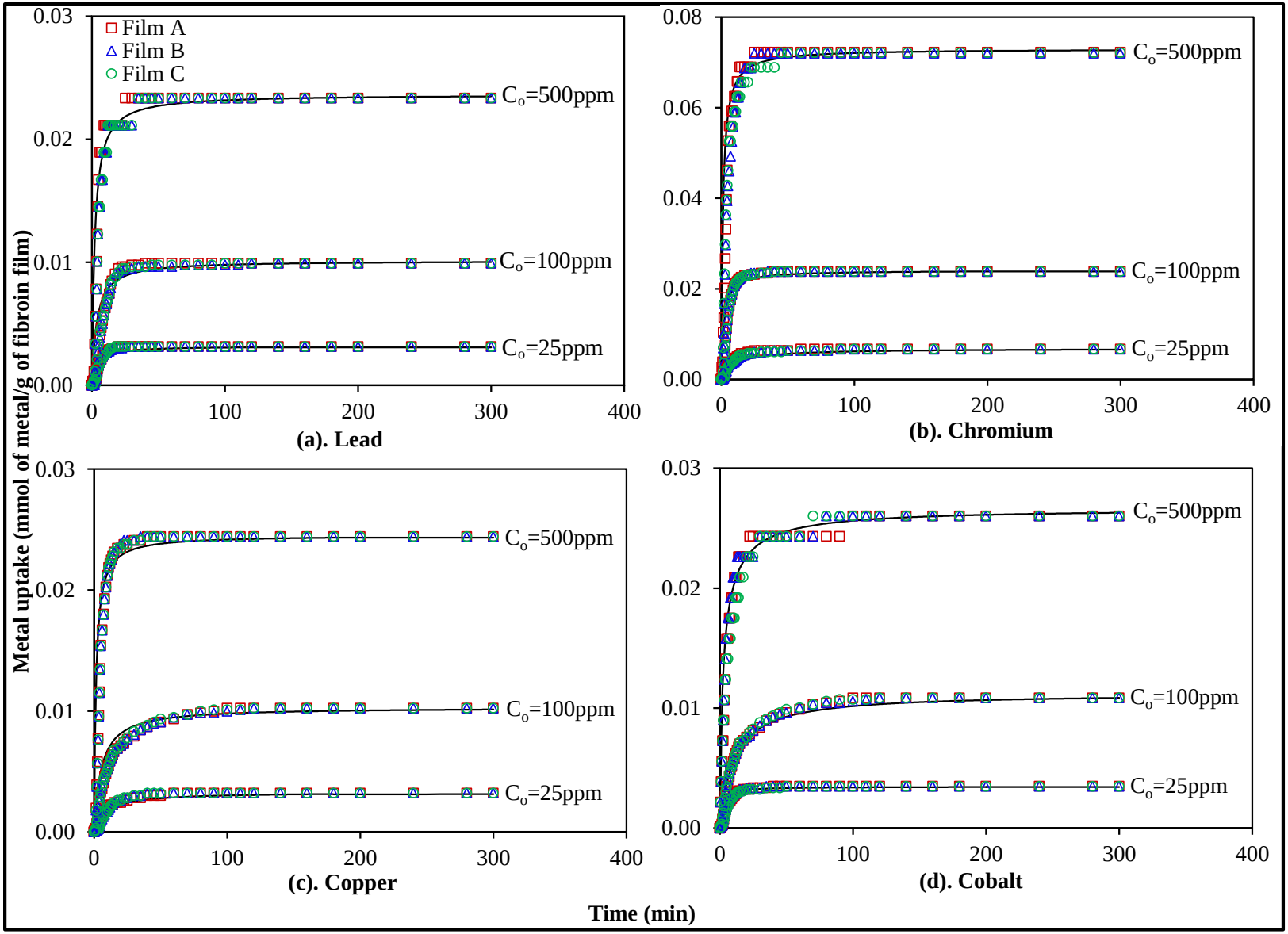

Figure 6.3 Comparison of experimental data and model calculations using average k_2 value for the adsorption of (a). *Lead* (b). *Chromium* (c). *Copper* and (d). *Cobalt* on ***fibroin films*** of three thicknesses.

The data fitting was done using a program in FORTRAN® (Appendix C). The metal uptake of all three films, when divided by their dry weight, fell on a single line and can be seen in Figure 6.2. Therefore, for a given initial metal concentration, a single set of data is fitted to equation 6.3, and the kinetic rate constant k_2 for metal adsorption on fibroin films are presented in Table 6.3.

Here, an error comes up for the values of k_2 at low initial concentrations (i.e., 25ppm). The reason for this error is primarily caused by experimental error in the concentration measurements, as discussed in Chapter 4. So, the k_2 values at 25ppm are neglected (shown by an " * " sign in Table 6.3) and an average k_2 is taken. The average k_2 value is used to calculate the metal uptake data for comparison between the experimental data and model calculations using equation 6.3. The same program in Fortran® was used (Appendix C). The comparison between the experimental data and model calculation is presented in Figure 6.3, which showed a good agreement. This indicates that the kinetic rate constant k_2 is independent of metal concentration and fibroin film thickness, suggesting that metal adsorption on fibroin does not follow diffusion mechanism.

The plots showing desorption of metal from the fibroin films are presented in Figures 6.4-6.6. The desorption kinetics followed the same pattern as the adsorption kinetics. The desorption data was also fitted to a kinetic model (Chapter 4),

$$\frac{dq_t}{dt} = k_d \left[\frac{q_m}{1+\frac{1}{b\,(C_e-\frac{mq_t}{V})}} - q_t \right]^2 \qquad (6.4)$$

The desorption rate constant k_d was determined from the data fitting, and the k_d values are presented in Table 6.4. For desorption, de-ionized water was used to "extract" adsorbed metal from the fibroin film. An equilibrium was established at the end of each desorption cycle, and the metal transfer from adsorbent to water stopped.

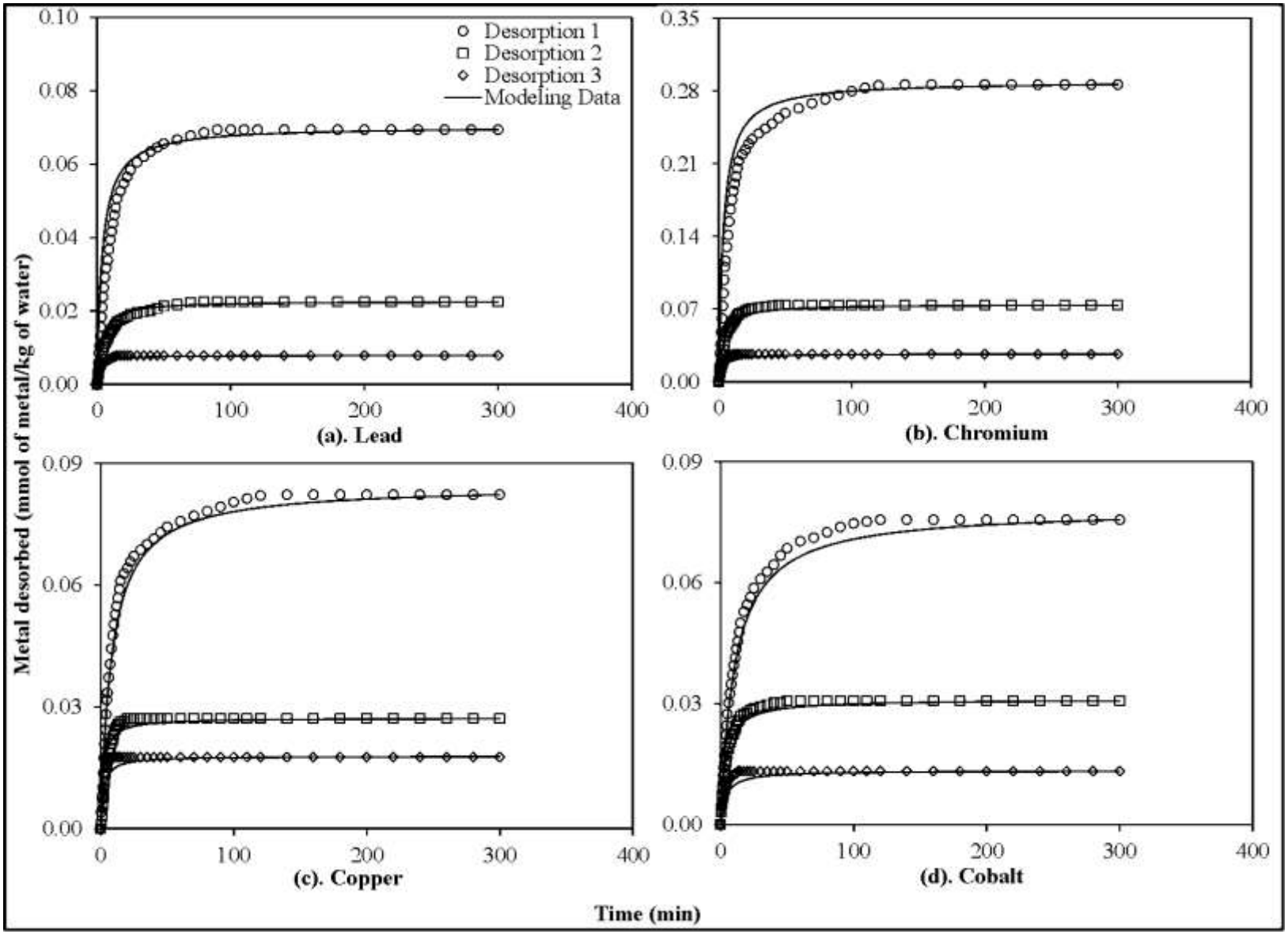

Figure 6.4 Comparison of experimental data and model calculations for the desorption of (a). *Lead* (b). *Chromium* (c). *Copper* and (d). *Cobalt* from ***fibroin film A.***

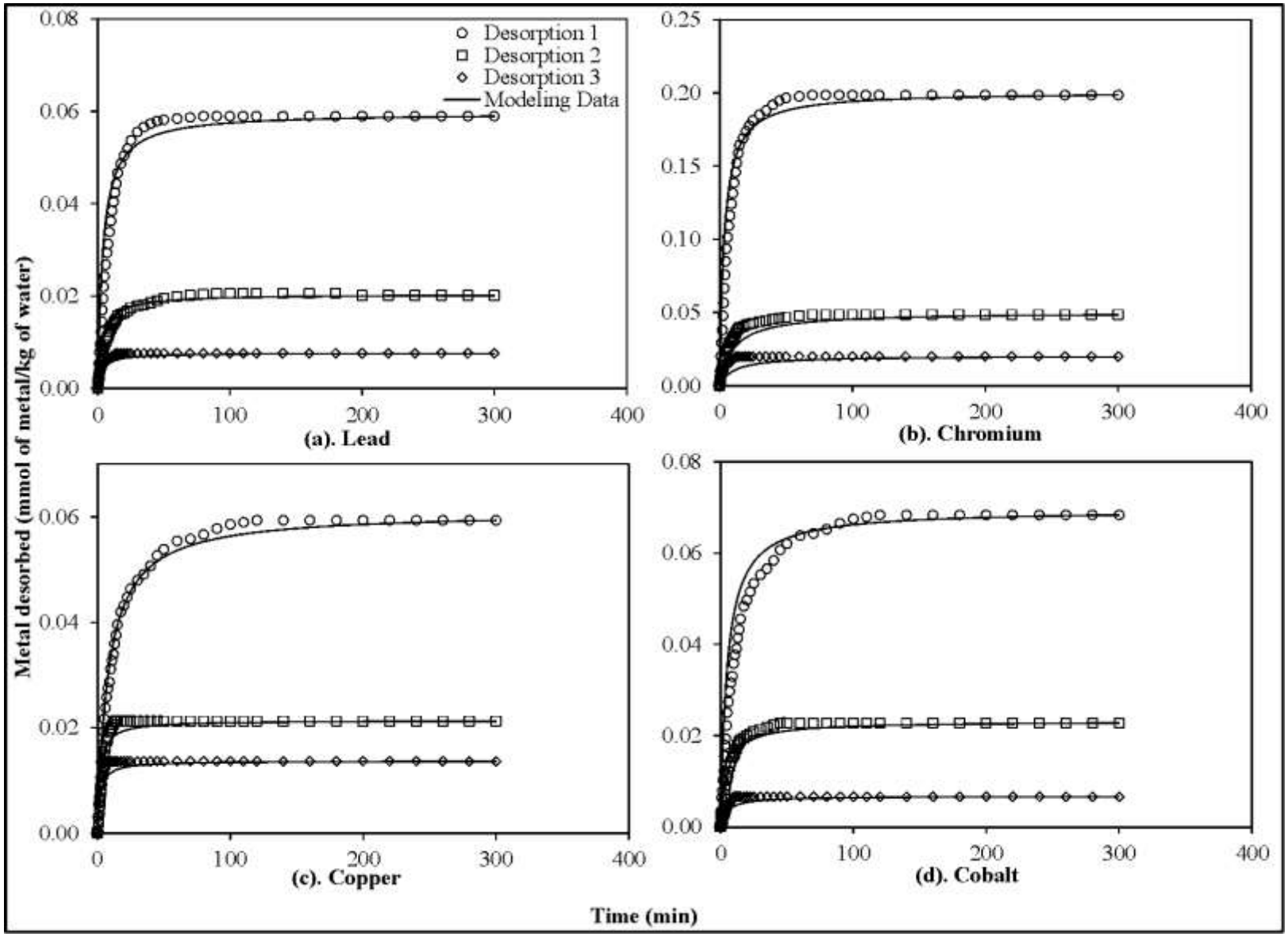

Figure 6.5 Comparison of experimental data and model calculations for the desorption of (a). *Lead* (b). *Chromium* (c). *Copper* and (d). *Cobalt* from ***fibroin film B.***

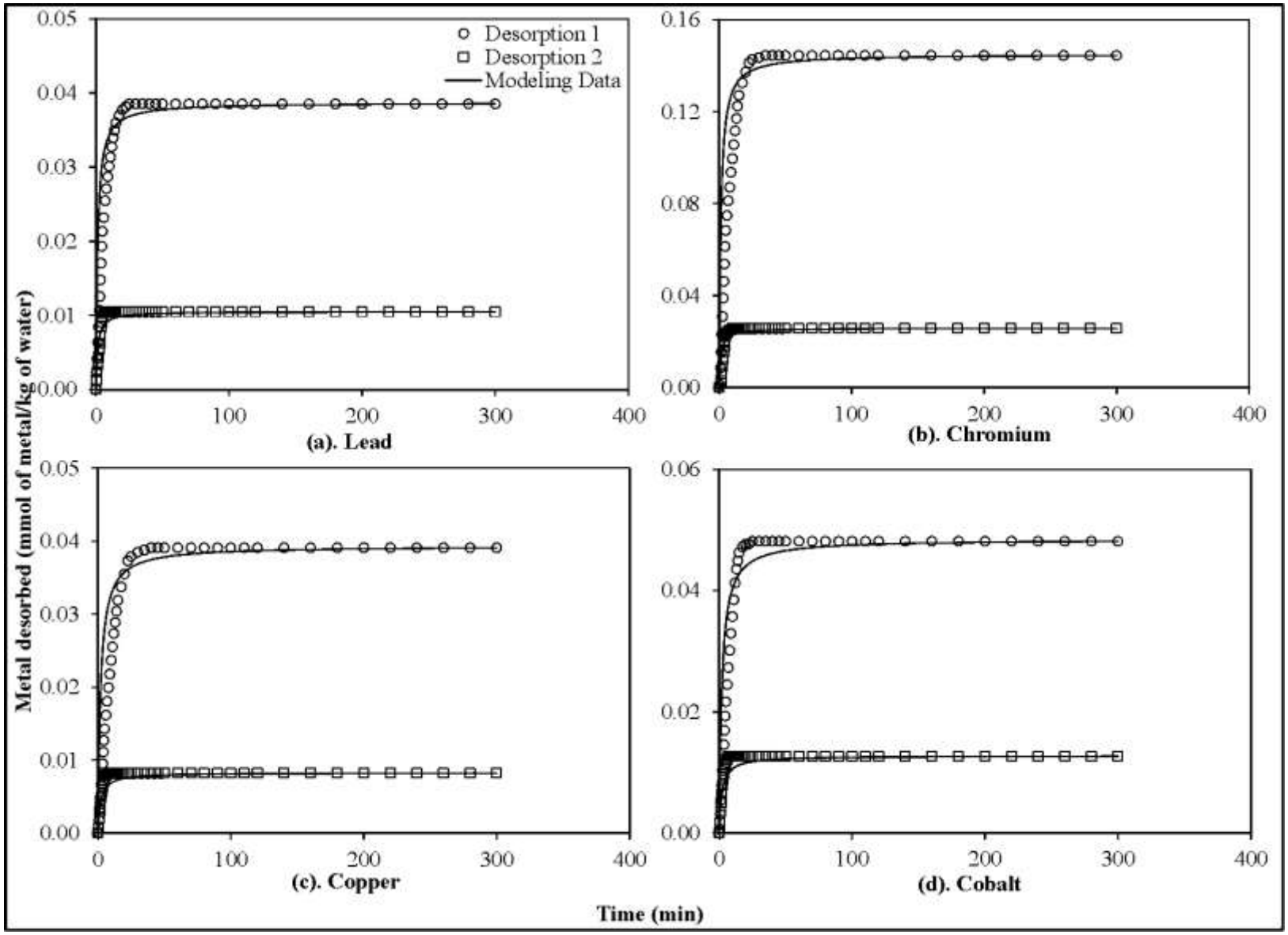

Figure 6.6 Comparison of experimental data and model calculations for the desorption of (a). *Lead* (b). *Chromium* (c). *Copper* and (d). *Cobalt* from ***fibroin film C.***

Table 6.4 Desorption rate constant k_d evaluated from kinetic desorption data fitting to equation 6.4 for the removal of all metals from *fibroin film* A, B and C.

Metal	Film	Desorption Cycle	Desorption Rate Constant k_d (g/mmol.min)	Amount of metal desorbed at equilibrium (mmol/kg of water)
Lead	A	1	0.13	0.069
		2	3.43	0.022
		3	4.40	0.008
	B	1	1.92	0.059
		2	4.84	0.020
		3	5.61	0.008
	C	1	3.32	0.039
		2	9.20	0.011
Chromium	A	1	4.43	0.286
		2	4.84	0.074
		3	4.00	0.026
	B	1	6.72	0.199
		2	6.93	0.048
		3	8.83	0.020
	C	1	10.13	0.144
		2	12.93	0.026
Copper	A	1	3.82	0.082
		2	6.72	0.027
		3	8.98	0.018
	B	1	7.41	0.059
		2	6.21	0.021
		3	11.23	0.014
	C	1	9.37	0.039
		2	8.12	0.008
Cobalt	A	1	0.21	0.076
		2	3.43	0.031
		3	3.72	0.013
	B	1	4.44	0.068
		2	3.59	0.023
		3	6.40	0.007
	C	1	9.73	0.048
		2	6.25	0.013

6.3.1 FTIR ANALYSIS

To examine the morphological characteristics of fibroin films, before and after metal adsorption (films of thickness *B*, loaded with lead, chromium, copper and cobalt ions with an initial solution concentration of 250ppm), FTIR spectra were recorded at room temperature using Bruker Tensor 27 spectrometer. To examine the chemical structure changes in fibroin films, Fibroin in the form of fibers was also analyzed. Figure 6.7(a) shows the spectra of fibroin films (before and after metal adsorption) with wavenumber range 400-4000cm^{-1}. A magnified image of the same diagram is shown in Figure 6.7(b) with a wavenumber 545-1755cm^{-1}. A comparison of IR spectra of fibroin film and fibroin fibers is presented in Figure 6.8(a) & (b).

The FTIR spectra in Figure 6.7(a) shows a wide absorption band at 3300cm^{-1}, assigned to the stretching of O–H group due to inter- and intramolecular hydrogen bonding of polymeric compounds (macromolecular associations), such as alcohols, phenols and carboxylic acids. The broad range of frequencies at 3300cm^{-1} is caused by the O–H stretching vibrations, indicating the presence of hydroxyl groups and bonded O–H bands of carboxylic acids.

There are three different types of distinguishable vibration peaks associated with amide groups in proteins. Protein shows characteristic vibration bands between 1615–1650cm^{-1} for amide I (C═O stretching), 1540–1520cm^{-1} for amide-II (secondary NH bending), and 1270–1230cm^{-1} for amide III (C–N and N–H functionalities) in their FTIR spectra [161]. The presence of amide-I, amide-II and amide-III can be observed in Figure 6.7(b) by the absorbance bands at 1620cm^{-1}, 1520cm^{-1}, and 1232cm^{-1}, respectively. The band at about 1700cm^{-1} is caused by the stretching of C═O in carboxyl groups. The bands at 1200–800cm^{-1} are dominated by C–O and C–N stretching. The band at about 1520cm^{-1} is assigned to the asymmetric stretching of N–O bond.

A sharp absorbance band at 1517cm^{-1} N–O can be observed and its peak shifted from 1515 to 1520cm^{-1} after lead, chromium, copper and cobalt adsorption. Another shift is also observed for (COOH) carboxyl absorbance band from 1697 to 1700 cm^{-1} after metal adsorption on fibroin films. The FTIR spectrum of fibroin films clearly showed the presence of carboxyl and hydroxyl groups. In biopolymers, these groups may act as proton donors; hence deprotonated hydroxyl and carboxyl groups may be involved in

coordination with metal ions [65]. The shift in wave number corresponds to a change in energy of the functional group [162], indicating that the bonding pattern of O–H, N–H and –COOH groups changes after sorption. This result confirms the involvement of hydroxyl, amino and carboxyl groups in binding of lead, chromium, copper and cobalt.

A comparison of spectra between fibroin film and fibroin fibers is presented in Figures 6.8(a) & (b). Some of the peaks in the spectrum of fibroin fibers are shifted once it was transformed into the film. Like peak at 1625cm^{-1} shifted to 1620cm^{-1} for the film spectrum. Similarly the peak at 1066cm^{-1} for fibroin fibers shifted to 1069cm^{-1} for film. The change in peak seems to be the result of variations in secondary protein structures during film synthesis procedure. The secondary protein structures consist of side chains (1605–1615 cm^{-1}), b-sheets (1619–1628 and 1697–1703cm^{-1}), random coil (1638–1655 cm^{-1}), a-helix (1656–1662 cm^{-1}), and turns (1663–1696 cm^{-1}) [163]. The FTIR spectrum of fibroin fibers also shows that the peaks get sharper for the fibroin film. The sharpness of peaks is also characterized by the secondary protein structures.

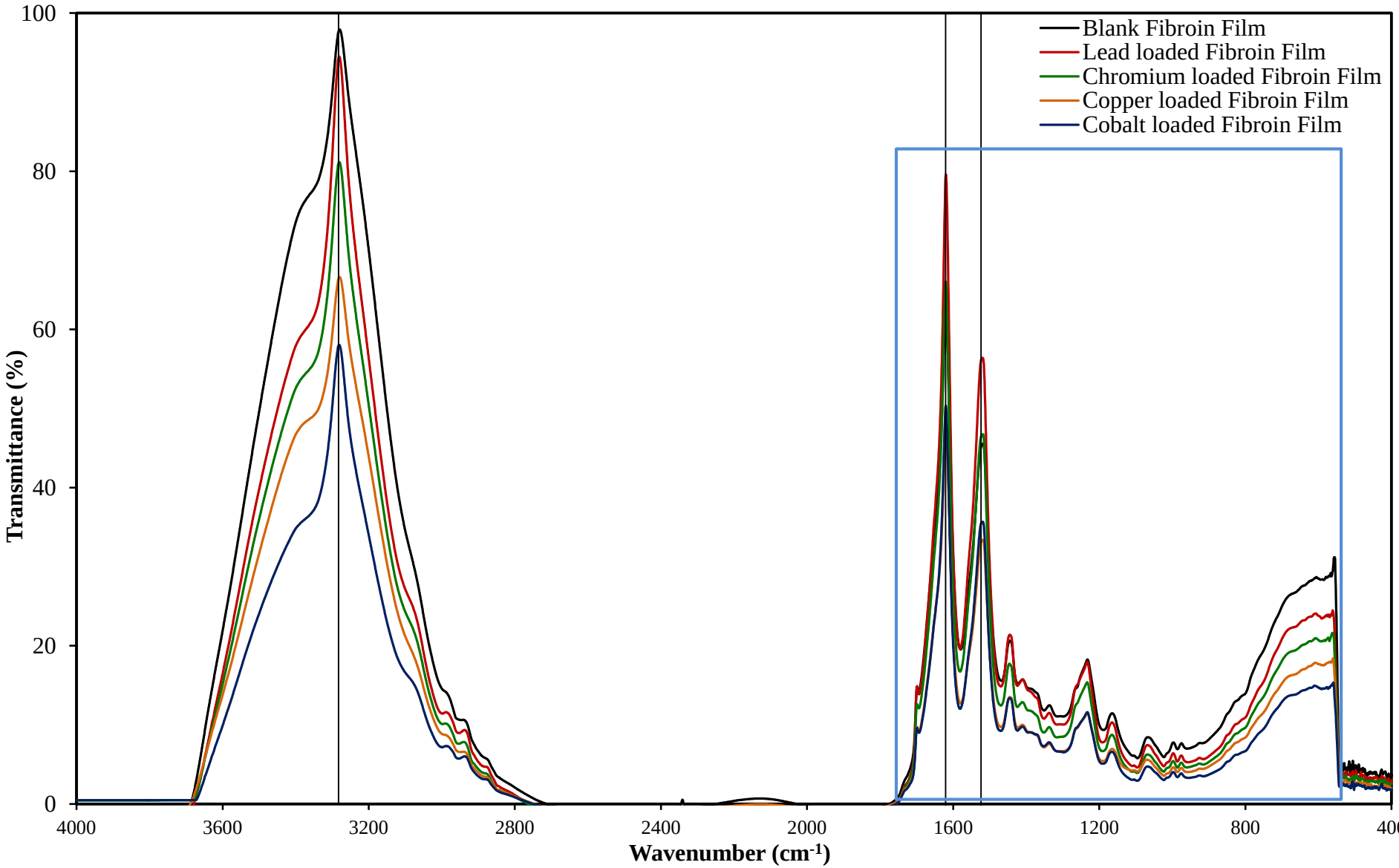

Figure 6.7(a) FTIR spectrum of fibroin films (Thickness B) before and after adsorption of lead, chromium, copper and cobalt. (Wavenumber 4000-400cm^{-1})

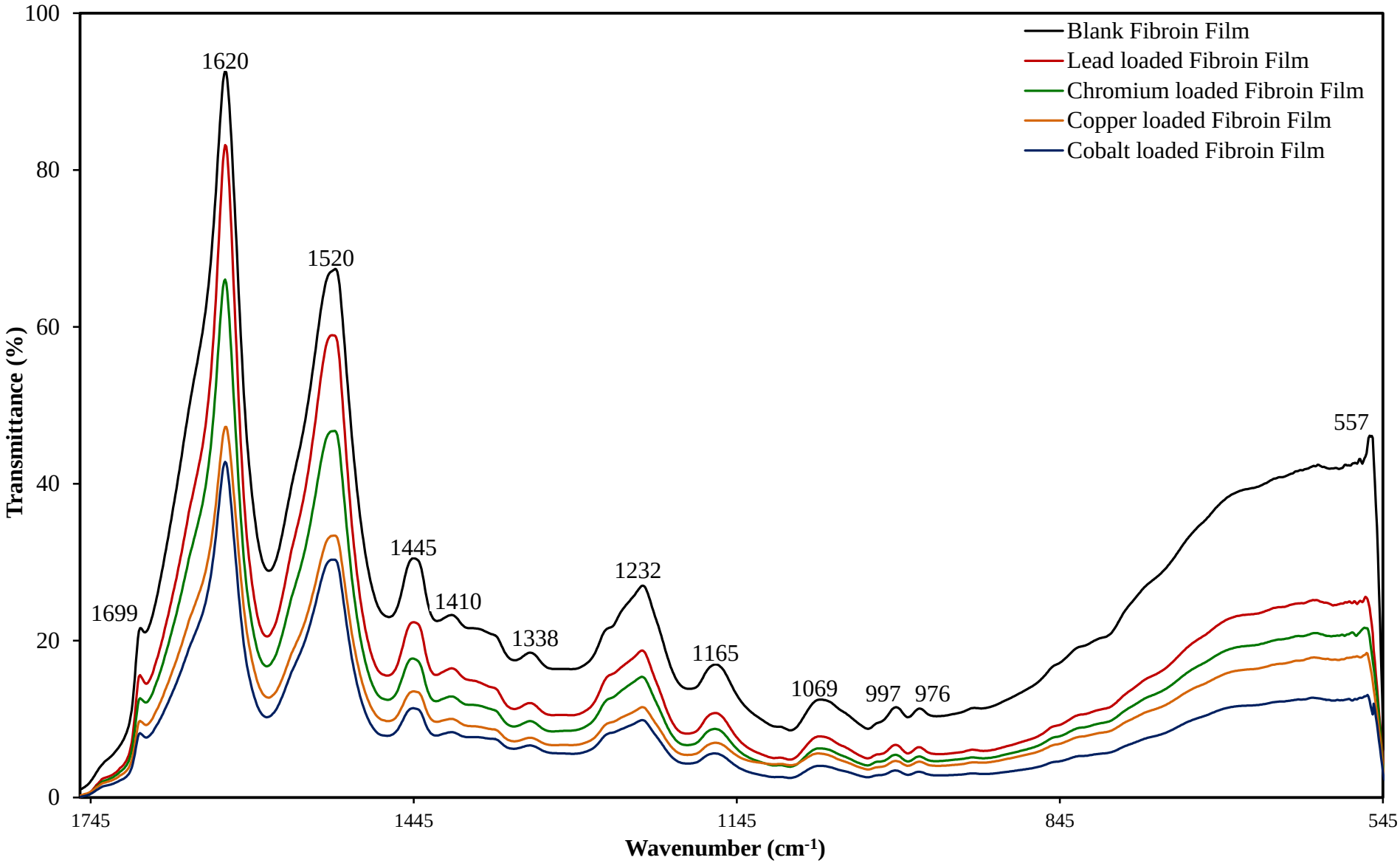

Figure 6.7(b) FTIR spectrum of fibroin films (Thickness B) before and after adsorption of lead, chromium, copper and cobalt. (Wavenumber 1755-545cm^{-1})

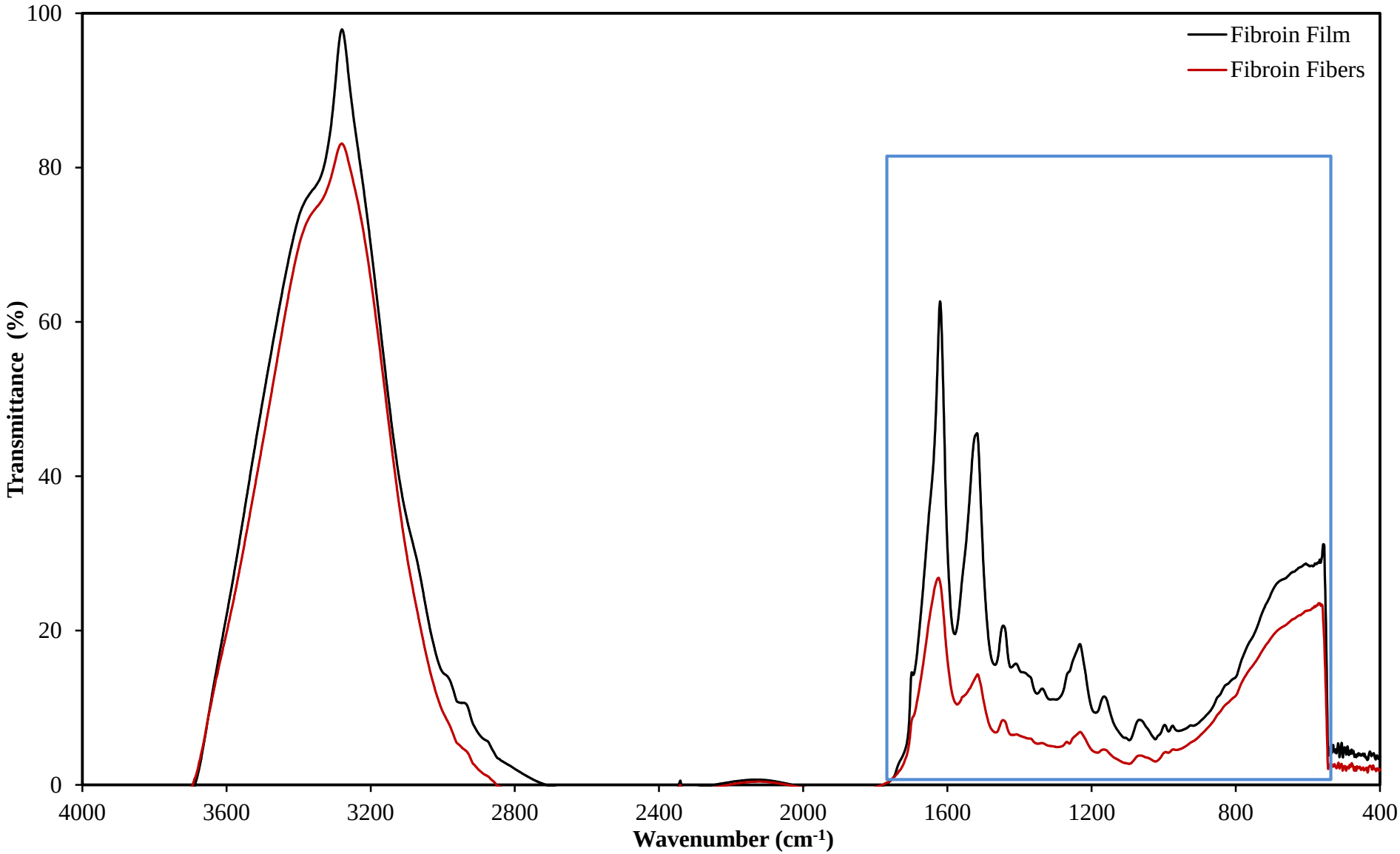

Figure 6.8(a) FTIR spectrum of fibroin film (Thickness B) and fibroin fibers. (Wavenumber 4000-400cm^{-1})

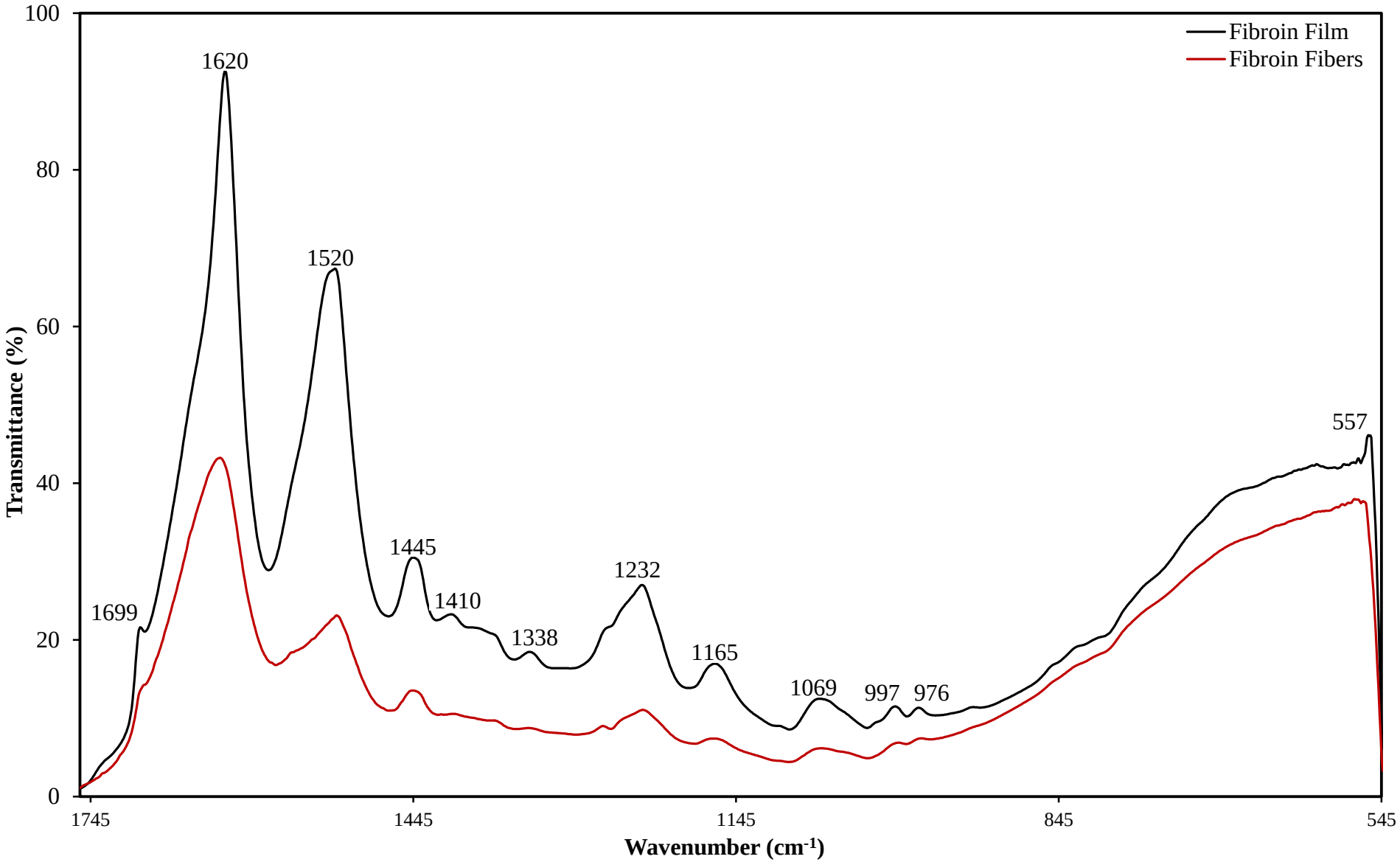

Figure 6.8(a) FTIR spectrum of fibroin film (Thickness B) and fibroin fibers. (Wavenumber 1755-545cm^{-1})

6.5 CONCLUSIONS

Adsorption-desorption tests on fibroin films of different thicknesses revealed the following:

- Silk fibroin films could be prepared by solution casting.
- The adsorption of lead, chromium, copper and cobalt ions on fibroin films was not a surface phenomenon, and the bulk body of the adsorbent was used for metal uptake.
- Adsorption kinetics was described by equation 6.3, and the rate constant k_2 was independent of initial metal concentration.
- Metal sorption into fibroin did not follow a simple diffusion mechanism as the rate constant is not significantly affected by the film thickness, which was further supported by the desorption experiments.

CHAPTER 7

CONCLUSIONS AND RECOMMENDATIONS

7.1 CONCLUSIONS

A thorough investigation for the degumming of silk cocoon to separate sericin from fibroin led to the development of an effective green separation process. Batch adsorption study helped to understand the mechanism involved in the removal of lead, chromium, copper, and cobalt ions by fibroin. Adsorption mechanism was investigated by the application of most appropriate adsorption models, which explained the kinetics and equilibrium of this system. An accurate evaluation of thermodynamics and reusability of the adsorbent, helped to whether prove this adsorption system is feasible or not. Dynamic adsorption study helped to find the empirical models which could explain the breakthrough of the column. Design parameters were evaluated which could be used to scale up the adsorption column operation. The conversion of fibroin fibers into fibroin films helped to answer questions related to the surface area of adsorbent. From the work completed in this study, a number of significant conclusions can be drawn and are discussed under.

Sericin extraction from cocoon with hot water is shown to be an effective process where no chemicals are needed. The rate of sericin extraction increases with an increase in extraction temperature, which results an increase in yield of sericin removed. The kinetics of sericin extraction can be approximated by the pseudo-second-order equation and intraparticle diffusion model, this appears to indicate that the intraparticle diffusion in not the only rate controlling step for this separation.

The adsorption of metal ions from aqueous solution to fibroin followed Langmuir isotherm. The calculated adsorption free energy ΔG for metal ions on fibroin suggested

that it is a physical adsorption. The thermodynamic evaluation of the adsorption, change in entropy (ΔS) and change in enthalpy (ΔH), indicated that the adsorption is spontaneous and endothermic in nature. For the adsorption of metal ions on fibroin, kinetic rate constant k_2 is independent of initial adsorbate concentration, but it is different for different metals. A multi linear trend of intraparticle diffusion model showed that the adsorption of all metals on fibroin is not only controlled by the intraparticle diffusion and possibly more than one mechanism is involved as a rate controlling step. The metal ions adsorbed in fibroin can be desorbed effectively by using 0.05M EDTA solution as a chelating agent. There is not a considerable change in the uptake capacity and the rate of adsorption even after ten cycles of adsorption and desorption, and thus fibroin can be reused repeatedly as an adsorbent.

Fibroin can be used for dynamic adsorption applications. Change in influent concentration affects the column performance since a decrease in breakthrough time is observed with an increased influent concentration. An increase in saturation capacity of the fibroin bed with an increase in the influent concentration was due to the increase in the equilibrium effluent concentration. All the three models (i.e., Yoon-Nelson model, BDST model and Thomas model) fit well with the experimental data; the bed depth service time model and Thomas model, which have essentially a common basis, described the adsorption breakthrough equally well. The same adsorbent can be used for multiple adsorption cycles after regeneration with 0.05M EDTA solution, and there was no change in its metal uptake capacity after regeneration.

Silk fibroin films could be synthesized from silk fibroin by solution casting. The adsorption of lead, chromium, copper and cobalt ions on fibroin films was not a surface phenomenon, and the bulk body of the adsorbent was used for metal uptake. Adsorption kinetics on fibroin films was also described by the modified pseudo-second-order equation, and again, the rate constant k_2 showed an independence of initial metal concentration. Metal sorption into fibroin did not follow a simple diffusion mechanism as the rate constant is not significantly affected by the film thickness, which was further supported by the desorption experiments.

7.2 FUTURE STUDIES/RECOMMENDATIONS

Silk fibroin has already been used in the field of biomedical, textile, pharmaceutical and cosmetic industries. The present research is an expansion of using this biomaterial as a potential adsorbent for metal recovery from wastewater. The followings are recommended for future study.

(1). Competitive sorption. When wastewater contains binary or tertiary metals, the interactions between the metals may influence the uptake of individual metals on fibroin. The interactions between the metals should be studied in order to get a full picture of metal removal from waste water with fibroin.

(2). Catalyst recovery. In many chemical reactions, catalysts are made up of precious metals (silver, gold, platinum, palladium, rhodium,). During the course of chemical reaction, these catalysts either get mixed with the product and/or with the by-products of reaction (e.g., water). Recovery of these precious metal ions from the reaction products could directly impact the economy of product and also reduces the environmental impacts. For example, the automotive catalytic converters deal with pollutants in vehicle exhaust (CO, NO_x, unburned or partially burned hydrocarbons), which use precious metals (Pt, Pd, Rh) and Ba- or La-oxides as catalysts. The precious metals are the most important components of the catalytic convertor, since the catalytic activity occurs at the precious metal center. It is generally agreed that Rh promotes the NO_x dissociation, while Pt and Pd promote the oxidation reaction. Palladium, rhodium and platinum should be recovered from spent automotive catalyst leachates[164] and fibroin may be a good adsorbent for this application.

(3). Hostile or toxic wastes, biosorption of metals onto dead biomass is generally suitable. One of the well documented examples of using biomass is the fungus *Rhizopus arrhizus* for the biosorption and recovery of uranium (uranyl ion) from wastewaters at Denison Mines, Canada [165]. Uranyl ion is deposited extensively as biomass bound uranyl hydroxide [166]. The adsorption could be done using fibroin, and if it works, it would be an attractive alternative for repeated uses after regeneration. It also seems attractive because the fibroin can easily be converted into different forms.

(4). Because of the hydroxyl, phenol and carboxyl groups, fibroin is a unique biomaterial, providing options for use in a range of biomedical and other applications such as controlled drug delivery [167]. However, pure silk fibroin films tend to get stiff and brittle in the dry state over time, exhibiting impressive tensile strength but low elongation. Therefore, there remains a need to modify fibroin to make it suitable for these applications [168].

REFERENCES

(1). R. Jain, Providing safe drinking water: a challenge for humanity, Clean technologies and environment policy 14 (2012) 1–4.

(2). J.S. Hawkes, Heavy metals, Journal of chemical education 74 (11) (1997) 1374.

(3). M. Shokrzadeh, S.S. Saravi, The study of heavy metals (zinc, lead, cadmium, and chromium) in sediments sampled from Gorgan coast (Iran), spring 2008, Toxicological and environmental chemistry 92 (2010) 67–69.

(4). P.K. Rai, Heavy metals in water, sediments and wetland plants in an aquatic ecosystem of tropical industrial region India, Environment monitoring and assessment 158 (2009) 433–457.

(5). J.O. Nriagu, Global inventory of natural and anthropogenic emission of trace metals to the atmosphere, Nature 279 (1979) 409–411.

(6). G. Capar, S.S. Aygun, M.R. Gecit, Treatment of silk production wastewaters by membrane processes for sericin recovery, Journal of membrane science 325 (2008) 920–931.

(7). D.M. Mamatha1, H.P. Cohly, A.H. Raju, M.R. Rao, Studies on the quantitative and qualitative characters of cocoons and silk from methoprene and fenoxycarb treated Bombyx mori (L) larvae, African journal of biotechnology 5 (15) (2006) 1422-1426.

(8). A.G. Khan, C. Kuek, T.M. Chaudhary, C.S. Khoo, W.J. Hayes, Role of mycorrhizae and phytochelators in heavy metal contaminated land remediation, Chemosphere 41 (2000) 197–207.

(9). P.K. Rai, Phytoremediation of Hg and Cd from industrial effluents using an aquatic free floating macrophyte azolla pinnata, International journal of phytoremediation 10 (5) (2008) 430–439.

(10). J.O. Nriagu, A history of global metal pollution, Science 272 (1996) 273–274.

(11). P.K. Rai, B.D. Tripathi, Heavy metals removal using nuisance blue green alga microcystis in continuous culture experiment, Environmental sciences 4 (1) (2007) 53–59.

(12). P. Miretzky, A. Saralegui, A.F. Cirelli, Aquatic macrophytes potential for the simultaneous removal of heavy metals, Chemosphere 57 (2004) 997–1005.

(13). P.M. Linnik, I.B. Zubenko, Role of bottom sediments in the secondary pollution of aquatic environments by heavy-metal compounds, Lakes and reservoirs: research and management 5 (2000) 11–21.

(14). P.H. Albers, M.B. Camardese, Effects of acidification on metal accumulation by aquatic plants and invertebrates: I. constructed wetlands, Environmental toxicology and chemistry 12 (1993) 959–967.

(15). P.K. Rai, Heavy metal pollution in aquatic ecosystems and its phytoremediation using wetland plants: an eco-sustainable approach, International journal of phytoremediation 10 (2) (2008) 133–160.

(16). S.R. Smith, A critical review of the bioavailability and impacts of heavy metals in municipal solid waste composts compared to sewage sludge, Environment international 35 (2009) 142–156.

(17). S. Amir, M. Hafidi, G. Merlina, J.C. Revel, Sequential extraction of heavy metals during composting of sewage sludge, Chemosphere 59 (2005) 801–810.

(18). K.Y. Chiang, S.D. Yoi, H.N. Lin, K.S. Wang, Stabilization of heavy metals in sewage sludge composting, Water science and technology 44 (2001) 95–100.

(19). L.M. Chu, M.H. Wong, Heavy metal contents of vegetable crops treated with refuse compost and sewage sludge, Plant and soil 103 (1987) 191–197.

(20). C. Ciavatta, M. Govi, A. Simoni, P. Sequi, Evaluation of heavy metals during stabilization of organic matter in compost produced with municipal wastes, Bioresource technology 43 (1993) 147–153.

(21). R. Aravindhan, A. Fathima, M. Selvamurugan, J.R. Rao, U.N. Balachandran, Adsorption, desorption, and kinetic study on Cr(III) removal from aqueous solution using bacillus subtilis biomass, Clean technologies and environmental policy 14 (2012) 727–735.

(22). V.J.P. Vilar, C.M.S. Botelho, R.A.R. Boaventura, Metal biosorption by algae gelidium derived materials from binary solutions in a continuous stirred adsorber, Chemical engineering journal 141 (2008) 42–50.

(23). G. Degirmen, M. Kilic, O. Cepeliogullar, A.E. Putun, Removal of copper(II) and cadmium(II) ions from aqueous solutions by biosorption onto pine cone, Water science and technology 66 (3) (2012) 564-572.

(24). H. Rezaei, S.D. Kulkarni, P.G. Saptarshi, Study of physical chemistry on biosorption of zinc by using chlorella pyrenoidosa, Russian journal of physical chemistry 86 (18) (2012) 1332–1339.

(25). M.A.H. Gazem, S. Nazareth, Isotherm and kinetic models and cell surface analysis for determination of the mechanism of metal sorption by aspergillus versicolor, World journal of microbiology and biotechnology 28 (2012) 2521–2530.

(26). F.A. Pavan, A.C. Mazzocato, Ponkan peel: a potential biosorbent for removal of Pb(II) ions from aqueous solution, Biochemical engineering journal 40 (2008) 357–362.

(27). M. Bulow, R. Micked, Determination of transport coefficients in microporous solids, Adsorption 1 (1995) 29-48.

(28). A.V.A. Kumar, S.A. Hashimi, N. Hilal, Investigation of kinetics and mechanism involved in the biosorption of heavy metals on activated sludge, International journal of green energy 5 (2008) 313–321.

(39). N. Azouaoua, Z. Sadaouia, A. Djaafri, H. Mokaddema, Adsorption of cadmium from aqueous solution onto untreated coffee grounds: equilibrium, kinetics and thermodynamics, Journal of hazardous materials 184 (2010) 126–134.

(30). F. Liua, L. Li, P. Linga, X. Jing, C. Li, A. Li, X. You, Interaction mechanism of aqueous heavy metals onto a newly synthesized IDA-chelating resin: isotherms, thermodynamics and kinetics, Chemical engineering journal 173 (2011) 106– 114.

(31). X. Zhao, G. Zhang, Q. Jia, C. Zhao, W. Zhou, W. Li, Adsorption of Cu(II), Pb(II), Co(II), Ni(II), and Cd(II) from aqueous solution by poly (aryl ether ketone) containing pendant carboxyl groups (PEK-L): equilibrium, kinetics, and thermodynamics, Chemical engineering journal 171 (2011) 152–158.

(32). V. Mishra, C. Balomajumder, V.K. Agarwal, Kinetics, mechanistic and thermodynamics of Zn(II) ion sorption: a modeling approach, Clean soil, air, water 40 (7) (2012) 718–727.

(33). W. Zhou, Y. Zhang, X. Ding, Y. Liu, F. Shen, X. Zhang, S. Deng, H. Xiao, G. Yang, H. Peng, Magnetotactic bacteria: promising biosorbents for heavy metals, Applied microbiology and biotechnology 95 (2012) 1097–1104.

(34). K. Vijayaraghavana, U.M. Joshi, S.K. Kannanb, An attempt to develop seaweed based treatment technology for the remediation of complex metal bearing laboratory wastewaters, Ecological engineering 47 (2012) 278– 283.

(35). C. Kirbiyik, M. Kilic, O. Cepeliogullar, A.E. Putun, Use of sesame stalk biomass for the removal of Ni(II) and Zn(II) from aqueous solutions, Water science and technology 66 (2) (2012) 231-238.

(36). B. Kizilkaya, F. Dogan, R. Akgul, G. Turker, Biosorption of Co(II), Cr(III), Cd(II), and Pb(II) ions from aqueous solution using nonliving neochloris pseudoalveolaris

deason and bold: equilibrium, thermodynamic and kinetic study, Journal of dispersion science and technology 33 (2012) 1055–1065.

(37). W.J. Weber, J.C. Morris, Advances in water pollution research: removal of biologically resistant pollutant from wastewater by adsorption, Proceedings of 1st international conference on water pollution symposium 2 (1962) 231–266.

(38). W.J. Weber, J.C. Morris, Kinetics of adsorption on carbon from solutions, Journal of the sanitary engineering division, American society of civil engineers 89 (1963) 31–59.

(39). F.C. Wu, R.L. Tseng, R.S. Juang, Initial behavior of intraparticle diffusion model used in the description of adsorption kinetics, Chemical engineering journal 153 (2009) 1–8.

(40). A. Serpen, B. Atac, V. Gokmen, Adsorption of maillard reaction products from aqueous solutions and sugar syrups using adsorbent resin, Journal of food Engineering 82 (2007) 342–350.

(41). W. Zhang, Z. Xu, B. Pan, L. Lu, Q. Zhang, W. Du, Assessment on the removal of dimethyl phthalate from aqueous phase using a hydrophilic hyper cross linked polymer resin, Journal of colloid and interface science 311 (2007) 382–390.

(42). F.C. Wu, R.L. Tseng, R.S. Juang, Role of pH in metal adsorption from aqueous solutions containing chelating agents on chitosan, Industrial and engineering chemistry research 38 (1999) 270–275.

(43). E. Lorenc-Grabowska, G. Gryglewicz, Adsorption characteristics of congo red on coal-based mesoporous activated carbon, Dyes and pigments 74 (2007) 34–40.

(44). S. Wang, H. Li, Kinetic modeling and mechanism of dye adsorption on unburned carbon, Dyes and pigments 72 (2007) 308–314.

(45). Z. Aksu, E. Kabasakal, Batch adsorption of 2,4-dichlorophenoxyacetic acid from aqueous solution by granular activated carbon, Separation and purification technology 35 (2004) 223–240.

(46). R.R. Sheha, H.H. Someda, Removal of some chelators from aqueous solutions using polymeric ingredients, Chemical engineering journal 114 (2005) 105–113.

(47). E. Lorenc-Grabowska, G. Gryglewicz, Removal of cyanocobal amine from aqueous solution using mesoporous activated carbon, Dyes and pigments 75 (2007) 136–142.

(48). A. Ozcan, A.S. Ozcan, S. Tunali, T. Akar, I. Kiran, Determination of the equilibrium, kinetic and thermodynamic parameters of adsorption of copper(II) ions onto seeds of *capsicum annuum*, Journal of hazardous materials 124 (2005) 200–208.

(49). A. Ozcan, E.M. Oncu, A.S. Ozcan, Kinetics, isotherm and thermodynamic studies of adsorption of acid blue from aqueous solutions onto natural sepiolite, Colloids and surfaces A: physicochemical and engineering aspects 277 (2006) 90–97.

(50). S. Tunali, A.S. Ozcan, A. Ozcan, T. Gedikbey, Kinetics and equilibrium studies for the adsorption of acid red from aqueous solutions onto calcined alunite, Journal of hazardous materials 135 (2006) 141–148.

(51). D. Ozer, G. Dursun, A. Ozer, Methylene blue adsorption from aqueous solution by dehydrated peanut hull, Journal of hazardous materials 144 (2007) 171–179.

(52). F.C. Wu, R.L. Tseng, R.S. Juang, Kinetic modeling of liquid-phase adsorption of reactive dyes and metal ions on chitosan, Water research 35 (2001) 613–618.

(53). Y. Onal, C. Akmil-Basar, D. Eren, C. Sarici-Ozdemir, T. Depci, Adsorption kinetics of malachite green onto activated carbon prepared from tuncbilek lignite, Journal of hazardous materials 128 (2006) 150–157.

(54). S. Lagergren, About the theory of so-called adsorption of soluble substances. Kungliga svenska vetenskapsakad, Handlingar 24 (1898) 1–39.

(55). Y.S. Ho, Citation review of Lagergren kinetic rate equation on adsorption reactions, Scientometrics 59 (2004) 171–177.

(56). Y.S. Ho, G. McKay, Pseudo-second order model for sorption processes, Process biochemistry 34 (1999) 451–465.

(57). Y.S. Ho, G. McKay, The kinetics of sorption of divalent metal ions onto sphagnum moss peat, Water research 34 (2000) 735–742.

(58). Y.S. Ho, G. McKay, Sorption of dye from aqueous solution by peat, Chemical engineering journal 70 (1998) 115–124.

(59). B.H. Hameed, J.M. Salman, A.L. Ahmad, Adsorption isotherm and kinetic modeling of 2,4-D pesticide on activated carbon derived from date stones, Journal of hazardous materials 163 (2009) 121–126.

(60). G. Crini, P.M. Badot, Application of chitosan, a natural aminopolysaccharide, for dye removal from aqueous solutions by adsorption processes using batch studies: a review of recent literature, Progress in polymer science 33 (2008) 399–447.

(61). L. Pontoni, M. Fabbricino, Use of chitosan and chitosan derivatives to remove arsenic from aqueous solution: a mini review, Carbohydrate research 356 (2012) 86–92.

(62). H.M.F. Freundlich, Uber die adsorption in losungen (adsorption in solution), International journal of research in physical chemistry and chemical physics 57 (1906) 385–470.

(63). I. Langmuir, The constitution and fundamental properties of solids and liquids, Journal of the American chemical society 38 (1916) 2221–2295.

(64). W. Ranke, Y. Josephy, Determination of adsorption energies and kinetic parameters by isosteric methods, Physical chemistry chemical physics 4 (2002) 2483–2498.

(65). H. Yazid, Z. Sadaoui, R. Maachi, Removal of Cd(II) ions from aqueous phase by biosorption on biological activated dates pedicels (kinetic, equilibrium and thermodynamic study), International journal of chemical reactor engineering 9 (2011) 1-25.

(66). H. Ucun, O. Aksakal, E. Yildiz. Copper(II) and zinc(II) biosorption on pinus sylvestris leaf, Journal of hazardous materials 161 (2009) 1040–1045.

(67). A. Sari, M. Tuzen, Biosorption of As(III) and As(V) from aqueous solution by macrofungus (inonotus hispidus) biomass: equilibrium and kinetic studies, Journal of hazardous materials 164 (2009) 1372–1378.

(68). X. Li, Q. Xu, G. Han, W. Zhu, Z. Chen, X. Heb, X. Tian, Equilibrium and kinetic studies of copper(II) removal by three species of dead fungal biomasses, Journal of hazardous materials 165 (2009) 469–474.

(69). C. Zhu, L. Wang, W. Chen, Removal of Cu(II) from aqueous solution by agricultural byproduct: peanut hull, Journal of hazardous materials 168 (2009) 739–746.

(70). S. Qaiser, A.R. Saleemi, M. Umar, Biosorption of lead from aqueous solution by ficus religiosa leaves: batch and column study, Journal of hazardous materials 166 (2009) 998–1005.

(71). A. Sari, M. Tuzen, Kinetic and equilibrium studies of biosorption of Pb(II) and Cd(II) from aqueous solution by macrofungus (amanita rubescens) biomass, Journal of hazardous materials 164 (2009) 1004–1011.

(72). G. Blazquez, M.A.M. Lara, E.D. Ruiz, G. Tenorio, M. Calero, Copper biosorption by pine cone shell and thermal decomposition study of the exhausted biosorbent, Journal of industrial and engineering chemistry 18 (2012) 1741–1750.

(73). M.O. Omorogie, J.O. Babalola, E.I. Unuabonah, J.R. Gong, Kinetics and thermodynamics of heavy metal ions sequestration onto novel nauclea diderrichii seed biomass, Bioresource technology 118 (2012) 576–579.

(74). B. Singha, S.K. Das, Removal of Pb(II) ions from aqueous solution and industrial effluent using natural biosorbents, Environmental science and pollution research 19 (2012) 2212–2226.

(75). J.H. Wu, Z. Wang, S.Y. Xu, Preparation and characterization of sericin powder extracted from silk industry wastewater, Food chemistry 103 (2007) 1255–1262.

(76). E. Servoli, D. Maniglio, A. Motta, R. Predazzer, C. Migliaresi, Surface properties of silk fibroin films and their interaction with fibroblasts, Macromolecular bioscience 5 (2005) 1175–1183.

(77). M.L. Gulrajani, R. Purwar, R.K. Prasad, M. Joshi, Studies on structural and functional properties of sericin recovered from silk degumming liquor by membrane technology, Journal of applied polymer science 113 (2009) 2796–2804.

(78). M.L. Gulrajani, K.P. Brahma, P.S. Kumar, R. Purwar, Application of silk sericin to polyester fabric, Journal of applied polymer science 109 (2008) 314–321.

(79). A. Anghileri, G. Freddi, R. Mossotti, R. Innocenti, Mechanical properties of silk yarn degummed with several proteases, Journal of natural fibers 4 (1) (2007) 13-23.

(80). Y. Shen, M.A. Johnson, D.C. Martin**,** Microstructural characterization of bombyx mori silk fibers, Macromolecules 31 (1998) 8857-8864.

(81). H. Zhang, J. Magoshi, M. Becker, J.Y. Chen, R. Matsunaga, Thermal properties of bombyx mori silk fibers, Journal of applied polymer science 86 (2002) 1817–1820.

(82). H.J. Jin, D.L. Kaplan, Mechanism of silk processing in insects and spiders, Nature 424 (2003) 1058-1061.

(83). B.M. Mina, G. Leea, S.H. Kimb, Y.S. Namb, T.S. Leeb, W.H. Parkb, Electrospinning of silk fibroin nano fibers and its effect on the adhesion and spreading of normal human keratinocytes and fibroblasts in vitro, Biomaterials 25 (2004) 1289–1297.

(84). G.H. Altman, F. Diaz, C. Jakuba, T. Calabro, R.L. Horan, J. Chen, H. Lu, J. Richmond, D.L. Kaplan, Silk based biomaterials, Biomaterials 24 (2003) 401–416.

(85). L.D. Miller, S. Putthanarat, R.K. Eby, W.W. Adams, Investigation of the nanofibrillar morphology in silk fibers by small angle X-ray scattering and atomic force microscopy, International journal of biological macromolecules 24 (1999) 159–165.

(86). X. Chen, L. Huang, R. He, Silk fibroin as a sorbent for online extraction and pre-concentration of copper with detection by electrothermal atomic absorption spectrometry, Talanta 78 (2009) 71–75.

(87). M.K. Sah, K. Pramanik, Regenerated silk fibroin from bombyx mori silk cocoon for tissue engineering applications, International journal of environmental science and development 1 (5) (2010) 404-408.

(88). N. Kasoju, R.R. Bhonde, U. Bora, Fabrication of a novel micro nano fibrous nonwoven scaffold with antheraea assama silk fibroin for use in tissue engineering, Materials letters 63 (2009) 2466–2469.

(89). Zainuddin, T.T. Le, Y. Park, T.V. Chirila, P.J. Halley, A.K. Whittaker, The behavior of aged regenerated bombyx mori silk fibroin solutions studied by 1H NMR and rheology, Biomaterials 29 (2008) 4268–4274.

(90). M.K. Sah, K. Pramanik, Regenerated silk fibroin from bombyx mori silk cocoon for tissue engineering applications, International journal of environmental science and development 1 (5) (2010) 404-408.

(91). M. Mukhopadhyay, T. Kaur, R. Khanna, Fixed bed and reduced lumped diffusion model parameter estimation of copper biosorption using aspergillus niger biomass, The canadian journal of chemical engineering 90 (2012) 1011-1016.

(92). C. Gerente, V.K.C. Lee, P.L. Cloriec, G. McKay, Application of chitosan for the removal of metals from wastewaters by adsorption: mechanisms and models review, Critical reviews in environmental science and technology 37 (2007) 41–127.

(93). I. Kavianinia, P.G. Pliegera, N.G. Kandileb, D.R.K. Harding, Fixed bed column studies on a modified chitosan hydrogel for detoxification of aqueous solutions from copper(II), Carbohydrate polymers 90 (2012) 875– 886.

(94). V.J.P. Vilar, C.M.S. Botelho, J.M. Loureiro, R.A.R. Boaventura, Biosorption of copper by marine algae gelidium and algal composite material in a packed bed column, Bioresource technology 99 (2008) 5830–5838.

(95). M. Karatas, Removal of Pb(II) from water by natural zeolitic tuff: kinetics and thermodynamics, Journal of hazardous materials 199 (2012) 383– 389.

(96). K.S. Rao, S. Anand, P. Venkateswarlu, Modeling the kinetics of Cd(II) adsorption on syzygium cumini leaf powder in a fixed bed mini column, Journal of industrial and engineering chemistry 17 (2011) 174–181.

(97). W. Zhang, L. Dong, H. Yan, H. Li, Z. Jiang, X. Kan, H. Yang, A. Li, R. Cheng, Removal of methylene blue from aqueous solutions by straw based adsorbent in a fixed bed column, Chemical engineering journal 173 (2011) 429– 436.

(98). F. Rashidi, R.S. Sarabi, Z. Ghasemib, A. Seif, Kinetic, equilibrium and thermodynamic studies for the removal of lead (II) and copper (II) ions from aqueous solutions by nanocrystalline TiO_2, Superlattices and microstructures 48 (2010) 577–591.

(99). V.J.P. Vilar, J.M. Loureiro, C.M.S. Botelho, R.A.R. Boaventura, Continuous biosorption of Pb/Cu and Pb/Cd in fixed bed column using algae gelidium and granulated agar extraction algal waste, Journal of hazardous materials 154 (2008) 1173–1182.

(100). V.J.P. Vilar, C.M.S. Botelho, R.A.R. Boaventura, Lead uptake by algae Gelidium and composite material particles in a packed bed column, Chemical engineering journal 144 (2008) 420–430.

(101). P. Agrawal, A.K. Bajpai, Dynamic column adsorption studies of toxic Cr(VI) ions onto iron oxide loaded gelatin nanoparticles, Journal of dispersion science and technology 32 (2011) 1353–1362.

(102). E. Worch, Fixed bed adsorption in drinking water treatment: a critical review on models and parameter estimation, Journal of water supply: research and technology aqua 57 (3) (2008) 171-183.

(103). Y.S. Ho, G. McKaya, Comparison of chemisorption kinetic models applied to pollutant removal on various sorbents, Process safety and environmental protection 76 (4) (1998) 332-340.

(104). I.M. Elnaggar, E.S. Zakaria, I.M. Ali, M. Khalil, M.F. Elshahat, Kinetic modeling analysis for the removal of cesium ions from aqueous solutions using polyaniline titanotungstate, Arabian journal of chemistry 5 (2012) 109–119.

(105). G. Issabayeva, M.K. Aroua, N.M. Sulaiman, Continuous adsorption of lead ions in a column packed with palm shell activated carbon, Journal of hazardous materials 155 (2008) 109–113.

(106). H.C. Thomas, Heterogeneous ion exchange in a flowing system, Journal of the American chemical society 66 (10) (1944) 1664-1666.

(107). H.M. Baker, A.M. Massadeh, H.A. Younes, Natural jordanian zeolite: removal of heavy metal ions from water samples using column and batch methods, Environmental monitoring and assessment 157 (2009) 319–330.

(108). A. Wolborska, Adsorption on activated carbon of p-nitrophenol from aqueous solution, Water research 23 (1989) 85–91.

(109). L. Wang, C. Lin, Equilibrium study on chromium (III) ion removal by adsorption onto rice hull ash, Journal of the Taiwan institute of chemical engineers 40 (2009) 110–112.

(110). R.M. Schneider, C.F. Cavalin, M.A.S.D. Barros, C.R.G. Tavares, Adsorption of chromium ions in activated carbon, Chemical engineering journal 132 (2007) 355–362.

(111). G.S. Bohart, E.Q. Adams, Some aspects of the behavior of charcoal with respect to chlorine, Journal of the American chemical society 42 (3) (1920) 523–544.

(112). R.A Hutchins, New method simplifies design of activated carbon systems, Chemical engineering journal 80 (1973) 133–138.

(113). Y.H. Yoon, J.H. Nelson, Application of gas adsorption kinetics I. a theoretical model for respirator cartridge service life, American industrial hygiene association journal 45 (8) (1984) 509-516.

(114). A.L. Laila, J.A. Bergendahl, R.W. Thompson, Adsorption of methyl tertiary butyl ether on granular zeolites: batch and column studies, Journal of hazardous materials 178 (2010) 363–369.

(115). A.D. Nandasana, A.K. Ray, S.K. Gupta, Applications of the non-dominated sorting genetic algorithm (NSGA) in chemical reaction engineering, International journal of chemical reactor engineering 1 (2003) 1-16.

(116). Z. Zhang, K. Hidajat, A.K. Ray, Application of simulated countercurrent moving bed chromatographic reactor for MTBE synthesis, Industrial and engineering chemistry research 40 (2001) 5305-5316.

(117). Z. Zhang, K. Hidajat, A.K. Ray, Multiobjective optimization of SMB and varicol process for chiral separation, Journal for the American institute of chemical engineers 48 (2002) 2800-2816.

(118). W. Li, D.R. Coffin, T.Z. Jin, N. Latona, C. Liu, B. Liu, J. Zhang, L. Liu, Biodegradable composites from polyester and sugar beet pulp with antimicrobial coating for food packaging, Journal of applied polymer science 126 (2012) 361–372.

(119). J.R. Ogez, J.C. Hodgdon, M.P. Beal, S.E. Builder, Downstream processing of proteins: recent advances, Biotechnology advances 7 (4) (1989) 467-488.

(120). G. Wider, L. Dreier, Measuring protein concentrations by NMR spectroscopy, Journal of American chemical society 128 (8) (2006) 2571-2576.

(121). G.C. Cunha, L.P.C. Romao, M.C. Santos, B.R. Araujo, S. Navickiene, V.L. Padua, Adsorption of trihalomethanes by humin: batch and fixed bed column studies, Bioresource technology 101 (2010) 3345–3354.

(122). S. Bunluesin, M. Kruatrachue, P. Pokethitiyook, S. Upatham, G.R. Lanza, Batch and continuous packed column studies of cadmium biosorption by hydrilla verticillata biomass, Journal of bioscience and bioengineering 103 (6) (2007) 509–513.

(123). E.A. Oluyemi, J.A.O. Oyekunle, S.O. Olasoji, A comparative study of the removal of heavy metal ions from synthetic wastewaters using different adsorbents, Adsorption science and technology 27 (5) (2009) 493-501.

(124). N. Ertugay, Y.K. Bayhan, Biosorption of Cr(VI) from aqueous solutions by biomass of *agaricus bisporus*, Journal of hazardous materials 154 (2008) 432-439.

(125). Y. Liu, Is the free energy change of adsorption correctly calculated, Journal of chemical and engineering data 54 (2009) 1981–1985.

(126). M. Erdem, A. Ozverdi, Kinetics and thermodynamics of Cd(II) adsorption onto pyrite and synthetic iron sulphide, Separation and purification technology 51 (2006) 240–246.

(127). R. Rakhshaee, M. Khosravi, M.T. Ganji, Kinetic modeling and thermodynamic study to remove Pb(II), Cd(II), Ni(II) and Zn(II) from aqueous solution using dead and living *azolla filiculoides*, Journal of hazardous materials 134 (2006) 120–129.

(128). E.F.S. Vieira, A.R. Cestari, C.D.S. Oliveira, P.S. De-lima, L.E. Almeida, Thermodynamics of pyrimethamine and sulfadiazine binding to a chitosan derivative, Thermochimica Acta 459 (2007) 9–11.

(129). B.H. Hameed, A.T.M. Din, A.L. Ahmad, Adsorption of methylene blue onto bamboo-based activated carbon: kinetics and equilibrium studies, Journal of hazardous materials 141 (2007) 819–825.

(130). S. Kubilay, R. Gurkan, A. Savran, T. Sahan, Removal of Cu(II), Zn(II) and Co(II) ions from aqueous solutions by adsorption onto natural bentonite, Adsorption *13* (2007) 41–51.

(131). K. Vijayaraghavan, Y.S. Yun, Biosorption of C.I. reactive black 5 from aqueous solution using acid-treated biomass of brown seaweed *laminaria* sp, Dyes and Pigments 76 (2008) 726–732.

(132). I. Langmuir, The adsorption of gases on plane surfaces of glass, mica, and platinum, Journal of the American chemical society 40 (1918) 1361–1403.

(133). D. Graham, The characterization of physical adsorption systems. I. The equilibrium function and standard free energy of adsorption, The journal of physical chemistry 57 (1953) 665–669.

(134). T.L. Brown, H.E. LeMay, Jr, B.E. Bursten, C.J. Murphy, Chemistry, Chapter 4 (2009).

(135). S.K. Milonjic, A consideration of the correct calculation of thermodynamic parameters of adsorption, Journal of the Serbian chemical society 72 (2007) 1363– 1367.

(136). H. Pahlavanzadeh, A.R. Keshtkarb, J. Safdarib, Z. Abadia, Biosorption of nickel(II) from aqueous solution by brown algae: equilibrium, dynamic and thermodynamic studies, Journal of hazardous materials 175 (2010) 304–310.

(137). N. Dizge, B. Keskinler, H. Barlas, Sorption of Ni(II) ions from aqueous solution by lewatit cation exchange resin, Journal of hazardous materials 167 (2009) 915–926.

(138). T. Fan, Y. Liu, B. Feng, G. Zeng, C. Yang, M. Zhou, H. Zhou, Z. Tan, X. Wang, Biosorption of cadmium(II), zinc(II) and lead(II) by penicillium simplicissimum: isotherms, kinetics and thermodynamics, Journal of hazardous materials 160 (2008) 655–661.

(139). X. Zhang, H. Su, T. Tan, G. Xiao, Study of thermodynamics and dynamics of removing Cu(II) by biosorption membrane of penicillium biomass, Journal of hazardous materials 193 (2011) 1– 9.

(140). V.K. Gupta, Equilibrium uptake, sorption dynamics, process development and column operations for the removal of copper and nickel from aqueous solution and wastewater using activated slag, a low cost adsorbent, Industrial and engineering chemistry research 37 (1998) 192-202.

(141). C. Chang, Y. Ku, The adsorption characteristics of EDTA chelated copper ion by activated carbon in a column test, Separation science and technology 33 (4) (1998) 483-501.

(142). T.S. Najim, S.A. Yassin, Removal of chromium from aqueous solution using modified pomegranate peel: mechanistic and thermodynamic studies, E-journal of Chemistry 6 (S1) (2009) 153-158.

(143). S. Paria, K.C. Khilar, A review on experimental studies of surfactant adsorption at the hydrophilic solid–water interface, Advances in colloid and interface science 110 (2004) 75– 95.

(144). G. Vidali, G. Ihm, H.Y. Kim, M.W. Cole, Potentials of physical adsorption, Surface science reports 12 (1991) 133-181.

(145). H. Qiu, L. Lv, B. Pan, Q. Zhang, W. Zhang, Critical review in adsorption kinetic models, Journal of zhejiang university science 10 (5) (2009) 716-724.

(146). S.S. Baral, S.N. Das, G.R. Chaudhury, Y.V. Swamy, P. Rath, Adsorption of Cr(VI) using thermally activated weed *Salvinia cucullata*, Chemical engineering journal 139 (2008) 245–255.

(147). M. Greluk, Z. Hubicki, Sorption of spadns azo dye on polystyrene anion exchangers: equilibrium and kinetic studies, Journal of hazardous materials 172 (2009) 289–297.

(148). E. Pehlivan, H.T. Kahraman, Hexavalent chromium removal by osage orange, Food chemistry 133 (2012) 1478–1484.

(149). M.I. Zaman, S. Mustafa, S. Khan, B. Xing, Heavy metal desorption kinetic as affected by of anions complexation onto manganese dioxide, Surfaces chemosphere 77 (6) (2009) 747–755.

(150). B.O. Shaughnessy, D. Vavylonis, Non-equilibrium in adsorbed polymer layers, Journal of physics: condensed matter 17 (2005) 63–99.

(151). M. Suzuki, Role of adsorption in water environment process, Water science and technology 35 (7) (1997) 1-11.

(152). M. Trgo, N.V. Medvidovic, J. Peric, Application of mathematical empirical models to dynamic removal of lead on natural zeolite clinoptilolite in a fixed bed column, Indian journal of chemical technology 18 (2011) 123-131.

(153). G.M. Nogueira, R.F. Weska, W.C. Vieira, B. Polakiewicz, A.C.D. Rodas, O.Z. Higa, M.M. Beppu, A new method to prepare porous silk fibroin membranes suitable for tissue scaffolding applications, Journal of applied polymer science 114 (2009) 617–623.

(154). N. Prabhu, K. Sharp, Protein solvent interactions, Chemical reviews 106 (2006) 1616-1623.

(155). A. Biswas, R.L. Shogren, D.G. Stevenson, J.L. Willett, P.K. Bhowmik, Ionic liquids as solvents for biopolymers: acylation of starch and zein protein, Carbohydrate polymers 66 (2006) 546–550.

(156). D.M. Phillips, L.F. Drummy, D.G. Conrady, D.M. Fox, R.R. Naik, M.O. Stone, P.C. Trulove, H.C.D. Long, R.A. Mantz, Dissolution and regeneration of bombyx mori silk fibroin using ionic liquids, Journal of the American chemical society 126 (2004) 14350-14351.

(157). S. Ghanaati, C. Orth, R.E. Unger, M. Barbeck, M.J. Webber, A. Motta, C. Migliaresi, C.J. Kirkpatrick, Fine tuning scaffolds for tissue regeneration: effects of formic acid processing on tissue reaction to silk fibroin, Journal of tissue engineering and regenerative medicine 4 (2010) 464–472.

(158). R. Rajkhowa, B. Levin, S.L. Redmond, L.H. Li, L. Wang, J.R. Kanwar, M.D. Atlas, X. Wang, Structure and properties of biomedical films prepared from aqueous and acidic silk fibroin solutions, Journal of biomedical materials research 97 (2011) 37-45.

(159). K. Matsumoto, H. Uejima, Regenerated protein fibers. Research and development of a novel solvent for silk fibroin, Polymer chemistry 35 (1997) 1949-1954.

(160). C.I.C. Silvestre, J.L.M. Santos, J.L.F.C. Lima, E.A.G. Zagatto, Liquid liquid extraction in flow analysis: a critical review, Analytica chimica acta 652 (2009) 54–65.

(161). B.B. Mandal, S.C. Kundu, Non-Bioengineered silk gland fibroin protein: characterization and evaluation of matrices for potential tissue engineering applications, Biotechnology and bioengineering 100 (6) (2008) 1237-1250.

(162). M. Boulet-Audet, T. L. Vre, T. Buffeteau, M.P. Zolet, Attenuated total reflection infrared spectroscopy: An efficient technique to quantitatively determine the orientation and conformation of proteins in single silk fibres, Applied spectroscopy 62 (9) (2008) 956-962.

(163). B.D. Lawrence, F. Omenetto, K. Chui, D.L. Kaplan, Processing methods to control silk fibroin film biomaterial features, Journal of material science 43 (2008) 6967-6985.

(164). K.V. Meel, A. Smekens, M. Behets, P. Kazandjian, R. Grieken, Determination of platinum, palladium, and rhodium in automotive catalysts using high energy secondary target X-ray fluorescence spectrometry, Analytical chemistry 79 (2007) 6383-6389.

(165). M. Tsezos, R.G.L. McCready, J.P. Bell, The continuous recovery of uranium from biologically leached solutions using immobilized biomass, Biotechnology and bioengineering 34 (1989) 10–17.

(166). L.E. Macaskie, P. Yong, T.C. Doyle, M.G. Roig, M. Diaz, T. Manzano, Bioremediation of uranium Bearing wastewater: biochemical and chemical factors influencing bioprocess application, Biotechnology and bioengineering 53 (1997) 100–109.

(167). C. Amorosi, V. Ball, J. Bour, P. Bertani, V. Toniazzo, D. Ruch, L. Averous, M. Michel, One step preparation of plasma based polymer films for drug release, Materials science and engineering 32 (2012) 2103–2108.

(168). M. Moritz, M. Laniecki, Application of SBA-15 mesoporous material as the carrier for drug formulation systems. Papaverine hydrochloride adsorption and release study, Powder technology 230 (2012) 106–111.

(169). C.M. Zvinowanda, J.O. Okonkwo, N.M. Agyei, M.M Sekhula, R. Sadiku, Application of maize tassel for the removal of Pb, Se, Sr, U and V from borehole water contaminated with mine wastewater in the presence of alkaline metals, ournal of hazardous materials 164 (2-3) (2009) 884-891.

(170). B. Yu, Y. Zhang, A. Shukla, S.S. Shukla, K.L. Dorris, The removal of heavy metals from aqueous solutions by sawdust adsorption, removal of lead and comparison of its adsorption with copper, Journal of hazardous materials 84 (2001) 83–94.

(171). G. Cimino, A. Passerini, G. Toscano, Removal of toxic cations and Cr(VI) from aqueous solutions by hazelnut shell, Water research 34 (2000) 2955–2962.

(172). K.G. Bhattacharyya, S.S. Gupta, Adsorptive accumulation of Cd(II), Co(II), Cu(II), Pb(II) and Ni(II) ions from water onto kaolinite: influence of acid activation, Adsorption science and technology 27 (2009) 47–68.

(173). K.S. Low, C.K. Lee, S.M. Mak, Sorption of copper and lead by citric acid modified wood, Wood science and technology 38 (2004) 629-640.

(174). N. Meunier, J. Laroulandie, J.F. Blais, R.D. Tyagi, Cocoa shells for heavy metal removal from acidic solutions. Bioresourse technology 90 (2003) 255–263.

(175). L.J. Yu, S.S. Shukla, K.L. Dorris, A. Shukla, J.L. Margrave, Adsorption of chromium from aqueous solutions by maple sawdust, Journal of hazardous materials 100 (1‐3) (2003) 53‐63.

(176). M. Dakiky, M. Khamis, A. Manassra, M. Mereb, Selective adsorption of chromium(VI) in industrial wastewater using low-cost abundantly available adsorbents, Advances in environmental research 6 (2002) 533‐540.

(177). T. Karthikeyan, S. Rajgopal, L.R. Miranda, Chromium(VI) adsorption from aqueous solution by hevea brasilinesis sawdust activated carbon, Journal of hazardous materials 124 (1‐3) (2005) 192‐199.

(178). H. Gao, Y. Liu, G. Zeng, W. Xu, T. Li, W. Xia, Characterization of Cr(VI) removal from aqueous solutions by a surplus agricultural waste, rice straw, Journal of hazardous materials 150 (2) (2008) 446‐452.

(179). M. Bansal, U. Garg, D. Singh, V.K. Garg, Removal of Cr(VI) from aqueous solutions using pre-consumer processing agricultural waste: a case study of rice husk, Journal of hazardous materials 162 (2009) 312‐320.

(180). M. Machida, J.R.M. Carvalho, J.N. Correia, Removal of trivalent chromium from solution by biosorption in cork powder, Journal of chemical technology 77 (12) (2002) 1340-1348.

(181). R. Gundogan, B. Acemioglu, M.H. Alma, Copper(II) adsorption from aqueous solution by herbaceous peat, Journal of colloid and interface science 269 (2004) 303‐309.

(182). J.M. Randall, R.L. Berman, V. Garret, A.C. Waiss, Use of bark to remove heavy metal ions, Forest product journal 24 (9) (1974) 80-84.

(183). N. Basci, E. Kocadagistan, B. Kocadagistan, Biosorption of copper(II) from aqueous solutions by wheat shell, Desalination 164 (2004) 135‐140.

(184). M. Sciban, M. Klasnja, B. Skrbic, Adsorption of copper ions from water by modified agricultural by-products, Desalination 229 (2008) 170‑180.

(185). A. Afkhami, T. Madrakian, Z. Karami, A. Amini, Effect of treatment of carbon cloth with sodium hydroxide solution on its adsorption capacity for the adsorption of some cations, Colloids and surfaces a physicochemical and engineering aspects 304 (1-3) (2007) 36-40.

(186). H.H. Sokker, S.M. Badawy, E.M. Zayed, F.A.N. Eldien, A.M. Farag, Rediation-induced grafting of glycidyl methacrylate onto cotton fabric waste and its modification for anchoring hazardous waste from their solutions, Journal of hazardous materials 168 (1) (2009) 137-144.

(187). M. Tabakci, S. Erdemir, M. Yilmaz, Preparation, characterization of cellulose grafted with calix[4]arene polymers for the adsorption of heavy metals and dichromate anions, Journal of hazardous materials 148 (1-2) (2007) 428-435.

(188). A. Nakajima, T. Sakaguchi, Selective accumulation of heavy metals by microorganisms, Applied microbiology and biotechnology 24 (1986) 59-64.

(189). J.H. Holland, Adaptation in natural and artificial systems: An introductory analysis with applications to biology, Control and artificial intelligence, University of Michigan press, Ann Arbor MI 1975.

(190). K. Deb, Nonlinear goal programming using multi-objective genetic algorithms, Journal of the Operational Research Society 52 (3) (2001) 291-302.

(191). N. Srinivas, K. Deb, Multiobjective function optimization using nondominated sorting genetic algorithms, Evolutionary Computation Journal 2 (3) (1995) 221-248.

(192). P.K. Kundu, A.K. Ray, A. Elkamel, Numerical simulation and optimisation of unconventional three-section simulated countercurrent moving bed chromatographic reactor for oxidative coupling of methane reaction, The Canadian journal of chemical engineering 90 (6) (2012) 1502-1513.

APPENDIX A

CALIBRATION CURVE FOR SERICIN CONCENTRATION

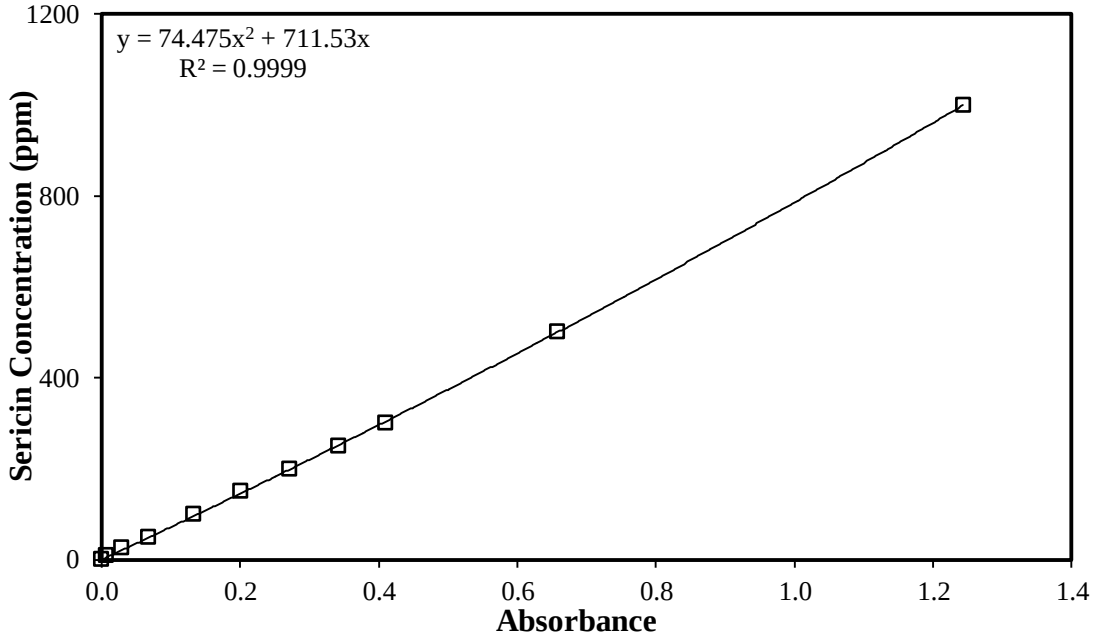

Figure A.1 Calibration curve used to calculate sericin concentration in water by using 282nm wavelength.

CALIBRATION CURVES FOR ALL METALS

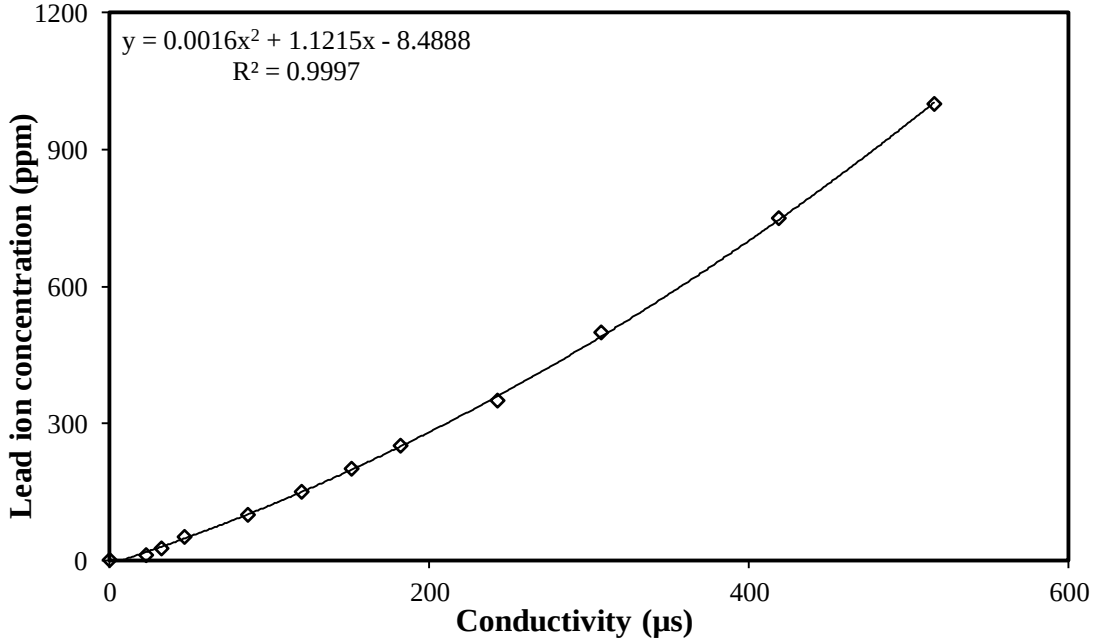

Figure A.2 Calibration curve used to calculate Lead ion concentration in water by using conductivity.

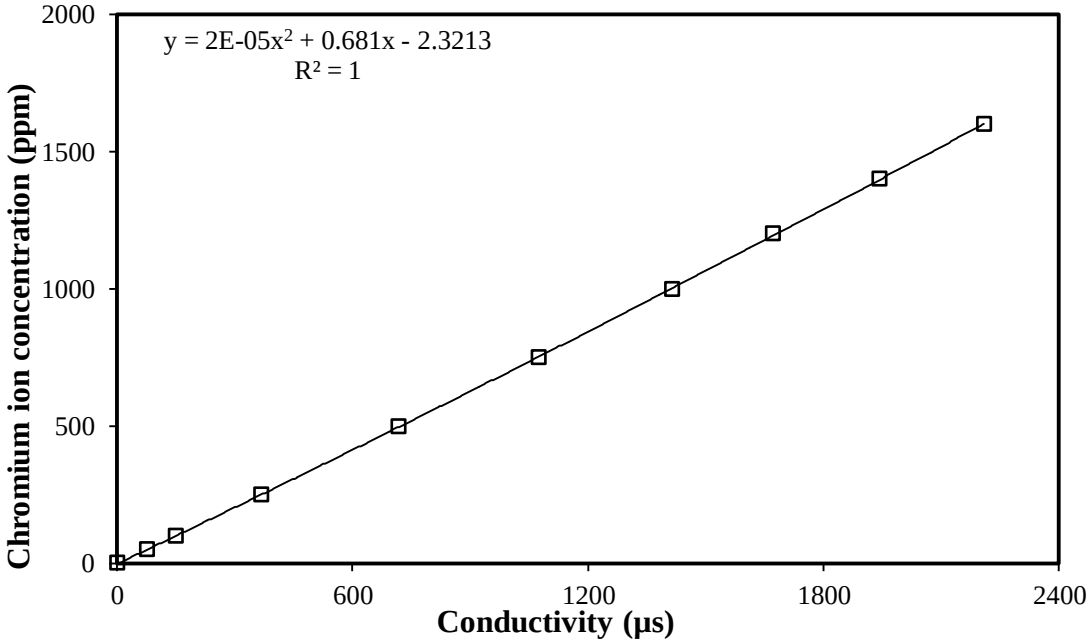

Figure A.3 Calibration curve used to calculate Chromium ion concentration in water by using conductivity.

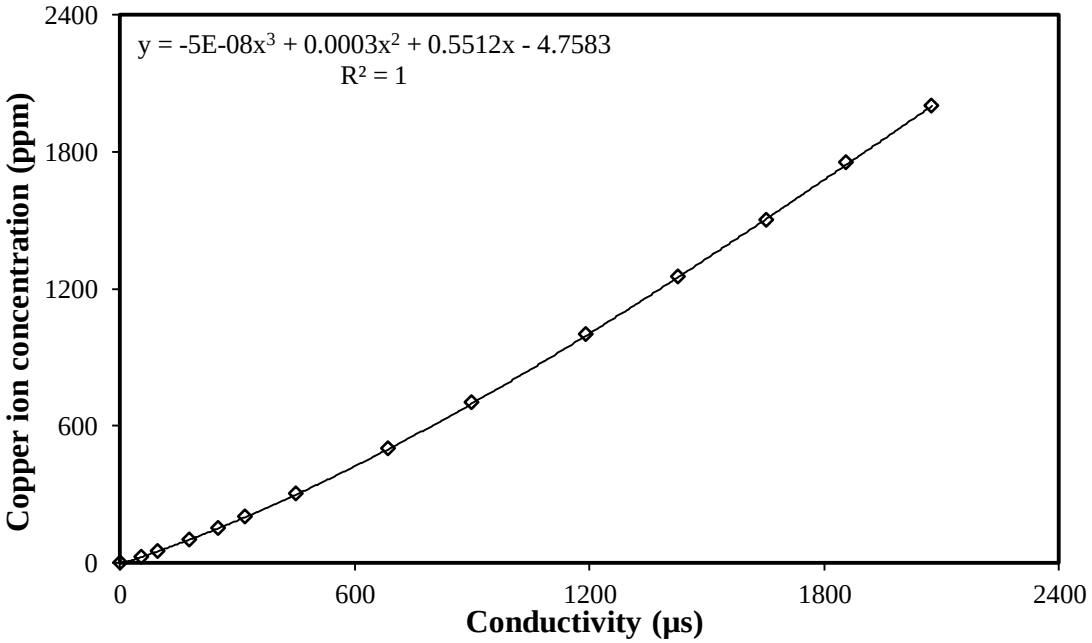

Figure A.4 Calibration curve used to calculate Copper ion concentration in water by using conductivity.

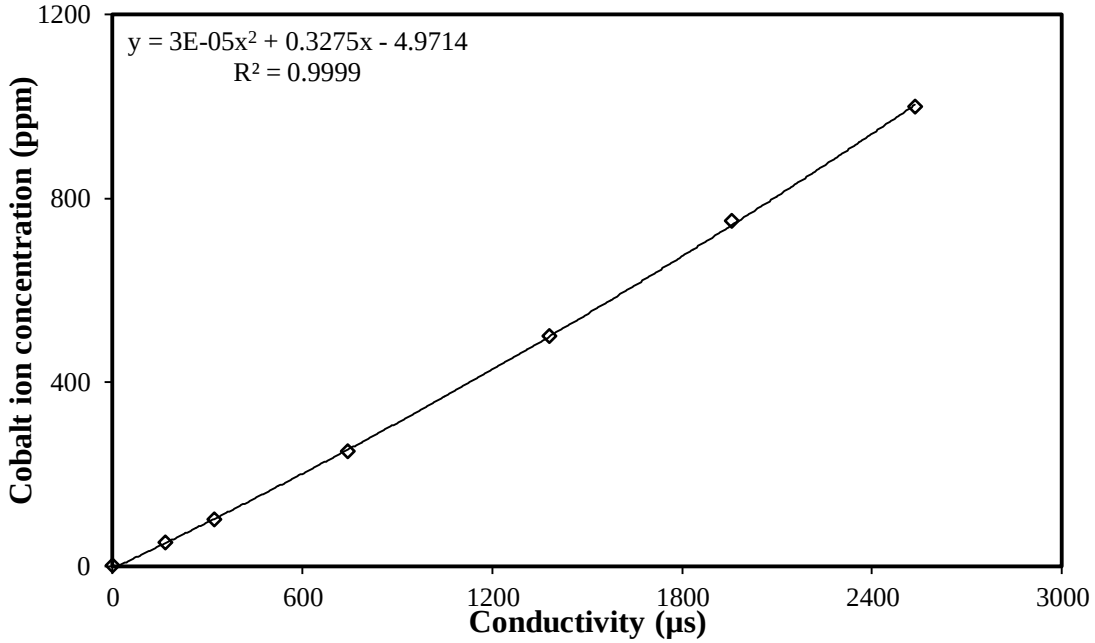

Figure A.5 Calibration curve used to calculate Cobalt ion concentration in water by using conductivity.

APPENDIX B

DATA FITTING TO PSEUDO-SECOND-ORDER KINETIC MODEL

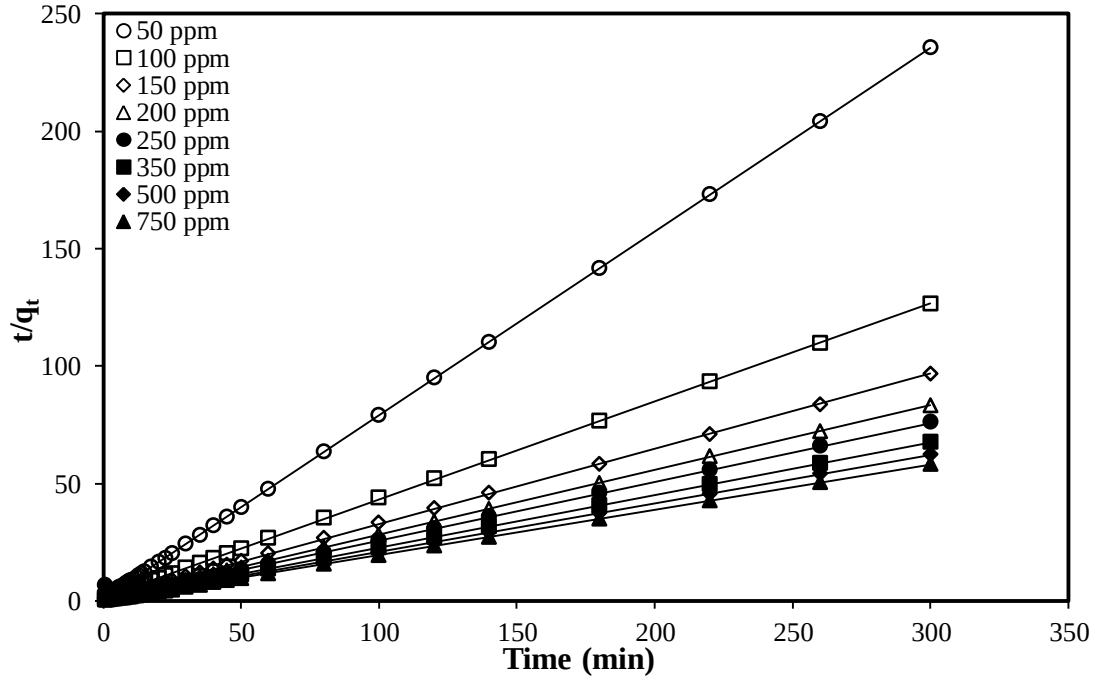

Figure B.1 Data fitted to pseudo 2nd order kinetic model for the adsorption of ***lead*** with variable inlet concentration.

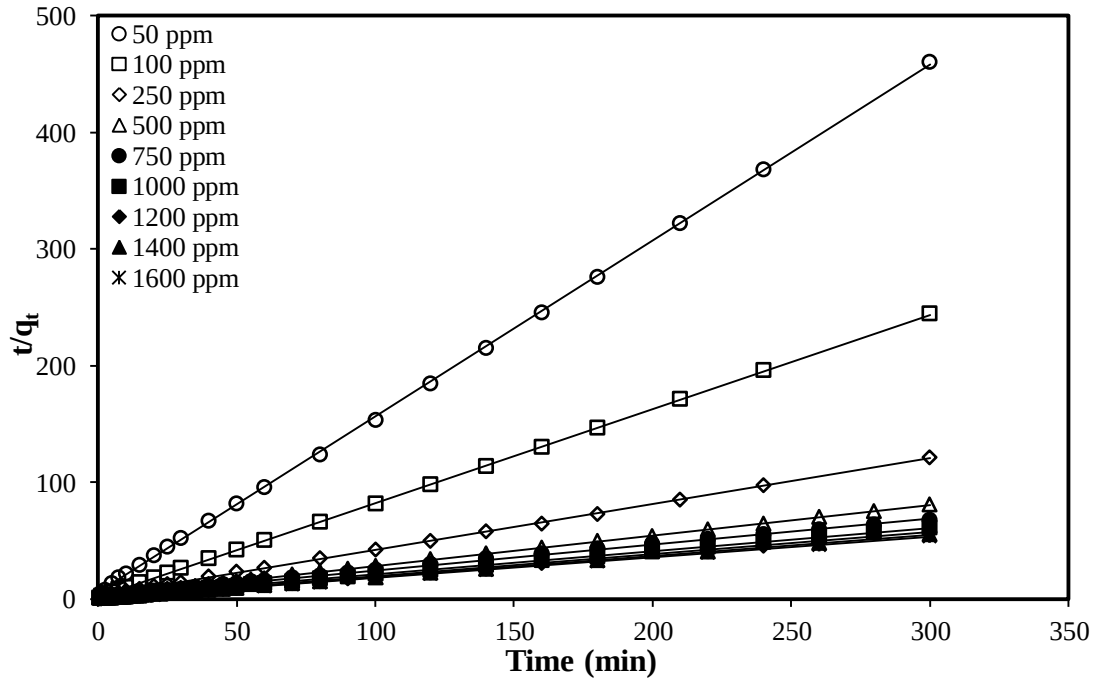

Figure B.2 Data fitted to pseudo 2nd order kinetic model for the adsorption of ***chromium*** with variable inlet concentration.

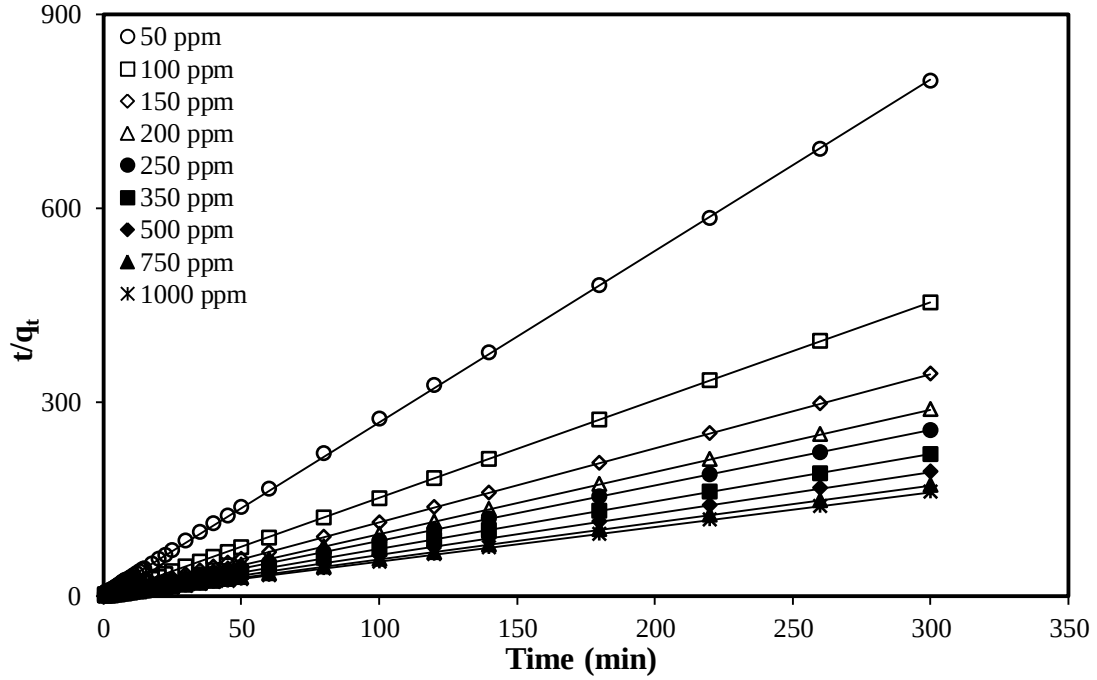

Figure B.3 Data fitted to pseudo 2nd order kinetic model for the adsorption of ***copper*** with variable inlet concentration.

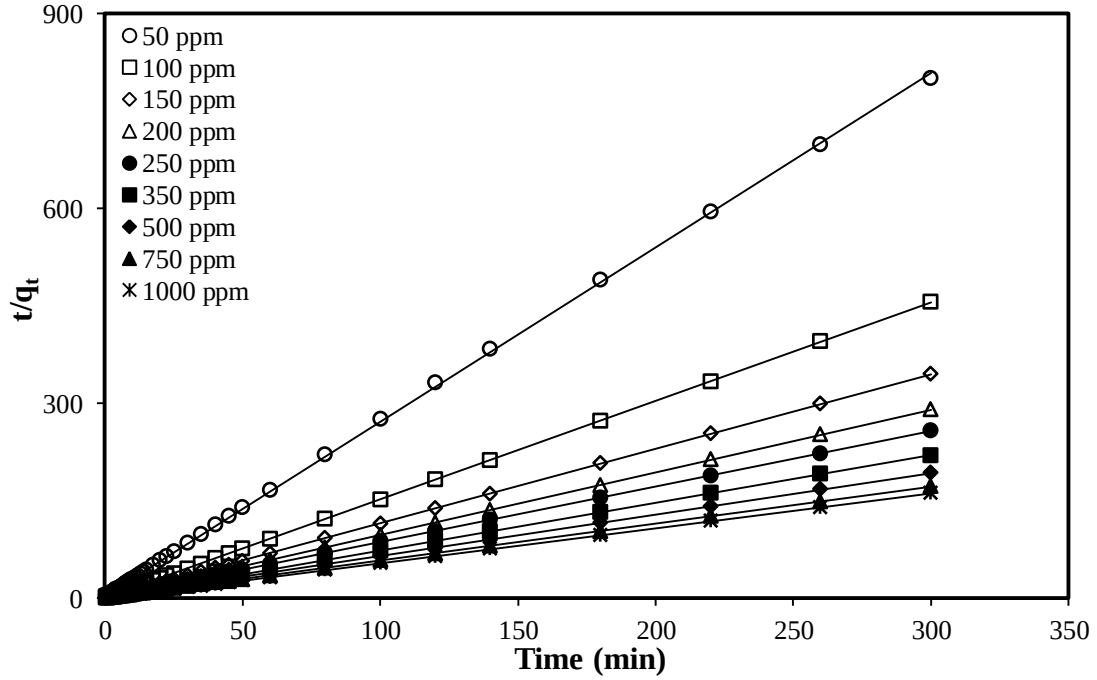

Figure B.4 Data fitted to pseudo 2nd order kinetic model for the adsorption of ***cobalt*** with variable inlet concentration.

DATA FITTING TO THE INTRAPARTICLE DIFFUSION MODEL

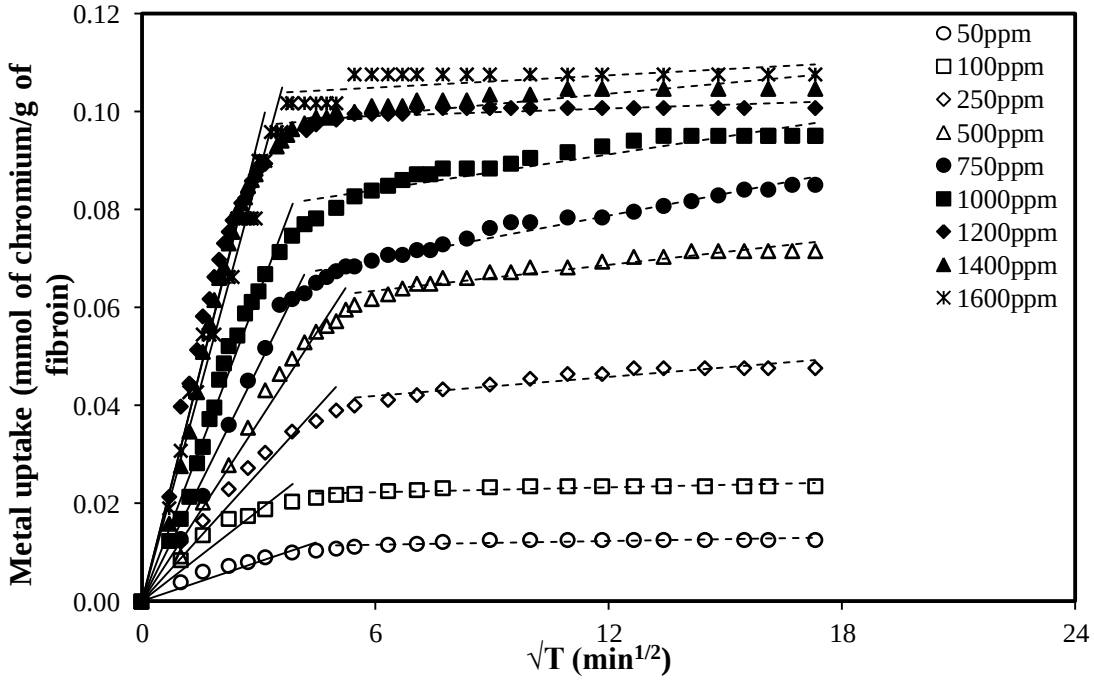

Figure B.5 Data fitted to intra particle diffusion model for the adsorption of ***chromium*** with variable inlet concentration.

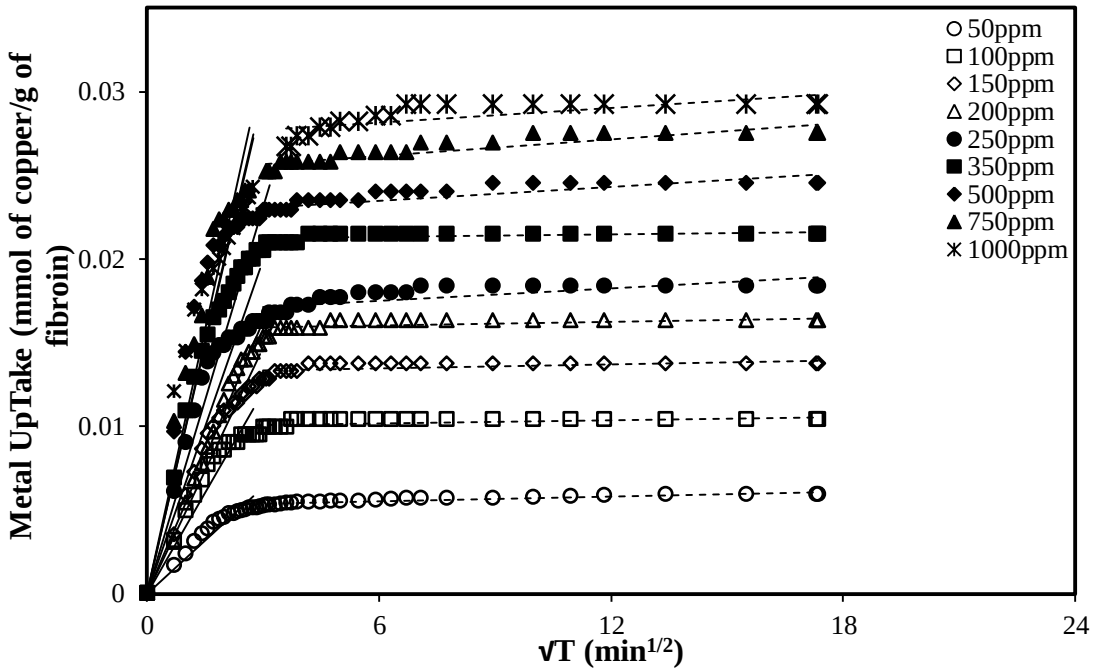

Figure B.6 Data fitted to intra particle diffusion model for the adsorption of ***copper*** with variable inlet concentration.

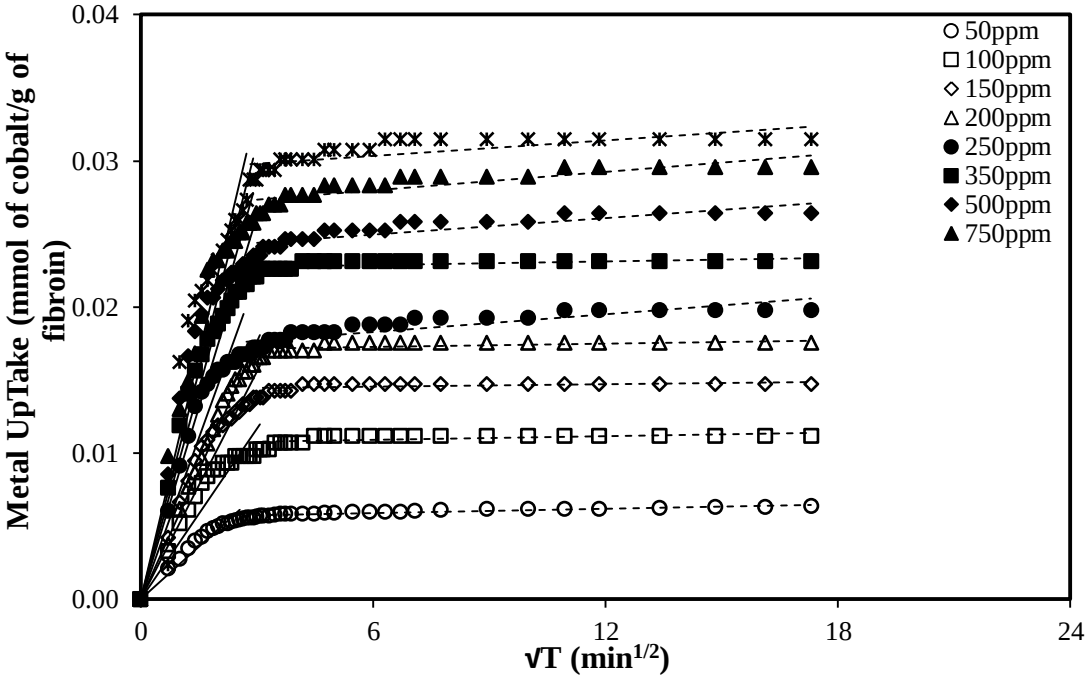

Figure B.7 Data fitted to intra particle diffusion model for the adsorption of ***cobalt*** with variable inlet concentration.

Table B.1 Number of samples with their flow rate collected to measure the influent flow rate flowing through the column.

OBSERVATIONS	Flow Rate I	Flow Rate II	Flow Rate III	Flow Rate IV
No.	(ml/min)			
1	0.149	0.182	0.209	0.238
2	0.148	0.179	0.212	0.242
3	0.151	0.181	0.211	0.239
4	0.149	0.178	0.208	0.241
5	0.149	0.181	0.213	0.240
6	0.151	0.179	0.207	0.241
7	0.148	0.178	0.212	0.239
8	0.152	0.182	0.213	0.241
9	0.151	0.181	0.207	0.239
10	0.152	0.179	0.209	0.241
Average	0.15	0.18	0.21	0.24

Table B.2 Comparison of maximum uptake capacity of fibroin with other sorbents reported in literature. (Adsorption temperature 25^{o}C)

Metal	Sorbent	Metal Uptake (mg/g)	Reference
Lead	Sphagnum moss peat	12.3	57
	Maize tassel	2.6	169
	Maple sawdust	3.2	170
	Hazelnut shell	1.8	171
	Kaolinite	11.1	172
	Wood	8.0	173
	Coca shells	6.2	174
	Fibroin	5.2	This Study
Chromium	Rice hull ash	7.0	109
	Osage orange	5.5	148
	Maple sawdust	5.1	175
	Cactus leaves	7.1	176
	Coconut tree sawdust	3.6	177
	Rice straw	3.2	178
	Rice husk	8.5	179
	Cork powder	6.3	180
	Fibroin	5.6	This Study
Copper	Wood	3.0	174
	Herbaceous peat	4.8	181
	Bark	18.0	182
	Wheat shell	8.3	183
	Wheat straw	4.5	184
	Soybean straw	5.4	184
	Corn	3.8	184
	Corn cob	2.2	184
	Fibroin	1.84	This Study
Cobalt	Bark	2.0	182
	Carbon cloth	12.0	185
	Cotton fabric waste	14.0	186
	Cellulose	4.7	187
	Aspergillus niger	2.4	188
	Rhizopus arrhizus	2.9	188
	Saccharomyces cerevisiae	5.8	188
	Fibroin	1.83	This study

APPENDIX C

GENETIC ALGORITHM USED TO SOLVE MODIFIED PSEUDO-SECOND-ORDER EQUATION IN FORTRAN®

The genetic algorithm (GA) [189] is a search technique that mimics the process of natural selection and natural genetics. In this algorithm, a set of decision variables is first coded in the form of a set of randomly generated binary numbers (0 and 1), called strings or chromosomes, thereby creating a "population (gene pool)" of such binary strings. Each chromosome is then mapped into a set of real values of the decision variables, using the upper and lower bounds of each of these. A model of the process is then used to provide values of the objective function for each chromosome. The value of the objective function of any chromosome reflects its "fitness". The Darwinian principle of "survival of the fittest" is used to generate a new and improved gene pool (new generation). This is done by preparing a "mating pool" that comprises copies of chromosomes, the number of copies of any chromosome being proportional to its fitness (Darwin's principle). Pairs of chromosomes are then selected randomly, and pairs of daughter chromosomes generated using operations similar to those in genetic reproduction. The gene pool evolves, with fitness improving over the generations.

Three common operators are used in GA [called simple GA (SGA), to distinguish it from its various adaptations] to obtain an improved (next) generation of chromosomes, i.e., reproduction, crossover, and mutation. Reproduction is the generation of the mating pool, where the chromosomes are copied probabilistically, based on their fitness values. However, no new strings are formed in the reproduction phase. New strings are created using the crossover operator by exchanging information among pairs of strings in the mating pool. A pair of daughter chromosomes is produced by selecting a crossover site (chosen randomly) and exchanging the two parts of the pair of parent chromosomes (selected randomly from the mating pool). The effect of crossover can be detrimental or beneficial. It is hoped that the daughter strings are superior. If they are worse than the parent chromosomes, they will slowly die a natural death over the next few generations (the Darwinian principle at work). In order to preserve some of the good strings that are already present in the mating pool, not all strings in the pool are used in crossover. A

crossover probability, P_{cross}, is used, where only $100P_{cross}$% of the strings in the mating pool is involved in crossover, while the rest continue unchanged to the next generation. After a crossover is performed, mutation takes place. The mutation operator changes a binary number at any location in a chromosome from a 1 to a 0 and vice versa, with a small probability, P_{mute}. Mutation is needed to create a point in the neighbourhood of the current point, thereby achieving a local search around the current solution and to maintain diversity in the population. The entire process is repeated until some termination criterion is met (the specified maximum number of generations is attained, or the improvements in the values of the objective functions become lower than a specified tolerance).

In order to handle multiple objective functions and find optimal Pareto solutions, the SGA has been modified. The new algorithm, non-dominated sorting genetic algorithm (NSGA), differs from the SGA only in the way the selection operator works. The NSGA uses a ranking selection method to emphasize the good points and a niche method to create diversity in the population without losing a stable subpopulation of good points. In the new procedure, several groups of non-dominated chromosomes from among all the members of the population at any generation are identified and classified into "fronts". Each of the members in a particular front is assigned a large, common, front fitness value (a dummy value) arbitrarily. To evenly distribute the points in this (or any other) front evenly in the variable decision domain, the dummy fitness value is then modified according to a sharing procedure by dividing it by the niche count of the chromosome. The niche count is a quantity that represents the number of neighbours around it, with distant neighbours contributing less than those nearby. The niche count, thus, gives an idea of how crowded the chromosomes are in the variable decision space. Using the shared fitness value for reproduction, thus, helps spread the chromosomes in the front, since crowded chromosomes are assigned lower fitness values. This procedure is repeated for all members of the first front. Once this is done, these chromosomes are temporarily removed from consideration, and all the remaining ones are tested for non-dominance. The non-dominated chromosomes in this round are classified into the next front. These are all assigned a dummy fitness value that is a bit lower than the lowest shared fitness value of the previous front. Sharing is performed thereafter. The sorting and sharing is continued until all the chromosomes in the gene pool are assigned shared

fitness values. The usual operations of reproduction, crossover, and mutation are now performed. It is clear that the non-dominated members of the first front with fewer neighbours will get the highest representation in the mating pool. Members of later fronts, which are dominated, will get lower representations (they are still assigned some low fitness values, rather than "killed" in order to maintain the diversity of the gene pool). Sharing forces the chromosomes to be spread out in the variable decision space. The population is found to converge very rapidly to the Pareto set. It should also be noted that any number of objectives (both minimization and maximization problems) can be solved using this procedure [190-192]. The parameters used in this technique are presented in Table C.1 and a flow chart describing the technique is presented in Figure C.1.

Table C.1 Computational parameters of Non-dominated Sorting Genetic Algorithm (NSGA) used in multi-objective optimization study.

PARAMETERS	NOTATION	VALES
No. of generations	N_{gen}	50
Population size	N_{pop}	50
Sub-string length coding for each decision variable	l_{substr}	32
Crossover probability	P_{cross}	0.7
Mutation Probability	P_{mute}	0.005
Jumping jene probability	P_{jump}	0.15
Seed for random number generator	S_r	0.45

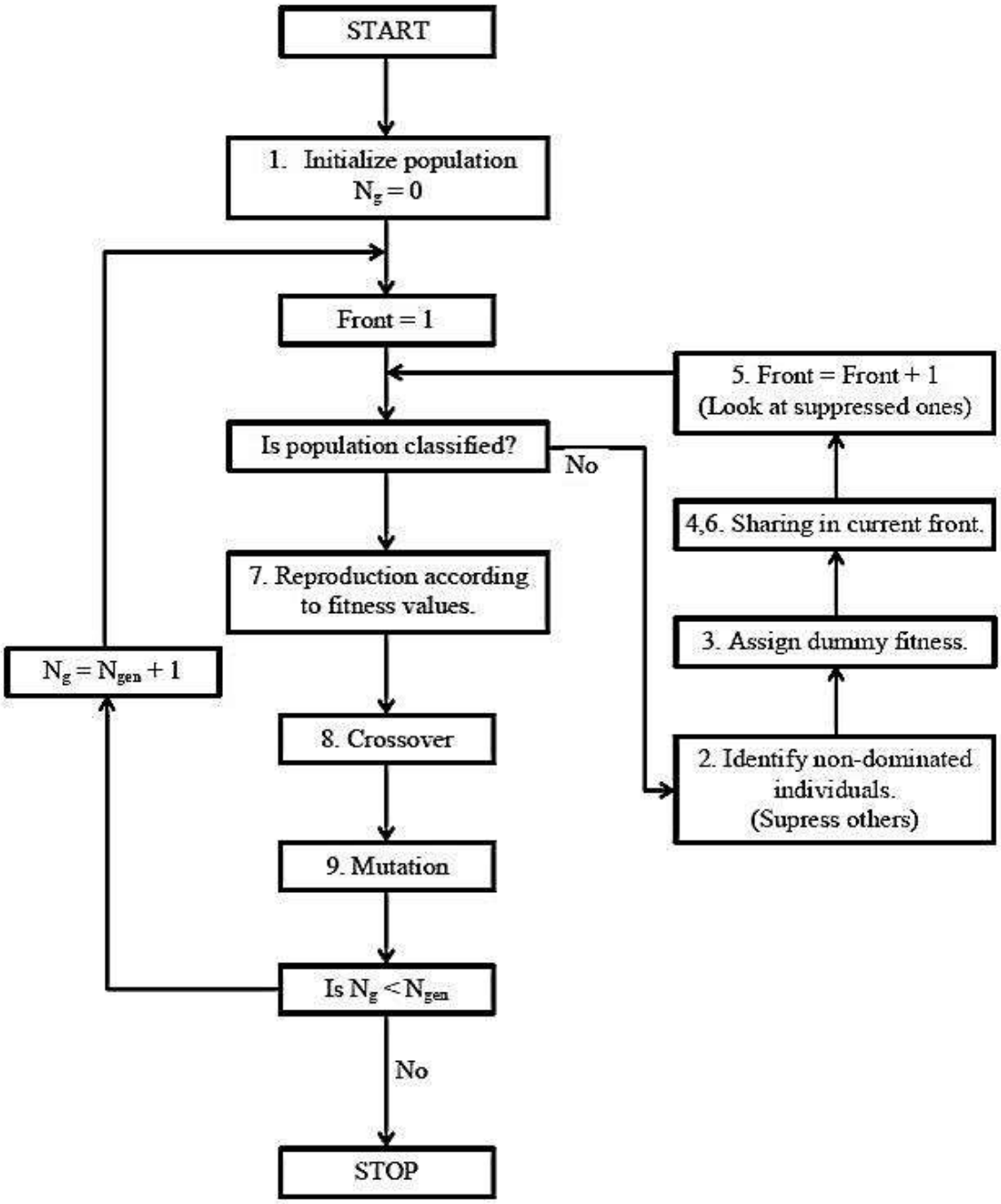

Figure C.1 Flow chart describing the technique to solve equation 4.29 and equation 4.31 in FORTRAN®.

FORTRAN® PROGRAMMING

FOR DATA FITTING TO EQUATION 4.29 FOR THE EVALUATION OF ADSORPTION RATE CONSTANT k_2.

```
PROGRAM MAIN
!    USE NUMERICAL_LIBRARIES
     Program main
     USE IMSLF90
     PARAMETER (NDATA=44)! This n data refers to the number of your experimental
data
     integer ipopsize, lchrom, maxgen, ncross, nmute, nparam
     integer lsubstr(10)
     integer I
     double precision pcross, pmute, pjump
     double precision alow(10),ahigh(10),factor(10)
     common/sgaparam/ipopsize,lchrom,maxgen,ncross,nmute,nparam
     common/sgaparam1/pcross,pmute,pjump
     DOUBLE PRECISION KA, Q, b, CO, m, V, TS
     DOUBLE PRECISION TEXP, CCEXP
     DIMENSION TEXP(NDATA), CCEXP(NDATA)
     COMMON /GA1/ TEXP, CCEXP
     COMMON /GA2/ TS
          COMMON /GA3/ KA, Q, b, CO, m, V
     EXTERNAL nsga2
     OPEN(unit=20, FILE='ads.txt')
     OPEN(unit=10, FILE='ads-res.res')
          READ(20, *) Q, b, CO, m, V
 ! Read the experimental data (time and concentration) from data file
     DO 27 I=1, NDATA
     READ(20, *) TEXP(I), CCEXP(I)
27   CONTINUE
     nparam=1 ! nparam refers to the number of the decision variables need to be tuned
! The following parameters are used in NSGA
          ipopsize=50          ! number of generations, decrease it to get quick result
     maxgen=50
     pcross=0.7d0
     pmute=0.005
     pjump=0.15d0
     nmute=0
     ncross=0
     lchrom=0.
     DO 2 i=1,nparam
     lsubstr(i)=10
     lchrom=lchrom+lsubstr(i)
     factor(i)=2.0**float(lsubstr(i))-1.0
```

```
2     continue
      alow(1)=0.010d0
!     alow(2)=30.0d0
!     alow(3)=0.4d0
!           alow(4)=0.15d0
      ahigh(1)=10.00d0
!     ahigh(2)=100.0d0
!           ahigh(3)=0.8d0
!           ahigh(4)=0.35d0
      write(10, 100) maxgen, ipopsize, nparam
      write(10, 200) pcross, pmute, pjump, lchrom
      Do 3 i=1, nparam
      write(10, 300) i, lsubstr(i), alow(i), ahigh(i)
3     continue
      write(10, *)
      write(10,350)
      call nsga2 (alow, ahigh, lsubstr, factor)
100   format(1x, 'No. of Generations=',I3,3X,'No. of population=',&
I3,3X,'No. of Variables=',I3,3X,'No. of objectives=1',I3)
200   format(1x,'crossover=',F5.3,3X,'mutation=',F6.4,3X,'jumping genes=',F5.3,&
3X,'chromosome length=',I3)
300   format(1x, 'variable No.',I3,3X,'stringlength=',I3,3X,&
'lowlimit=',F14.6,3X,'highlimit=',F14.6)
350   format(15X,'X(1)',8X,'simulout(1)',8X,'F')
      end
          subroutine simul(nparam,x,simulout)
            IMPLICIT double precision (A-H,O-Z)
            parameter (ndatas=10, NDATA=44)     ! Change only NDATA here.....
       integer ipopsize,lchrom,maxgen,ncross,nmute,nparamm,igen,nobjfn, I, J
          double precision x(nparam),simulout(ndatas),pen,pcross, pmute,pjump
       double precision F
       double precision TEXP, CCEXP, CCAL
       dimension TEXP(NDATA)
       dimension CCEXP(NDATA), CCAL(NDATA)
       common/sgaparam/ipopsize,lchrom,maxgen,ncross,nmute,nparamm
             common/sgaparam1/pcross,pmute,pjump
       common/statist/igen                !avg,amax,aminO,sumfitness
       common/GA1/ TEXP, CCEXP
          EXTERNAL Isosimul
        call Isosimul(X, NDATA, TEXP, CCAL)
  ! Define the objective
        F=0.0d0
        DO 111 J=1, NDATA
        F=F+(CCEXP(J)-CCAL(J))**2.0
!                   print*, CCEXP, CCAL
!                   Pause
```

```
111     CONTINUE
        simulout(1)=1.0/(1.0+F)
!             simulout(2)=1.0/(1.0+F)
        if(mod(igen,1) .eq. 0) then
        write(10,100) X, simulout(1), F
        end if
100     format(8X, 3F14.6)
        return
        end
      Subroutine Isosimul(X, NDATA, TEXP, CCAL)
      INTEGER MXPARM, N, NDATA, I, J
      PARAMETER (MXPARM=50, N=1)
      INTEGER MABSE,MBDF
      PARAMETER (MABSE=1,MBDF=2)
      INTEGER IDO,NOUT,ISTEP
      DOUBLE PRECISION A(1,1), PARAM(MXPARM),T,TEND, TT, TOL
      DOUBLE PRECISION Y, X
      DOUBLE PRECISION TEXP, CCAL
      DOUBLE PRECISION KA, Q, b, CO, m, V, TS
      DIMENSION Y(N),X(10),TEXP(NDATA), CCAL(NDATA)
      EXTERNAL DIVPAG, SSET, UMACH
      EXTERNAL FCN, FCNJ
      COMMON /GA2/ TS
      COMMON /GA3/ KA, Q, b, CO, m, V
      KA=X(1)
!           Q=6.138735421d0
!           b=0.00825437d0
!           CO=150.0d0
!           m=1.0d0
!           V=0.08d0
            TS=300.0d0
      CALL UMACH(2, NOUT)
      CALL SSET(MXPARM, 0.0, PARAM, 1)
      PARAM(4)=100000000
      PARAM(10)=MABSE
      PARAM(12)=MBDF
      TOL=10E-7
      DO 56 I=1,N
      Y(I)=0.0
56    CONTINUE
      T=0.0
      IDO=1
      ISTEP=1
      DO 20 WHILE(ISTEP .LE. 30001)
      IF(ISTEP .EQ. 30001) IDO=3
```

```
!     IF(ISTEP .GT. 60000) KZF=0.0  ! use the KZF value to initiate the rectangular pulse injection
      TEND=TS*ISTEP/30000.
      TT=TEND
      CALL DIVPAG(IDO, N, FCN, FCNJ, A, T, TEND,TOL, PARAM, Y) ! This function is used to solve the ODE
            DO 30 J=1, NDATA
      IF(TT .EQ. TEXP(J)) THEN
      CCAL(J)=Y(N)
      END IF
 30   CONTINUE
      ISTEP=ISTEP+1
20    CONTINUE
      RETURN
      END
      SUBROUTINE FCN(N, T, Y, YPRIME)
      INTEGER I, N
      DOUBLE PRECISION T, Y(N), YPRIME(N)
      DOUBLE PRECISION KA, Q, b, CO, m, V
      COMMON /GA3/ KA, Q, b, CO, m, V
YPRIME(1)=KA*(((Q/(1+(1/(b*(CO-((m*Y(1))/V))))))-Y(1))**2.0) ! First plate for component 1
      RETURN
      END
      SUBROUTINE FCNJ(N, X, Y, DYPDY)
      INTEGER N
      DOUBLE PRECISION X, Y(N), DYPDY(N,*)
      RETURN
      END
     subroutine nsga2(alow,ahigh,lsubstr,factor)
     integer oldchr1(400,400), newchrom(400,400),oldrank(400)
     integer chr(400),lsubstr(400),dummychr(400),oldrankno(400)
     integer oldrankar(400,400),keepchrom(400,400),globchrom(800,800)
     integer oldmaxrank,grank(800),grankno(800),igen
     integer ipopsize,lchrom,maxgen,ncross,nmute,nparam
     integer jrand
     double precision oldx(400,20),factor(20),oldcub_len(400),globx(800,20)
     double precision dummyx(20),alow(20),ahigh(20),newx(400,20),a11(400)
     double precision oldfit1(400),oldfit2(400),newfit1(400),globfit1(800)
     double precision newfit2(400),keepx(400,20),globfit2(800)
     double precision keepfit1(400),keepfit2(400),gcub_len(800),a22(400)
     double precision pcross,pmute,pjump
     double precision oldrand(55), fix
     common/sgaparam/ipopsize,lchrom,maxgen,ncross,nmute,nparam
     common/sgaparam1/pcross,pmute,pjump
     common/randvar/oldrand,jrand
```

```
      common/consts/fix
```

FOR SIMULATION OF KINETIC ADSORPTION CURVES OF ADSORPTION USING EVALUATED k_2.

```
PROGRAM MAIN
      USE IMSLF90
      INTEGER MXPARM, N, NPLATE, NG, I
      PARAMETER (MXPARM=50, NPLATE=1, N=1)
      INTEGER MABSE,MBDF
      PARAMETER (MABSE=1,MBDF=2)
      INTEGER IDO,NOUT,ISTEP
      DOUBLE PRECISION A(1,1), PARAM(MXPARM),T,TEND, TT, TOL
      DOUBLE PRECISION Y
      DOUBLE PRECISION KA, Q, b, CO, m, V, TS
      DIMENSION Y(N)
      EXTERNAL DIVPAG, SSET, UMACH
      EXTERNAL FCN, FCNJ
      COMMON /GA2/ TS
            COMMON /GA3/ KA, Q, b, CO, m, V
      OPEN(unit=20, FILE='SC-ads.txt')
      OPEN(unit=10, FILE='SC-ads-res.res')
      READ(20, *) KA, Q, b, CO, m, V
!           Q=6.7659d0
!           b=0.00567d0
!           CO=50.0d0
!           m=1.0d0
!           V=0.08d0
            TS=300.0d0
      CALL UMACH(2, NOUT)
      CALL SSET(MXPARM, 0.0, PARAM, 1)
      PARAM(4)=100000000
      PARAM(10)=MABSE
      PARAM(12)=MBDF
      TOL=0.000001
      DO 10 I=1,N
      Y(I)=0.0d0
10    CONTINUE
      T=0.0
      IDO=1
      ISTEP=1
      WRITE(10, 99994) T, Y(N)
      DO 25 WHILE(ISTEP .LT. 301)
      IF(ISTEP .EQ. 301) IDO=3
!     IF(ISTEP .GT. 6) KZF=0.0d0
      TEND=TS*ISTEP/300.
```

```
      TT=TEND
      CALL DIVPAG(IDO, N, FCN, FCNJ, A, T, TEND,TOL, PARAM, Y)
      IF(MOD(ISTEP, 1) .EQ. 0) THEN
      WRITE(10, 99994) TT, Y(N)
      END IF
      ISTEP=ISTEP+1
25    CONTINUE
99994  FORMAT(4X, F10.5, 4X, F10.5)
      END
      SUBROUTINE FCN(N, T, Y, YPRIME)
      INTEGER I, J, N
      DOUBLE PRECISION T, Y(N), YPRIME(N)
      DOUBLE PRECISION KA, Q, b, CO, m, V, TS
      COMMON /GA2/ TS
            COMMON /GA3/ KA, Q, b, CO, m, V
      YPRIME(1)=KA*(((Q/(1+(1/(b*(CO-((m*Y(1))/V))))))-Y(1))**2.0) ! First plate for
component 1
      RETURN
      END
      SUBROUTINE FCNJ(N, T, Y, DYPDY)
      INTEGER N
      DOUBLE PRECISION T, Y(N), DYPDY(N, T)
      RETURN
      END
```

Table C.2 Film thicknesses measured at ten different spots of each film to get an average value.

OBSERVATIONS	**FILM THICKNESS (mm)**		
No.	**A**	**B**	**C**
1	0.161	0.068	0.039
2	0.163	0.070	0.041
3	0.162	0.069	0.042
4	0.161	0.069	0.041
5	0.162	0.070	0.042
6	0.163	0.068	0.039
7	0.161	0.069	0.042
8	0.162	0.069	0.041
9	0.163	0.070	0.041
10	0.161	0.069	0.042
Average	0.162	0.069	0.041